PICOSECOND SPECTROSCOPY OF MOLECULAR AGGREGATES

by

MIIN-LIANG HORNG, B.S., M.S.

A DISSERTATION

IN

CHEMISTRY

Submitted to the Graduate Faculty of
Texas Tech University
in Partial Fulfillment of
the Requirements for
the Degree of

DOCTOR OF PHILOSOPHY

Approved

December, 1992

ACKNOWLEDGMENTS

I am deeply indebted to Professor Edward L. Quitevis for his invaluable direction and support throughout this work. His enthusiasm for science was both contagious and an inspiration to me. His insight, patience, and guidance made graduate school an exciting learning experience.

I would also like to thank my committee members, Professor Richard L. Redington, Professor Richard E. Wilde, Professor Thomas L. Gibson, and Professor Gregory Gellene, for their helpful discussions and guidance of this dissertation.

I should like to express my thanks to Professor Robert D. Walkup for making many valuable suggestions and advice throughout my Ph.D. Program. I am also grateful to Professor G. Wilse Robinson for use of the Picosecond and Quantum Radiation Laboratory.

It gives me great pleasure to acknowlege the help and cooperation I have received from many persons during this work. The help given by Dr. Jamine Lee, Dr. Kelly G. Casey, Mr. Yavuz Onganer, and Mr. Ningyi Luo are much appreciated. I also thank the Department of Chemistry and Biochemistry, the Graduate School, and the R. A. Welch Foundation for their financial support.

I would like to apologize to my wife and children for the many hours of my time spent on chemistry instead of with them. Finally I am greatly indebted to my parents and my wife for their continued support and encouragement without which this work could not have been completed.

TABLE OF CONTENTS

ABSTRACT

Cyanine dyes in aqueous solutions at higher concentrations are known to deviate from Beer's law. These spectral changes have been attributed to the formation of dimers and higher polymers, and may consist of a shift of the absorption peak or a splitting of the monomer band due to excitonic interactions. Dimerization of 1,1'-diethyl-2,2'-carbocyanine has been studied over a certain concentration range. The value of the dimerization equilibrium constant K has been determined. The dimer spectrum has been extracted from the composite spectra and analyzed in terms of a vibronic exciton coupling theory.

The study of exciton transport in simple molecular aggregates is crucial in understanding the dynamics of excitation energy transfer in light-harvesting antennae. The optical dynamics of J-aggregates of 1,1'-diethyl-2,2'-cyanine in sodium chloride solution, on colloidal silica and poly(vinylsulfonic acid, sodium salt) have been studied by using picosecond polarized pump-probe spectroscopy. The picosecond transient photobleaching signal of colloidal silica system decays biexponentially and appears to be independent of the laser intensity. The absorption anisotropy is constant and discussed in terms of the coherence properties of excitons. For the J-aggregates in the systems of sodium chloride and polyelectrolyte solutions, the absorption anisotropy decay and ground-state recovery kinetics are excitation-intensity dependent. The excitation-intensity dependence of the decay kinetics of J-aggregates in these two systems indicates that exciton annihilation is occurring. The results are discussed in terms of the dynamics of delocalized and localized excitons.

LIST OF TABLES

LIST OF FIGURES

CHAPTER I

INTRODUCTION

Solar generation of electricity is one of the most promising areas of technological development for reducing consumption of fossil fuels. Today, silicon photovoltaic cells have been used for converting solar energy directly to electricity and the maximum realized energy conversion has reached 16% in the laboratory.[1,2] However, a natural photosynthesis-type photoelectric system can provide as high as 90% quantum yield of solar energy conversion without the use of the superpure crystallinity of light-absorbing materials as required by manmade inorganic semiconductor photocells.[3,4] Much evidence exists showing that generation of microcurrent in the photosynthetic electron transport chain is determined by the processes of energy transfer from light-harvesting antenna to reaction centers. Apparently, a new line of highly efficient solar converters may be advanced from investigations of ultrafast primary stages of photosynthesis. It is clear that understanding the excitation energy transport mechanisms of photosynthesis is our most important task.

Light-harvesting antennae in photosynthetic bacteria, algae, and higher plants contain numerous pigment molecules [Figures 1.1, 1.2] that are highly ordered.[5,6] The trapped light energy migrates from one pigment molecule in the antenna to the next through nonradiative interactions.[7] This energy is directed to photochemical electron-transfer complexes known as the reaction centers where the absorbed energy is used to drive a sequence of reactions leading to the separation of charge and ultimately results in the synthesis of high-energy chemical products [Figure 1.3].[7]

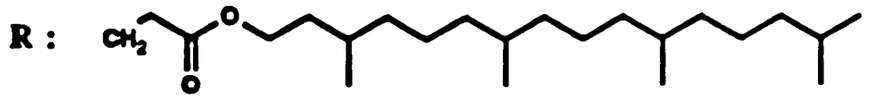

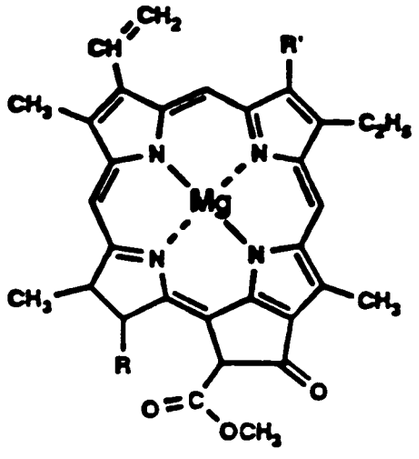

Chlorophyll a: R' = CH_3
Chlorophyll b: R' = CHO

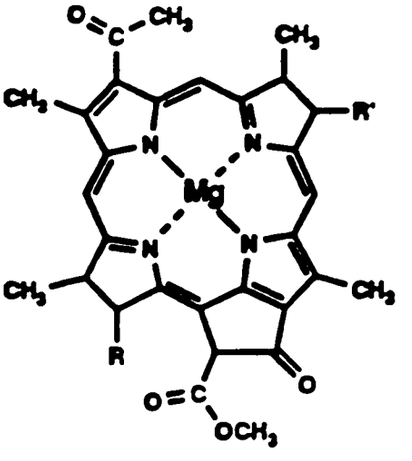

Bacteriochlorophyll a: R' = CH_2-CH_3
Bacteriochlorophyll b: R' = CH-CH_3

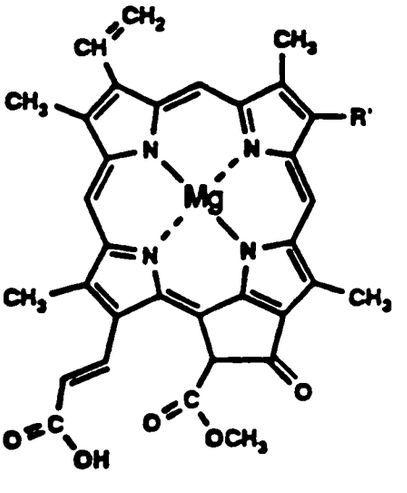

Chlorophyll c_1: R' = -CH_2-CH_3
Chlorophyll c_2: R' = -CH=CH_2

Figure 1.1. The structures of the chlorophylls.

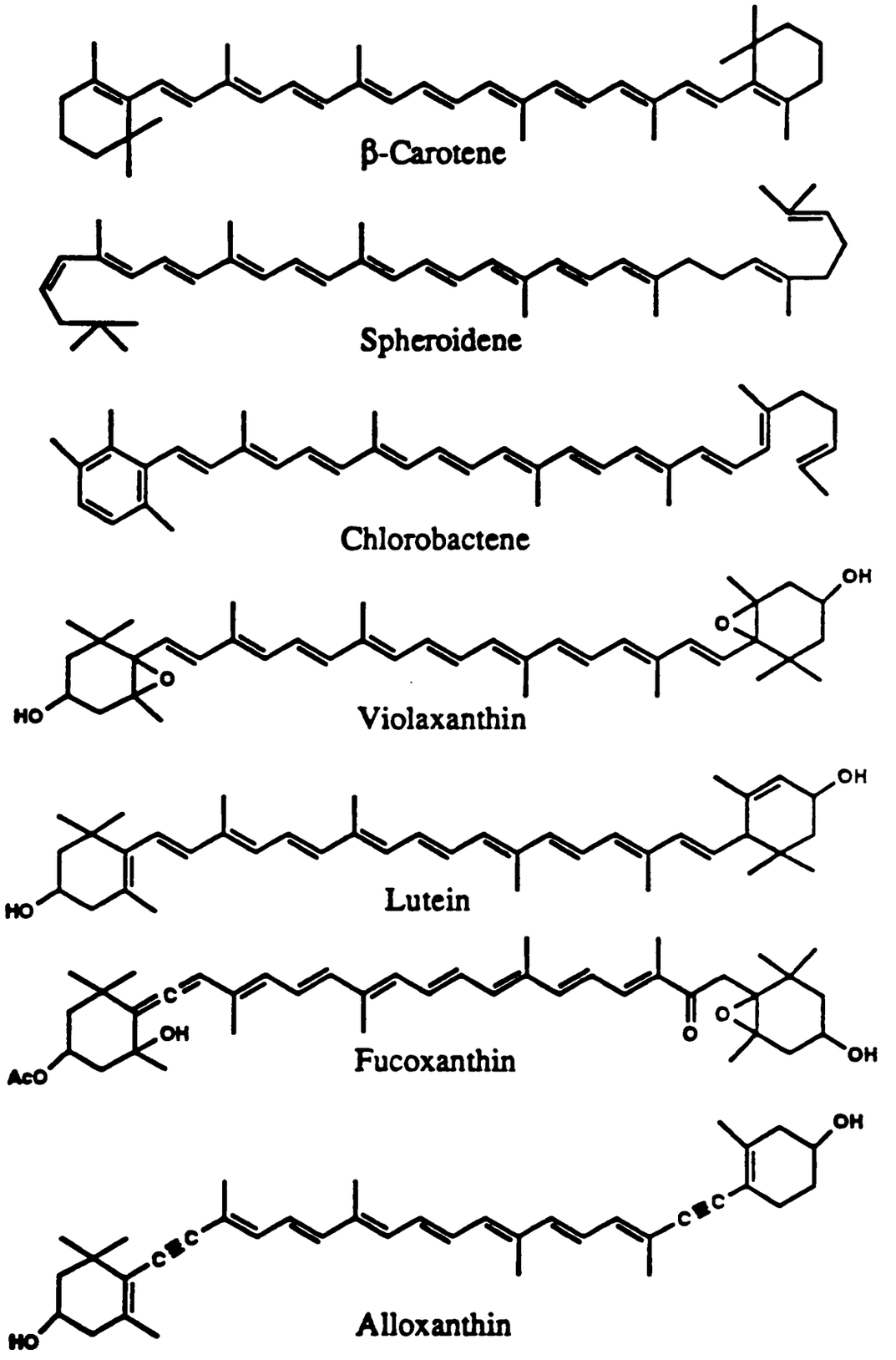

Figure 1.2. Structures of some carotenoids found in plants and bacteria.

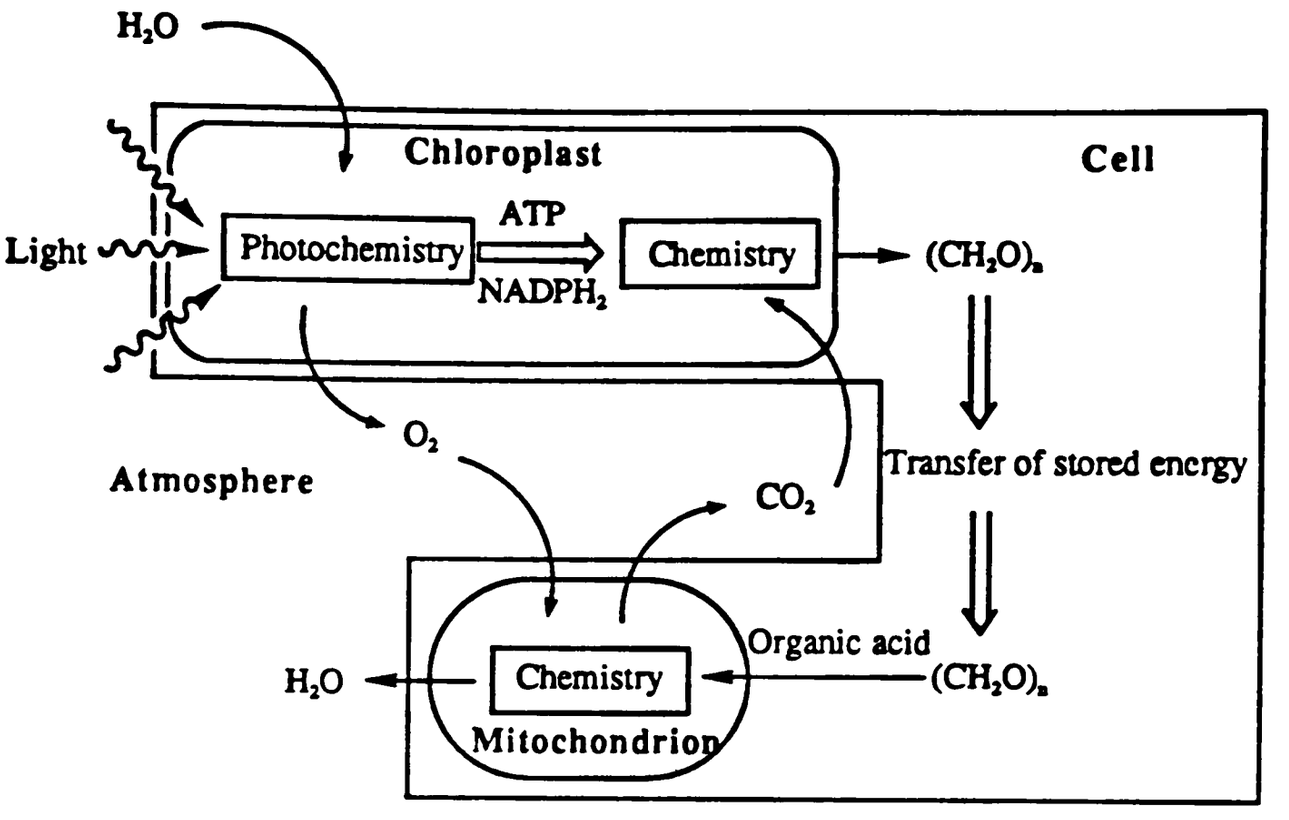

ATP: adenosine triphosphate;
$NADPH_2$: reduced nicotinamide adenine dinucleotide phosphate.

Figure 1.3. Scheme of photosynthesis.

The dynamics of excitation energy transport in these antenna systems are not well understood, in part because detailed structural data is lacking. To understand the dynamics of excitation energy transport in these complex systems, it is logical to choose model systems that are ordered but less complicated. Aggregates of cyanine dyes are ideally suited for many reasons. The molecules are in well-defined structures.[8-10] An analogous situation exists in the aggregates of cyanine dyes bearing a chromophore at every repeating unit on the ordered arrays, such molecular aggregates also display efficient electronic energy transfer to low-energy traps.[11,12] The function of dyes adsorbed on polymer chain and the biological membrane of plants is similar, both supporting high concentrations of chromophores.[13] Aggregates of cyanine dyes can thus mimic the function of the light-harvesting pigment layers, without reproducing their exact structure.

1.1. Cyanine Dyes

Cyanine dyes have been studied as sensitizers in photoelectrochemical solar energy conversion systems[14-16] and chemotherapy.[17] Recently, these dyes have shown great promise for use in the fields of opto-electronics[18] and optical communications.[19] However, most practical uses of cyanine dyes are in photographic processes.[20] In normal photographic practice, the sensitivity of undyed emulsions is limited to wavelengths absorbed by the silver halide. But in color photography, the desired color separations often require dyes that sensitize over rather narrow spectral ranges with sharp decreases in spectral sensitivities at long wavelength. Dyes that have made color photography and high speed photography possible belong to the cyanine or related group almost exclusively. Cyanine dyes bound to the silver halide microcrystals are being used as spectral sensitizers and

color images. Cyanine dyes have accomplished spectral separation in either the visible or infrared and extended the responses of photoconductors to longer wavelengths. Spectral sensitization has been extended to wavelengths well beyond 1000 nm.[20] Certain cyanines that are not useful as photographic sensitizers have proved valuable as dyes for optical data disks[21,22] and laser dyes[23,24] in computers and dye laser applications, respectively.

Numerous investigations are conducted on the photophysics of cyanine dyes since the discovery of the first cyanine dye, bis-[4-(1-pentylquinoline)]-methinecyanine iodide (may be called 1-pentyl-4-[(1-pentyl-4(1H)-quinolylidene)-methyl]quinolinum iodide or Quinoline Blue) [Figure 1.4(a)], by C. H. Greville Williams in 1856.[25] The term "Cyanine" was originally applied to one compound [Figure 1.4(b)][14,26] but was subsequently extended to a group of dyes. Many of the early cyanine dyes are recognized as composed of two heterocyclic rings like quinoline or benzothiazole joined together by a chain with an odd number of methine carbon atoms (-CH=).[27,28] Traditionally, the dyes with the general structures shown in Figure 1.4(c) from quinoline or benzothiazole with one, three or five methine carbon atoms are designated by the terms simple cyanine, carbocyanine or dicarbocyanine respectively. The N-substituent and the positions of linking of the heterocyclic ring are usually specified for cyanines from quinoline. For example, 1,1'-diethyl-2,4'-cyanine iodide (Isocyanine iodide) is the dye structure shown in Figure 1.4(d) with R = CH_2CH_3, X = I, Y = CH=CH and n = 0. For the dyes from other heterocycles, the 2-position of the heterocyclic rings is attached to the methine chain (for instance, 3,3'-diethylthiacarbo-cyanine iodide is the dye shown in Figure 1.4(e) with R = CH_2CH_3, X = I, Y = S and n = 1).

(a)

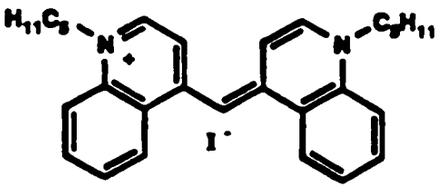

Williams' Cyanine

(b)

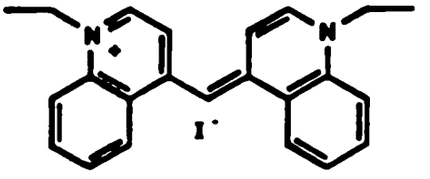

Cyanine

(c)

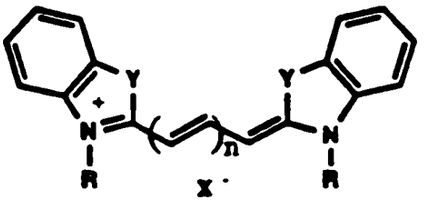

n = 0, simple cyanine
n = 1, carbocyanine
n = 2, dicarbocyanine
n = 3, tricarbocyanine

(d)

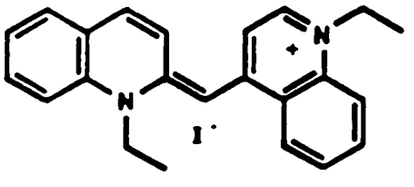

Isocyanine iodide

(e)

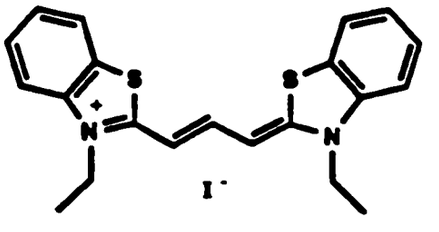

3,3'-Diethylthiacarbocyanine iodide

Figure 1.4. Structures of cyanine dyes.

Sensitizing dyes are characterized by high extinction transitions in the visible or infrared regions of the spectrum. The important characteristics that influence the absorption wavelengths for these dyes are the length of the conjugated chain and the nature of the terminal group. In large conjugated molecules like the cyanines, the filled orbitals of the ground states contain sigma (σ), pi (π) and lone-pair (n) electrons. The possible electronic transitions in the visible and infrared spectral regions include $\pi \rightarrow \pi^*$ and $n \rightarrow \pi^*$, but the latter are low extinction bands and can be obscured by the strong $\pi \rightarrow \pi^*$ transitions. There are two extreme resonance structures in the resonance picture of symmetrical ground-state dyes, the formal charges are located at the ends of the chromophore. After excitation, more of the formal charge is located on the methine carbons than on the terminal atoms.[29] The redistribution of electron charge density following various electronic transitions is characteristic of an ionic bond between a negatively charge chlorine atom and a conjugated cation species. For symmetrical dyes, this leads to more positive charge near the center of system.

Dyes that differ only by the number of vinyl groups (-CH=CH-) in the conjugated chain are termed a vinylogous series [Figure 1.5]. Absorption maxima for these dyes shift to longer wavelengths as the length of the chromophoric chain increases. This behavior is readily understood by the simple model of a particle in a box[30] and the shift approximates 100 nm per vinyl group in the most symmetric cyanine dyes [Figure 1.6]. Frequently transitions occur from the ground vibrational level of the ground electronic state to many different vibrational levels of a particular excited electronic state. Such transitions may give rise to vibrational fine structure in the main peak of the electronic transition. Absorption spectra for typical symmetrical cyanine dyes exhibit a band shape with a single absorption band in the visible

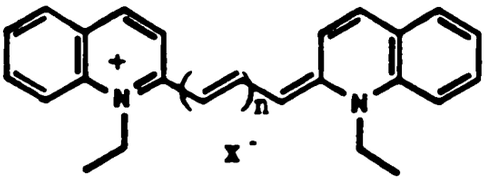

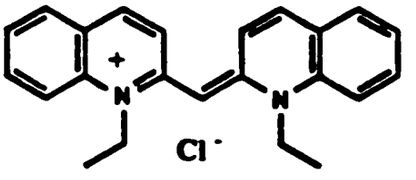

PIC
(Pseudoisocyanine chloride)
1,1'-Diethyl-2,2'-cyanine chloride

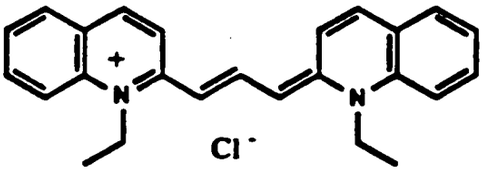

DCC
1,1'-Diethyl-2,2'-carbocyanine chloride

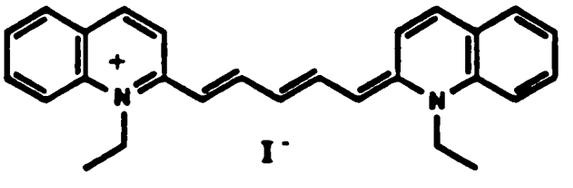

DDC
1,1'-Diethyl-2,2'-dicarbocyanine Iodide

Figure 1.5. Structures of a vinylogous series.

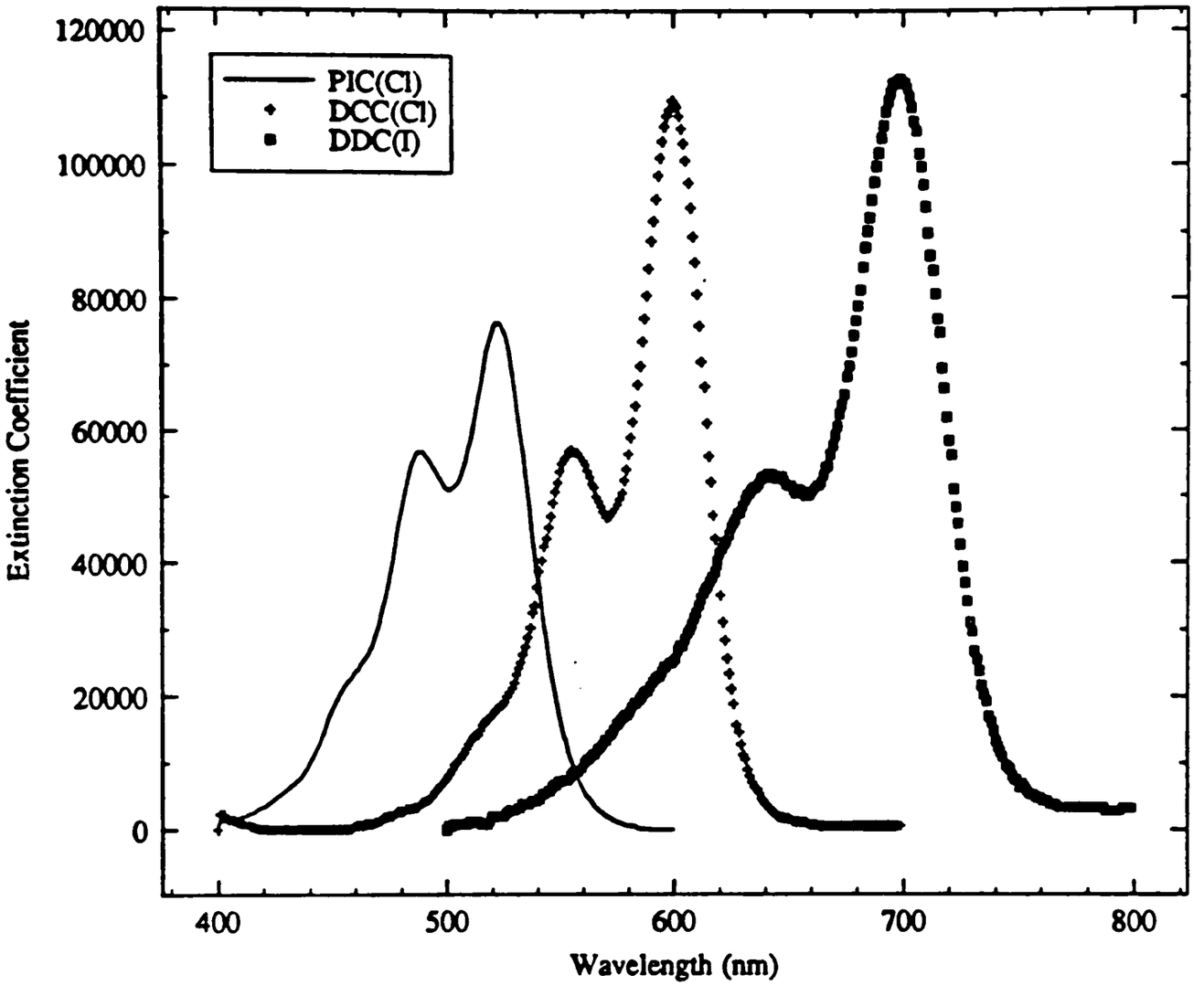

Figure 1.6. Absorption spectra of a vinylogous series.

spectrum and prominent vibrational shoulders on the short wavelength side of the band. The shoulders included one or two vibrational quanta ($0 \rightarrow 1'$, $0 \rightarrow 2'$) relative to the absorption maximum ($0 \rightarrow 0'$). Intensity ratios for the $0 \rightarrow 0'/0 \rightarrow 1'$ bands increase as the chromophoric chain is lengthened.

Industrially numerous colored compounds of the same basic structure are generally synthesized, differing only in the position of a substituent or other minor details. The absorption spectra of such related dyes are normally found to vary. Shifts of the absorption maximum to longer and shorter wavelengths are called bathochromic and hypsochromic shifts, respectively. An increase and a decrease in the magnitude of the extinction coefficient are termed hyperchromic and hypochromic changes, respectively [Figure 1.7].[14]

1.2. Aggregates of Cyanine Dyes

The cyanine dyes exhibit interesting aggregation properties in solution and on surfaces, having both sharp absorption bands and large dipole strengths.[31] Interactions among dye molecules produce large spectral shifts and distinct changes in band shape. Generally, aqueous solutions of these dyes have a visible absorption spectrum that depends strongly upon dye concentration. For sufficiently diluted solutions, most of these dyes can be shown to produce the spectrum of the unassociated dye molecule. The spectral changes observed upon increasing concentration have been attributed to dye association. Increasing dye concentration produces at least one, and often several, new absorption bands that are shifted to shorter or longer wavelengths compared to the diluted-solution spectrum. The first new band that appears at shorter wavelength is usually ascribed to a dimer. For many cyanines, dimerization is followed by a generally unspecified degree of

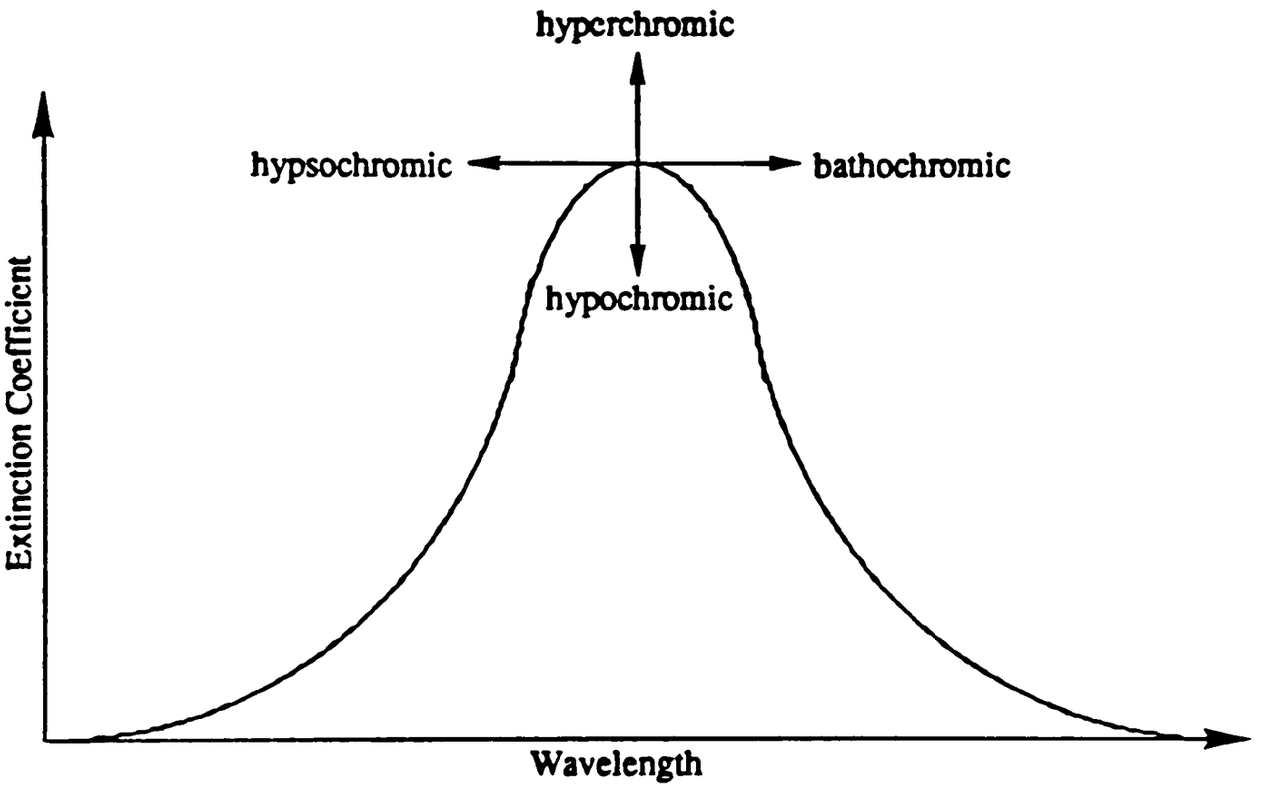

Figure 1.7. Scheme of designations for wavelength shifts and changes of extinction of absorption bands.

aggregation, which results in further shifts in the main band to even shorter wavelengths. At higher concentrations, certain of the cyanine dyes exhibit an intense and unusually sharp absorption at longer wavelengths. The most well-known example of the sharp band formation is aqueous 1,1'-diethyl-2,2'-cyanine chloride (Pseudoisocyanine chloride or PIC-Cl), which has n = 0 in the series shown in Figure 1.5 and is the subject of this dissertation. Spectroscopic studies on PIC aggregates date back to the midthirties when E. E. Jelley and G. Scheibe independently discovered that concentrated solutions of PIC-Cl develop a sharp absorption band.[32,33] This band, now referred to as J-band probably "J" for Jelley, was interpreted by them as arising from an aggregate of the PIC molecule.

In alcohol, as in diluted water solutions, PIC appears to exist only in an extended configuration and has its maximum absorption near 523 nm [Figure 1.8]. This transition is associated with isolated molecules and is referred to as the monomer band (M-band). On increasing the dye concentration beyond about 100 μM, the intensity of the monomer band decreases and a new maximum appears near 485 nm; this band is associated with formation of a dimer and is accordingly called the D-band. At concentrations above 0.01 M, an abnormal increase of viscosity is observed, together with the appearance of a narrow band of high absorptivity which is located at approximately 572 nm; and is referred to as the J-band. This J-band is thought to be caused by aggregates of stacked cyanine molecules held together by van der Waals forces in a close-packed and possibly helical configuration.[34,35] Aggregation occurs because of the strong dispersion forces associated with the high polarizability of the chromophoric chain. J-aggregates of pseudoisocyanine can be formed in aqueous solutions at high concentrations, or upon addition of either NaCl [Figure 1.9], colloidal silica [Figure 1.10], or poly(vinylsulfonic acid, sodium salt)

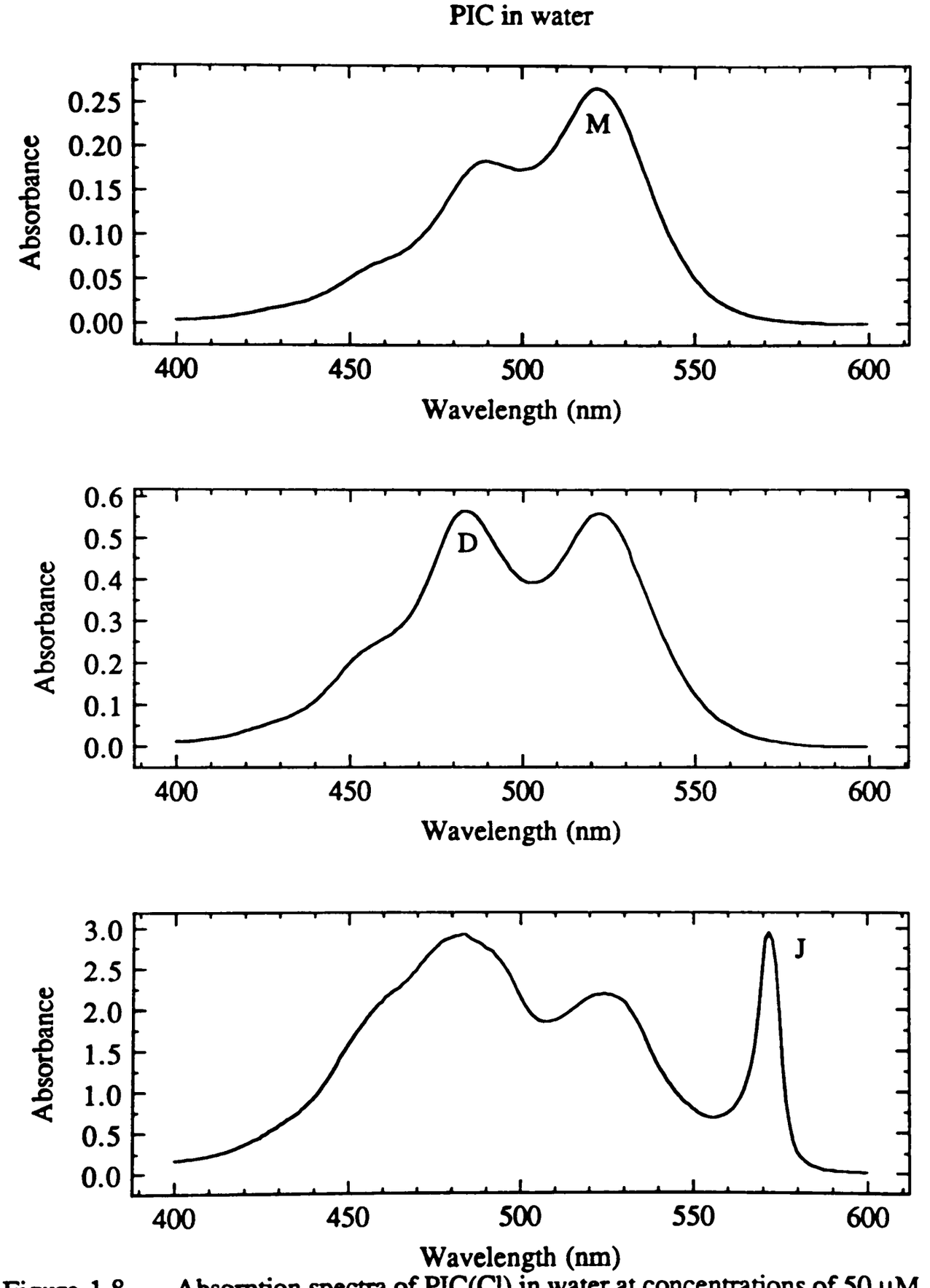

Figure 1.8. Absorption spectra of PIC(Cl) in water at concentrations of 50 μM, 100 μM, and 10 mM.

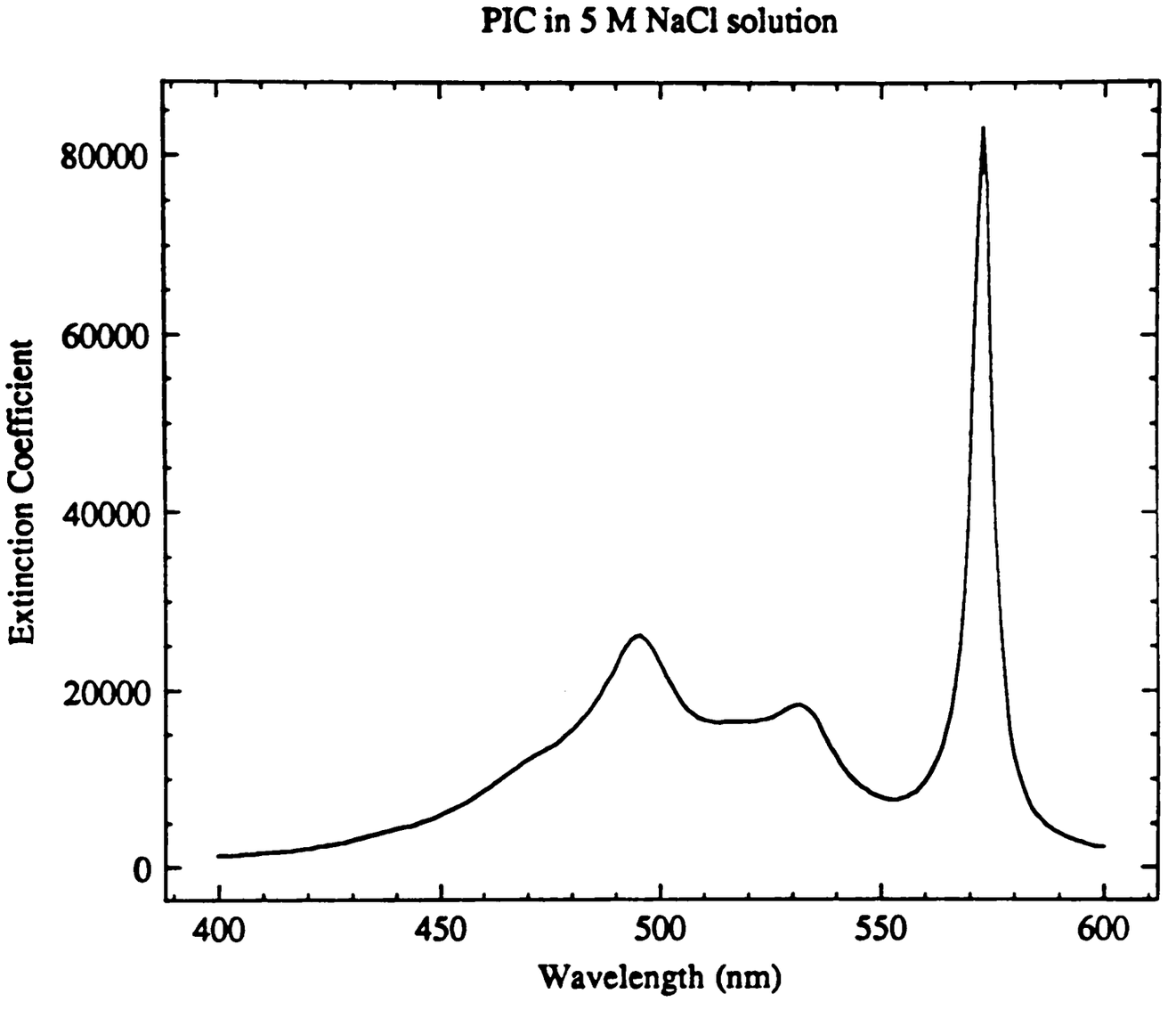

Figure 1.9. The absorption spectrum of 50 μM PIC(Cl) in 5 M NaCl solution.

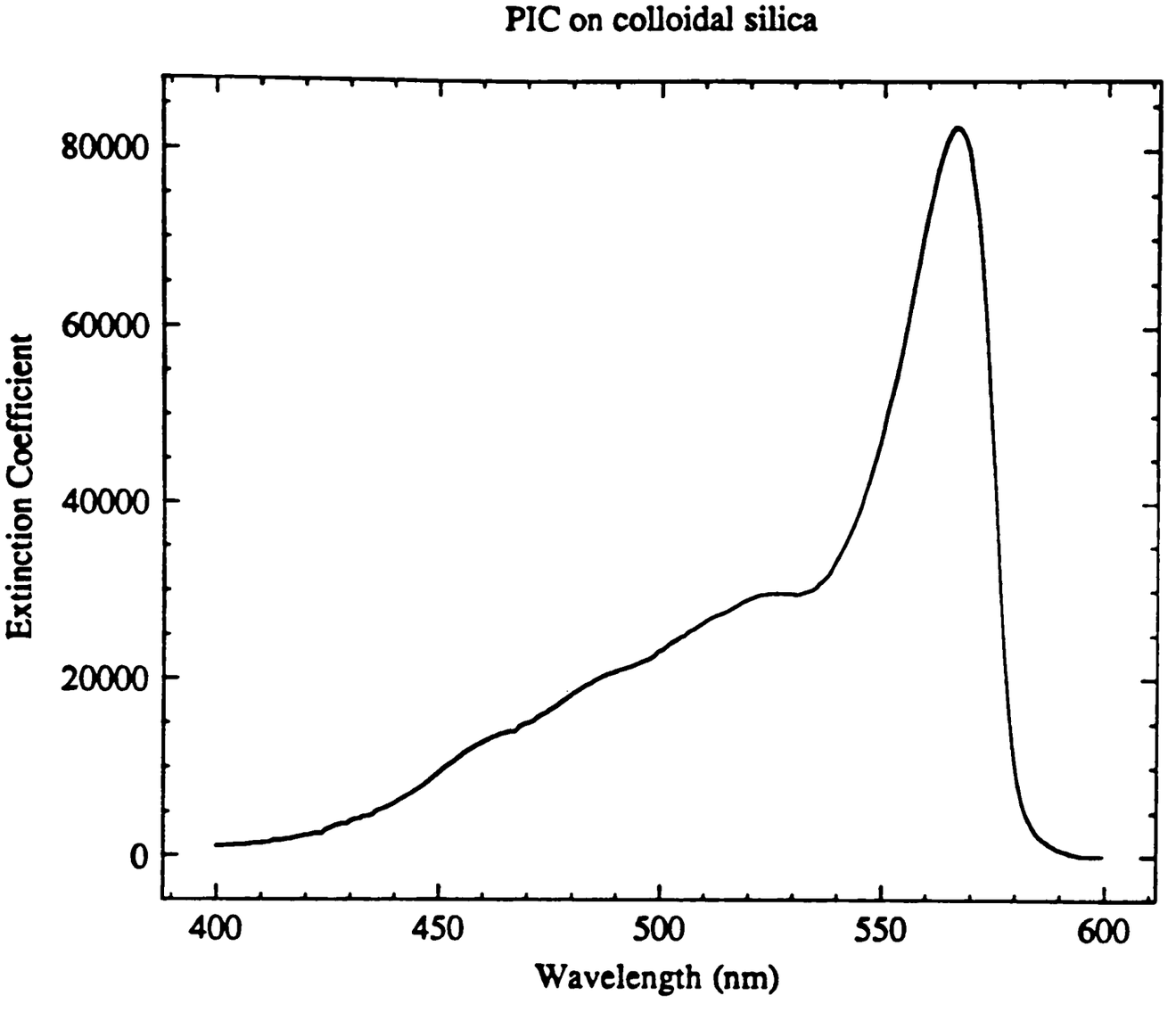

Figure 1.10. The absorption spectrum of 50 μM PIC(I) in 7.5% colloidal silica.

(or PVS polymer) [Figure 1.11] to dilute aqueous solutions of PIC, or in low-temperature glasses and polycarbonate resin matrix [Figure 1.12]. Electrostatic attraction of polyelectrolytes for oppositely charged anionic or cationic dyes can be particularly effective for inducing aggregation. For diluted solutions of polyelectrolytes, induced aggregation will vary with the sign, number, and spacing of ionic sites in the polyelectrolyte and also with the "stacking coefficient" of the particular dye, that is, its preference for attachment to sites adjacent to those already occupied by dye ions rather than random attachment to available sites.[36] This coefficient is expected to parallel the free energy of aggregation. Ionic PVS polymer contains negative charges all along the polymer chain, facilitating electrostatic binding of the positively charged PIC molecules. In colloidal silica, the aggregates are bound to the surfaces of 4-nm-diameter colloidal particles. Dye adsorption occurs because of the electrostatic attraction between the cationic dye and the ionized silanol groups on the surface of the colloids. Added inorganic salts generally increase the dielectric constant of a solvent and facilitate aggregation, but a high dielectric constant is not a unique requirement for aggregation since formamide (dielectric constant 109) does not promote dye aggregation. Simple organic additives diminish the effective dielectric constant of a solvent and enhance the repulsion between similarly charged dye ions. Cyanine aggregates are less basic than the corresponding monomers. Dye cations were shown to act as electron acceptors for a variety of Lewis bases, including oxygen, nitrogen, and carbanionic bases. Aggregation in solution is a moderately exothermic process, the enthalpy for J-aggregation of PIC is -22 Kcal/mole.[37] Brooker suggests that planar dyes aggregate more readily than nonplanar dyes.[38] Carbocyanine and dicarbocyanine dyes in the benzimidazole series aggregate readily in solution, but a decrease in chain length to the simple

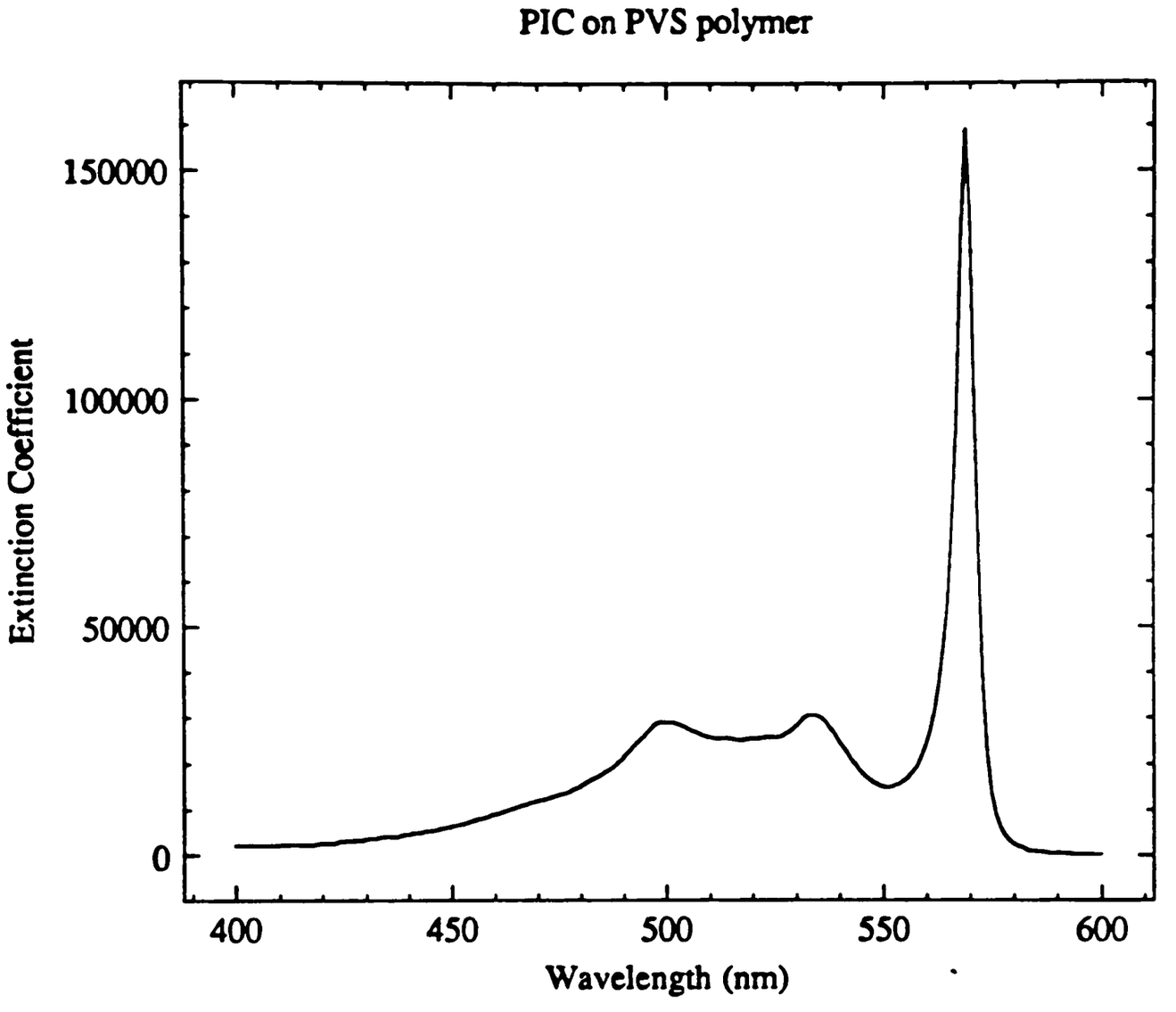

Figure 1.11. The absorption spectrum of 100 μM PIC(Cl) in 0.05 g/dl poly(vinyl-sulfonic acid, sodium salt) solution.

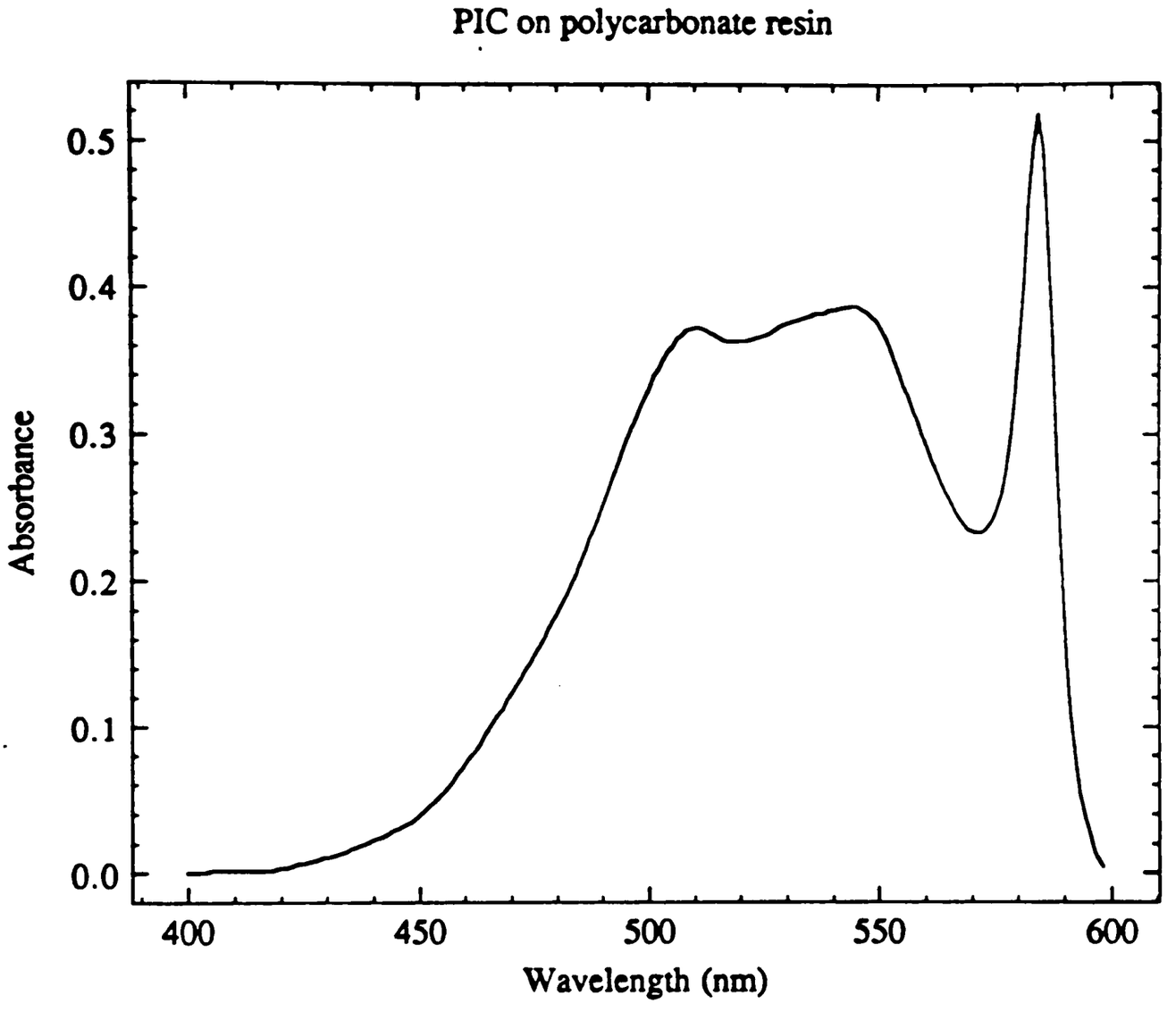

Figure 1.12. The absorption spectrum of PIC(I) in polycarbonate resin matrix.

cyanine leads to nonplanar dyes and no observable aggregation.[39] Increased methine chain length, chloro substituents, and fused benzene rings on the heterocycle enhance dimerization or blue-shifted aggregation.[39] The blue-shifted aggregates are designated as H aggregates ("H" for hypsochromic). J aggregation, however, is less prevalent for longer chain dyes. For example, PIC J aggregates readily, but the higher vinylog pinacyanol with only two additional methine carbons rarely forms J aggregates.

The spectra of PIC in 5 M NaCl, PVS polymer, and colloidal silica all exhibit the familiar J-band between 560 and 574 nm, which are red-shifted to the M-band due to excitonic interactions between the chromophores.

1.3. Exciton Theory for Electronic Spectra of Cyanine Aggregates

The appearances of excited states of a molecular crystal are much different from those of the isolated molecule. This phenomenon is quite common to all the nonmetallic solids such as semiconductors, molecular aggregates, molecular crystals, ionic crystals, and rare gas crystals.[40] These different physical phenomena can be treated with the various aspects of exciton theory just as valence-bond method and molecular-orbital approximation are used by theoretical chemists to treat the problem of chemical bonding and to determine a single molecule's geometry. According to this theory, the electronic excitation of a nonmetallic solid of interacting atoms or molecules can lead to an excited state whose energy resides on more than one of the atoms or molecules in the crystalline solid during the lifetime of the state. Such a state is treated as an exciton.[41] A coherent exciton is an excitation that is delocalized over the aggregate. The aggregate band is spectral evidence for the coherent properties of the excitons at the moment of excitation. However, molecular

dephasing can cause the loss of this coherence.[42] The excitation transfer becomes slower and must be described by an incoherent hopping mechanism involving localized excitons.[43] The excitaton energy transport from one molecule to another does not take place by emission and reabsorption of radiation, but through the electrostatic coupling of the two molecules in a radiationless transition.[44] These interactions result in the splitting of the energy level into a number of new levels equal to the number of equivalent interacting molecules.

The exciton concept was first introduced by J. I. Frenkel in 1931 as a general excitation delocalization mechanism to account for the capacity of argon crystals to take up the big quantum of energy without local melting.[45] In 1948, A. S. Davydov extended the molecular exciton model, and applied to the problem of the spectrum of naphthalene crystals which consists of very sharp line-like spectra at low temperatures.[46] Since then there have been numerous spectral studies exploring all aspects of the model.

The nomenclature of excitons is somewhat confusing for most people approaching this theory for the first time. The classification of excitons helps to clear up this broad subject. A diagrammatic classification of excitons is shown in Figure 1.13, and the general characters of the various excitons are also indicated in this diagram. The longitudinal excitons, in which the colliding particle transfers momentum parallel to the direction of motion in atomic collisional excitation, will not be considered further.[47] Instead, the transverse excitons, in which the perturbation of the system by the electric vector of the light wave is perpendicular to the direction of photon propagation in optically excited system, will be described.[48]

A transverse exciton consists of an electron and a hole performing various correlated motions, such as relative motion of the electron and the hole and

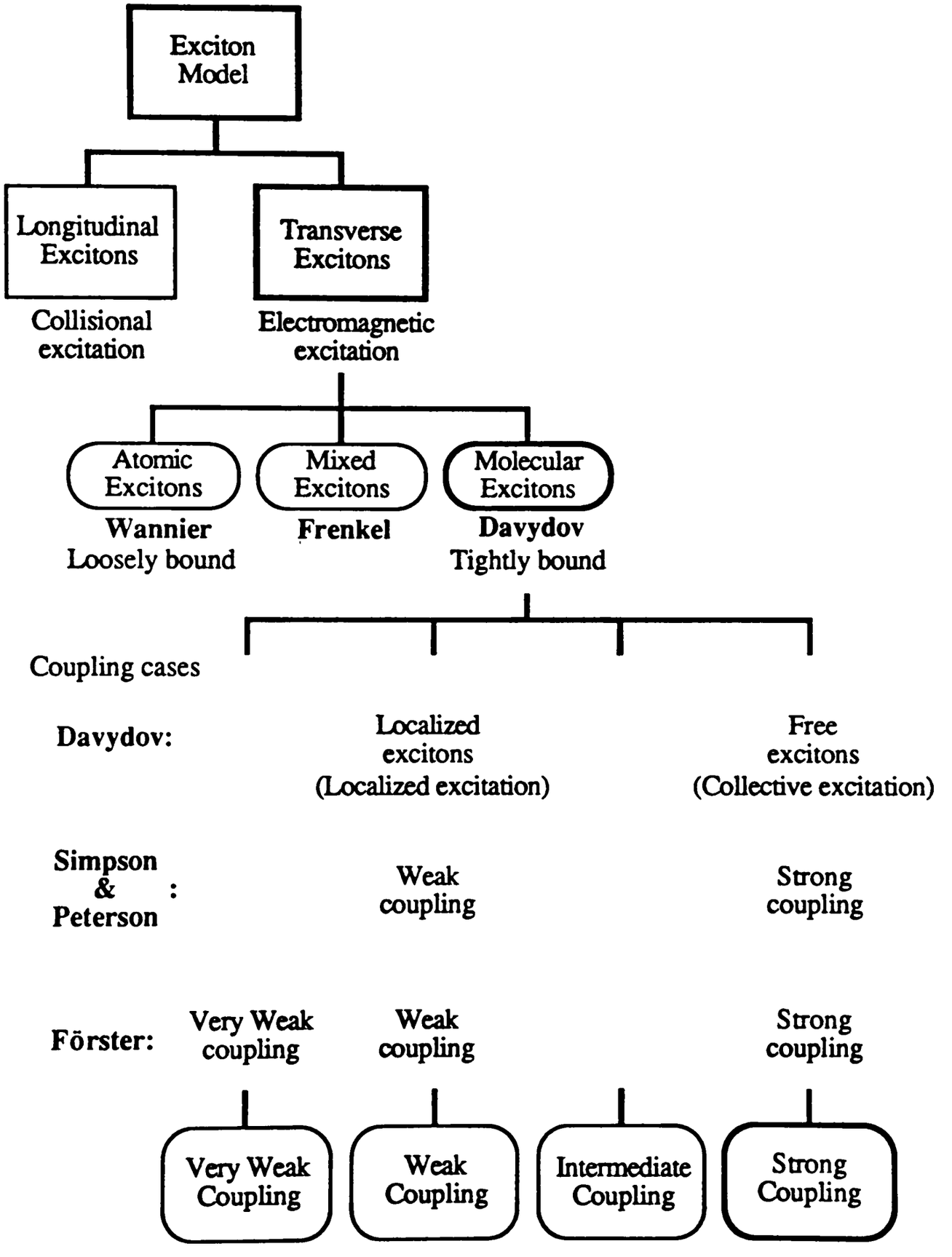

Figure 1.13. The classification of excitons.

translational motion as a whole. In the rigid lattice, there are two types of transverse excitons that are well understood, namely, atomic exciton[49] and molecular exciton.[50] For most ionic crystals, semiconductors and insulators, with strong bonding between components of the lattice, the atomic exciton description is most appropriate. The atomic exciton is composed of a hole of the valence-band and an electron of the conduction-band, these quasi-particles are usually separated by a distance which is large compared to the lattice constant (numbers specifying the size of a unit cell). The quasi-particles share certain properties with real particles, such as wave-particle duality. Thus, their dynamics can be expressed in terms of mass, momentum, and energy, but the effective mass depends on the forces between the systems making up the solid, showing that it is a collective property, unlike the rest mass of an electron. In this case, the distribution function for the excited electron may extend up to and beyond the nearest neighbor positive centers of the lattice. Hence, this exciton is described as a loosely bound exciton. In the atomic exciton model, excited states are described in terms of two coordinates, either "electron and hole" or "relative and translational" coordinates. This type of excited states is called Wannier excitons.[49]

Obviously, the molecular exciton is applicable to molecular crystals or Van der Waals aggregates of molecules, and is regarded as essentially atomic or molecular excitations in which the electron stays together with its hole, and both may jump from site to site. An electron and a hole may be bound together by their attractive coulomb interaction, just as an electron is bound to a proton in a neutral hydrogen atom. Here the molecular exciton is described as tightly bound exciton, since the wave function for the excited electron is bound closely to its molecular framework (positive center), with negligible electron exchange to neighboring molecules. The molecular exciton model is referred to as Davydov excitons (or Frenkel excitons),[50]

which have only translational degree of freedom. The bound electron-hole pair can move through the crystal and transport energy; it does not transport charge because it is electrically neutral. The argon crystal case chosen for study by Frenkel shows both the atomic and the molecular exciton spectral consequences, and is classified into mixed excitons.[51]

If a crystal has N atoms or molecules, Davydov exciton can take N states for a given type of atomic or molecular excitation, while Wannier excitons take N^2 states. Thus, when the relative motion is confined to a small region of atomic size, the former may be regarded as a limiting case of the latter. In order to apply the theory to optically excited aggregate systems, this dissertation will deal only with molecular excitons.

There are three theoretically different but somewhat parallel classifications of the molecular excitons. According to the rate of excitation transfer relative to the rate of lattice displacement as a result of excitation, Davydov classified the molecular excitons into free excitons and localized excitons.[50] By comparing the exciton band width with the spectral band width of the individual molecule, Simpson and Peterson proposed the criterion $2U/\Delta\varepsilon >> 1$ for their strong-coupling excitons and $2U/\Delta\varepsilon << 1$ for the weak-coupling criterion,[52] where 2U is the exciton band width and $\Delta\varepsilon$ is the spectral band width of the corresponding molecular electronic transition in the individual molecule. Thus, if the related spectral shift for the exciton states of a molecular aggregate is greater than the total electronic band width of the corresponding transition in the individual molecule, the strong coupling case prevails. These seem to be the most operationally practicable criteria for the strength of intermolecular electronic interaction between excited states relative to the strength of intramolecular vibrational-electronic coupling. Förster[53] suggested a slightly

modified designation of Simpson and Peterson's criteria to strong and medium in order to fit his energy transfer model into a common scheme with the exciton models. Later, in a revision of the earlier proposal, he then agreed to call the medium case the case of weak coupling; and his energy transfer model, the very weak coupling.[54] Of course, the intermediate coupling case is an important molecular exciton case, and comes between the extreme cases covered by the Simpson and Peterson criteria.

Accordingly, we summarize four theoretical coupling cases, in the molecular exciton or energy transfer theory. We shall examine the types of spectral effect which can be observed for the strong-coupling, intermediate-coupling, weak-coupling, and very-weak-coupling exciton cases.[48] When a pair of molecules are in excitation resonance, the electronic motions in one molecule are coupled to those in others and also internally coupled to the nuclear motions of the same molecule. If the electron-electron intermolecular coupling is much stronger than the intramolecular electron-nuclear coupling, energy transfer and delocalization take place independently of nuclear motion. This is the strong-coupling limit. Strong coupling requires the Born-Oppenheimer separability of intramolecular electronic and vibrational wave functions for a molecule.[52,55] Thus, the allowed excited electronic states of identical molecules in a molecular aggregate will interact, and the vibrational envelope will follow along. Figure 1.14 schematically illustrates the spectral effects for such a case. The upper curve shows a Franck-condon band envelope for a strong electric-dipole molecular electronic transition in a unit molecule. In a dimer, a splitting occurs in principle, although one of the components may be forbidden and not observable. However, in the dimer, the excitation is now distributed over both molecules, so the vibrational frequencies in the excited state will change. In the infinite linear polymer, a much larger exciton splitting will be observed, but the band

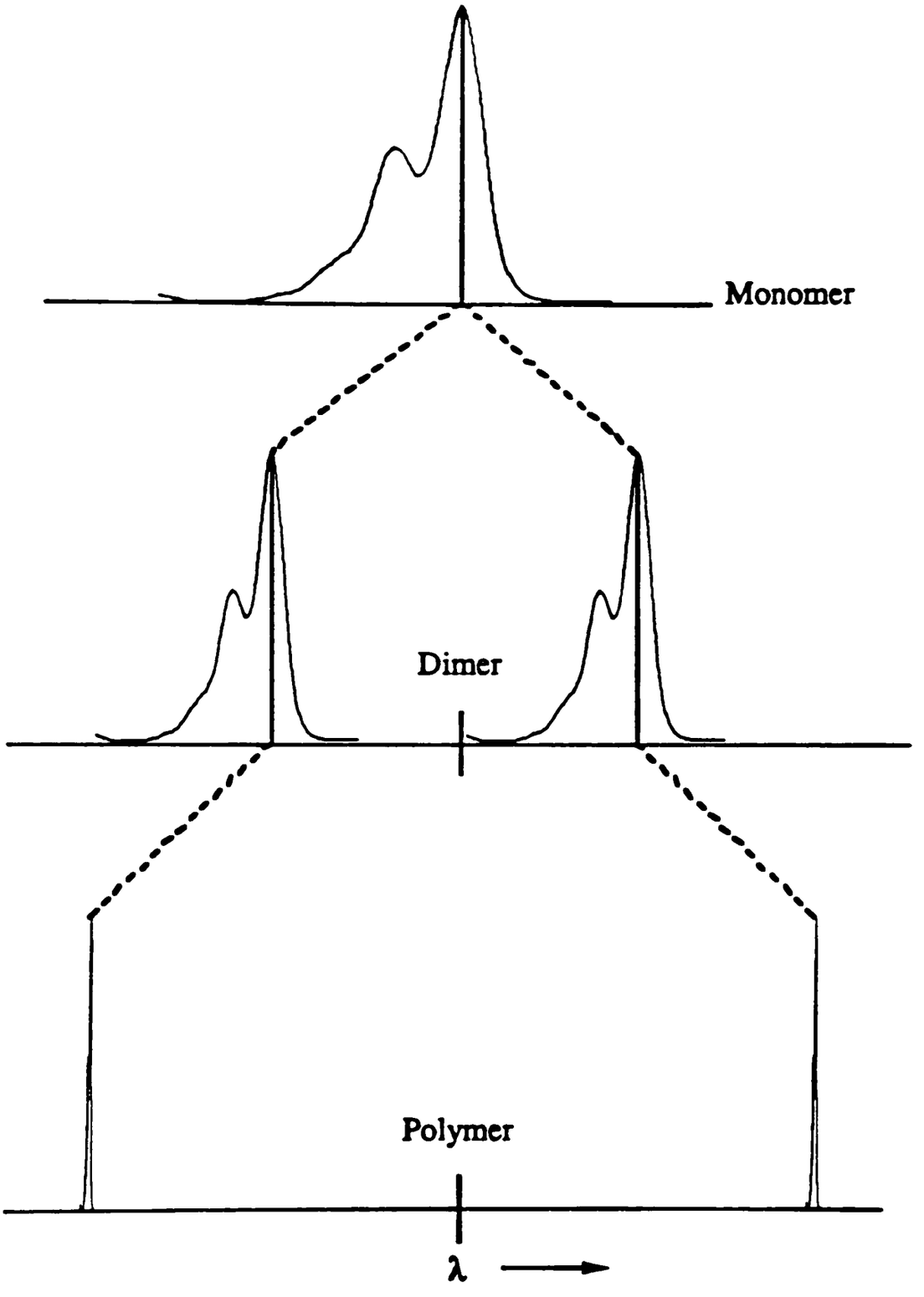

Figure 1.14. Spectral effects of the strong-coupling exciton.

width of the allowed components now becomes characteristically very narrow. The latter effect is caused by the fact that the excitation is now spread over many molecules, so that each molecule has approximately the same electronic structure as a ground-state molecule. In spectroscopic language, only the 0,0 or vibrationless electronic transition is now allowed by Franck-condon principle.[48] The actual geometry for a real case would modify the observed spectral components of the exciton band. Furthermore, the splitting would be symmetrical about the origin only for a molecule with no permanent dipole moment.

If, on the other hand, the coupling of the electrons in one molecule to those of another is sufficiently weaker than the intramolecular coupling to nuclear motion, the energy transfer is necessarily accompanied by a transfer of nuclear motion because the excitation is localized for long enough on one molecule to permit the nuclei to adopt a new motion for the changed electronic state.[56] This is the weak coupling limit. Weak coupling corresponds to the failure of Born-Oppenheimer separability of intramolecular electronic and vibrational wave functions for a molecule. In the limit of weak coupling, no spectral band shape change is observed, but instead second-order effects such as hypochromism or hyperchromism may be observed.

Intermediate coupling constitutes one of the difficult unsolved problems of exciton theory.[57,58] The electronic and vibrational wave functions are not separable, so that individual vibronic sub-bands interact according to their individual oscillator strengths (intensities). However, here the splitting of vibronic sub-bands degenerated in the molecular aggregate is comparable with the vibronic spacings in the original electronic transition for the individual molecule.

The interaction of light with matter that gives rise to resonance phenomena, such as electronic and vibrational absorption, can be related formally to the transition

dipole moment in the material. The absorption of light is directly proportional to the square of the electric dipole transition moment. The transition moment μ_{0a} is the dipole moment associated with the transition from ground state 0 to state a in the molecule. Its magnitude is easily determined from the area under an absorption curve, but its direction must be obtained from a study of oriented systems with polarized light. The transition moment is characteristic of the electronic structure of the molecule or group, therefore any change in bonding will in general change the spectrum. We would expect then that a polymer would have a different spectrum from the monomer.[59-62] The changes would be associated with the quantum mechanical interactions of electron exchange, overlap, etc., but coulombic forces would also contribute. The quantum mechanical overlap effects are very short range and primarily influence the groups directly bonded; therefore in certain polymers, the main interactions affecting the spectrum may be coulombic.[63] This hypothesis is strengthened by the observation of spectral changes with no concurrent change in primary chemical bonding. We shall ascribe the hypochromism in aggregates solely to the coulombic interaction between electrons in different bases. The leading term in the interaction is dipole-dipole and is the only one we will consider. If the group, i.e., their transition moments, are randomly oriented with respect to each other there is no net effect on the spectrum. However, if the aggregate contains colinear transition moments there will be an increase in absorption (hyperchromism), while parallel stacking of the moments will cause a decrease in absorption (hypochromism). The strength of the effect will depend on the cube of the distance between groups.[63]

We shall start by reviewing the theory of the splitting of the monomer levels upon formation of the dimer. It is assumed that the molecular planes of the dye

cations are parallel in the dimer, forming a sandwich structure.[9,64] Accordingly in the following discussion, only the sandwich structure will be considered. Two possible arrangements are shown in Figure 1.15. While not unique, it may be considered as a working model. As the notation tends to be confusing we shall give a summary of it first. The electronic wave functions of the monomers are ϕ while those of the dimer are Φ or ψ; subscripts u and v label the monomer, and the asterisk represents the wave function of the excited molecule. The starting point in the molecular exciton model treatment will be the singlet electronic energy states and their corresponding electronic state wave functions for a component molecule of the dimer. It is assumed that the electronic singlet state energies and wave functions are known, satisfying the individual molecule Schrödinger equation

$$H\phi = E\phi. \qquad (1)$$

The entire molecule in an electronic state is represented by ϕ_u, or ϕ_u^* for ground or excited singlet state wave functions, respectively, for molecule u. Both molecules of a dimer will be considered to be identical. We should now seek to construct correct zeroth-order wave functions for molecular aggregates in order to derive first-order energies for the electronic states of the dimer. The ground state wave function for a molecular dimer consisting of two identical molecules will be

$$\Phi_G = \phi_u\phi_v. \qquad (2)$$

It is totally symmetric with respect to all symmetry operations of the dimer. The first excited state wave functions of the dimer are degenerate and do not describe stationary states of the system. They can be described equally well by two possible wave functions

$$\Phi_1 = \phi_u\phi_v^* \qquad (3)$$

and

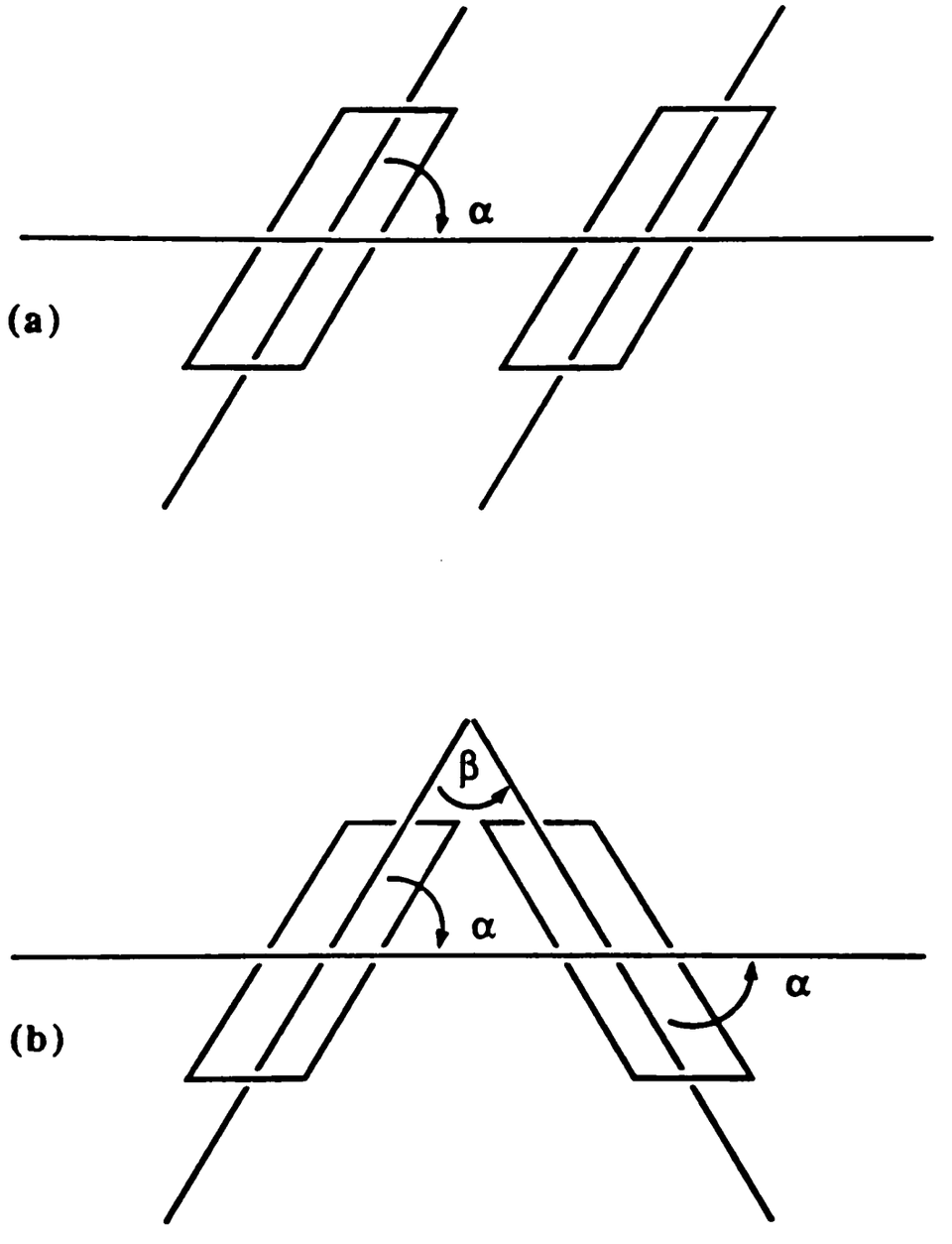

Figure 1.15. The sandwich structure arrangements of dimer.

$$\Phi_2 = \phi_u^* \phi_v. \tag{4}$$

The correct zeroth-order wave functions are

$$\psi_I = \frac{1}{\sqrt{2}}(\Phi_1 + \Phi_2) = \frac{1}{\sqrt{2}}(\phi_u \phi_v^* + \phi_u^* \phi_v) \tag{5}$$

and

$$\psi_{II} = \frac{1}{\sqrt{2}}(\Phi_1 - \Phi_2) = \frac{1}{\sqrt{2}}(\phi_u \phi_v^* - \phi_u^* \phi_v). \tag{6}$$

Interchange of molecular labels u, v indicates that the first function is totally symmetric and the second function is antisymmetric. In both of the stationary state exciton states ψ_I, ψ_{II}, the excitation is on both molecules, i.e., the excitation is collective or delocalized. The exciton states for a system of two nonrigid molecules is obtained through the use of perturbation theory. Thus the energy states and wave functions for a molecular dimer are determined by adding to the total Hamiltonian for the collection of unperturbed molecules a term V_{uv} where V_{uv} is the intermolecular interaction operator acting between molecules u and v. If two molecules are at a distance r from each other which is so large that there is no appreciable overlapping of their charge distributions, the classical potential energy of the system can be expressed as a series in inverse powers of r. In the case of two ions, this series would start with a term in 1/r; in the case of an ion and a neutral molecule, it would start with a term in $1/r^2$; since the neutral molecule has an instantaneous dipole moment whose potential is proportional to $1/r^2$; in the case of two neutral atoms, the only case to be considered here in more detail, the series starts with a term in $1/r^3$ (since the potential of two dipoles is proportional to $1/r^3$)[65], that is , we have

$$V_{uv} = -\frac{a}{r^3} + \frac{b}{r^4} + \frac{c}{r^5} \tag{7}$$

where

$$a = e^2 \sum_i \sum_j (2Z_u^i Z_v^j - X_u^i X_v^j - Y_u^i Y_v^j). \tag{8}$$

Here, in the classical dipole-dipole potential, X_u^i, Y_u^i, Z_u^i are the coordinates of the electrons of the molecule u and X_v^j, Y_v^j, Z_v^j those of the molecule v. The coordinate system being chosen with the z-axis parallel to the line of molecular centers, and the summation is over all electrons in each molecule. The constant b is cubic, the constant c quartic in the coordinates. While the first term in V_{uv} is due to dipole-dipole interaction, the second is due to dipole-quadrupole interaction, and the third to quadrupole-quadrupole interaction. Most of the present considerations will be concerned with the first term only. For allowed electric-dipole transitions, the dipole-dipole potential term becomes the leading one and higher multipoles are neglected. Moreover, in most cases, electron displacement along only one coordinate is affected by the light wave causing the excitation at a particular frequency, so that in general only one term in the dipole-dipole interaction may remain. For the excited state of an x-polarized transition in a dimer consisting of two molecules u and v, whose transition moments are both parallel to the x-axis, the perturbation potential reduces to

$$V_{uv} \approx \frac{e^2}{r^3}\Sigma_{i,j}(X_u^i X_v^j). \qquad (9)$$

In order to understand the spectral properties of such a molecular dimer, we must evaluate the excited state interaction energy to measure the exciton splitting, and the transition moment in order to determine the selection rules. In evaluating the excited state interaction energy, we shall examine merely the exciton splitting for simplicity. The energy of interaction will be given by the expectation value of the interaction potential with respect to the degenerate excited states of the dimer:

$$U = \iint \phi_u \phi_v^* V_{uv} \phi_u^* \phi_v d\tau_u d\tau_v. \qquad (10)$$

Inserting the form of V_{uv} appropriate to an x-polarized electric-dipole transition in molecules u and v,

$$U = \frac{e^2}{r^3}\int\int \phi_u\phi_v^*(\Sigma_{i,j}X_u^iX_v^j)\phi_u^*\phi_v d\tau_u d\tau_v. \qquad (11)$$

Because of the form of V_{uv}, equation may be factored to yield

$$U = \frac{1}{r^3}[\int \phi_u(\Sigma_i eX_u^i)\phi_u^* d\tau_u]\cdot[\int \phi_v^*(\Sigma_j eX_v^j)\phi_v d\tau_v]. \qquad (12)$$

We recognize immediately that each of the integrals is now precisely the transition moment integral for the excitation of the individual molecules u and v,

$$M_u = \int \phi_u(\Sigma_i eX_u^i)\phi_u^* d\tau_u. \qquad (13)$$

In order to make the totally symmetric exciton stationary state wave function correspond to a lowering of energy of the dimer excited state ψ_I is chosen to lie lower than ψ_{II}.[40] Accordingly, we have

$$M_u = - M_v. \qquad (14)$$

The expression for the energy lowering or interaction energy for the parallel dimer becomes

$$U = - \frac{M_u^2}{r^3}. \qquad (15)$$

The exciton band width will be twice this value or 2U. Thus we see that the energy lowering for the simple dimer case at hand is given by the monomer transition moment squared, i.e., is proportional to the probability or intensity of the electric dipole allowed transition in the monomer, divided by the intermolecular distance cubed. Thus, the stronger the absorption band, the greater will be the exciton band splitting. One observes also that the r-dependence makes this a comparatively long-range interaction. For a dimer with arbitrary mutual orientations of molecular axes with respect to an x, y, z coordinate frame, the energy of interaction is given by

$$U = -\frac{M_u^2}{r^3}(2\cos\alpha_u^z\cos\alpha_v^z - \cos\alpha_u^x\cos\alpha_v^x - \cos\alpha_u^y\cos\alpha_v^y) \qquad (16)$$

where again M_u represents the transition moment in a free molecule, and $\cos\alpha_u^z$, $\cos\alpha_u^y$, $\cos\alpha_u^x$ represent the cosines of the angles which the transition moment M_u for molecule u makes with the x, y, and z axes. Let us examine the spectral selection rules by evaluating the matrix elements of the electric dipole operator between the ground state and the stationary exciton states of the dimer. Thus, the transition moment vector of the dimer is given by

$$M^I = \iint\Psi_G(\mu_u + \mu_v)\Psi_I d\tau_u d\tau_v \qquad (17)$$

and

$$M^{II} = \iint\Psi_G(\mu_u + \mu_v)\Psi_{II} d\tau_u d\tau_v \qquad (18)$$

where μ_u,μ_v are the electric dipole operators corresponding to the molecular electronic coordinates of molecules u and v. Evaluating these, the two transition moments are

$$M^{I,II} = \frac{1}{\sqrt{2}}\iint\phi_u\phi_v(\mu_u + \mu_v)(\phi_u\phi_v^* \pm \phi_u^*\phi_v)d\tau_u d\tau_v. \qquad (19)$$

These lead to, because of orthogonality and normalization properties of the intramolecular state wave functions,

$$M^I = \frac{1}{\sqrt{2}}\int\phi_v\mu_v\phi_v^* d\tau_v + \frac{1}{\sqrt{2}}\int\phi_u\mu_u\phi_u^* d\tau_u \qquad (20)$$

or

$$M^I = \frac{1}{\sqrt{2}}(M_v + M_u). \qquad (21)$$

Similarly,

$$M^{II} = \frac{1}{\sqrt{2}}(M_v - M_u). \qquad (22)$$

Therefore, for the parallel dimer of Figure 1.15, the transition moments corresponding to the stationary exciton states are:

$$M^{I} = \frac{1}{\sqrt{2}}(M_v - M_v) = 0 \qquad (23)$$

and

$$M^{II} = \frac{1}{\sqrt{2}}(M_v + M_v) = \sqrt{2}\, M_v. \qquad (24)$$

Thus, the transition moments for the dimer are given as superpositions of the transition moments for the individual molecules.

Therefore, the simplest theoretical model to describe the interaction between aggregated molecules is exciton theory neglecting vibrations, leading to exciton bands and optical selection rules which allow electronic transitions to the lower or the upper exciton band edge depending on the relative orientation of the monomer units. The spectral shifts thus can be explained by exciton theory for linear aggregates. According to this theory, the lowest excited singlet level of the monomer is spread out upon N-fold aggregation into an N-fold band of levels. The frequency of the optically allowed transition in the aggregate is shifted from the monomer transition frequency by

$$U = 2\,\frac{1}{h}\,\frac{N-1}{N}\,\frac{\langle M^2\rangle}{r^3}\,(1 - 3\cos^2\alpha); \qquad (25)$$

where M is the transition dipole moment of the monomer, α is the angle between the transition dipole moment of a molecule in the aggregate and the long axis of the aggregate, r is the intermolecular seperation, and h is Planck's constant. A red-shifted band (the J-band) is predicted for $0^\circ < \alpha < 54^\circ 44'$ and a blue-shifted band (the H-band) for $54^\circ 44' < \alpha < 90^\circ$. The large spectral shifts in these aggregates thus may be described semiquantitatively by use of this one-dimension molecular exciton model.

The exciton band structure in linear molecular aggregates with various geometrical arrangements of transition dipoles is shown in Figure 1.16. By variation of the angle α between the aggregates axis and the molecules axises, one can go from a card-pack chain aggregates to a head-to-tail chain aggregates as α goes from 90° to 0°. For a red-shift J-band of our system, an α angle between 0° and 54.7° is expected.

While in the past much of the work on aggregates was aimed at understanding the spectroscopy in terms of an excitonic model, recently the focus has changed to comprehend the dynamical properties of aggregates due to the advent of picosecond optical spectroscopy. In this work, we focus our attention on the optical dynamics of aggregates of the molecule PIC.

The large spectral shifts in these aggregates may be described semiquantitatively by use of the molecular exciton model. The N-fold degenerate excited states of N dye molecules are split into N separated sublevels when the aggregate is formed, but the transition intensity accumulates in the longest wavelength transition for an α angle less than 54.7° or in the shortest wavelength transition for α angles greater than this value.

1.4. Exciton Dynamics

When several excitons are created simultaneously in a given domain, bimolecular exciton-exciton annihilation processes are possible.[66-69] It is assumed that excitons in different domains cannot interact with each other. When the initial exciton density is not too large (less than 1 exciton per 10 pigment molecules, for instance), the simultaneous encounter and annihilation of more than 2 excitons at one time is considered to be negligible.[67] It is now generally accepted that bimolecular

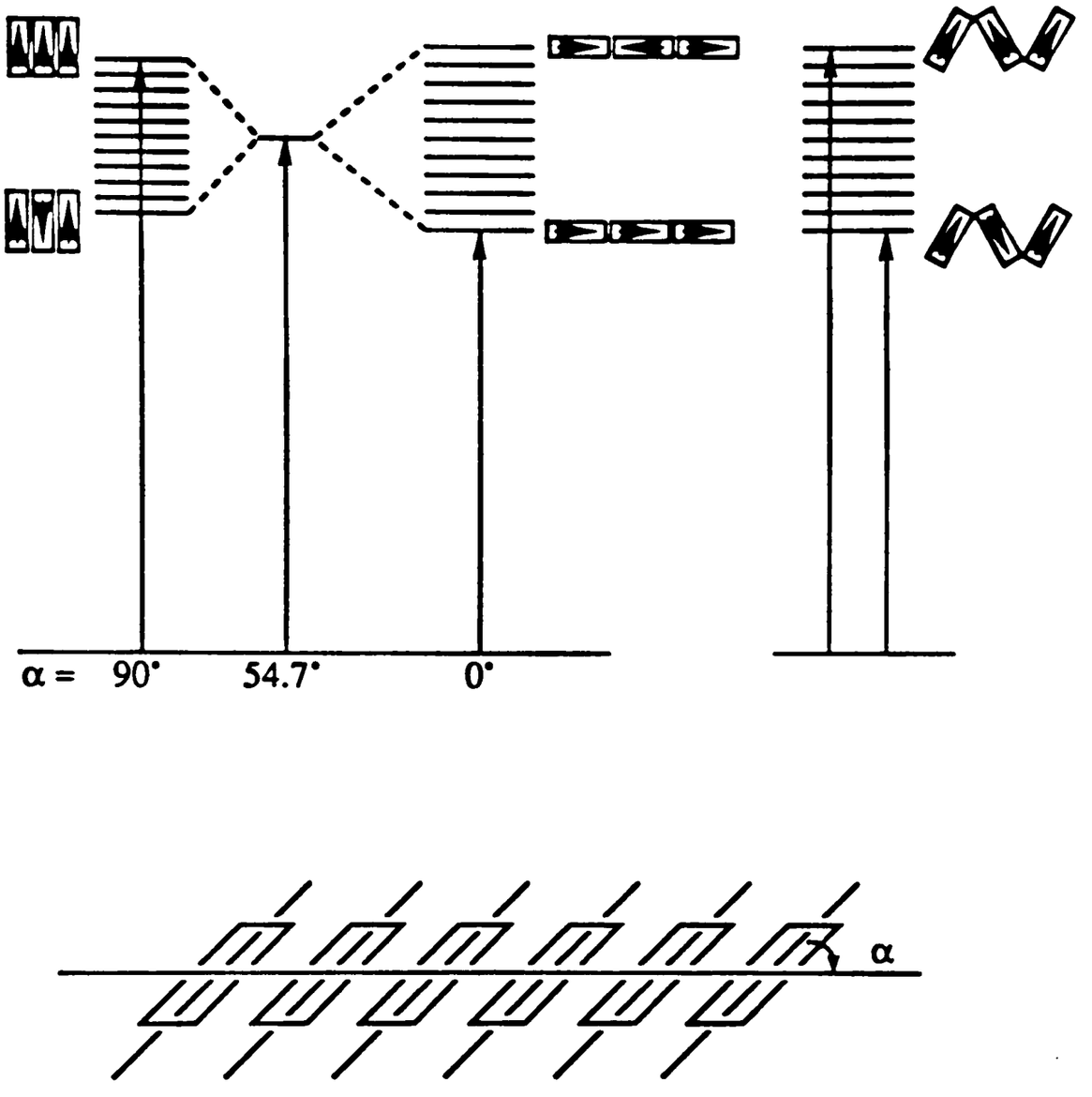

Figure 1.16. The exciton band structures for linear chain polymer.

exciton interactions occur in photosynthetic membranes when intense laser excitation sources are employed. When a single picosecond laser pulse is used for excitation of the fluorescence, singlet-singlet exciton annihilation is dominant. However, when a pulse sequence or microsecond duration excitation pulses are employed, annihilation of singlet excitons by triplet excitons is important. Experimentally, exciton annihilation manifests itself by a decrease in the lifetime of the fluorescence and by a decrease in the integrated quantum yield of fluorescence, ϕ, as the intensity I of the excitation is increased. When picosecond pulses are used for excitation, the major bimolecular exciton deactivation process is believed to be singlet-singlet annihilation. Singlet-triplet annihilation does not play an important role.[69] Singlet-singlet exciton annihilation may lead to the disappearance of either one or both excitons:

$$S_1 + S_1 \text{ -- } \gamma_{ss} \text{ --> } S_1 + S_0 \qquad (26)$$

or

$$S_1 + S_1 \text{ -- } \gamma \text{ --> } \begin{cases} S_0 + S_0 \\ T_1 + S_0 \\ T_1 + T_1 \end{cases} \qquad (27)$$

where T_1 represents the lowest triplet state, and $\gamma^{(1)}$ and $\gamma^{(2)}$ denote the appropriate bimolecular rate constants.[67] For our purposes, the relative probabilities of the three different channels in equation (27) need not be considered. The equation governing the singlet exciton population and including singlet-singlet exciton annihilation is the second order rate law[70,71]

$$\frac{dN_{ex}}{dt} = -\frac{N_{ex}}{\tau_{ex}} - \frac{\gamma_{ss}}{2}N_{ex}^2 \qquad (28)$$

where N_{ex} is the exciton population in an aggregate, τ_{ex} is the exciton lifetime and γ_{ss} is the singlet-singlet exciton annihilation rate constant.[43] Integration of equation (28) leads to the following expression :

$$\tau_{ex}\ln\left(\frac{\frac{1}{\tau_{ex}}+\frac{\gamma_{ss}}{2}N_{ex}(t)}{-N_{ex}(t)}\right)=t+C \qquad (29)$$

where

$$C=\tau_{ex}\ln\left(\frac{\frac{1}{\tau_{ex}}+\frac{\gamma_{ss}}{2}N_0}{-N_0}\right). \qquad (30)$$

The expression for the exciton population can be written as

$$N_{ex}(t)=\frac{\frac{2}{\tau_{ex}\gamma_{ss}}}{\left(\frac{2}{\tau_{ex}\gamma_{ss}N_0}+1\right)\exp\left(\frac{t}{\tau_{ex}}\right)-1} \qquad (31)$$

where N_0 is the initial exciton density, which is proportional to the excitation intensity. This equation can be simplified to give

$$K(t)=\frac{A}{B\exp\left(\frac{t}{\tau_{ex}}\right)-1} \qquad (32)$$

where A is a normalization constant and B is defined by

$$B=\frac{2}{\tau_{ex}\gamma_{ex}N_0}+1. \qquad (33)$$

Equation (32) was used to fit our data for J-aggregates in 5 M NaCl solution.

This dissertation consists of two major parts. The first study involves picosecond spectroscopies of three different J-aggregate systems of PIC, whereas the other study concerns the steady state absorption spectra of 1,1'-diethyl-2,2'-carbocyanine chloride (DCC) dimers.

In Chapter II of this dissertation, we apply picosecond pump-probe method to study electronic energy relaxation in molecular aggregates of PIC. Our goal is to understand exciton properties of the systems by using picosecond pump-probe spectroscopy. At the start, this chapter describes the experimental apparatus in detail together with the preparation of samples (2.1). The data obtained by the

experimental methods and methods of data analysis are also presented (2.2). The results of the different systems are compared and discussed (2.3). The results are discussed in terms of the dynamics of delocalized and localized excitons. Briefly, the transient photobleaching signals at 570 nm for J-aggregates of PIC on colloidal silica are independent of the laser excitation intensity and can be well fitted by a biexponential decay function consisting of short and long components. The absorption anisotropy for these J-aggregates is constant. In contrast, the transient photobleaching signals for J-aggregates in concentrated aqueous solutions of NaCl and on PVS decayed faster as the excitation intensities is increased. They decay nonexponentially at high laser excitation intensities but exponentially at very low excitation intensities. The absorption anisotropy decays for these J-aggregates. The picosecond polarized pump-probe experiments substantiate the view point that the excitation transfer involves delocalized excitons in J-aggregates on colloidal silica and localized excitons in J-aggregates in NaCl solution. Transient bleaching signals for pseudoisocyanine on PVS were measured at four different wavelengths. The results suggested that there exist densely spaced excited states which were strongly absorbing.

In Chapter III, we investigate the aggregation of two DCC monomeric units. The mutual orientation of the two molecules in the dimer is derived from the experimental results. This chapter is presented in the same logical order of experimental (3.1), results (3.2), and discussion (3.3). In short, absorption spectra of DCC in water as function of concentration are obtained at a fixed temperature by using a double-beam spectrometer. All measured spectra are digitized and stored in a microcomputer. Several computer programs (as listed in the appendix) written by the author are used to do the analysis. The true dimer spectrum is extracted from the

composite spectra. As has been found with other dyes,[72-75] the dimer shows two absorption maxima. The geometry structure of the dimer is determined by.the informations obtained from deconvolution of the dimer spectrum into two component bands. The results give a distance of 10 Å between the two monomers and an angle of 72° between the transition moments of the monomer units in the dimer. Knowing the arrangements of the transition dipoles, it seems advisable to study electronic energy relaxation in the dimer by using picosecond pump-probe spectroscopy.

The final chapter (IV) of this dissertation concludes with recommendations for future experiments.

CHAPTER II

PICOSECOND SPECTROSCOPY OF J-AGGREGATES

2.1. Experimental

2.1.1. Sample Preparation

PIC(Cl) (1,1'-diethyl-2,2'-cyanine chloride, Exciton), PIC(Br) (1,1'-diethyl-2,2'-cyanine Bromide, Exciton), PIC(I) (1,1'-diethyl-2,2'-cyanine Iodide, 99%, Kodak), DCC(Cl) (Pinacyanol Chloride, 98%, Kodak), DDC(I) (1,1'-diethyl-2,2'-dicarbocyanine Iodide, 99%, Kodak), colloidal silica (Nalco 1115, Lot No. 7K825 and Lot No. B8K828), were used without further purification. Absorption spectra were obtained on a Shimadzu UV-265 spectrometer at room temperature 21 ± 0.5 °C. Cuvette lengths of 0.1 and 1.0 cm were used according to the molar extinction coefficients of the dyes.

The stock solution of colloidal silica was a 15% (w/v) aqueous suspension at pH 10.4. The average particle size in this polydispersed suspension was 4 ± 1 nm. There are 60-65 binding sites on each colloid particle. Samples of PIC in colloidal silica were made by diluting 0.5 mL of a 0.01 M methanol solution of PIC(I) with 49.5 mL of deionized water and 50 mL of the colloidal silica stock solution. Centrifugation of aliquots of this sample at 64,000 g for 15 h and spectrophotometry of the supernatant revealed that most of the dye is adsorbed on the colloid particles.

Samples of PIC(I) in salt solution were made by mixing 0.5 mL of 0.01 M PIC in methanol with 99.5 mL of 5 M NaCl.

PVS was purified and fractionated by the Breslow and Kutner method.[76] Briefly, 25% polymer solution from Polyscience (Polysciences, Lot # 94950) was

purified by two precipitations with methanol. Seventy percent methanol by weight was used for each precipitation. When two sharply defined layers have formed in a separatory funnel, the lower precipitated oil layer was collected and separated as completely as possible. The methanol was removed under reduced pressure on a rotary evaporator at 60°C. The polymer was generally dried under vacuum at 110°C overnight, and the yield was about 52%. The polymer appeared to be hydrated by contact with atmospheric moisture; therefore, it should either be stored in a desiccator or in a bottle with a plug seal.

The product was used to make up 0.26, 0.43, 0.72, 1.2 and 2.0 % in 0.1 molar sodium sulfate solutions, and the intrinsic viscosities were determined. Briefly, a routine viscometer of size 100 (Industrial Research Glassware LTD) was used to measure the viscosities of the solutions. Calibration Factor B of the viscometer is given by the following equation.

$$B = 1.5887 \times 10^{-2} - 1.1667 \times 10^{-6}T \qquad (34)$$

where T is the temperature of the bath in °C. The coefficient of viscosity η of a fluid is given as

$$\eta \text{ (in centistokes)} = Bt \qquad (35)$$

where t is the efflux time in seconds. The specific viscosity η_{sp} of a fluid is related to the viscosity η_0 of the pure fluid (solvent) by the expression

$$\eta_{sp} = \frac{\eta}{\eta_0} - 1 \qquad (36)$$

The intrinsic viscosity $[\eta]$ is defined as the ratio of the specific viscosity to the weight concentration of solute, in the limit of zero concentration

$$[\eta] = \lim_{c \to 0} \frac{\eta_{sp}}{c} \qquad (37)$$

where c is usually defined as the concentration in grams of solute per 100 ml of solution. Plot η_{sp}/c versus c and extrapolate linearly to $c = 0$ to obtain $[\eta]$ for the polymer. The molecular weight of the polymer was determined by relating the intrinsic viscosities to the weight-average molecular weights as determined by light-scattering measurements. The results are shown in Tables 2.1 and 2.2 and Figure 2.1. The unpurified PVS sample was prepared by adding 1.6 ml 25% polymer solution (density = 1.26 g/ml) to 98.4 ml 102 μM PIC(Cl) solution. The stock solution of purified PVS polymer was a 0.05 g/dL aqueous solution. Samples of PIC(Cl) on purified PVS polymer were made by adding 1mL 0.05 g/dL purified PVS polymer stock solution to 99.0 mL of 42.4 μM PIC(Cl) aqueous solution. The absorption spectrum of PVS solution showed a red-shifted J-band at 563.4 nm.

2.1.2. Pump-probe Configuration

Time-resolved spectroscopy provides a powerful technique for investigating electronic properties in physical, chemical, and biological systems. The simplest type of time-resolved pump-probe configuration is one in which both pump and probe pulses are derived from the same laser pulse, that is, they have the same wavelength. A strong pump pulse is used to bleach a ground-state absorption, and a weak delayed replica of the pump pulse is used to monitor the decay of the bleaching. The return of molecules to the ground state can be followed by the change in transmission of a weak probe pulse through the sample as a function of time delay after the arrival of the strong pump pulse. The change in probe beam intensity is too small to see for this type of ground-state recovery experiment. The lock-in amplifier (LIA or phase-sensitive detector) offers a solution to these problems. This method of increasing sensitivity in applications of CW mode-locked lasers is to use a modulator

Table 2.1. Data of the weight-average molecular weight for the purified PVS polymer.

Measurements / Samples	Efflux time (second)	η_{sp} / C, dℓ/g	Intrinsic Viscosity = 3.6786e-2
0.1 M Na_2SO_4	62.56	———	
0.26 g/dl PVS in 0.1M Na_2SO_4	63.10	0.0331819	
0.43 g/dl PVS in 0.1M Na_2SO_4	63.64	0.0398183	
0.72 g/dl PVS in 0.1M Na_2SO_4	64.58	0.0446850	Weight-Average molecular weight 9671.2
1.20 g/dl PVS in 0.1M Na_2SO_4	65.62	0.0406147	
2.01 g/dl PVS in 0.1M Na_2SO_4	68.02	0.0434816	

Table 2.2. Data of the weight-average molecular weight for the unpurified PVS polymer.

Measurements / Samples	Efflux time (second)	η_{sp} / C, dℓ/g	Intrinsic Viscosity = $1.8426e^{-2}$
0.1 M Na_2SO_4	62.56	———	Weight-Average molecular weight 5012.3
0.26 g/dl PVS in 0.1M Na_2SO_4	62.78	0.0134955	
0.43 g/dl PVS in 0.1M Na_2SO_4	63.28	0.0265005	
0.72 g/dl PVS in 0.1M Na_2SO_4	63.64	0.0238506	
1.20 g/dl PVS in 0.1M Na_2SO_4	64.58	0.0267657	
2.01 g/dl PVS in 0.1M Na_2SO_4	66.16	0.0286207	

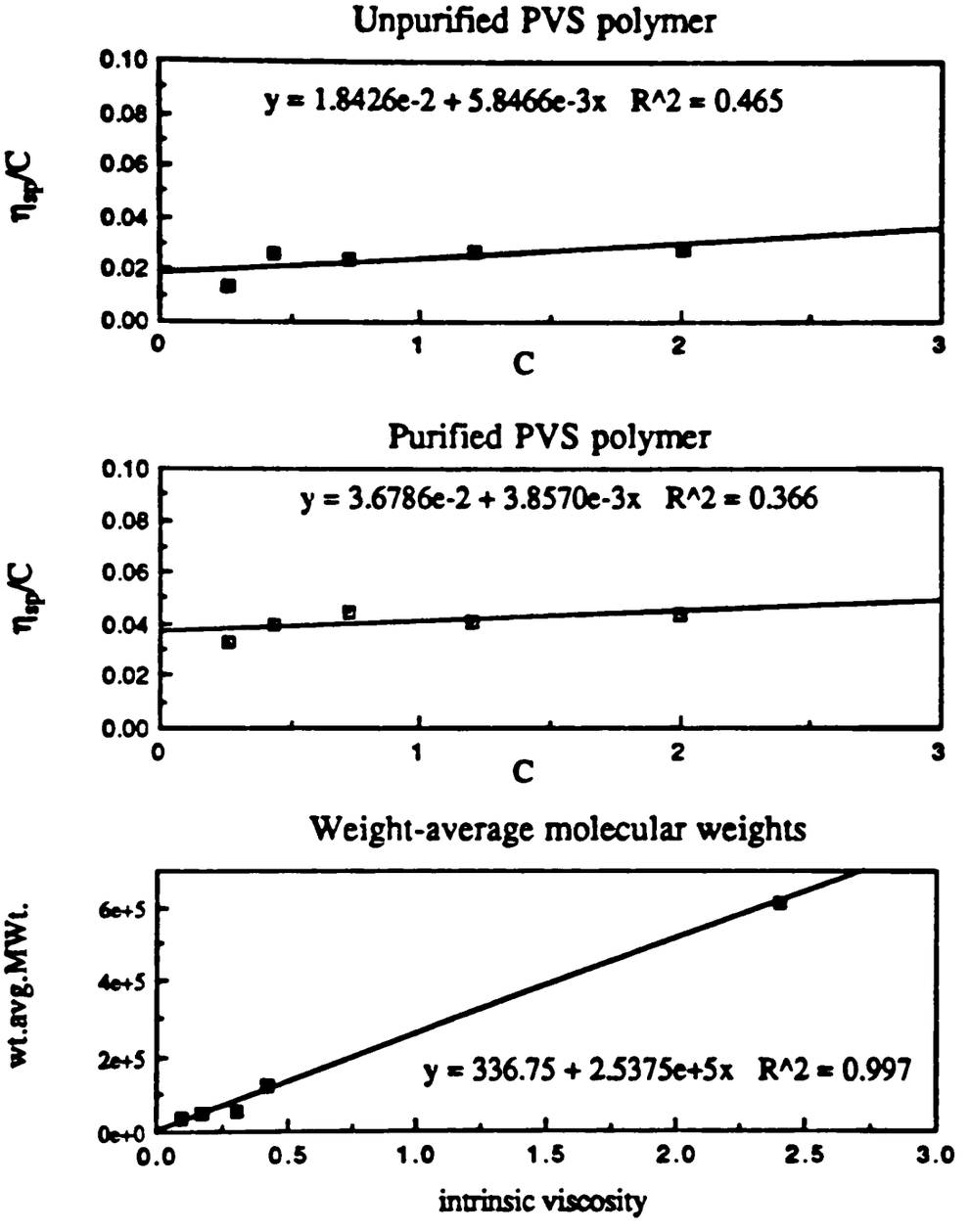

Figure 2.1. The results of our intrinsic viscosities measurements and the weight-average molecular weights determined by Breslow et. al..

(or beam chopper) and a lock-in amplifier. The modulator imposes a frequency modulation on the intensity of laser beam reaching the sample; the frequency of modulation is generally in the kilohertz or megahertz region depending on the nature of the application. The lock-in amplifier is fed two signals; one is a reference signal from the modulator, and the other is a response signal from a detector monitoring the sample. The job of the lock-in amplifier is then to selectively amplify only components of the response signal which oscillate at the same frequency as the reference signal. To minimize low-frequency noise, the pump beam is modulated and the component of the probe beam at the pump modulation is detected. The result is a very effective discrimination against noise, and hence a large increase in the signal-to-noise ratio. The dynamic range can be improved to as much as 10^7 by electronically pre-filtering the input to discriminate against noise frequencies away from the frequency of interest.[77] The time resolution of pump-probe spectroscopy is determined by the shortness of the laser pulses used in the measurement. The molecular orientational contribution can be studied directly by making measurements of the ground-state recovery with the probe beam polarized first parallel and then perpendicular to the pump beam. If isotropic decay due to ground-state recovery is desired, the probe beam should have a polarization of 54.7° with respect to that of the pump beam.

The optical arrangement is illustrated in Figure 2.2. The pump laser, a mode-locked argon ion laser (mode locked Coherent Supergraphite CR-12 SG), was operated at 514.5 nm and used to pump synchronously a Rhodamine 110 dye laser (Coherent Model 700). Mode locked operation of the ion laser was achieved with the use of a Coherent 467 SEM Frequency Synthesizing Mode Locker. The mode locker head, driven by the 38-MHz resonance frequency from the mode locker synthesizer

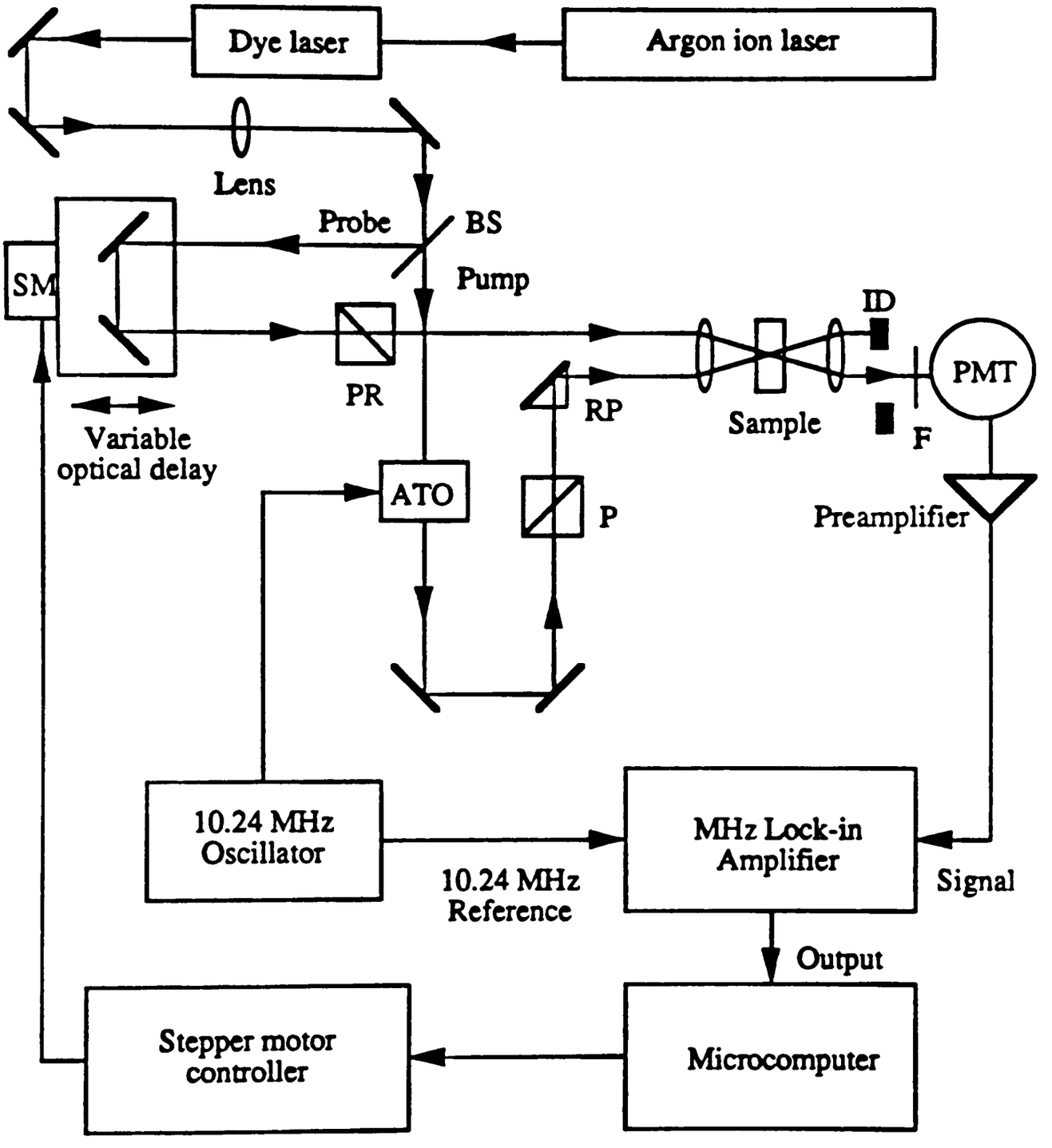

Figure 2.2. Block diagram for pump-probe apparatus.

driver, acted like a repetitive shutter in front of the high reflector mirror. This caused the laser output to become a continuous train of optical pulses; the pulse width was 200 picoseconds and the pulse repetition rate was 76 MHz. The delay arm within the dye laser matched the cavity length of the dye laser to the cavity length of the ion laser, thereby enabling synchronous pumping. Because it was synchronously pumped, the dye laser delivered a pulse train with a pulse width of 7 picoseconds. A continuous pulse train of these pulses was delivered. The wavelength of the dye laser output depended on the dye used and the birefringent filter tuning element of the dye laser. The dye laser was tuned to 570 nm or 560 nm, near the absorption maximum of the J-band. Continuous-wave (CW) [or continuous pulse train] autocorrelation measurements of picosecond pulses was obtained by using an audio loudspeaker driven at 30 Hz in one arm of the correlator to permit autocorrelation display at this frequency. The laser beam was split into a pump beam and a probe beam by a pellicle beam splitter (BS) with a reflectivity of 8%. The resulting pump beam was then directed into a Matsushita ELF-M120 acoustooptic modulators (ATO) operating with approximate modulation depth of 60-80% at 10.24 MHz. The probe beam was subjected to a variable delay consisting of two mirrors mounted on a computer-controlled translation stage. The probe pulse delay corresponded to 2.0 ps/step. The polarization of the probe beam with respect to the pump beam was produced by passing the probe beam through a polarization rotator (PR). Noncolinear, copropagating pump and probe beams were made by reflecting the pump beam through a roof top prism (RTP). The beams were focused with a 10-cm focal length achromat to a spot size of $\approx$ 300 μm in a sample contained in a rotating 3.1-mm pathlength cell. The average incident laser powers of the pump and probe beams at the sample were 25.5 and 7.5 mW, respectively. After the pump beam was

blocked with a iris diaphragm (ID), the probe beam passed through neutral density filters and an interference filter at the wavelength of the laser and was detected with a photodiode. Noise sources were largely eliminated by using a low-noise preamplifier (Trontech W50ATC, 0.01-50 MHz, 50dB, NF = 1.5dB).[78] The output from the preamplifier was fed into an EG&G megahertz lock-in amplifier (LIA). The analog output of the LIA was digitized and stored in a Apple IIe microcomputer. Raw signals were transferred to a DEC VAX 11/730 minicomputer for data analysis. The background-free second-order autocorrelation of the pulse was determined by replacing the sample with a potassium dihydrogen phosphate (KDP) crystal and measuring the second harmonic generation (SHG) signal as a function of the probe delay with a phtomultiplier tube (PMT). Optimum autocorrelation measurements were made by using standard chopping techniques. The vertically polarized probe beam was chopped at ≈1 KHz, and the modulated SHG signal was detected with a kilohertz LIA. The maximum of the autocorrelation was used to establish the position of zero delay. The measurements were carried out at room temperature (21°C ± 1).

In ground-state recovery experiments, a polarized pump pulse initially creates an anisotropic distribution of excited molecular aggregates whose transition dipoles are mainly aligned along the polarization of the pump light. Molecular rotation and energy transfer will cause this anisotropic distribution to decay to a uniform distribution. The subsequent transmission of probe light through such a system will differ for polarization parallel or perpendicular to that of the pump light. Hence, the time dependence of the depolarization is described by the absorption anisotropy r(t). The time-dependent bleaching signals $S_{//}(t)$, $S_{\perp}(t)$, and $S_{54.7}(t)$ obtained with the

probe light polarized parallel, perpendicular, and 54.7° to the polarization of the pump beam are governed by the following functions

$$S_{//}(t) = [1 + 2r(t)]K(t) \quad (38)$$

$$S_{\perp}(t) = [1 - r(t)]K(t) \quad (39)$$

$$S_{54.7}(t) = K(t) \quad (40)$$

where K(t) is the isotropic decay component of ground-state recovery decay law. Hence, the isotropic curve is given by

$$S_{is}(t) = \frac{S_{//}(t) + 2S_{\perp}(t)}{3}. \quad (41)$$

In principle, the signal at the magic angle of 54.7° should equal to the isotropic curve. The absorption anisotropy r(t) is easily calculated:

$$r(t) = \frac{S_{//}(t) - S_{\perp}(t)}{S_{//}(t) + 2S_{\perp}(t)} \quad (42)$$

In the same wavelength pump-probe experiments, both pulses are derived from the same pulse show an unexpected peaking or sharp spike at zero delay. This sharp coherent spike results from the diffraction of pump photons into the beam direction. This artifact is always present in pump-probe measurements with coherent pump and probe beams having the same frequency. Straightforward deconvolution over the entire decay range can lead to an inaccurate description of the signal due to the coherent spike at zero delay. In order to correct for the coherent coupling artifact, the antisymmetrization procedure of Engh et al.[79] was used. Briefly, for noncollinear copropagating beams, the observed signal as a function of delay time τ can be written as

$$S(\tau) = \beta(\tau) + \gamma(\tau). \quad (43)$$

$\beta(\tau)$ is the coherent contribution to the signal and is symmetric with respect to delay. For times long compared to the dephasing time,[80] $\gamma(\tau)$ is given by the convolution of

the molecular response R(t) with the second-order pulse intensity autocorrelation G(t). Forming the antisymmetrized function

$$S_a(\tau) = \frac{1}{2}[S(\tau) - S(-\tau)] = \frac{1}{2}[\gamma(\tau) - \gamma(-\tau)] \quad (44)$$

removes the coherent coupling artifact. The antisymmetrized signal can be expressed as

$$S_a(\tau) = \int_{-\infty}^{\infty} G(t')R_a(t' + \tau)dt', \quad (45)$$

where $R^a(t)$ is the antisymmetrized response function

$$R_a(t) = (1/2)[R_i(t) - R_i(-t)]. \quad (46)$$

Because of the low signal-to-noise ratio, it was difficult to distinguish between different model decay functions. The signals were therefore simply fit to single exponentials. For a single exponential response function, $R^a(t)$ is simply given by

$$R_a(t) = -A\exp(t/\tau), \; t < 0 \quad (47)$$

$$= A\exp(-t/\tau), \; t \geq 0. \quad (48)$$

To obtain the decay time τ, transient bleaching signals were antisymmetrized about zero delay time. The antisymmetrized signals were fit to the convolution of the pulse autocorrelation with the antisymmetrized response function. For a highly nonexponential transient bleaching curve, the signal was antisymmetrized about $\tau = 0$ and fitted to the convolution of the pulse autocorrelation with the antisymmetrized form of the biexponential decay function

$$R_i(t) = A_1\exp(-t/\tau_1) + A_2\exp(-t/\tau_2). \quad (49)$$

The fitting was done with a nonlinear convolute-and-compare analysis using a Marquardt-Levenberg algorithm which minimized the sum of the squares of the residuals by varying the parameters of response function.[81,82]

The fluorescence decay was measured with standard time-correlated single photon counting (TCSPC) techniques using excitation from a synchronously pumped Rhodamine 6G dye laser, which was cavity-dumped to yield an interpulse spacing of ≈ 78 ns. The details of the apparatus have been previously described.[83,84] The solutions were excited at 566 nm and fluorescence was collected with a lens at right angles to the excitation and passed through a double monochromator set at 580 nm to a multichannel plate photomultiplier. The power in the excitation beam was less than 1 mW.

2.2. Results

The experimental results cover four different systems. There are J-aggregates of PIC on colloidal silica, in 5 M sodium chloride solution and on PVS polymer, and DCC dimers. Both colloidal silica and PVS polymer consist of two types of sample. These will be treated separately below.

2.2.1. Colloidal Silica

Transparent colloidal dispersions are convenient systems in which to apply a variety of spectroscopic techniques in order to study molecular interactions at surfaces.[85] Colloids are well-suited for spectroscopic studies because the small particle dimensions help to minimize light scattering, the large surface-to-volume ratio enhances the optical detectability of surface interactions, and they can be readily prepared or are commercially available. Colloidal silica was chosen because surface interactions can be studied in the absence of either surface-enhanced optical effects[86] or electron transfer between adsorbed molecules and the colloid.[87,88] The physical properties of colloidal silica have been well-documented,[89] and there have been a number of photochemical studies on colloidal silica during the past several

years.[90,91] At pH > 6, the silanol groups on the surface are ionized. Cationic organic molecules, such as PIC, will bind very strongly to the negatively charged surface of colloidal silica, principally through electrostatic attraction. Because the adsorbed molecules cannot penetrate the solid silica surface, these molecules face a water environment. Rather than dispersing uniformly on the silica surface as in anionic micelles, the adsorbed cationic dye molecules tend to cluster.[92] Although this property is undesirable when studying isolated adsorbed molecules, it is advantageous when studying aggregates of organic molecules on surfaces.

PIC aggregates prepared from different lot numbers of colloidal silica yield different J-band spectra. Since the colloidal silica of lot number B7K825 and B6M821 were received prior to lot number B8K828 and give the same spectra, the formers are labeled as sample F and the latter is labeled as sample L. These two samples are treated separately below.

2.2.1.1. Sample F

The absorption spectra of PIC at a concentration of 50 μM in water with and without 7.5% colloidal silica are shown in Figure 2.3. It is very clear that the presence of adjacent binding sites on these colloids facilitates aggregation at this low dye concentration. The J-band is located at 570 nm, which is red shifted from the monomer band at 523 nm. Absorption linewidth of the J-band $\Delta\nu_{1/2}(J)$ as a function of aggregate size N which are coherently coupled is given by[10,93]

$$\frac{\Delta\nu_{1/2}(M)}{\Delta\nu_{1/2}(J)} = \sqrt{N} \qquad (50)$$

where $\Delta\nu_{1/2}(M)$ is the bandwidth of the monomer. Simulations of the absorption bandwidths show that the full width at half maximum (FWHM) are approximately 1222 cm^{-1} for M-band and 411 cm^{-1} for J-band, respectively [Figures 2.4, 2.5].

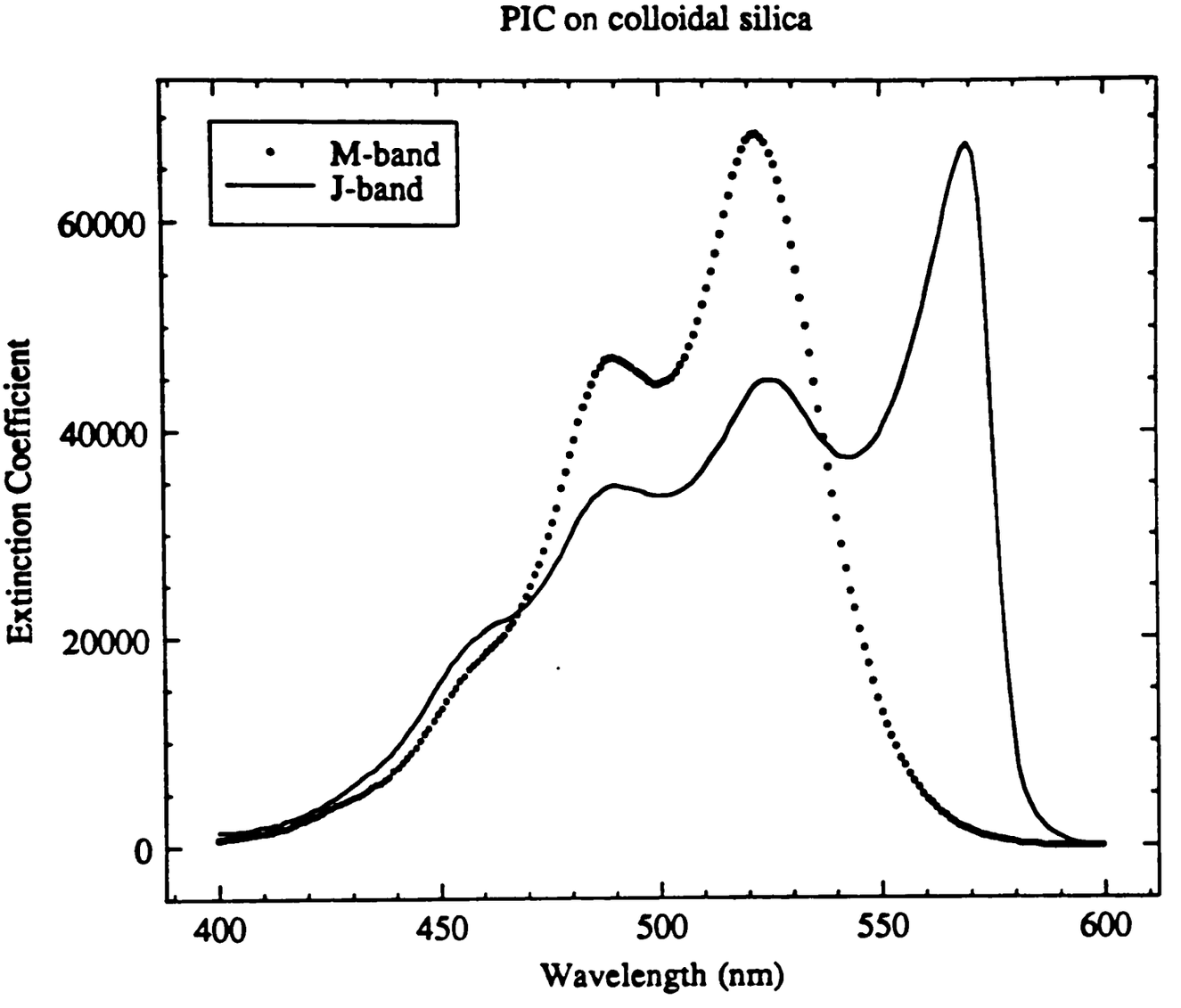

Figure 2.3. The absorption spectra of 50 mM PIC(I) in water with and without 7.5% colloidal silica (sample F).

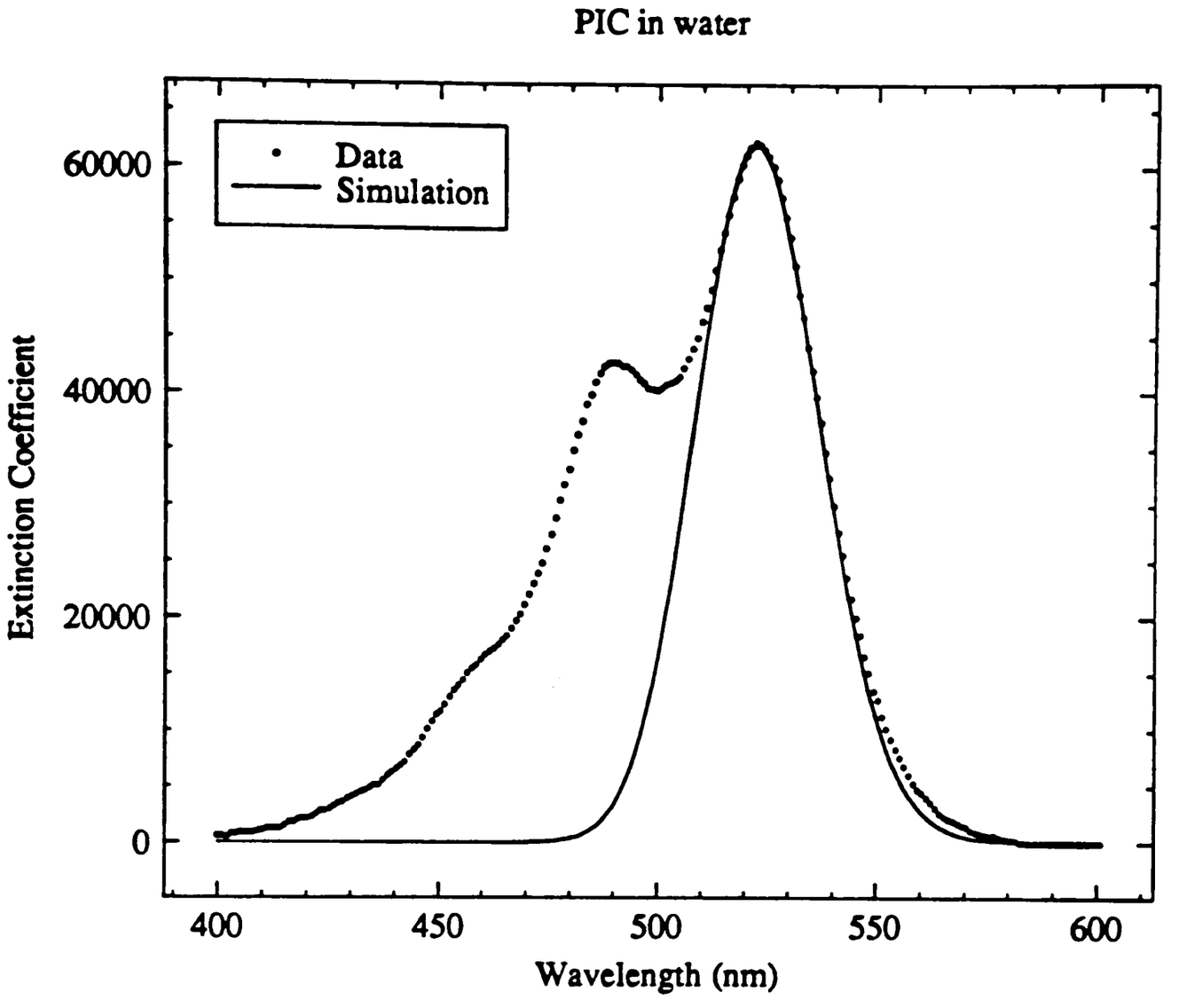

Figure 2.4. The absorption linewidth of PIC M-band (sample F).

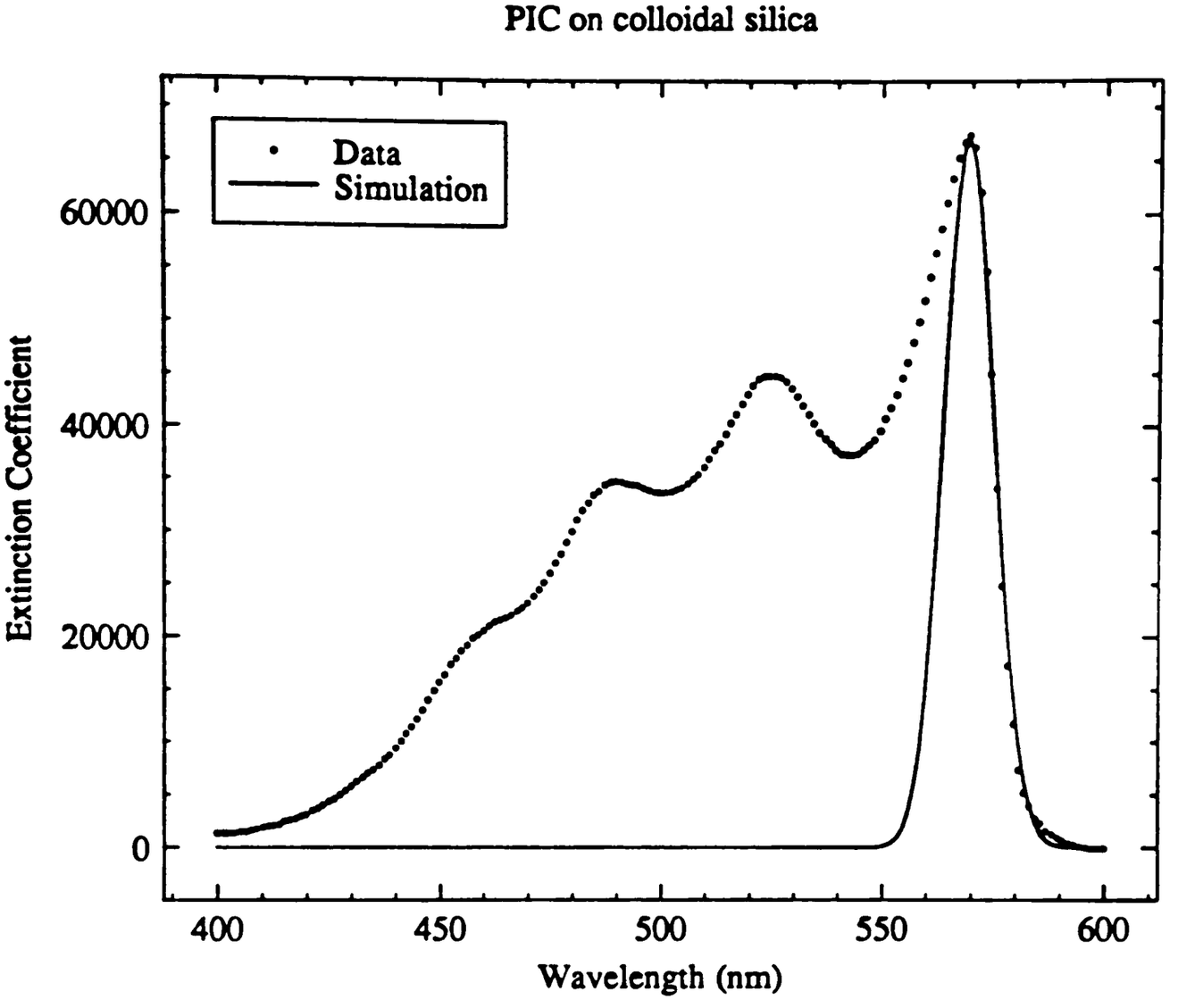

Figure 2.5. The absorption linewidth of PIC J-band (sample F).

The result suggests that an average aggregate size of 9 monomer units are coherently coupled in the system. It needs to be emphasized that no method exists so far for precisely determining the size N of a given J-aggregate, and that the value of N determined above is only approximate. The bandwidth of adsorbed species can be inhomogeneously broadened due to a distribution of aggregate size.[94-96]

Typical transient bleaching signals for J-aggregates on colloidal silica are shown in Figure 2.6. The curves $S_{//}(t)$, $S_{54.7}(t)$, and $S_{\perp}(t)$ are obtained, respectively, with probe beam polarized parallel, 54.7°, and perpendicular to the polarization of the pump beam at 570 nm. Experimentally, the isotropic component of the ground-state recovery can be obtained from $S_{//}(t)$ and $S_{\perp}(t)$ without taking the signal at the magic angle of 54.7°; however, the comparison between the signal taken at the magic angle and the isotropic curve calculated from $S_{//}(t)$ and $S_{\perp}(t)$ does provide a way of checking the goodness of experimental data. The calculated isotropic curve and the signal at the magic angle of 54.7° are shown in Figure 2.7. The curves isotropic and 54.7° are equal to each other within experimental error. Hence, these measurements are valid for analysis.

The decay of these signals appeared to be highly nonexponential. Part of the nonexponential behavior is caused by the coherent coupling artifact, which is a distortion around zero time delay. In order to extract the true decay behavior, we used the method of antisymmetrization to remove the coherent coupling artifact before fitting the data. The fits of the antisymmetrized form of $S_{//}(t)$, $S_{54.7}(t)$, and $S_{\perp}(t)$ to antisymmetrized biexponential over the delay range indicated are shown in Figures 2.8, 2.9, and 2.10. The fitting parameters obtained for the transient bleaching signals in Figure 2.6 are listed in Table 2.3. The $S_{//}(t)$ signal exhibits a dominant short component with a decay time of 23.9 ps and a long component with a

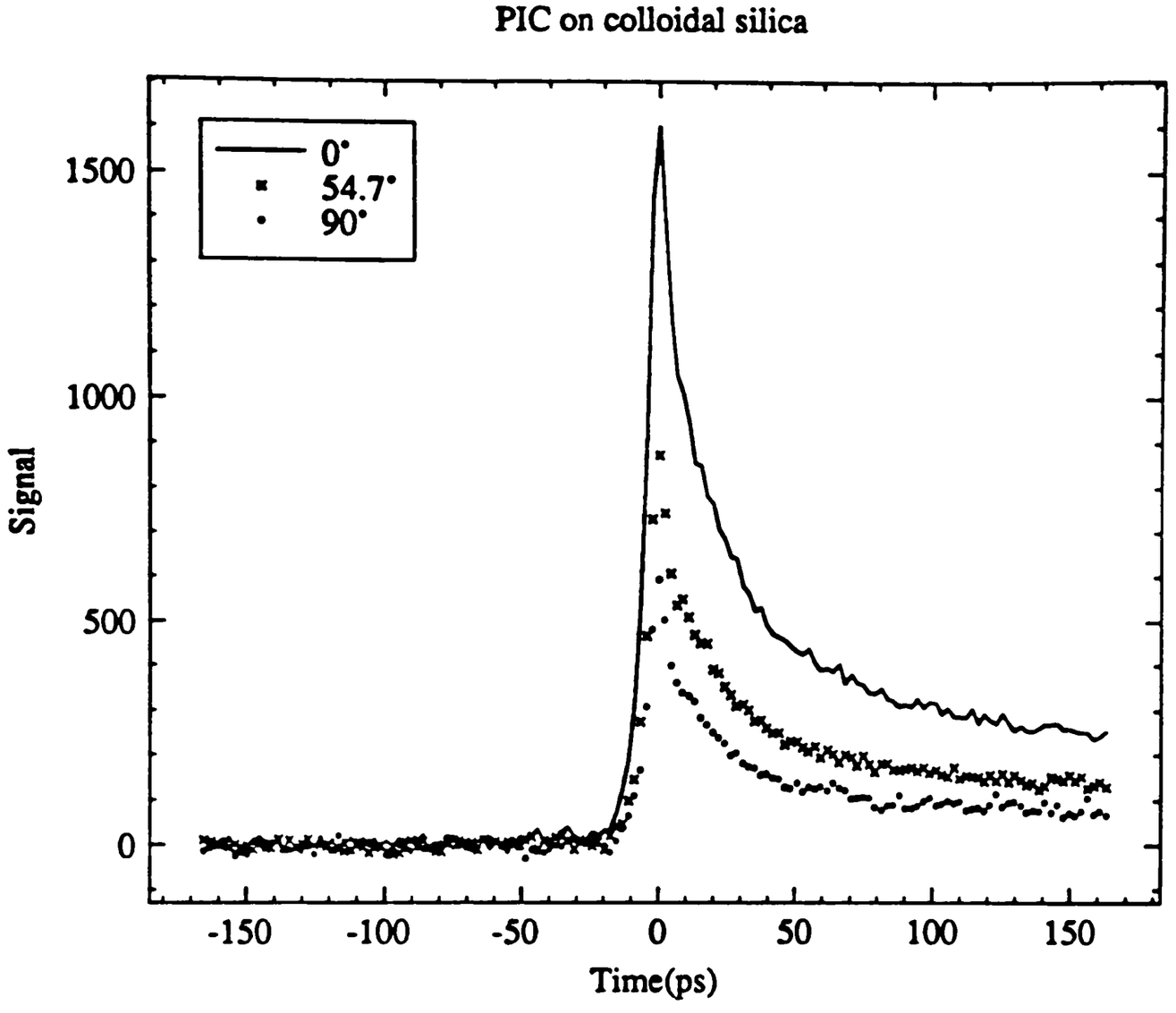

Figure 2.6. Transient bleaching signals for J-aggregates on colloidal silica at 570 nm (sample F).

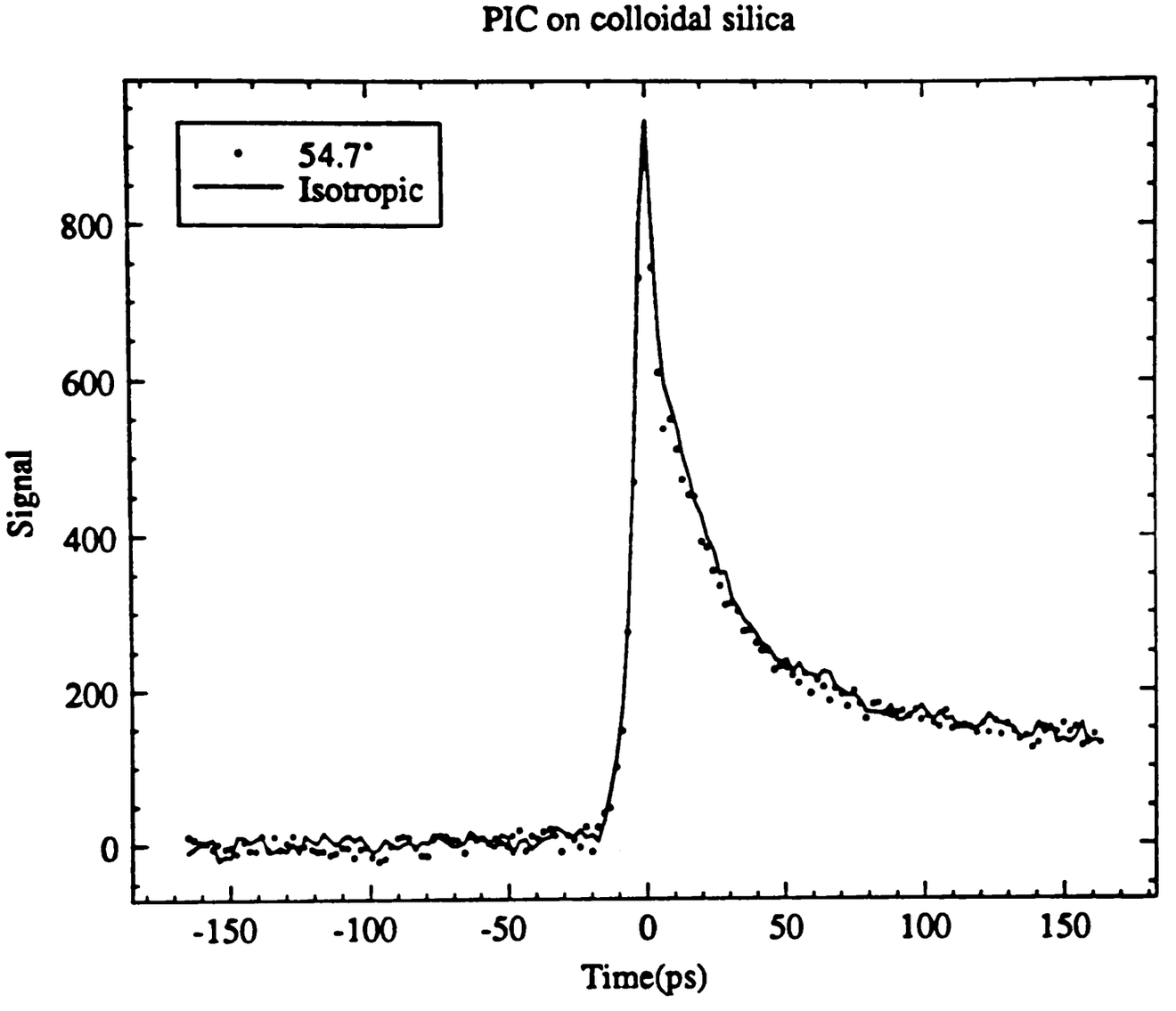

Figure 2.7. The curves isotropic and magic angle of sample F.

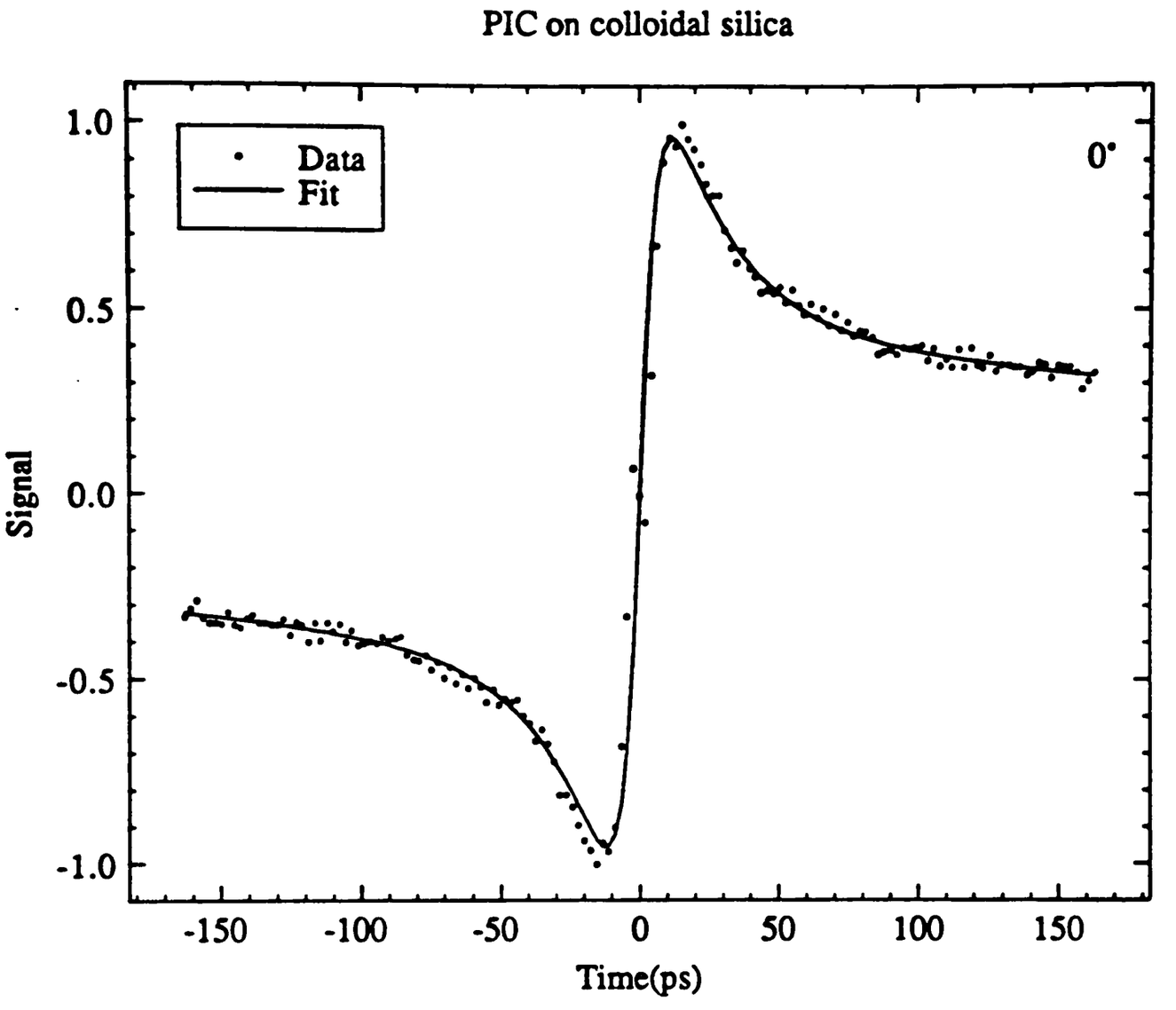

Figure 2.8. Antisymmetrized parallel signal from Figure 2.6 (points) and the convolution of the pulse autocorrelation with an antisymmetrized form of eq 49 (solid curve). See Table 2.3 for fitting parameters.

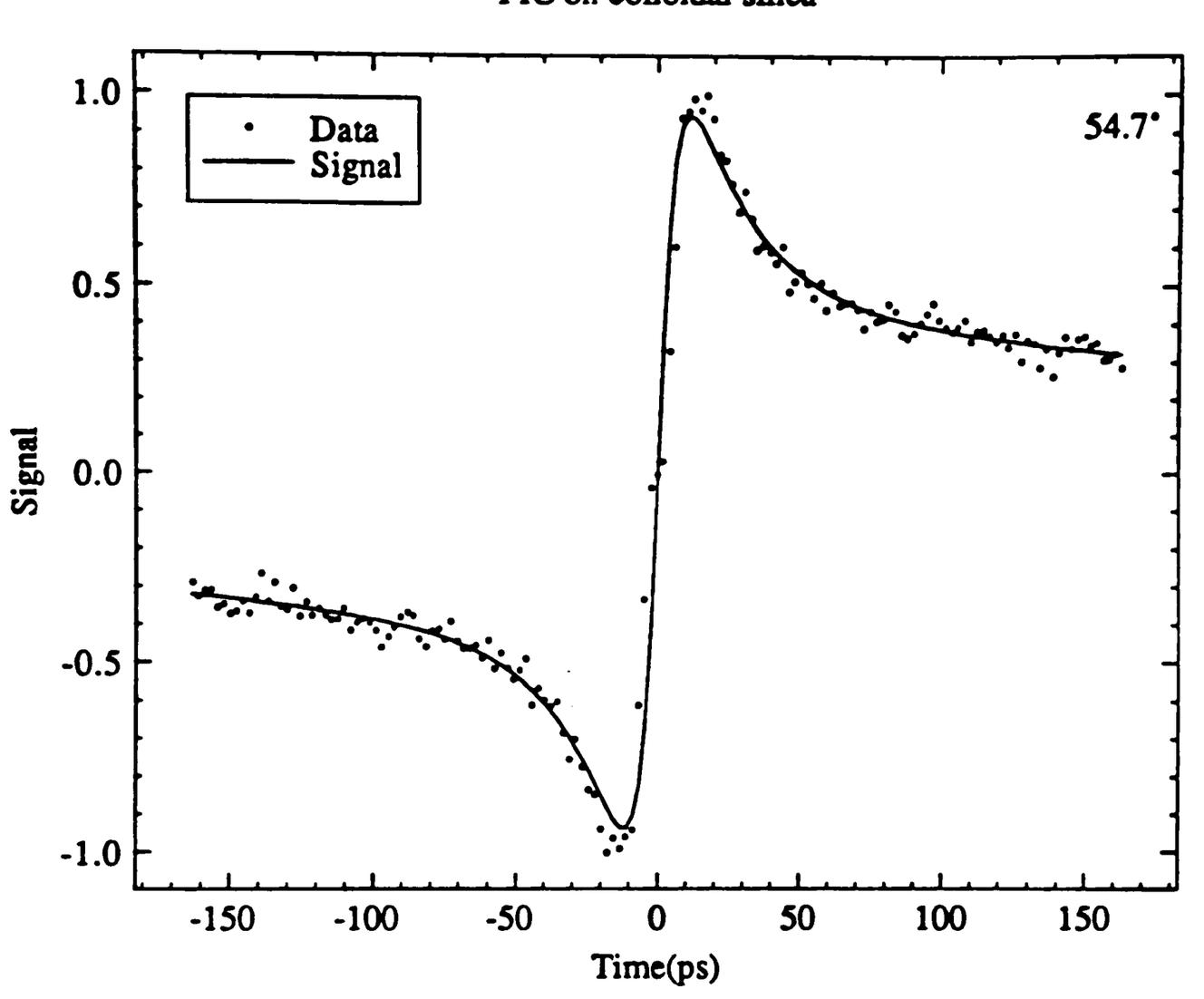

Figure 2.9. Antisymmetrized magic angle signal from Figure 2.6 (points) and the convolution of the pulse autocorrelation with an antisymmetrized form of eq 49 (solid curve). See Table 2.3 for fitting parameters..

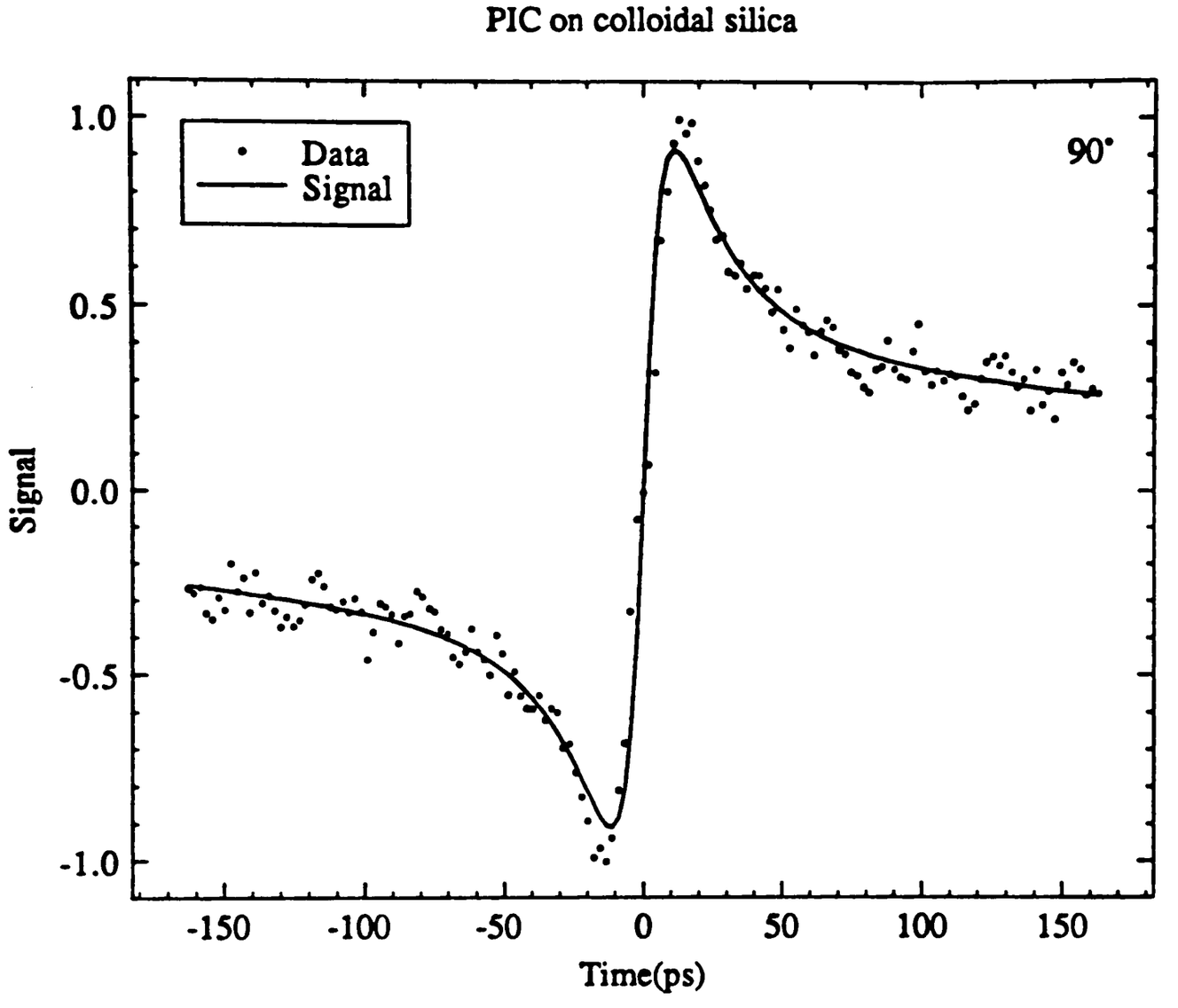

Figure 2.10. Antisymmetrized perpendicular signal from Figure 2.6 (points) and the convolution of the pulse autocorrelation with an antisymmetrized form of eq 49 (solid curve). See Table 2.3 for fitting parameters..

Table 2.3. Biexponential fitting parameters for the polarized transient bleaching signals in Figure 2.6.

Parameters / Signals	A_1	τ_1, ps	A_2	τ_2, ps	χ^2
Parallel	0.66	23.94	0.34	335.91	5.5×10^{-3}
Magic angle	0.66	22.40	0.34	336.43	5.0×10^{-3}
Perpendicular	0.66	20.75	0.34	334.31	5.6×10^{-3}

decay time of 336 ps. A comparison of parameters obtained in the biexponential fits reveals that the transient bleaching signals were independent of the polarization of the probe light. Using the following equation for the average relaxation time,[95]

$$<\tau> = \frac{A_1\tau_1^2 + A_2\tau_2^2}{A_1\tau_1 + A_2\tau_2}, \qquad (51)$$

we find that $S_{//}(t)$, $S_{\perp}(t)$, and $S_{54.7}(t)$ are characterized by similar average relaxation time: 298, 301, and 300 picoseconds, respectively.

Figure 2.11 compares a magic angle signal with one obtained with the laser intensity halved. The excellent overlap between the two curves indicates that the transient bleaching signals varied linearly with the laser intensity. Antisymmetrization analysis of the signal obtained with the laser intensity halved yielded a biexponential function, $R_i(t) = 0.7\exp(-t/26.0\text{ ps}) + 0.3\exp(-t/382\text{ ps})$, with $\chi^2 = 2.2 \times 10^{-3}$ and an average relaxation time of 330 ps. The biexponential parameters in this fit are similar to those in Table 2.3.

Plot of the anisotropy versus time for J-aggregates on colloidal silica is shown in Figure 2.12. Absorption anisotropy r(t) are calculated from Equation (42) using the signals in Figure 2.6. Despite the uncertainty near zero delay due to the presence of the coherent coupling artifact, the decay of anisotropy was not noticeable. For $0 < t < 160$ ps considerable residural anisotropy appeared. The value of this anisotropy is equal to 0.42 ± 0.04. $S_{//}(t)$, $S_{\perp}(t)$, $S_{54.7}(t)$; therefore, differ by only multiplicative constants and have the same decay behavior because of the constancy of the anisotropy in this time range.

2.2.1.2. Sample L

The spectra of sample L are different than those of sample F and have their maximum absorption at 567nm [Figure 2.13]. The monomer band is not as evident

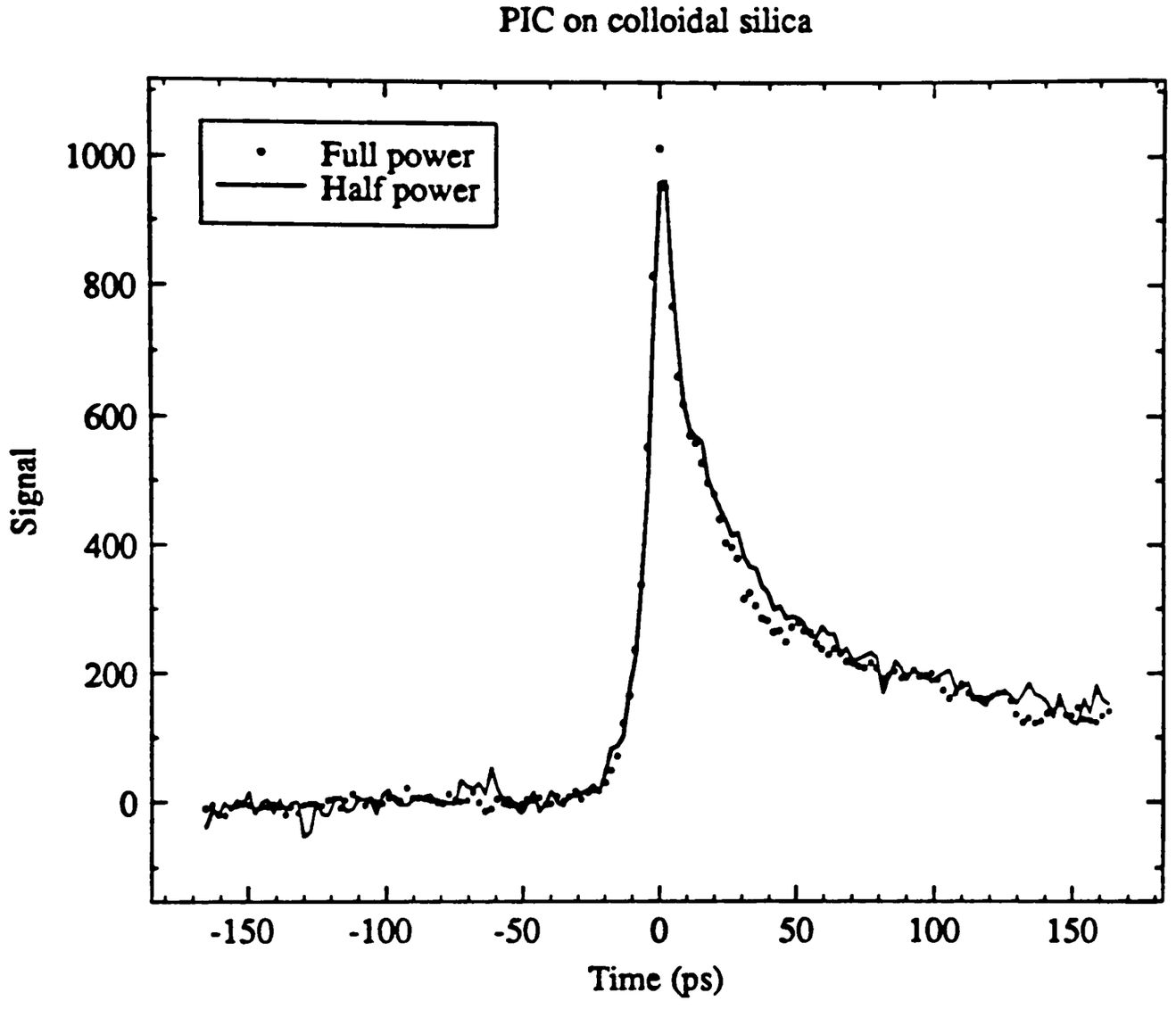

Figure 2.11. Comparison of a magic angle curve (points) and one obtained with the laser intensity halved (solid curve). The magic angle curve obtained with the laser intensity halved has been multiplied by a factor of 2.

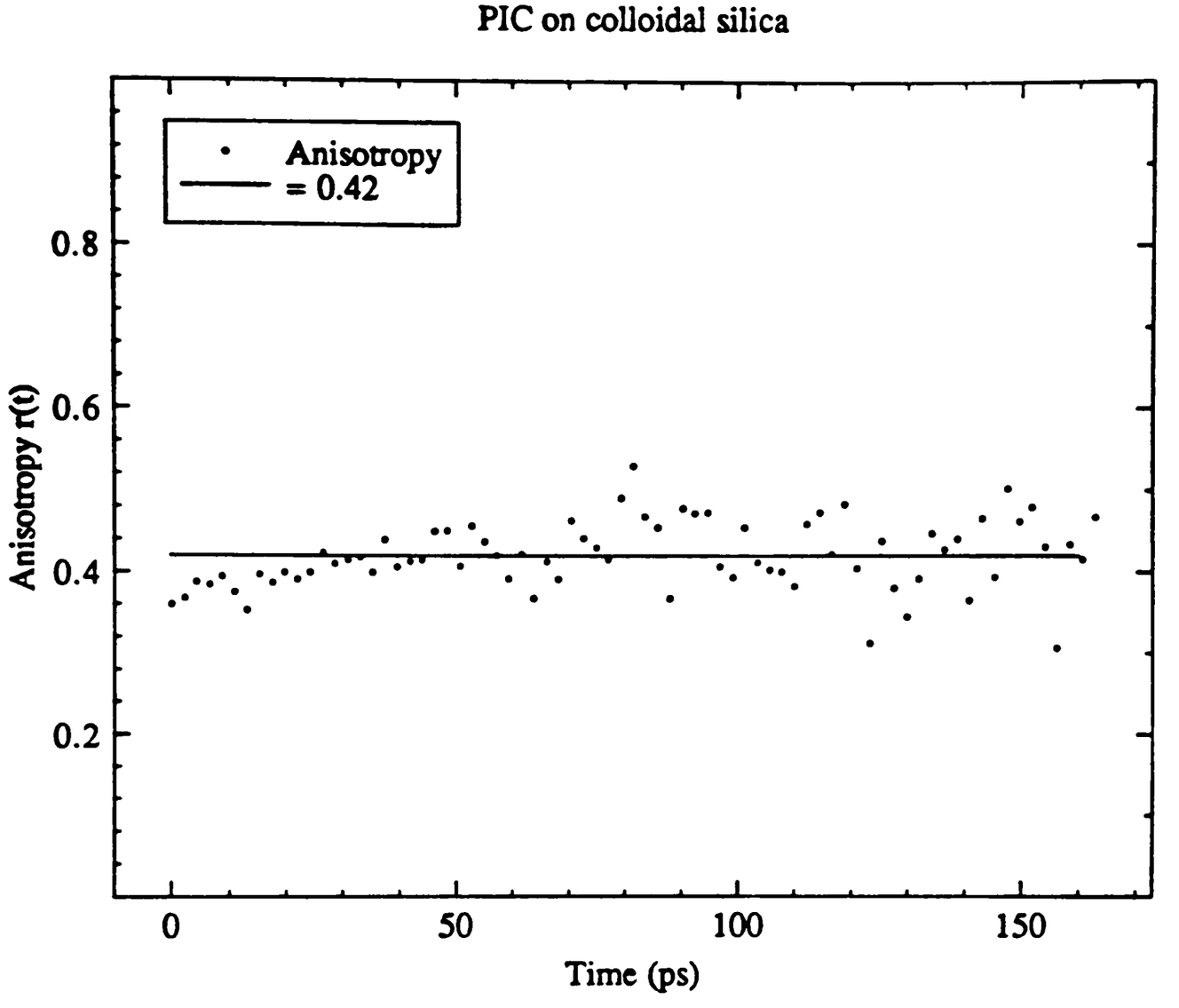

Figure 2.12. Absorption anisotropy r(t) calculated from eq 42 using the signals in Figure 2.6. The straight line corresponds to an average anisotropy of 0.42.

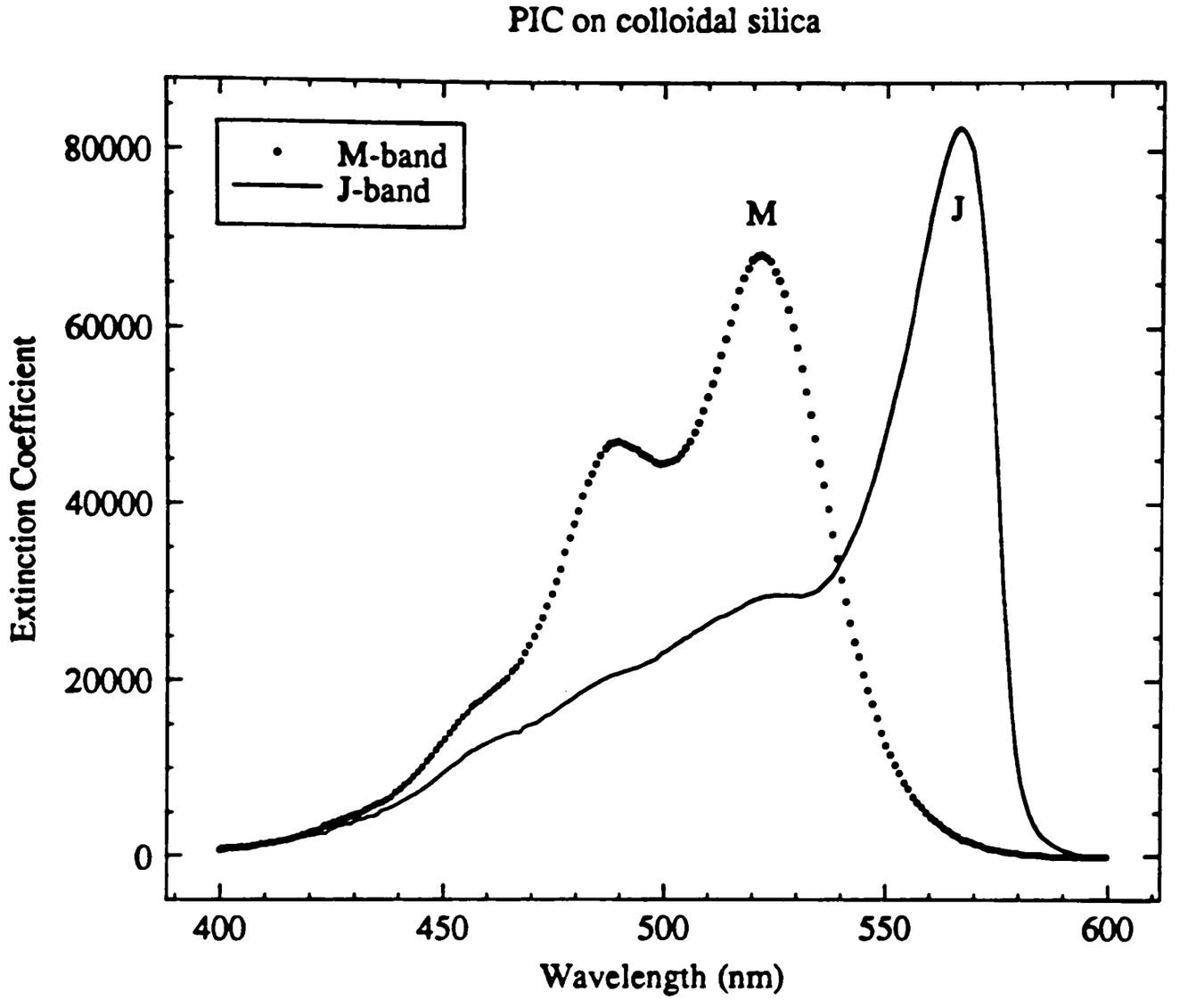

Figure 2.13. The absorption spectra of 50 mM PIC(I) in water with and without 7.5% colloidal silica (sample L).

in these spectra as in the former ones. An analysis of the linewidth shows that the FWHM is about 503 cm^{-1} for the J-band [Figure 2.14], which is also different from that of sample F. The result suggests that an average aggregate size of 6 monomer units are coherently coupled in the system.

Typical transient bleaching signals for this system are shown in Figure 2.15. The curves are $S_{//}(t)$, $S_{54.7}(t)$, and $S_{\perp}(t)$ signals obtained at 570 nm. The calculated isotropic curve and the signal at the magic angle of 54.7° are shown in Figure 2.16. The curves isotropic and 54.7° are equal to each other within experimental error.

Reducing the excitation intensity by a factor of two, Figure 2.17 compares a magic angle signal with one obtained with the laser intensity halved. These signals have been normalized. The excellent overlap between the two curves indicates that the transient bleaching signals varied linearly with the laser intensity.

Excited singlet-state decay gives rise to fluorescence, whereas both excited singlet-state and triplet-state decays can contribute to transient photobleaching. Clearly, the time dependence of the fluorescence should be different than the time dependence of transient photobleaching for these J-aggregates if triplet-state decays. Transition-metal ions shorten triplet-state lifetimes[97-100] and bind strongly to colloidal silica.[89] If the long component in the transient photobleaching signal is due to the triplet state, it should exhibit a faster decay in presence of adsorbed transition-metal ions. Transient photobleaching signals for zero, 1.0 x 10^{-3} M Cu^{+2}, and 1.0 x 10^{-3} M Co^{+2} are shown in Figure 2.18. The signals have been normalized at the peak of the coherent coupling artifact. The antisymmetrized form of $S_{//}(t)$ in Figure 2.18 and fit to the antisymmetrized form of the biexponential decay function are shown in Figure 2.19. Different runs resulted in similar values for the decay times. The average decay times were τ_1 equal to 20 ± 2 picosecond and τ_2 equal to 250 ± 32

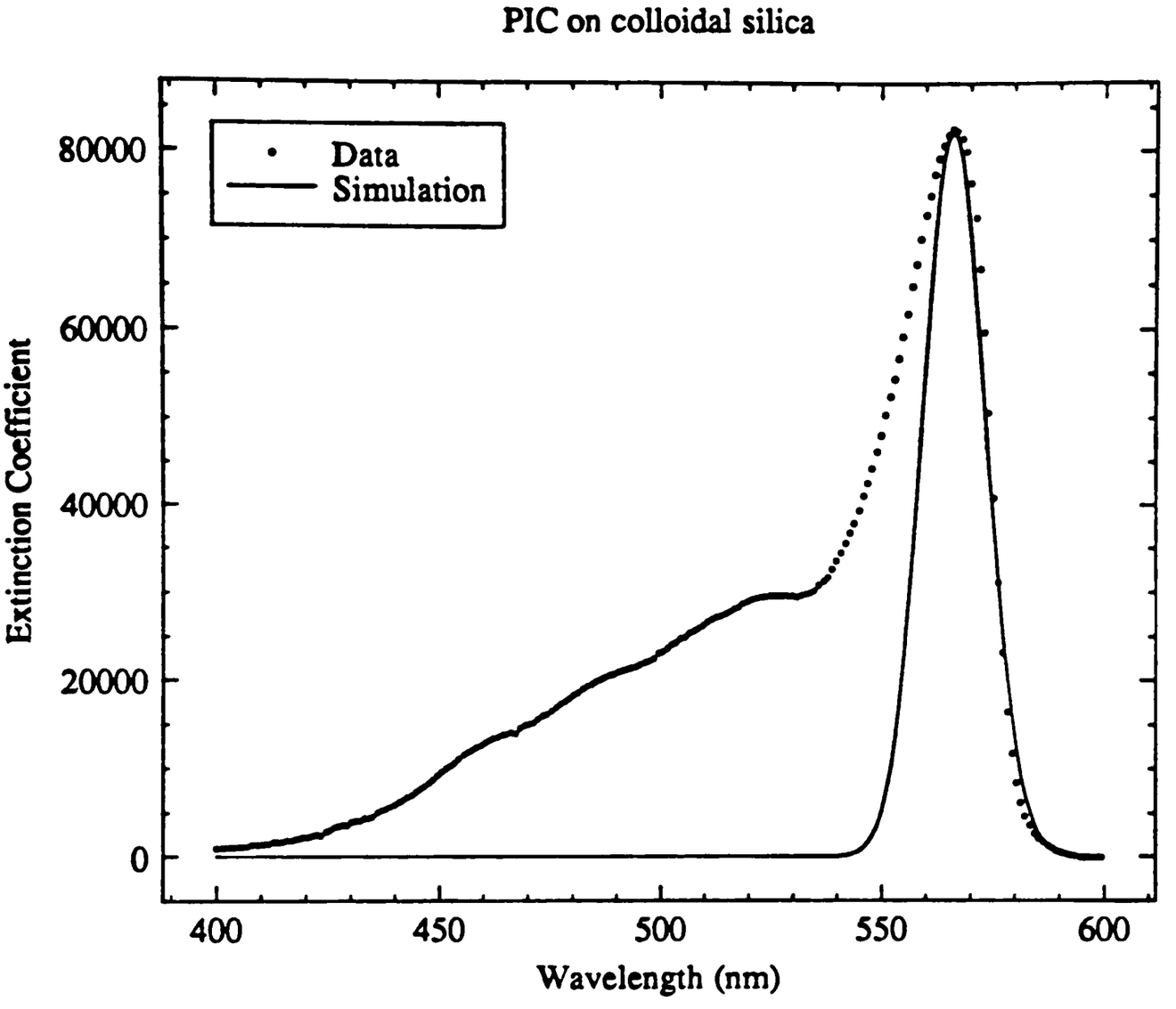

Figure 2.14. The absorption linewidth of PIC J-band (sample L).

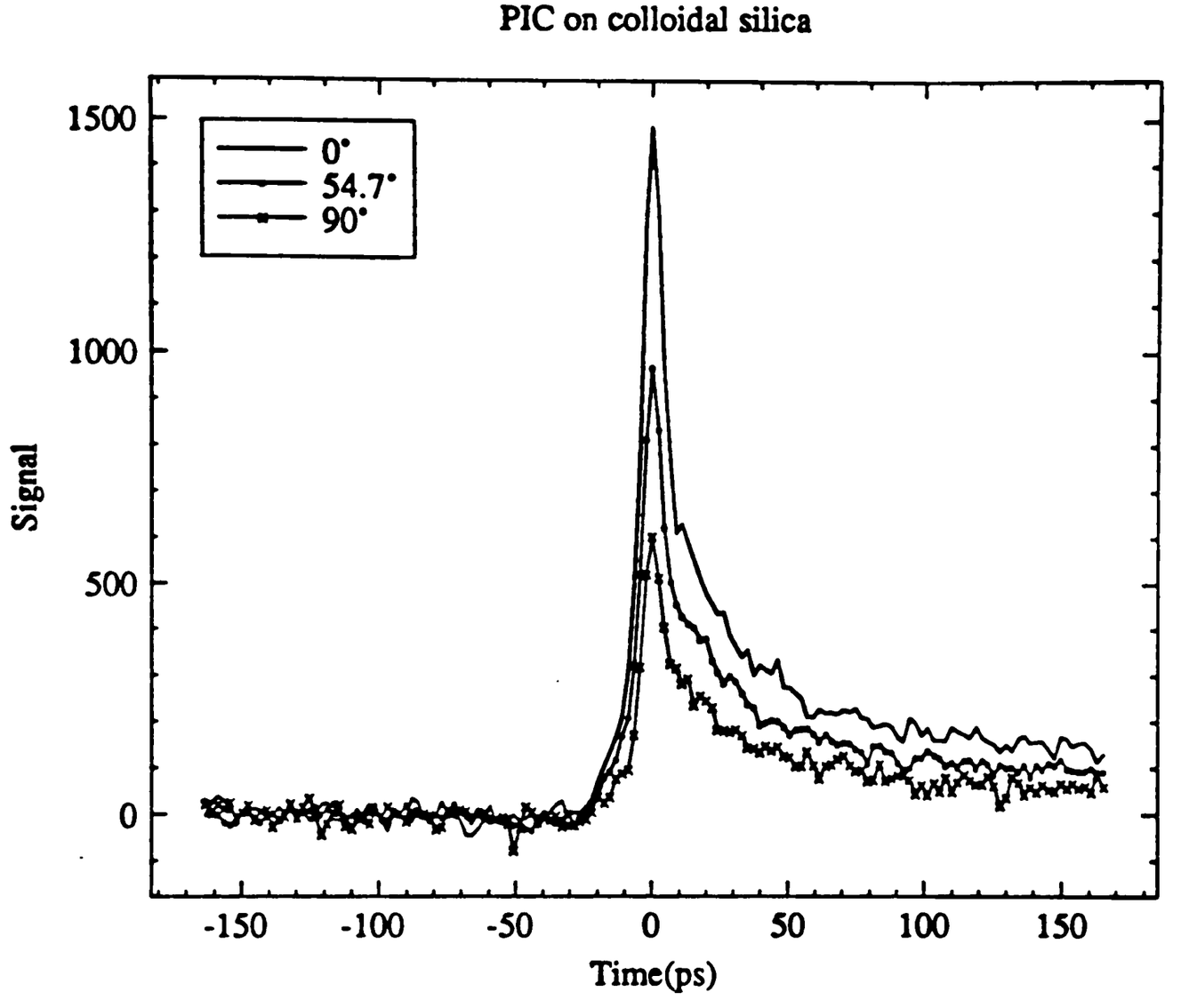

Figure 2.15. Transient bleaching signals for J-aggregates on colloidal silica at 570 nm (sample L).

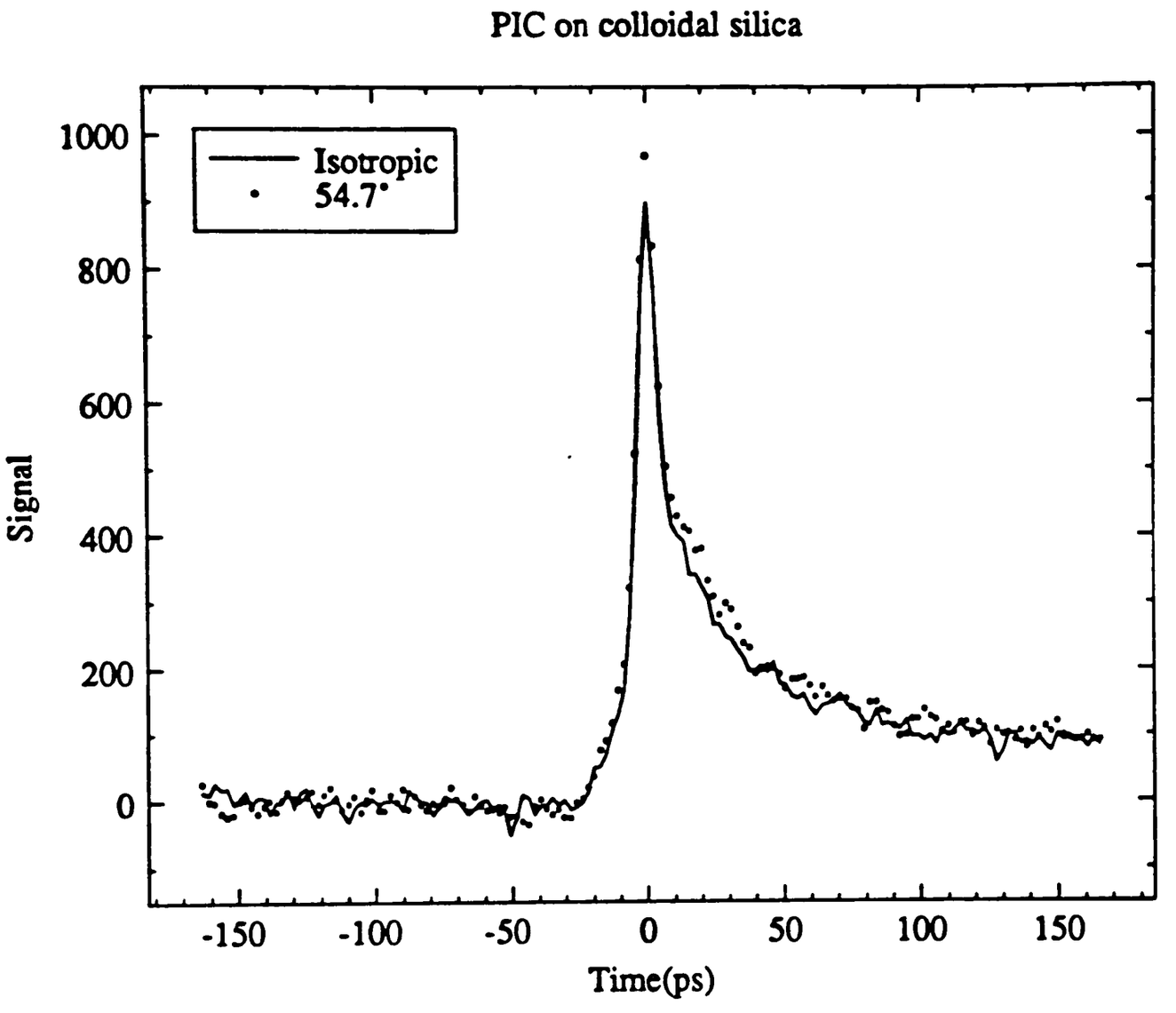

Figure 2.16. The curves isotropic and magic angle of sample L.

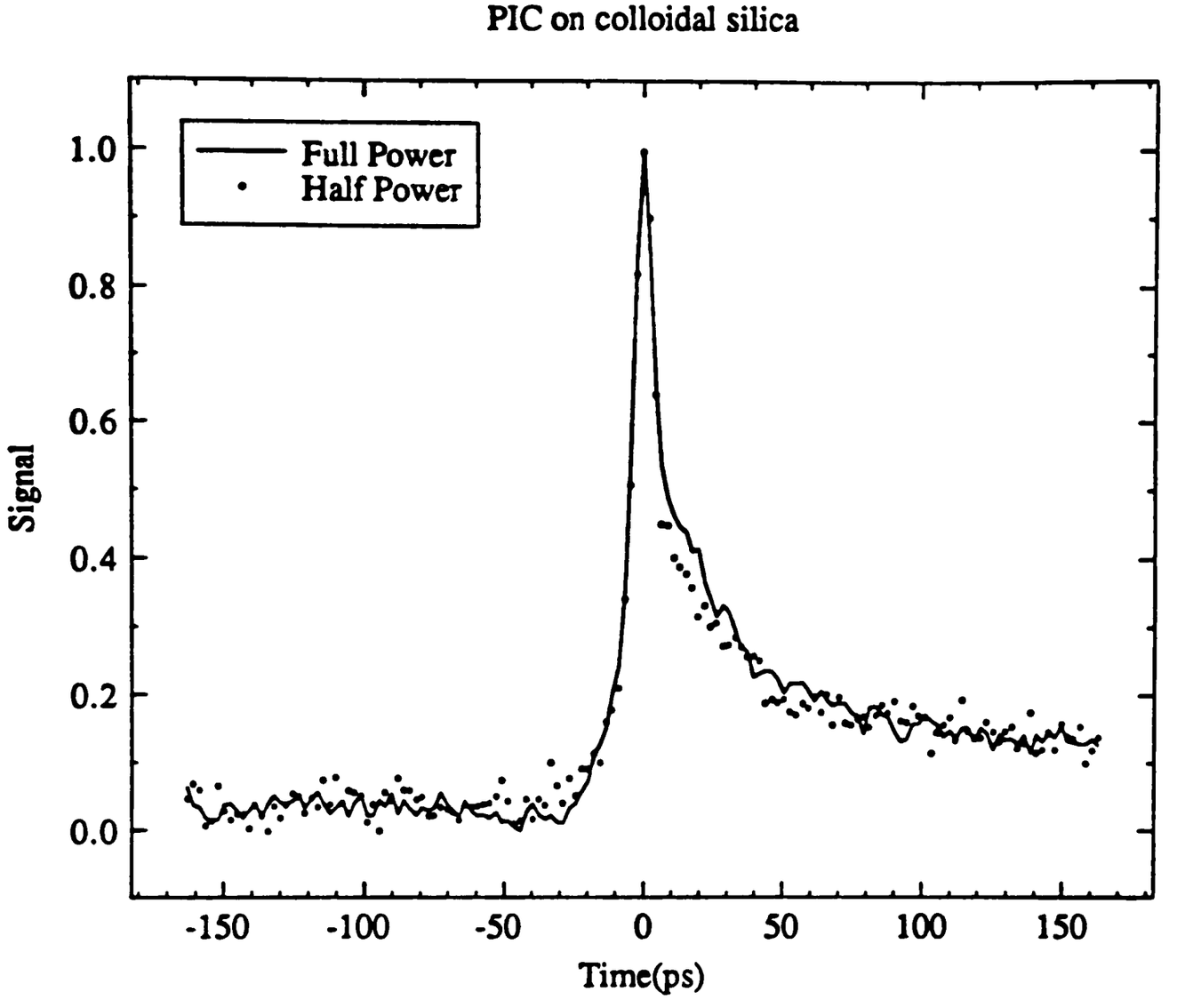

Figure 2.17. Comparison of a magic angle curve (points) and one obtained with the laser intensity halved (solid curve). The curves have been normalized.

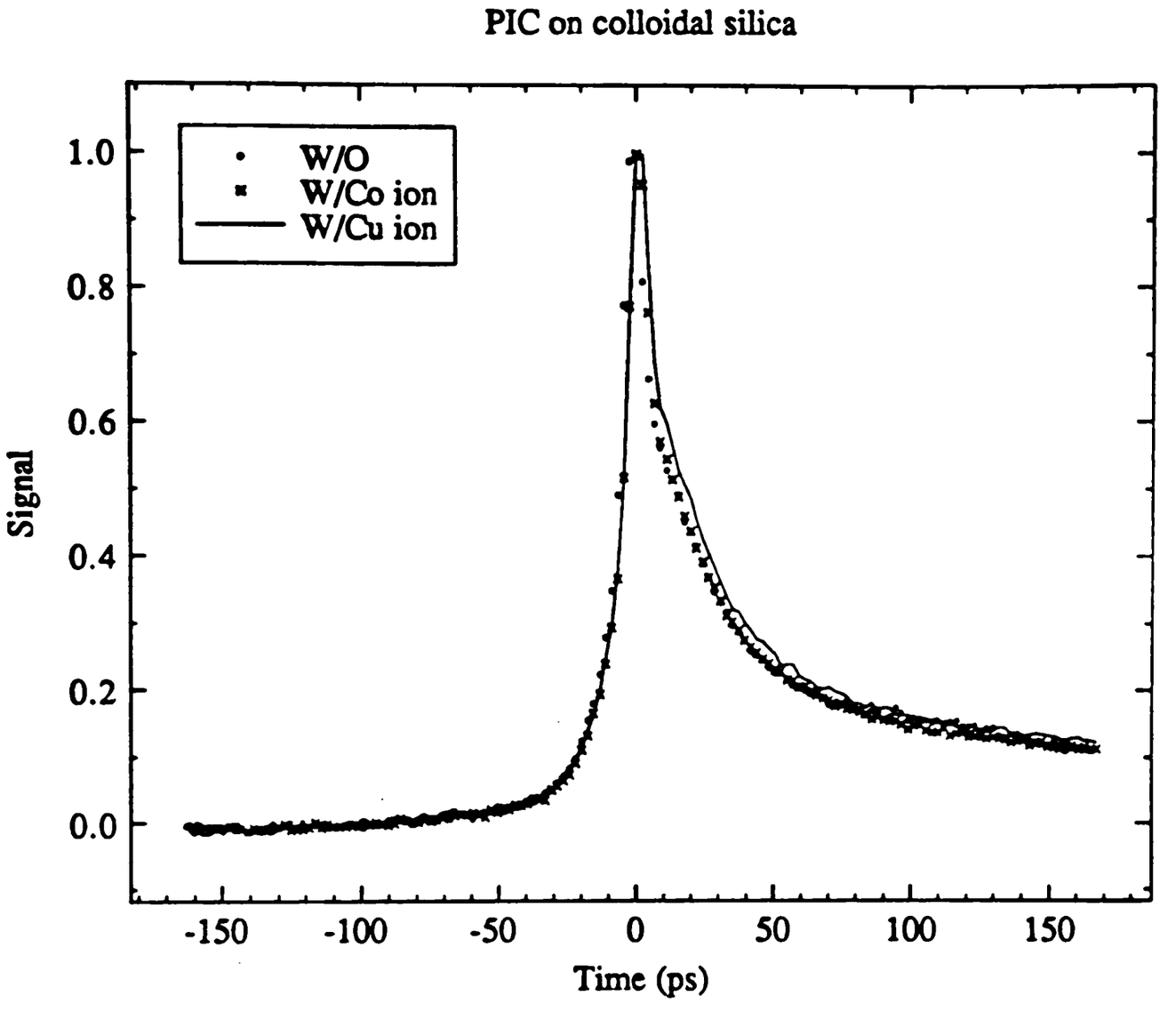

Figure 2.18. Representative transient photobleaching signals for J-aggregates of PIC on colloidal silica without heavy metal ions and with $CoCl_2$ and $CuSO_4$. The signals have been normalized at the peak of the coherent coupling artifact.

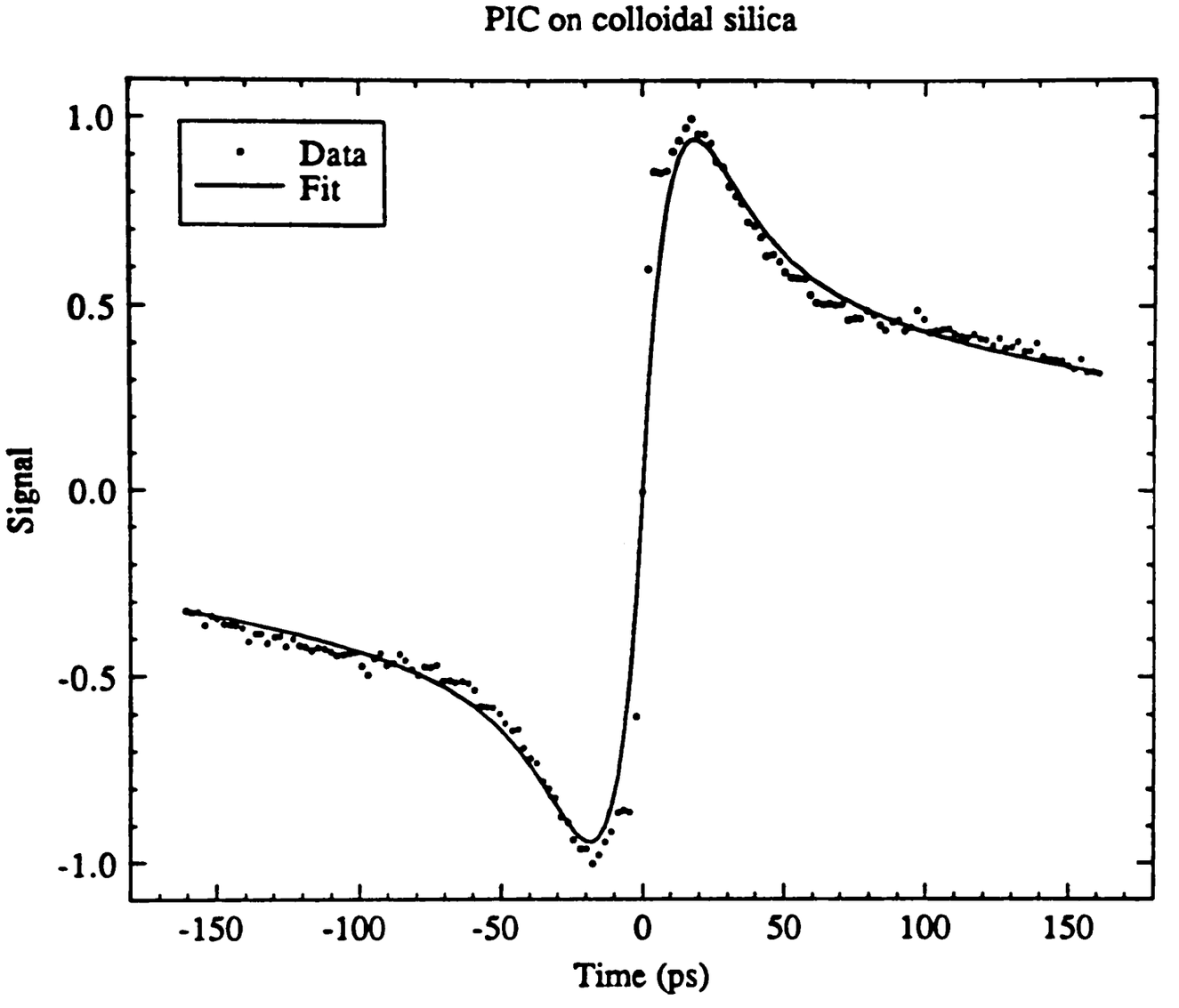

Figure 2.19. Antisymmetrized parallel signal from Figure 2.18 (points) without heavy metal ions and the convolution of the pulse autocorrelation with an antisymmetrized form of eq 49 (solid curve). See Table 2.4 for fitting parameters.

picosecond. Although the value of τ_1 obtained in these experiments compares well with values obtained from sample F, the values of the other biexponential parameters are different. We should not surprised at the 20% difference of τ_2 between sample F and sample L because the absorption spectra are quite different. Different exciton band structure may resulted in different decay time. One experimental point should also be noted that the signal to noise ratio of the measurements shown in Figure 2.13 are lower than those of sample F. It is not clear whether a change in weight of the short and long components would not lead to a lengthening rather than a shortening of the long decay component. Besides, to deduce decay times of 300 ps from a biexponential decay that extends only over 160 picoseconds may also result in a great uncertainty. Thus, there is no point to focus on the τ_2 difference between samples F and L. It is more important to know if this long component arises from excited triplet state decay. Examination of the fits in Figures 2.19, 2.20, and 2.21 suggests that the decay rates of the short and long components in the samples with and without triplet quancher are close to indistinguishable. This results suggest that triplet quenching is not observed in this time range. Table 2.4 summarizes the biexponential fitting parameters for zero, 1.0×10^{-3} M Cu^{+2}, and 1.0×10^{-3} M Co^{+2}.

The results of these experiments show that excitons in J-aggregates on colloidal silica are delocalized independent of different silica lot number. Because the decay kinetic is independent of the excitation intensity, exciton annihilation is not occurring in the J-aggregates on colloidal silica.

2.2.2. NaCl Solution

As can be judged from the spectral analysis of the J-aggregate spectrum, it is best characterized as a case of strong exciton interaction. It is of great fundamental

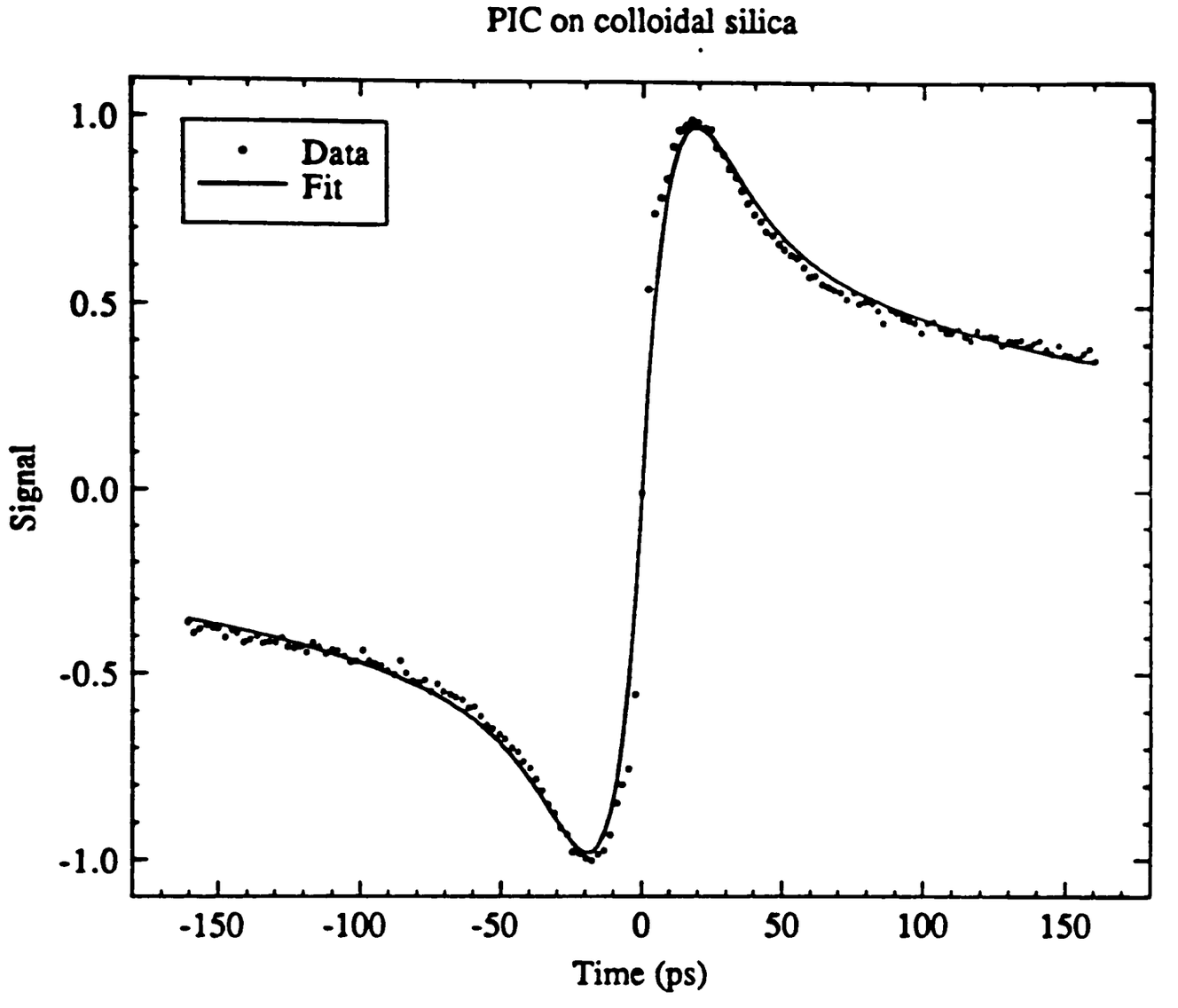

Figure 2.20. Antisymmetrized parallel signal from Figure 2.18 (points) with $CoCl_2$ and the convolution of the pulse autocorrelation with an antisymmetrized form of eq 49 (solid curve). See Table 2.4 for fitting parameters.

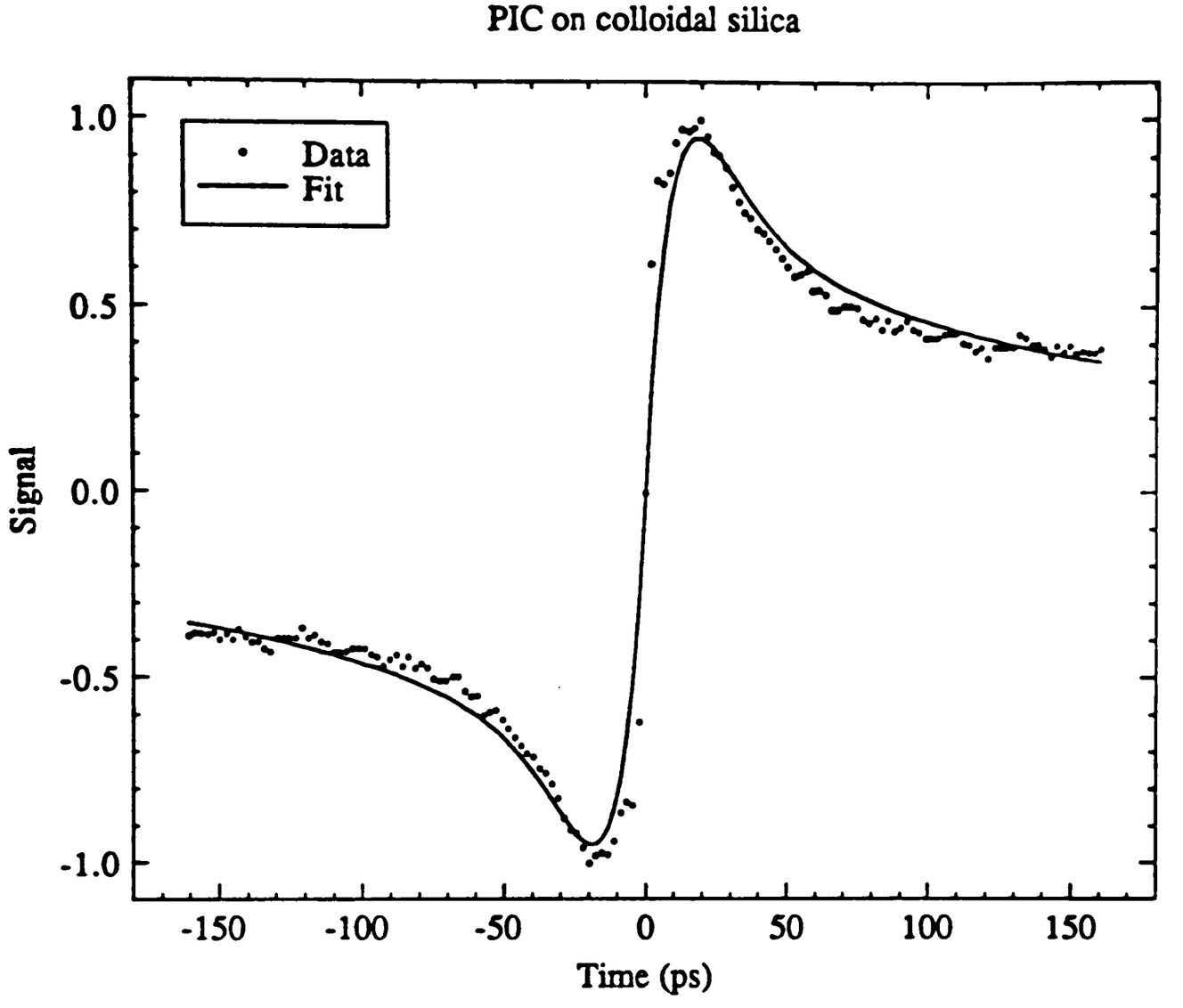

Figure 2.21. Antisymmetrized parallel signal from Figure 2.18 (points) with $CuSO_4$ and the convolution of the pulse autocorrelation with an antisymmetrized form of eq 49 (solid curve). See Table 2.4 for fitting parameters.

Table 2.4. Biexponential fitting parameters for the polarized transient bleaching signals in Figure 2.18.

Parameters / Signals	A_1	τ_1, ps	A_2	τ_2, ps	χ^2
Without heavy metal ions	0.75	21.3	0.25	259.5	4.6×10^{-3}
With Co^{+2}	0.74	22.2	0.26	268.5	2.4×10^{-3}
With Cu^{+2}	0.74	21.1	0.26	276.6	5.0×10^{-3}

interest to study the excited state dynamics and energy transport of such a strongly coupled system. In addition evidence is accumulating that strongly coupled chromophores also exist in natural photosynthetic systems. Thus, in order to learn more about the consequences of strong exciton coupling in natural systems it may be useful to study the J-aggregate which possibly is a simpler system.

The absorption spectrum of 50 μM PIC in 5 M NaCl solution is shown in Figure 2.22. Obviously, the presence of 5 M sodium chloride induces the aggregation of PIC. This J-aggregate system exhibits the familiar J-band at 574 nm. An analysis of the linewidth of the J-band shows that the FWHM is about 146 cm^{-1} [Figure 2.23], which is much narrower than that of colloidal silica system. The result gives an average aggregate size of 70 monomer units, which is larger than the size of aggregates on colloidal silica.

Figure 2.24 shows typical transient bleaching signals of PIC in 5 M sodium chloride solution with the polarization of the probe beam parallel, 54.7°, and perpendicular to the polarization of the pump beam. The coherent spike are not as intense as those of colloidal silica due to stronger signal of the system. The excellent overlap between the curves, magic angle and isotropic is shown in Figure 2.25.

Plot of the anisotropy versus time for J-aggregates in 5 M sodium chloride solution is shown in Figure 2.26. The zero time anisotropies are not exactly equal to the theoretical value of 0.4 because of the coherent coupling artifact. Nonetheless, outside the region of the coherent coupling artifact the anisotropy decays.

The normalized magic-angle transient bleaching signal and one obtained with the excitation intensity reduced by a factor of two for 50 mM PIC in 5M NaCl are shown in Figure 2.27. These magic-angle transient bleaching signals show that the decay kinetics of J-aggregates in sodium chloride solutions are excitation-intensity

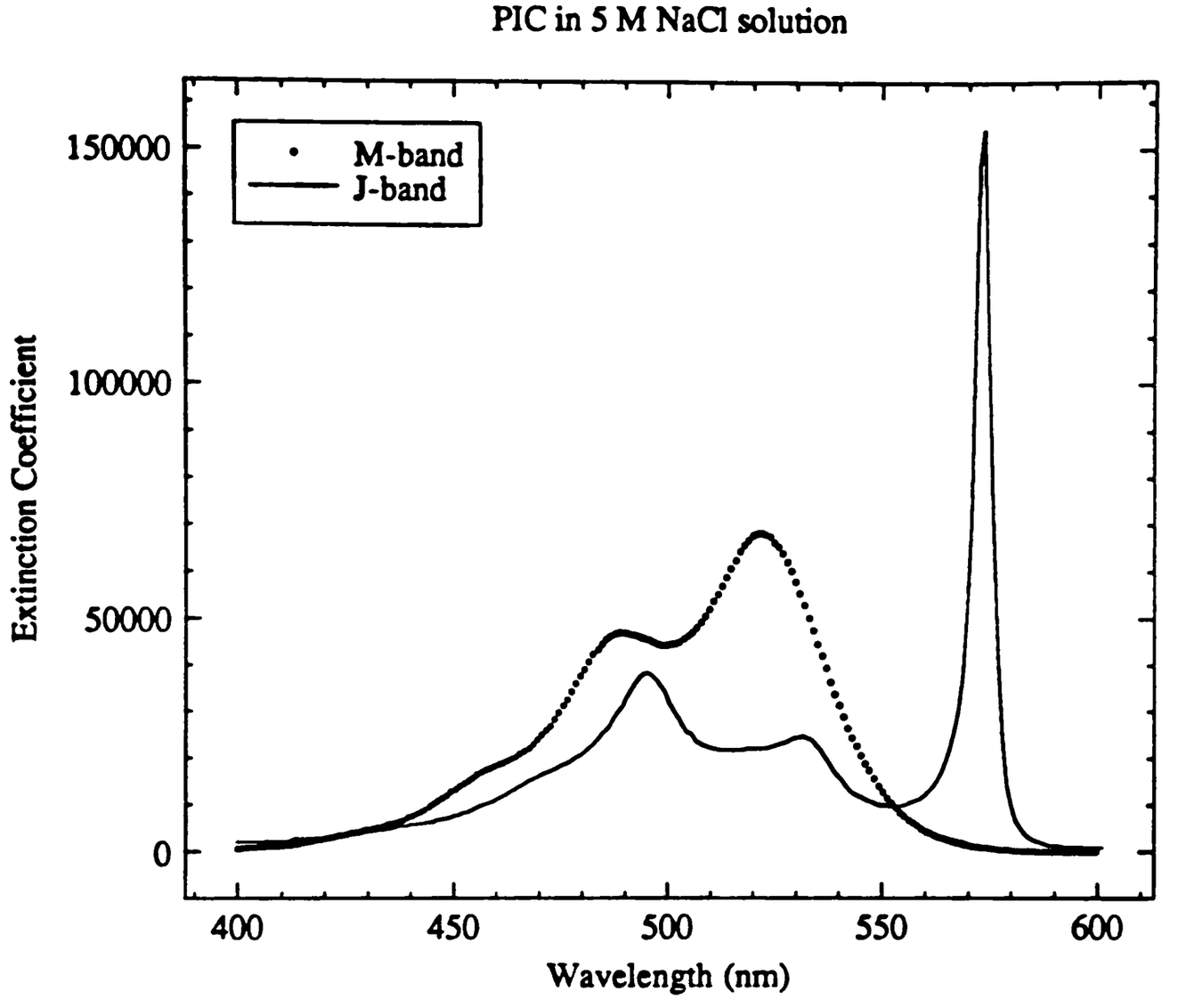

Figure 2.22. The absorption spectra of 50 μM PIC(Cl) in water and in 5 M NaCl solution.

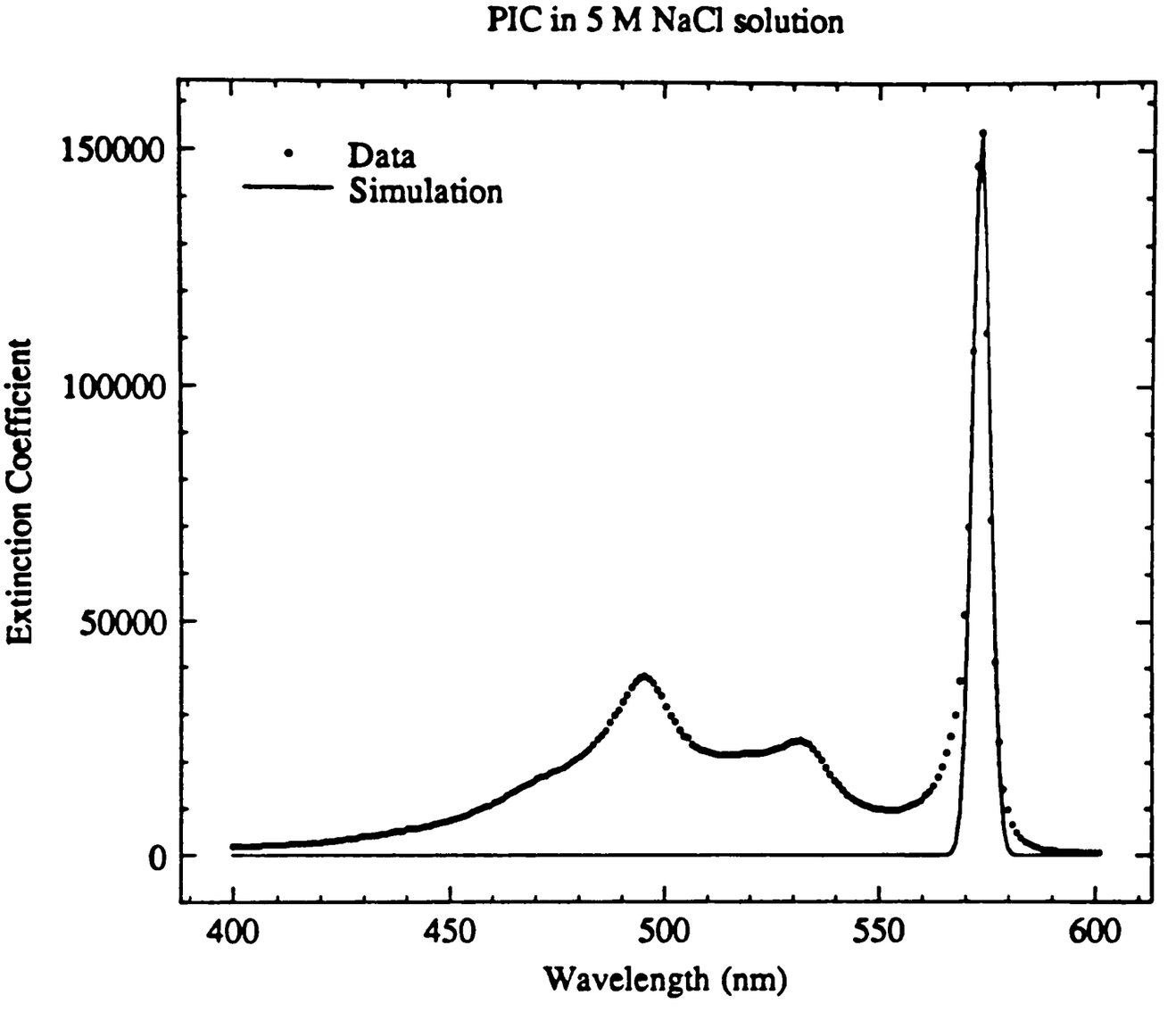

Figure 2.23. The absorption linewidth of PIC J-band in 5 M NaCl solution.

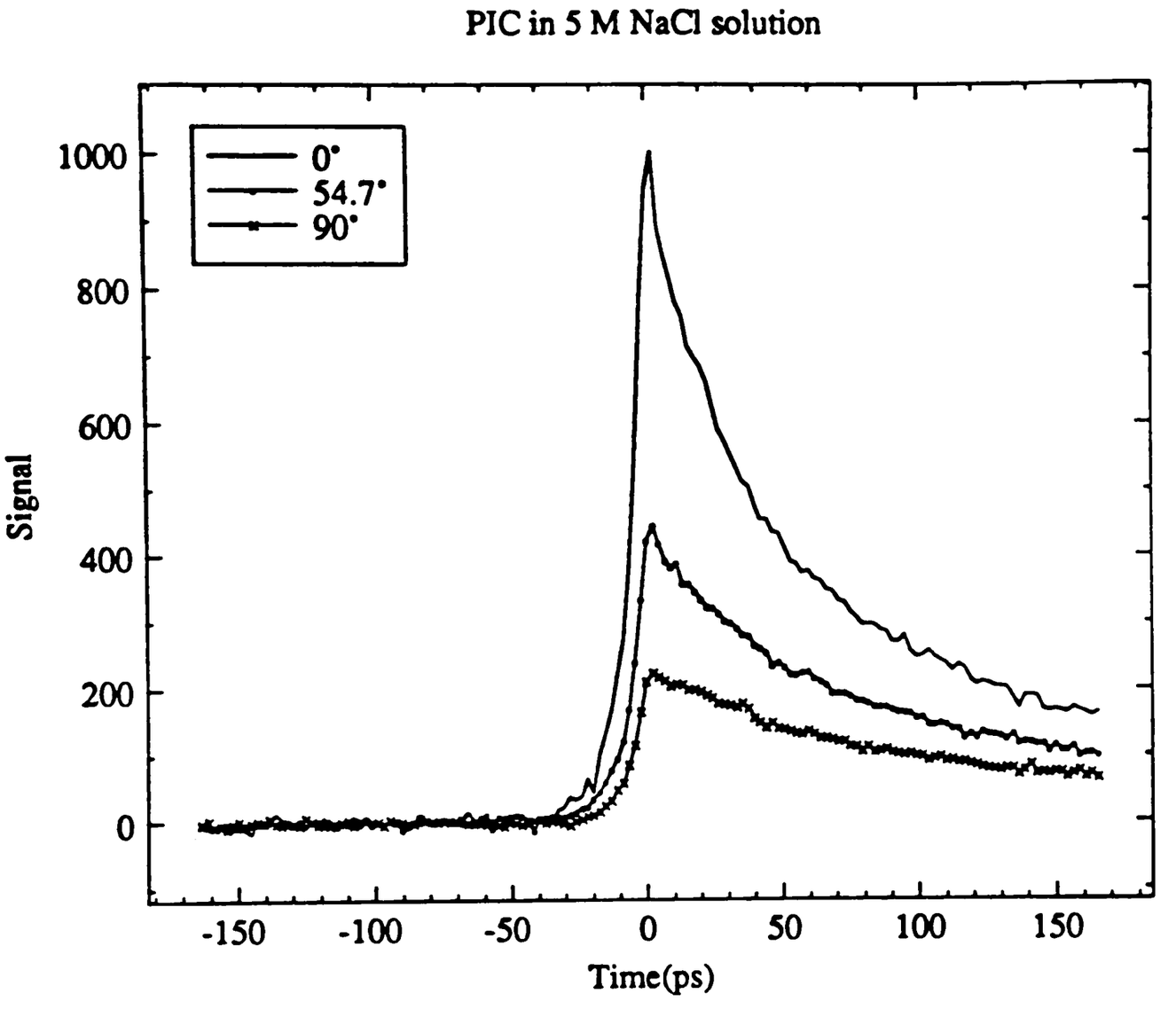

Figure 2.24. Transient bleaching signals for J-aggregates in 5 M NaCl solution at 570 nm.

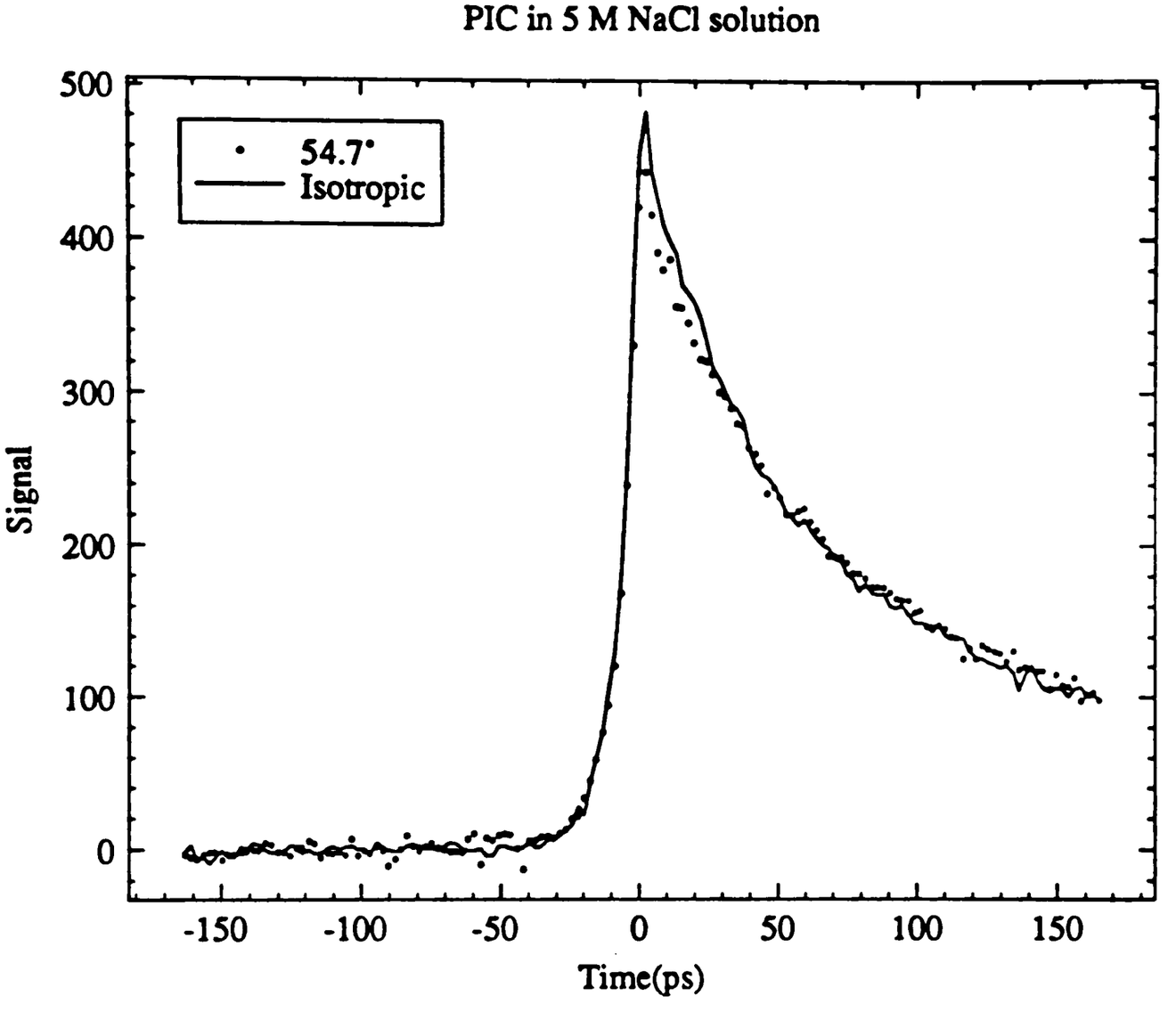

Figure 2.25. The curves isotropic and magic angle of PIC in 5 M NaCl solution.

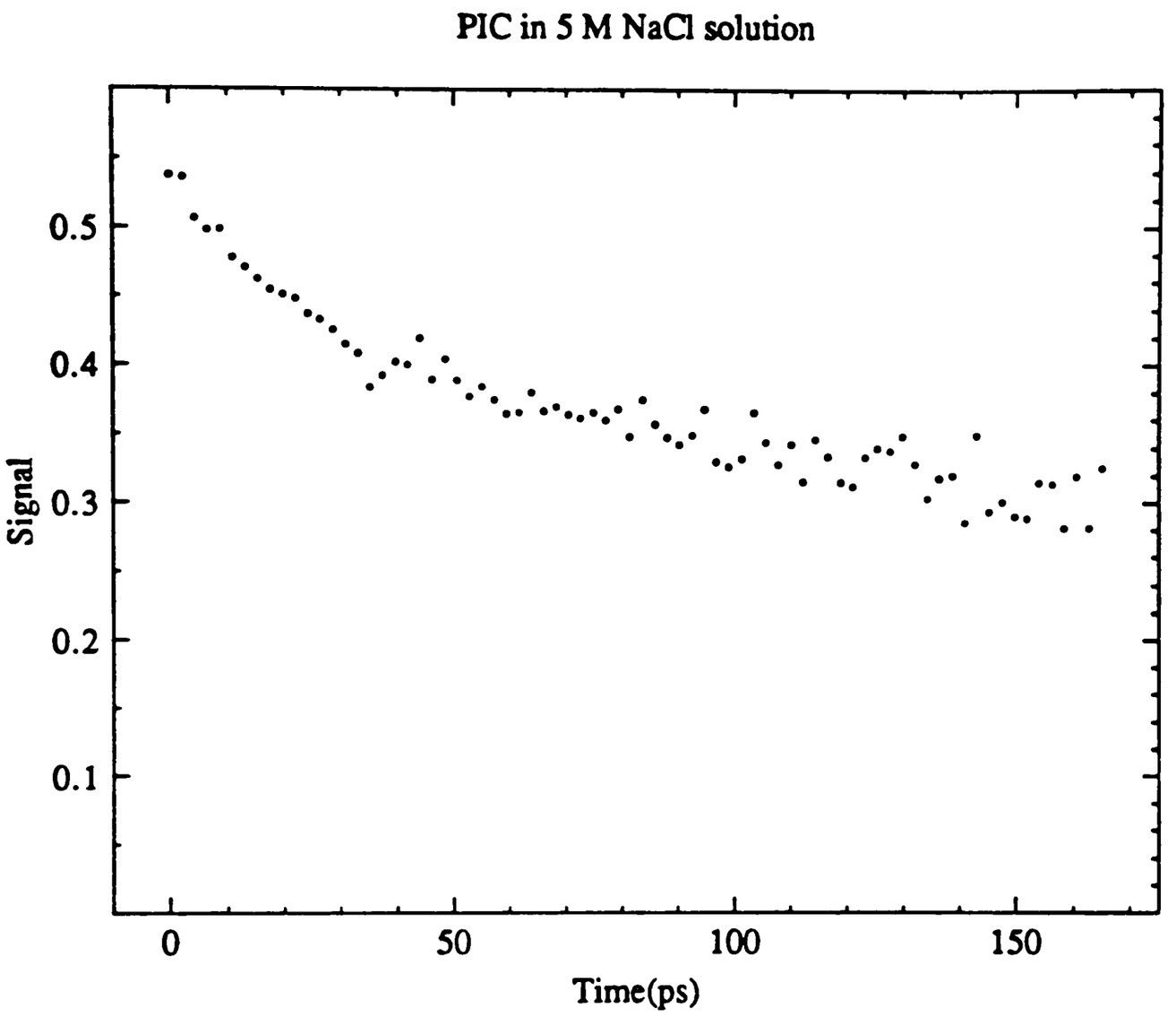

Figure 2.26. Absorption anisotropy for PIC in 5 M NaCl solution.

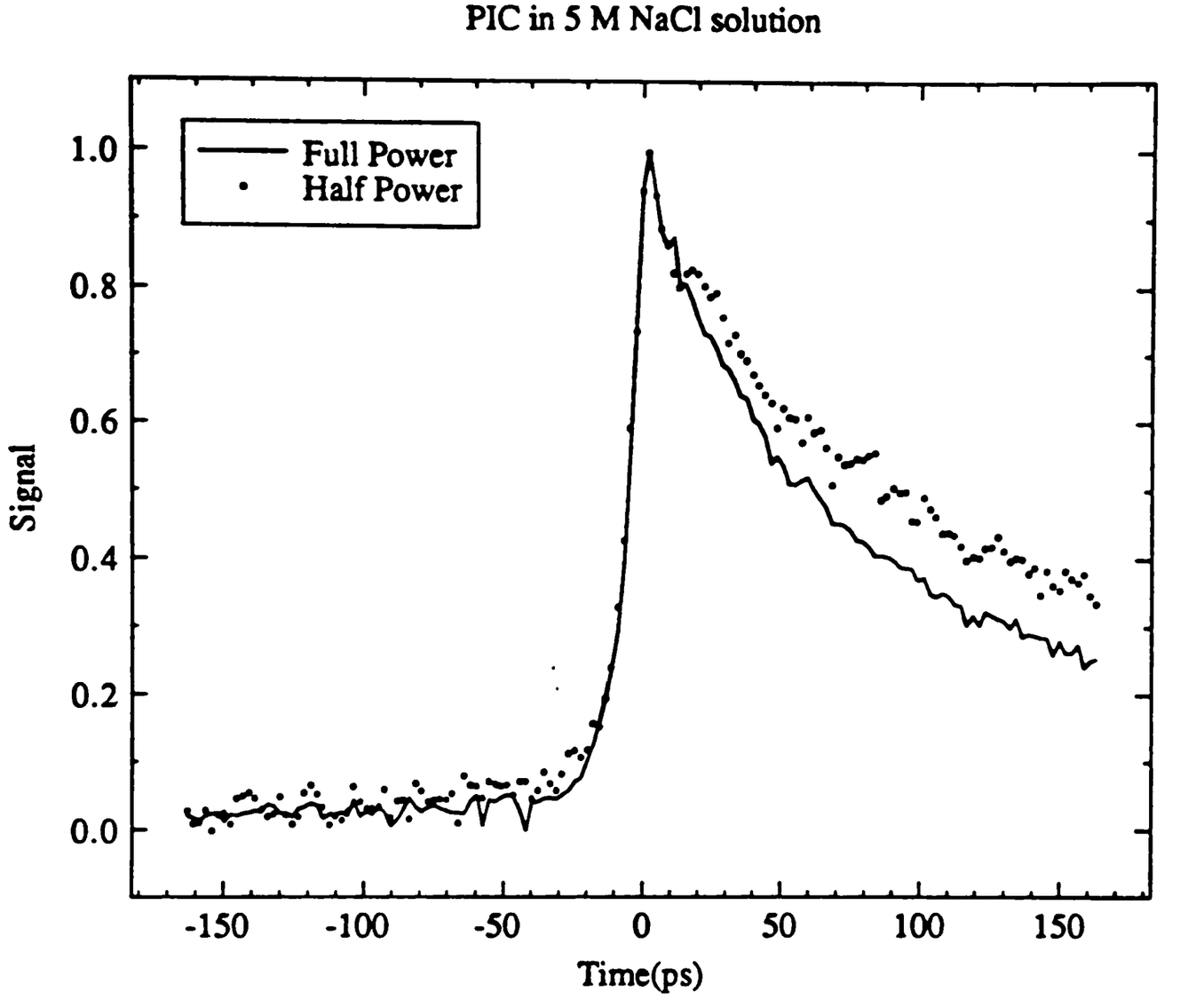

Figure 2.27. Magic angle transient bleaching signal (solid curve) and one obtained with the excitation intensity reduced by a factor of two (dotted curve) for 50 μM PIC in 5 M NaCl.

dependent. This result indicates that exciton annililation is occurring.

Fits of the magic angle signals over the delay range indicated for J-aggregates in solution at excitation intensities of 2.4×10^{12} and 1.2×10^{12} photons $cm^{-2}pulse^{-1}$ are shown in Figures 2.28 and 2.29. Table 2.5 summarizes the analysis for the excitation-intensity-dependent study. The fitting parameters A, B, and τ_{ex} were allowed to vary during the fit for both excitation intensities. Although the values of τ_{ex} are not exactly the same for the two excitation intensities, as one would have predicted from the model, they differ by only 5% from the average value of 195 ps. This average value is in agreement with value of 200 ps obtained from an analysis of fluorescence decay data of J-aggregates in solution.[101] If the value of γ_{ss} is assumed to be the same for both excitation intensities, the initial population N_0 determined from the parameters τ_{ex} and B are in the ratio of 1/2.1, which is in agreement with the ratio of 1/2 of the excitation intensity.

2.2.3. PVS Polymer

Dye-polyanion complexes provide interesting examples of systems in which efficient transfer of excitation energy is possible. Studies of the excitation energy transfer between dye molecules bound to polymer molecules are of great interest in relation to the function of chlorophyll in chloroplast lamellae. The results of picosecond pump-probe measurements are very different for J-aggregates on unpurified and purified PVS and will be discussed separately.

2.2.3.1. Unpurified PVS

When a solution of the unpurified PVS polymer is added to a diluted aqueous PIC solution, a narrow band of high absorptivity appears at approximately 570 nm [Figure 2.30]. This J-band is associated with aggregates of cyanine dyes bound to

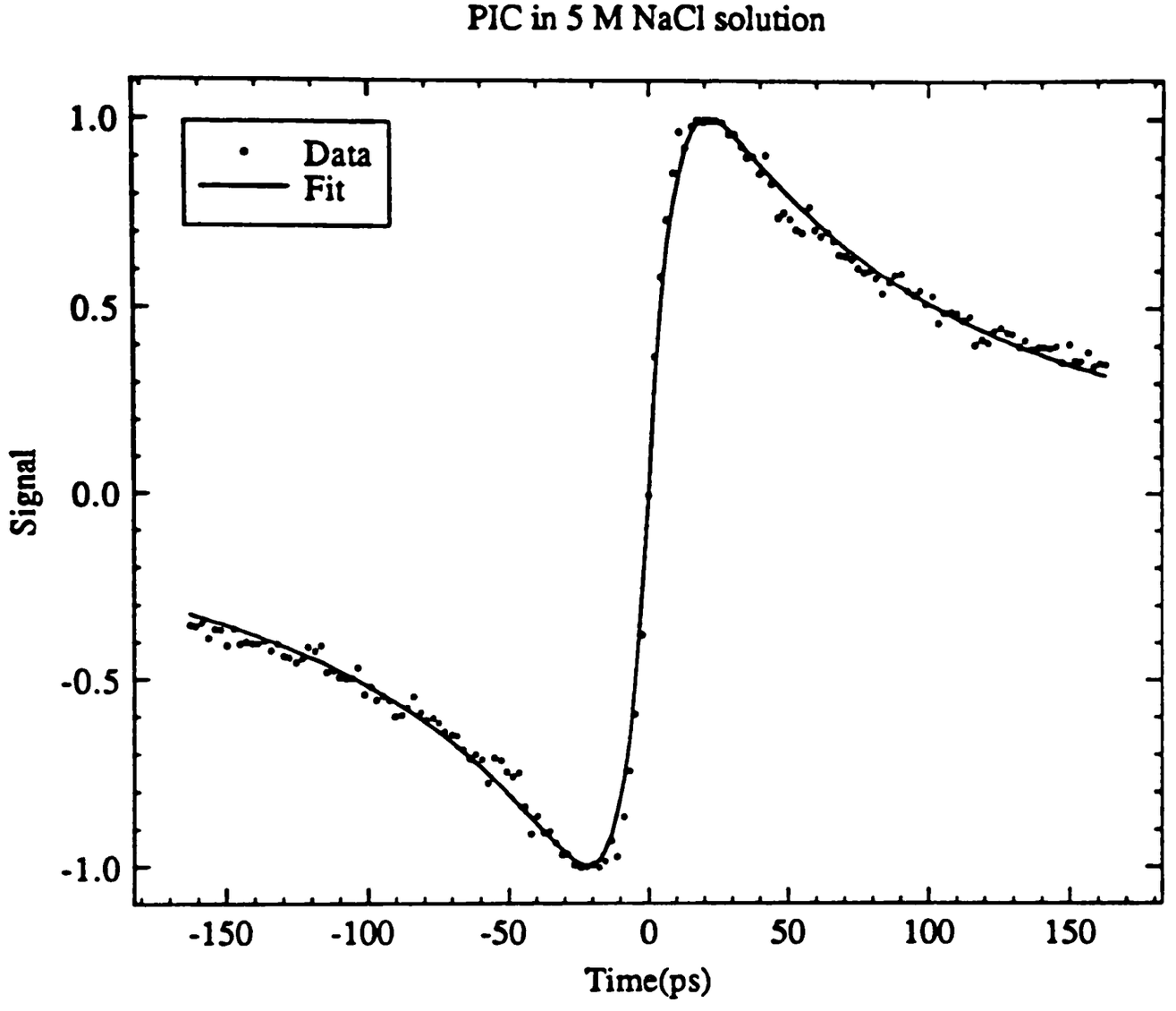

Figure 2.28. Antisymmetrized magic angle signal for PIC in 5 M NaCl (points) and the convolution of the pulse autocorrelation with an antisymmetrized form of eq 32 (solid curve). See Table 2.5 for fitting parameters.

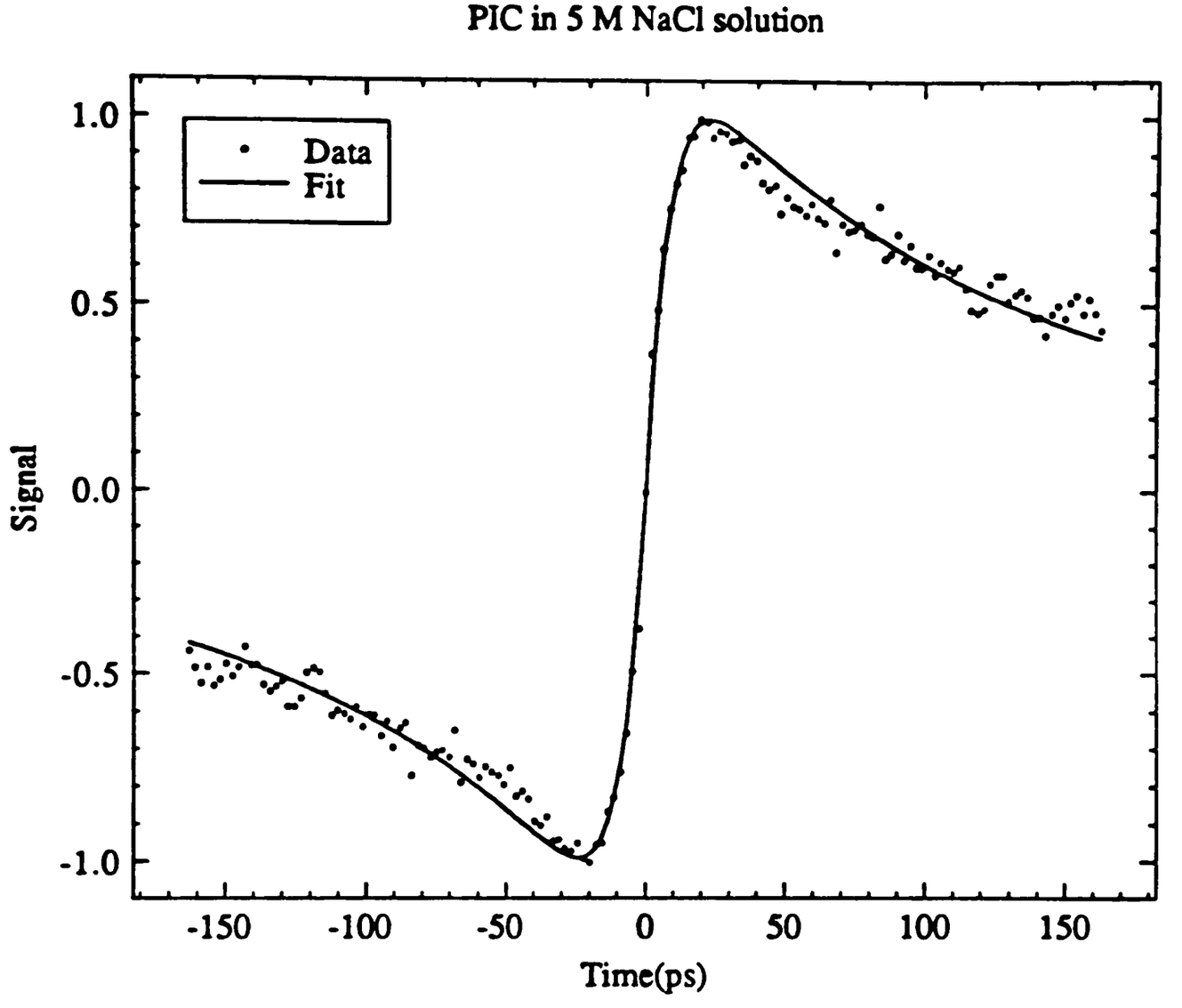

Figure 2.29. Antisymmetrized magic angle signal for PIC in 5 M NaCl with the excitation intensity reduced by a factor of two (points) and the convolution of the pulse autocorrelation with an antisymmetrized form of eq 32 (solid curve). See Table 2.5 for fitting parameters.

Table 2.5. Fit of transient bleaching signals for J-aggregates in 5 M NaCl solution to exciton-annihilation model.

Parameters / Excitation Intensity photons cm^{-2} $pulse^{-1}$	A	B	τ_{ex}, ps	χ^2
2.4×10^{12}	0.115	1.7	185	1.37×10^{-3}
1.2×10^{12}	0.196	2.3	205	2.43×10^{-3}

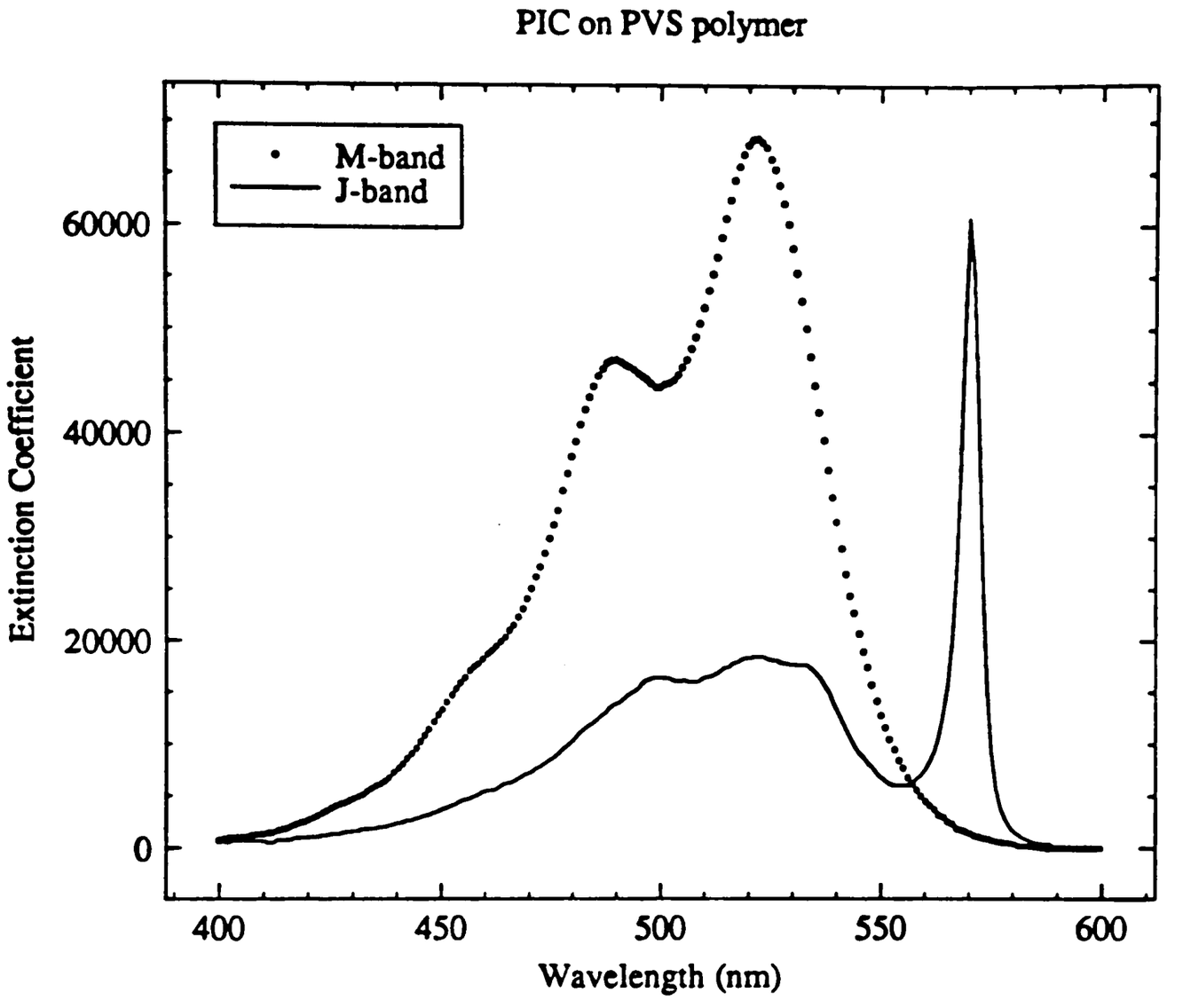

Figure 2.30. The absorption spectra of 50 μM PIC(Cl) in water and 100 μM PIC(Cl) in 0.05 g/dl unpurified PVS solution.

PVS polymer, and red shifted to the M-band. The linewidth of the J-band is approximately 165 cm^{-1} [Figure 2.31], which corresponds to an average aggregate size of 55 monomer units.

Transient photobleaching signal of pump-probe measurement at 574.4 nm with the highest intensity used is shown in Figure 2.32. The initial bleaching is seen to decay with a pulse limited rate to a state absorbing more strongly than the initial ground state. A very similar decay curve but with an opposite sign is observed when the kinetic is monitored at 570 nm [Figure 2.33]. For this wavelength, the initial signal is observed as an increasing absorption that very rapidly recover to a negative signal level, followed by a slower decay of the negative signal. These results suggest that there exist densely spaced excited states that are strongly absorbing.

By varying laser power, the results of these measurements [Figure 2.34] show that the lifetime is strongly dependent on excitation pulse intensity. At a relatively high light intensity, the excited-state lifetime is essentially pulse limited. Upon decreasing, the light intensity a gradual increase of the excited-state lifetime is observed. The observed intensity dependence of the excited-state dynamics is attributed to efficient exciton annihilation between the highly mobile singlet excitons.

Typical transient bleaching signals for PIC on PVS at lowest excitation intensity are shown in Figure 2.35, with parallel, magic-angle (54.7°), and perpendicular relative polarizations of the excitation and analyzing light. A difference curve is obtained, according to

$$S_D(t) = \frac{S_{//}(t) - S_{\perp}(t)}{3}. \qquad (52)$$

The difference function is given by the convolution of the autocorrelation with the anisotropy function r(t) and the ground-state-recovery decay function K(t)

$$d(t) = r(t)K(t). \qquad (53)$$

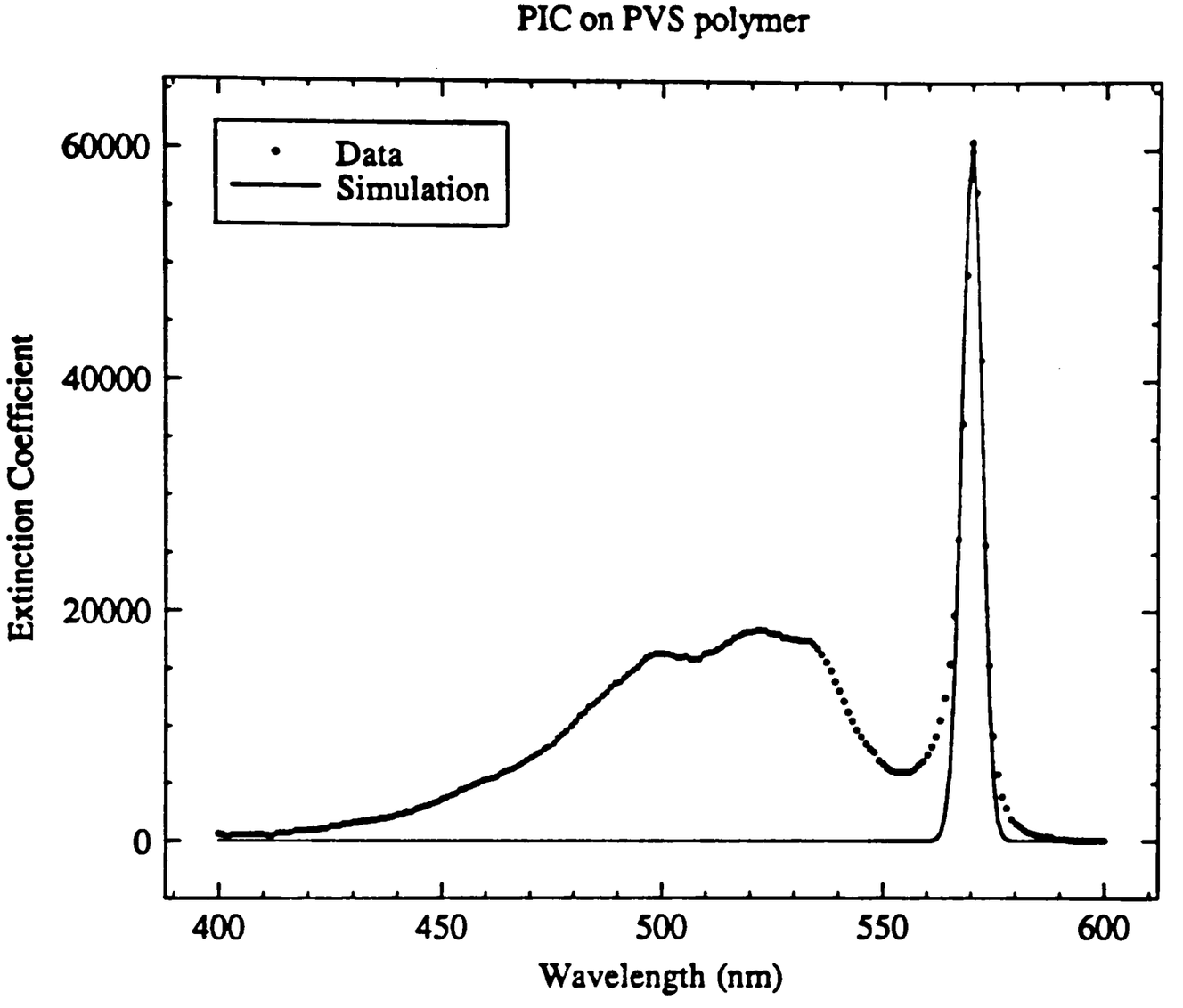

Figure 2.31. The absorption linewidth of PIC J-band for 100 μM PIC(Cl) in 0.05 g/dl unpurified PVS solution.

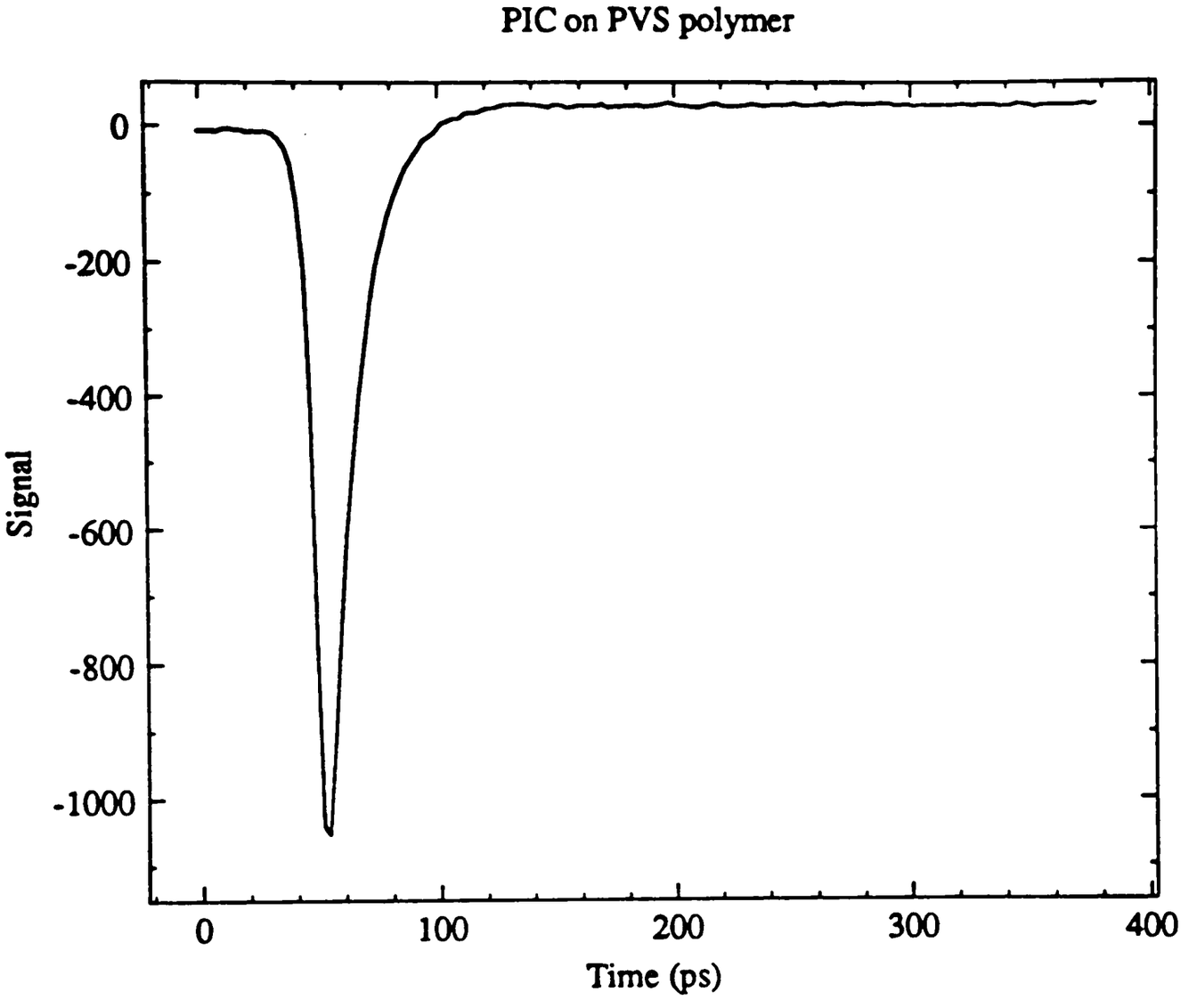

Figure 2.32. Transient bleaching signals for J-aggregates in 0.05 g/dl unpurified PVS solution at 574.4 nm with the highest intensity used.

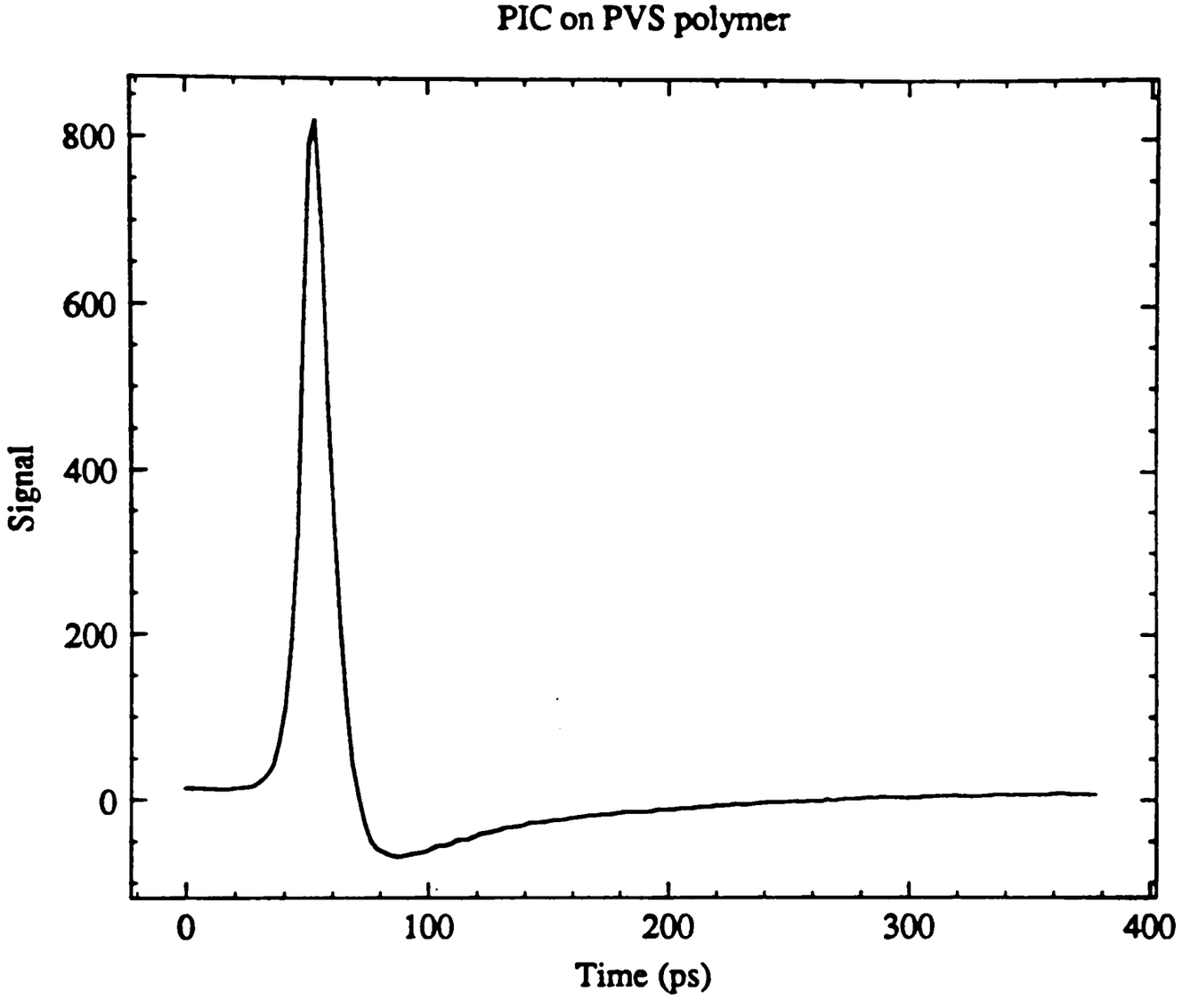

Figure 2.33. Transient bleaching signals for J-aggregates in 0.05 g/dl unpurified PVS solution at 570 nm with the highest intensity used.

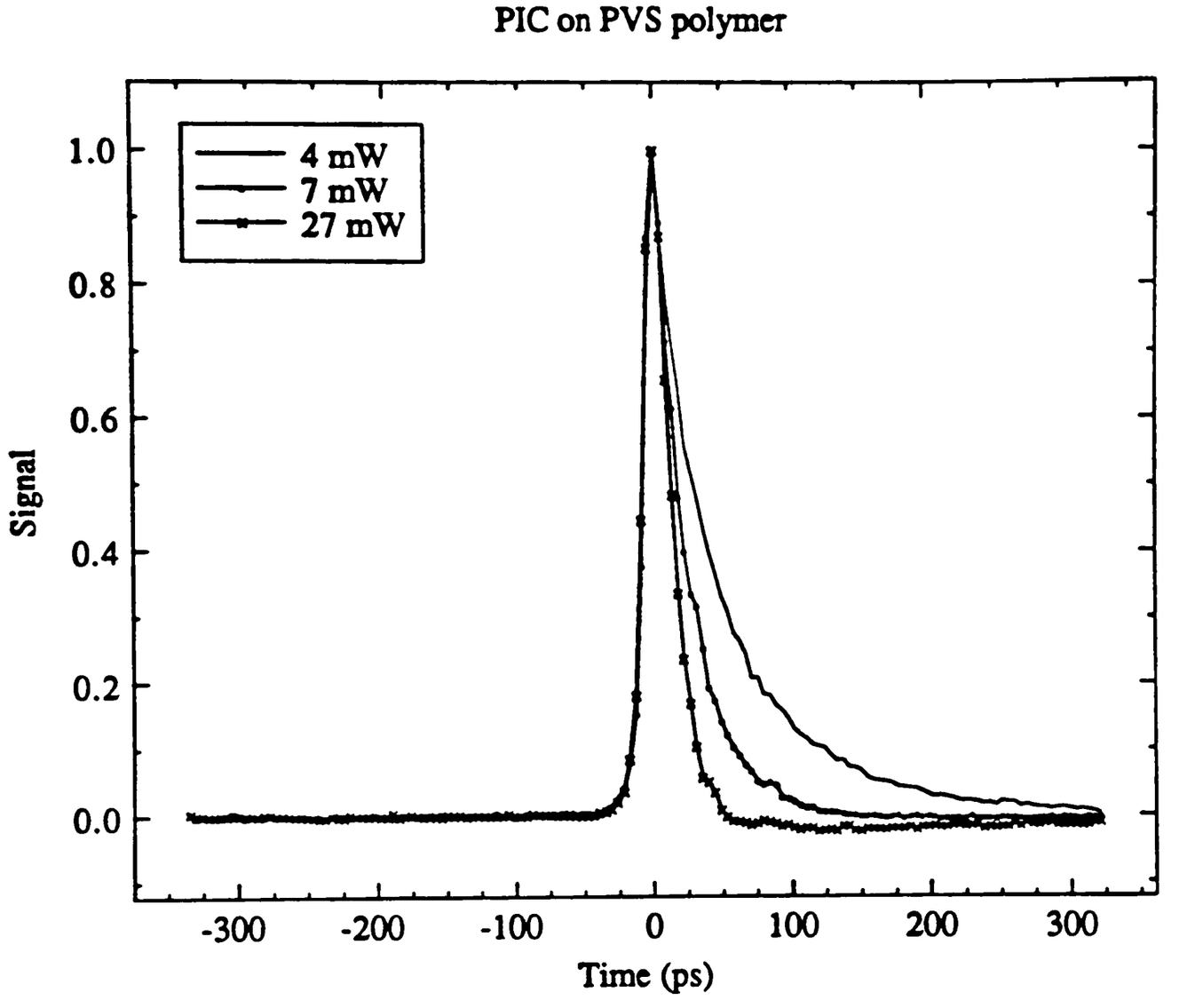

Figure 2.34. Excitation intensity dependence of transient bleaching signals for J-aggregates in 0.05 g/dl unpurified PVS solution at 574.4 nm.

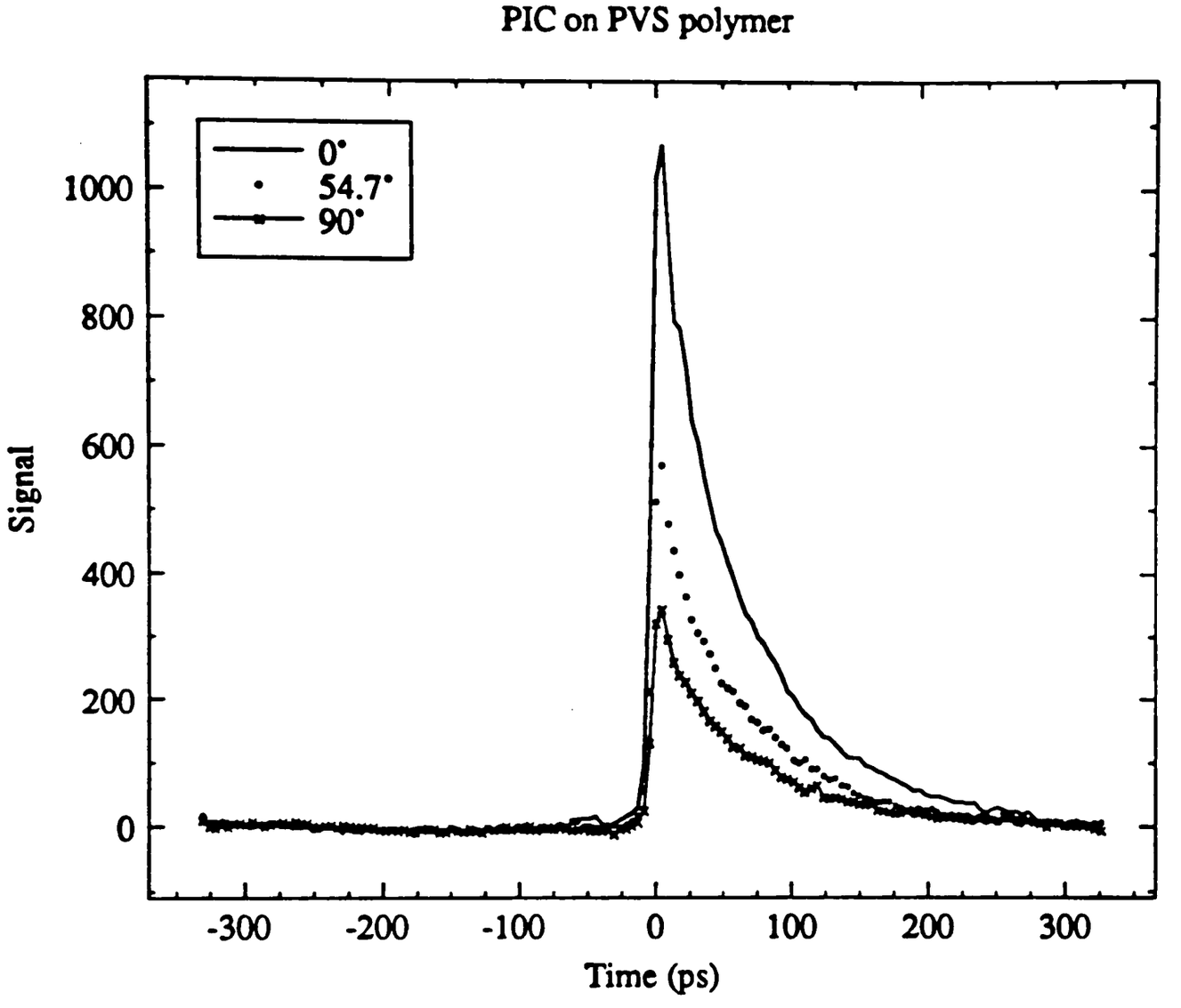

Figure 2.35. Transient bleaching signals for J-aggregates in 0.05 g/dl unpurified PVS solution at 574.4 nm with excitation intensity of 1.6×10^{11} photons cm^{-2} $pulse^{-1}$.

The calculated difference curve is shown in Figure 2.36. If the curves of isotropic and magic angle are equal to each other within experimental error, then the difference curve is valid for analysis. The excellent overlap between the curves of magic angle and isotropic is shown in Figure 2.37.

The magic angle curve can be fitted by a single exponential function with the ground-state-recovery time about 63 picoseconds [Figure 2.38]. The difference curve is fitted by a biexponential function [Figure 2.39], with τ_1 about 14 picoseconds, and τ_2 equal to the ground-state-recovery time within 4 % error. This result consists with our model. Our model is discussed below.

The ground-state-recovery decay function K(t) is given by

$$K(t) = A_0 \exp(-t/\tau_{gsr}) \tag{54}$$

which decays exponentially with decay time τ_{gsr}. The anisotropy function is given by[102-104]

$$r(t) = 0.4[(1 - a)\exp(-t/\tau_{depol}) + a] \tag{55}$$

with decay time τ_{depol}, where a is the residue anisotropy. Substituting Equation for r(t) and K(t), we have $d(t) = 0.4(1 - a)\exp(-t/\tau_{depol})A_0\exp(-t/\tau_{gsr}) + 0.4aA_0\exp(-t/\tau_{gsr})$. d(t) can then be expressed as a biexponential function

$$d(t) = A_1\exp(-t/\tau_1) + A_2\exp(-t/\tau_2). \tag{56}$$

It turns out that the long decay component τ_2 of the biexponential function is equal to τ_{gsr}, which consists with our result. The short decay component τ_1 corresponds to τ_D, which is given by

$$\frac{1}{\tau_D} = \frac{1}{\tau_{depol}} + \frac{1}{\tau_{gsr}}. \tag{57}$$

The value of residual anisotropy can then be obtained from the ratio of the preexponential factors

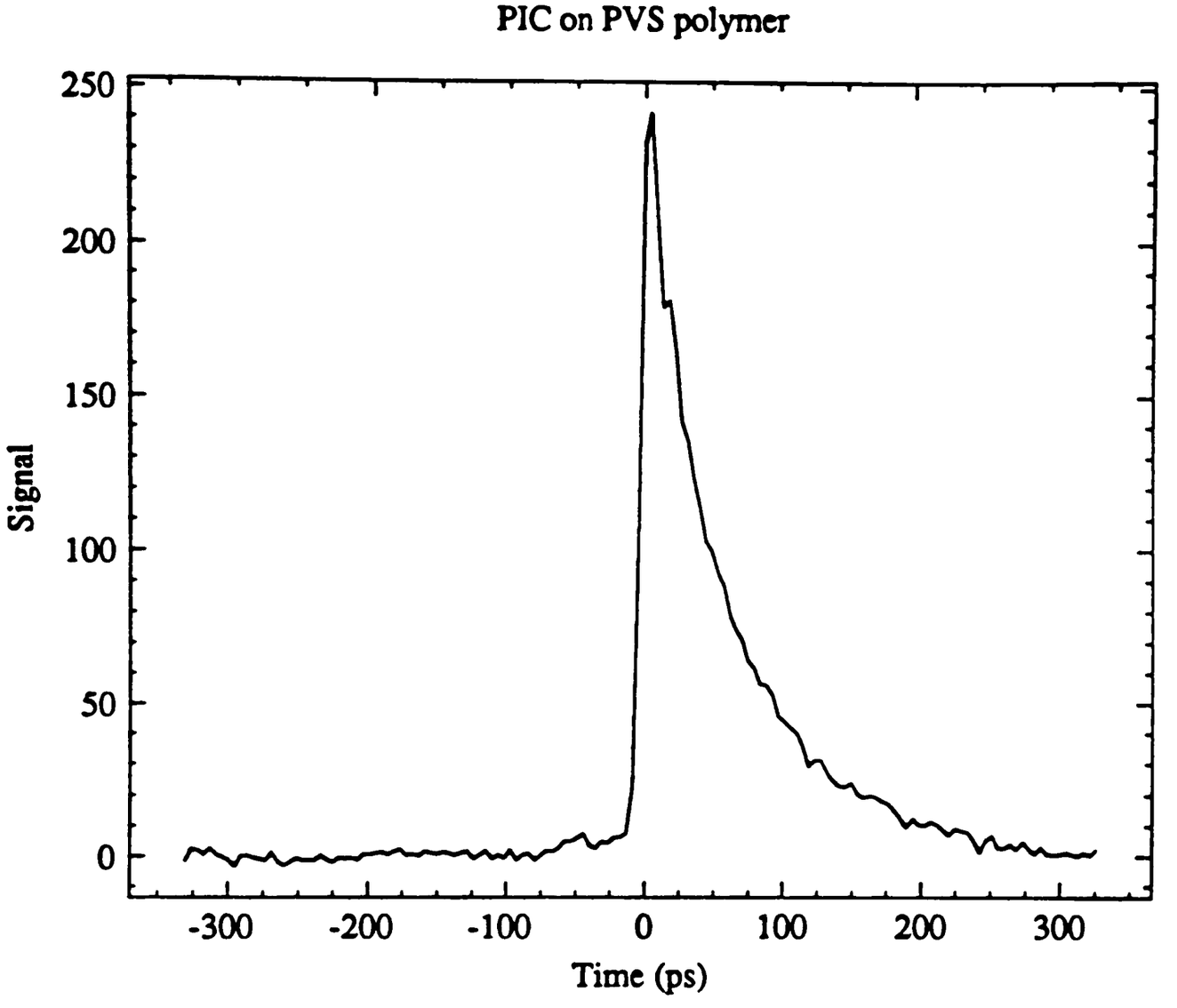

Figure 2.36. The calculated difference curve for J-aggregates in 0.05 g/dl unpurified PVS solution at 574.4 nm with excitation intensity of 1.6×10^{11} photons cm^{-2} $pulse^{-1}$.

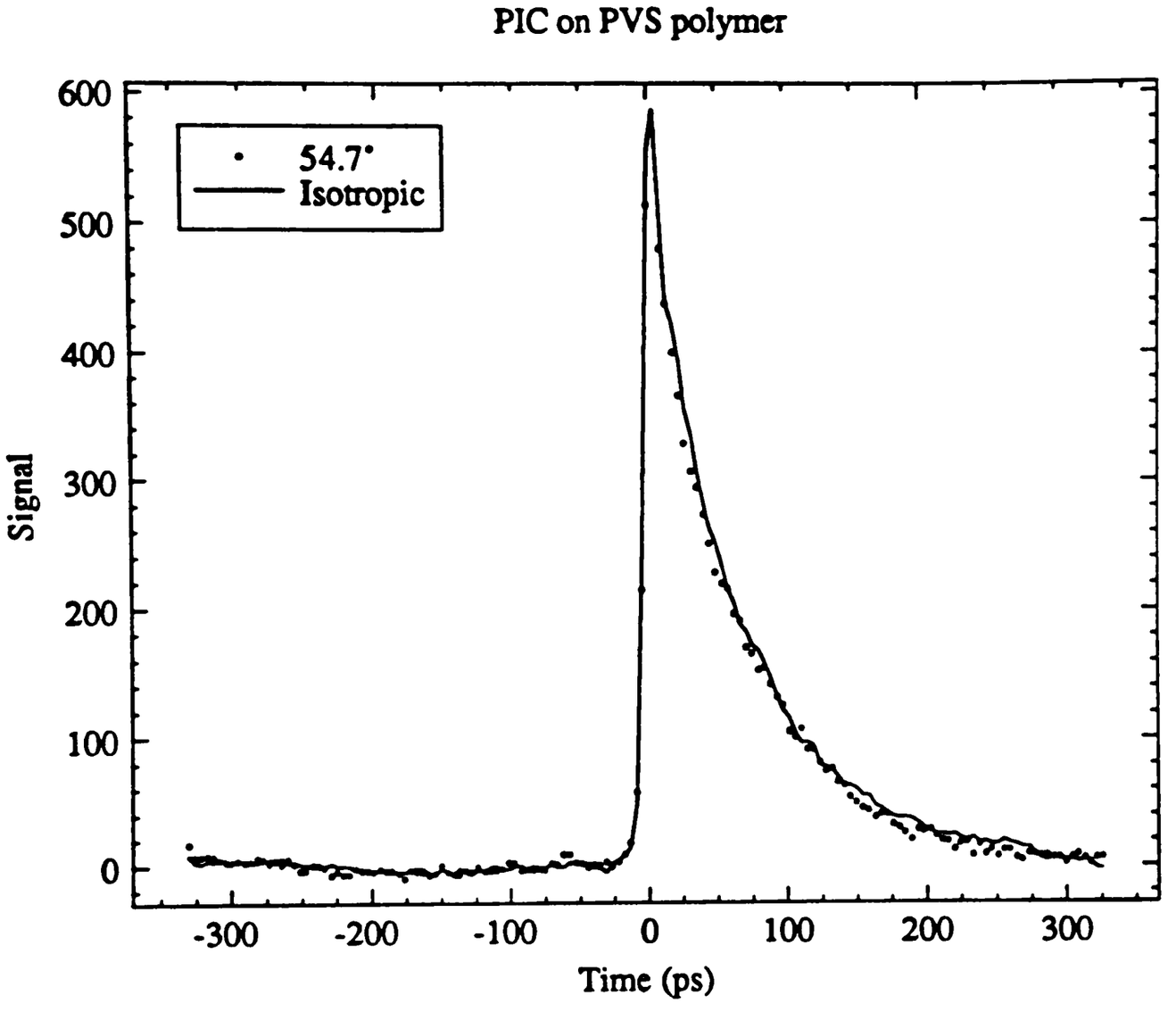

Figure 2.37. The curves isotropic and magic angle for J-aggregates in 0.05 g/dl unpurified PVS solution at 574.4 nm with excitation intensity of 1.6 x 10^{11} photons cm^{-2} $pulse^{-1}$.

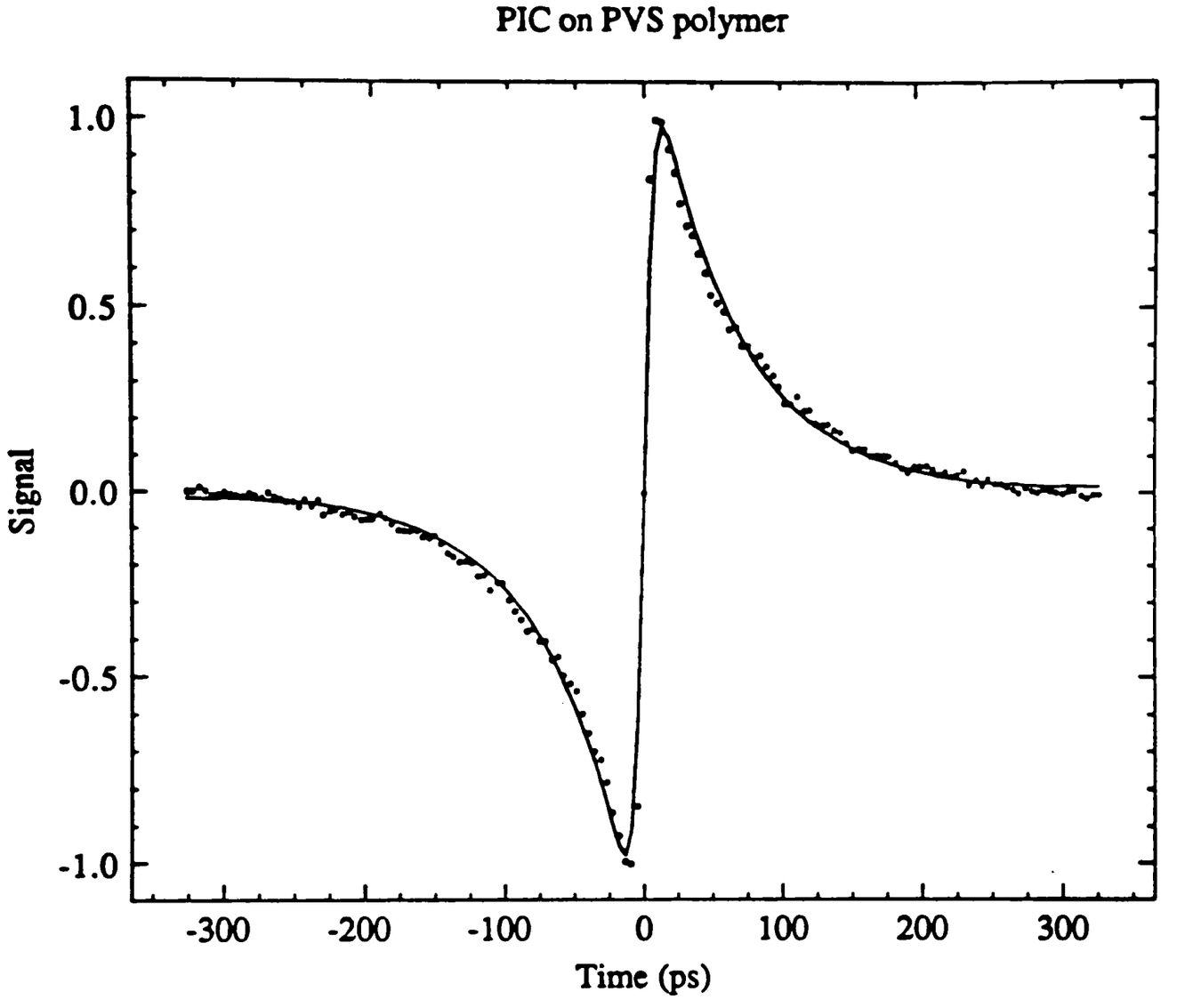

Figure 2.38. Antisymmetrized magic angle signal for J-aggregates in 0.05 g/dl unpurified PVS solution (points) and the convolution of the pulse autocorrelation with an antisymmetrized form of eq 54 (solid curve). See Table 2.6 for fitting parameters.

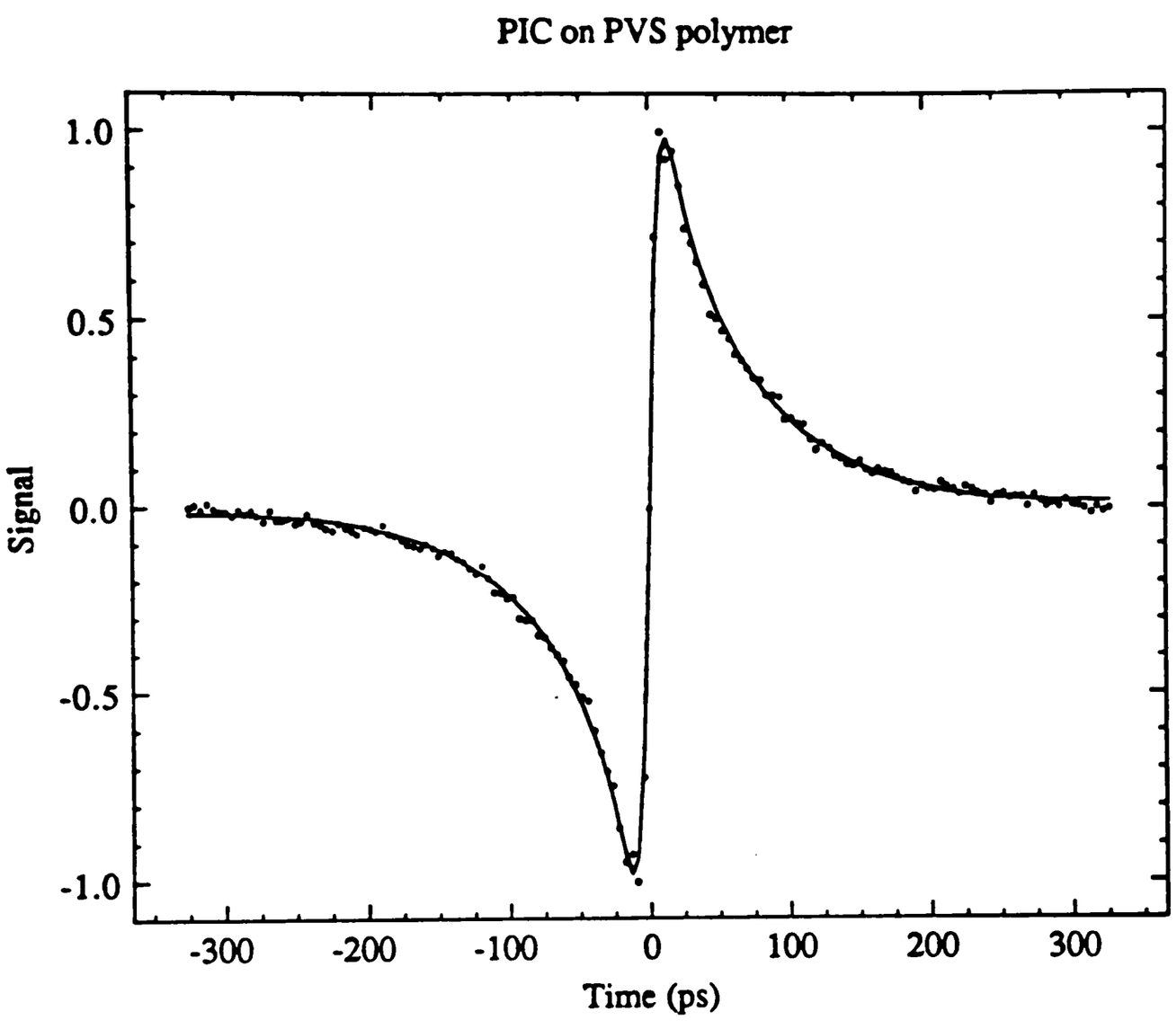

Figure 2.39. Antisymmetrized difference signal for J-aggregates in 0.05 g/dl unpurified PVS solution (points) and the convolution of the pulse autocorrelation with an antisymmetrized form of eq 56 (solid curve). See Table 2.6 for fitting parameters.

$$\frac{A_2}{A_1} = \frac{a}{1 - a}. \qquad (58)$$

The value of residual anisotropy is also determined by the order parameter, S, of the system according to:[103,104]

$$a = S^2. \qquad (59)$$

where

$$S = <\frac{3\cos^2\alpha - 1}{2}> \qquad (60)$$

where α is the angle between the symmetry axis of the aggregate and the direction of the absorption transition moment of molecules. Knowing the order parameter, the value of the angle α can then be calculated. The results are summarized in Table 2.6.

2.2.3.2. Purified PVS

The absorption spectra in Figure 2.40 show that, with progressive additions of PIC to constant concentration of purified PVS solution, the intensity of the M-bands diminished, with the J-bands increased in intensity until a maximum value was reached. Addition of further PIC resulted in supersaturation of the available PVS binding sites and hence precipitation of neutralized polymers. An analysis of the J-band of the saturated PVS solution is shown in Figure 2.41. The linewidth of the J-band is about 306 cm^{-1}, which gives a smaller aggregate size of 16 monomer units that are coherently coupled.

The transient photobleaching signals of pump-probe measurement at 560 nm with the highest intensity (3×10^{12} photons $pulse^{-1}$ sec^{-1}) used are shown in Figure 2.42. The initial bleaching is seen to decay with a pulse limited rate to a very short-lived of strongly absorbing state then following by a nonexponential decay. When the kinetic was monitored at 565 nm [Figure 2.43], sign of the signal remained

Table 2.6. Fitting parameters of transient bleaching signals for J-aggregates in 0.05 g/dl unpurified PVS solution.

Difference curve

Excitation intensity photons cm^{-2} $pulse^{-1}$	A_1	τ_1, ps	A_2	τ_2, ps	χ^2
1.6×10^{11}	0.25	14	0.75	65	4.1×10^{-4}

Magic angle curve

Excitation intensity photons cm^{-2} $pulse^{-1}$	A	τ_{gsr}, ps	a	S	α	χ^2
1.6×10^{11}	0.4	63	0.75	0.87	17°	1.3×10^{-3}

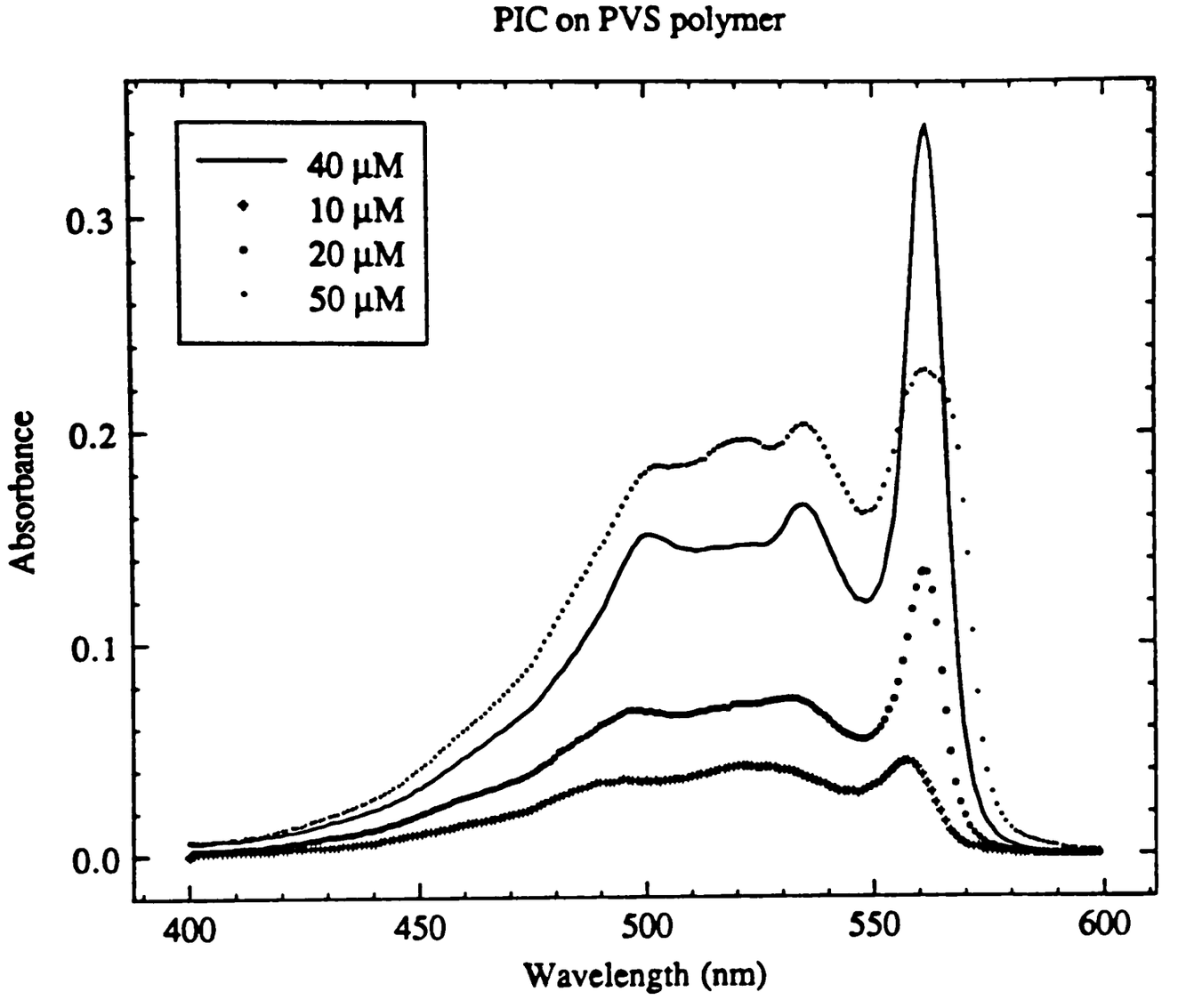

Figure 2.40. The absorption spectra of 0.5 mg/dl purified PVS solution with 10, 20, 40 and 50 µM PIC.

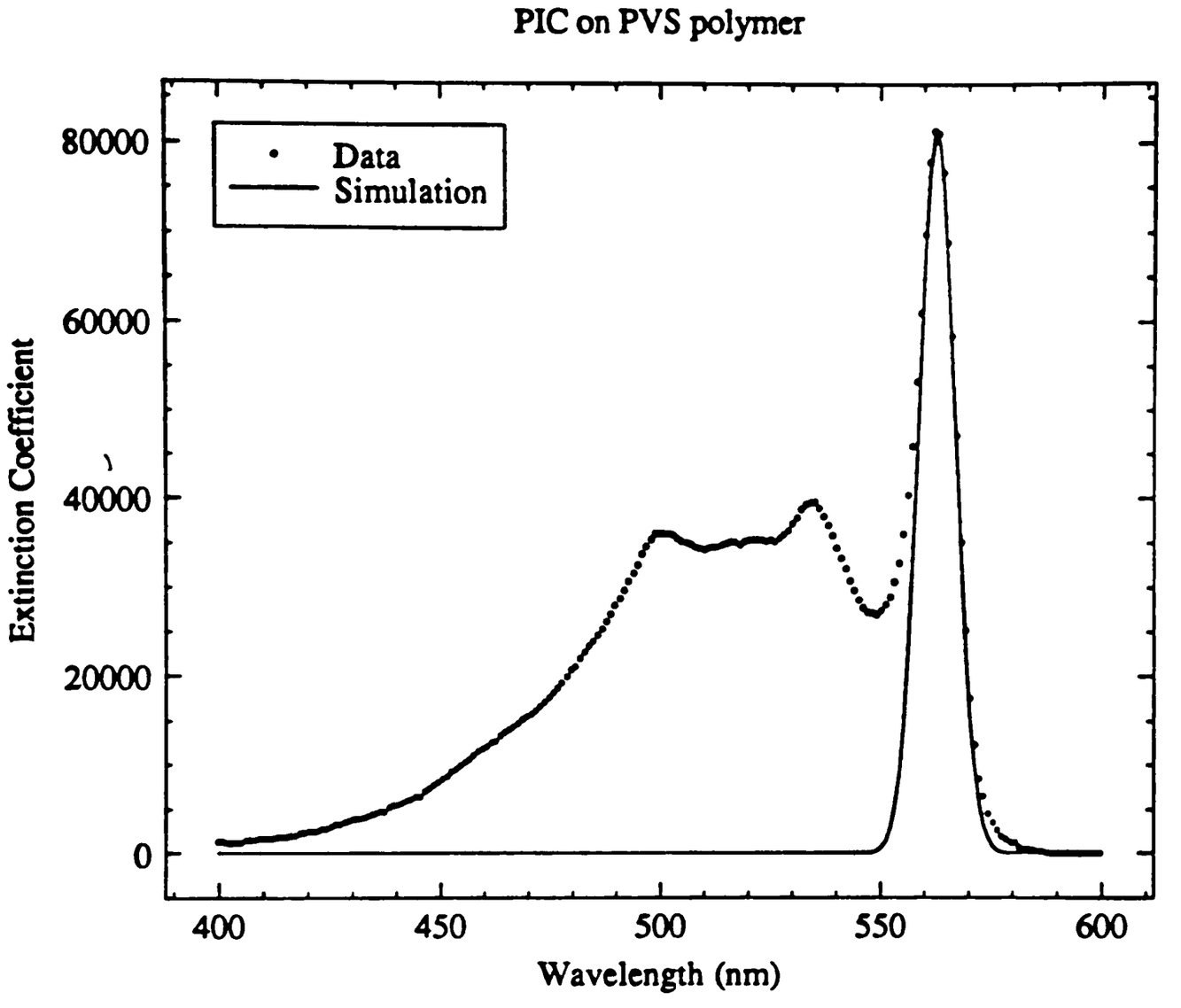

Figure 2.41. The absorption linewidth of PIC J-band for 40 μM PIC(Cl) in 0.5 mg/dl purified PVS solution.

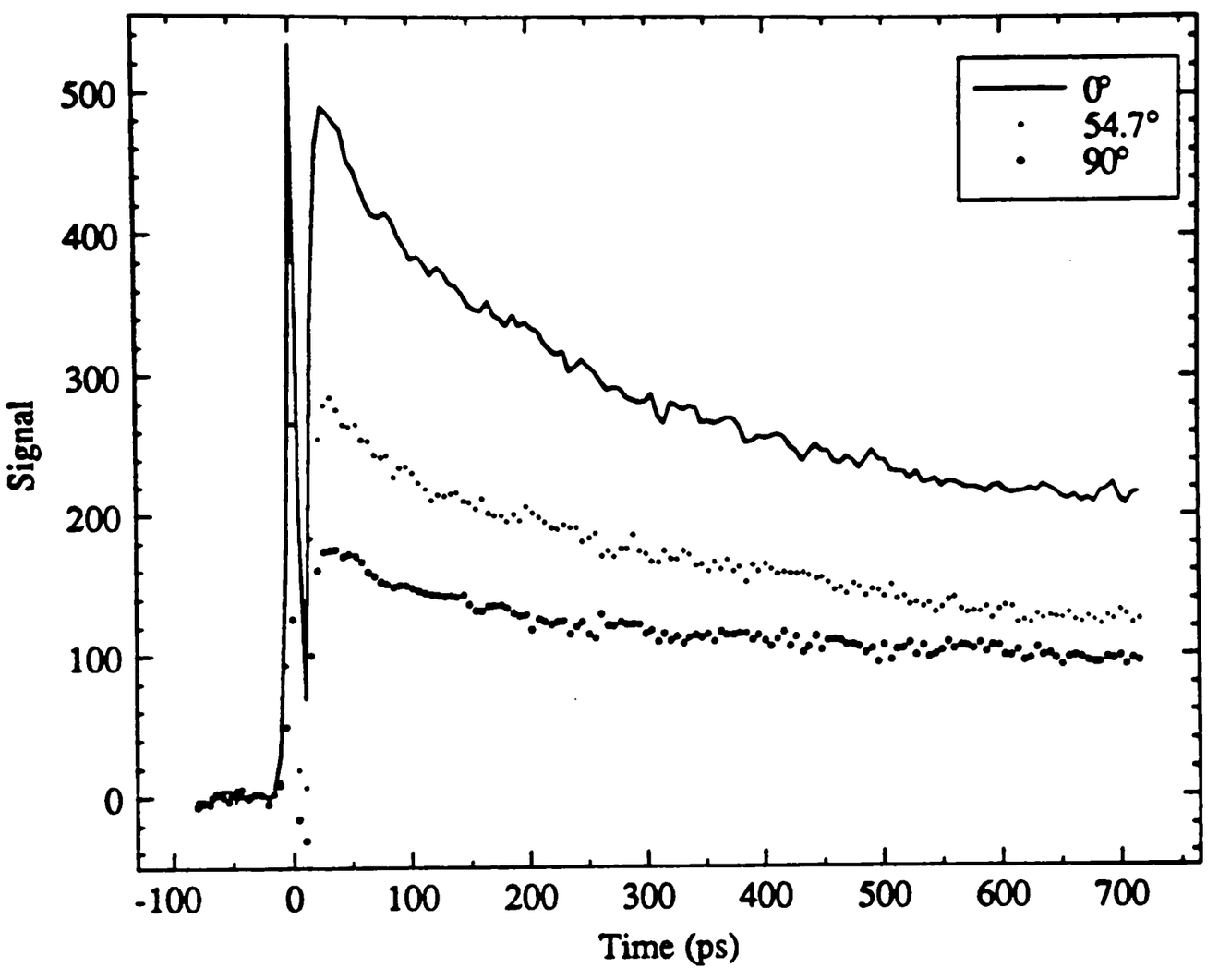

Figure 2.42. Transient bleaching signals for J-aggregates in 0.5 mg/dl purified PVS solution at 560 nm with the highest intensity used.

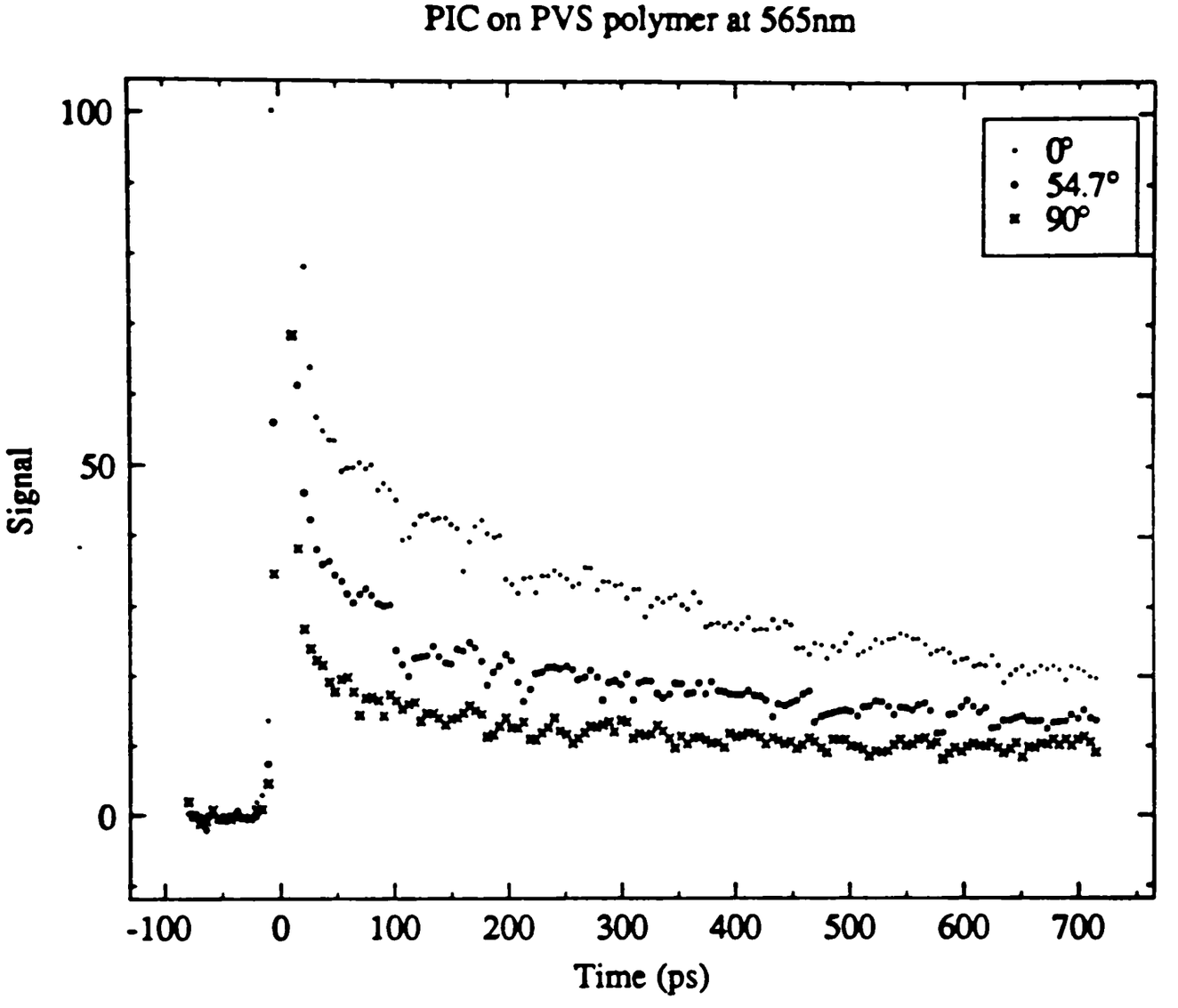

Figure 2.43. Transient bleaching signals for J-aggregates in 0.5 mg/dl purified PVS solution at 565 nm with the highest intensity used.

unchanged and the coherent spike to signal ratio became large. The excellent overlap between the curves of magic angle and isotropic is shown in Figures 2.44 and 2.45 for 560 nm and 565 nm, respectively. Reducing laser power by a factor of two, the results of these measurements gave indistinguishable $<\tau>$ and are 4240 ps and 4205 ps. Fits of signals are shown in Figures 2.46 and 2.47 and the fitting parameters are summarized in Tables 2.7 and 2.8. A detailed discussion of the decay kinetic will be given in the next section. Unfortunately, further reduction of the excitation intensity resulted in poor signals. Consequently we were unable to analyze these low quality signals.

2.3. Discussion

Cyanine dyes in solution undergo rapid torsional relaxation which induce rapid nonradiative decay,[105] and hence have low quantum yields and short excited-state lifetimes in solution. PIC monomers are practically non-fluorescent in fluid solvents at room temperature.[106-108] A lifetime of 15 ± 3 ps was measured for the ground state recovery time for PIC monomers.[109,110] Upon cooling fluorescence is observed with decay time increasing to a value of 1,734 ps at 84 °K.[111] In very high viscosity solvents or adsorption onto a surface can inhibit the torsional-induced nonradiative decay channel,[112,113] thereby increasing the excited state lifetime of the molecule. PIC aggregates fluoresce strongly at room temperature. The fluorescence quantum yield of the monomers is smaller than 10^{-3}, but that of the J-aggregate band amounts to 30%.[114] However, the very strong reabsorption of the aggregate fluorescence usually lead to prolonged decay times in fluorescence decay measurements.[115] Stiel and Sundström found unequivocal evidence that the disparity in the reported values of the excited-state lifetime of J-aggregates of PIC in

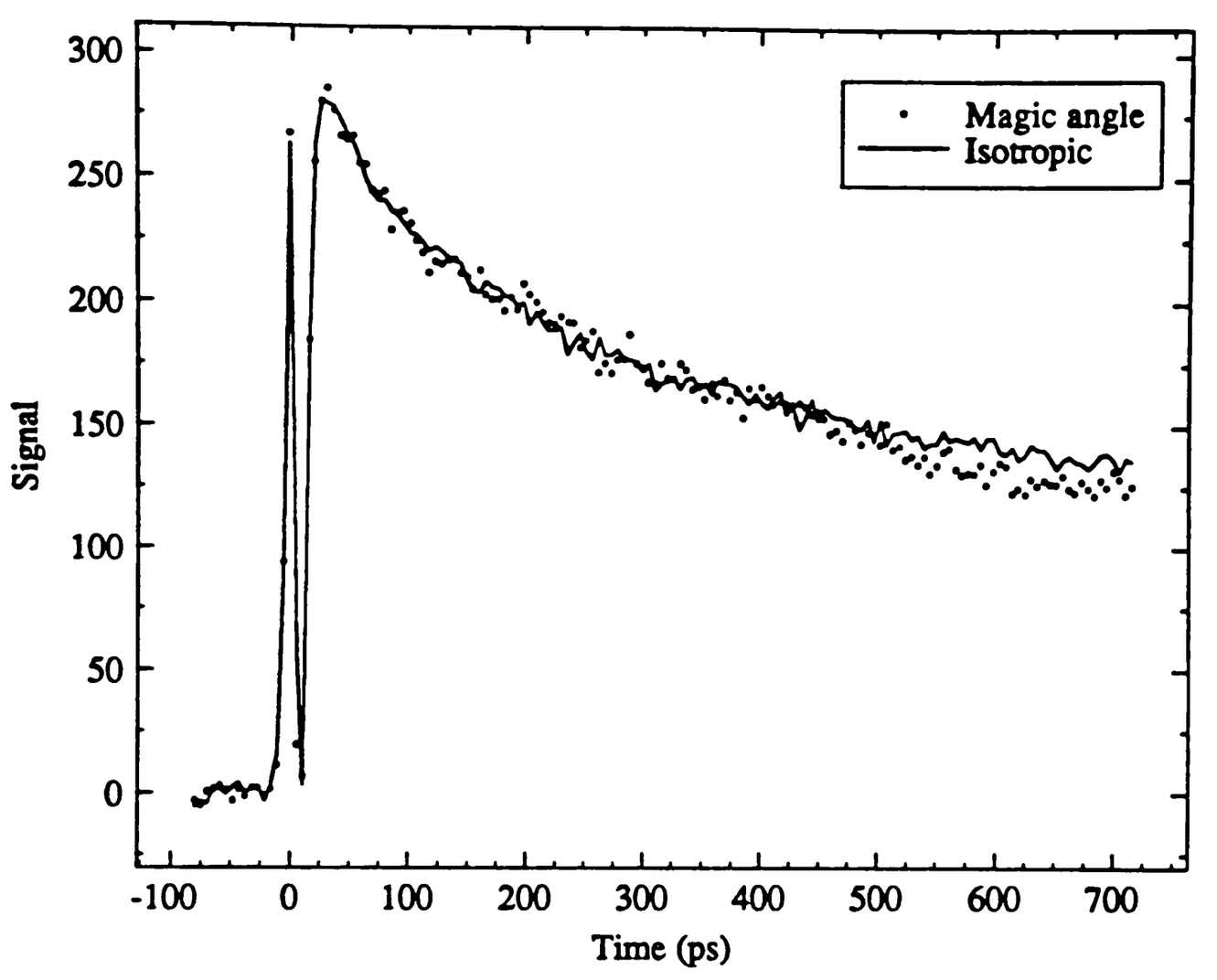

Figure 2.44. The curves isotropic and magic angle for J-aggregates in 0.5 mg/dl purified PVS solution at 560 nm with excitation intensity of 3.0×10^{12} photons cm^{-2} $pulse^{-1}$.

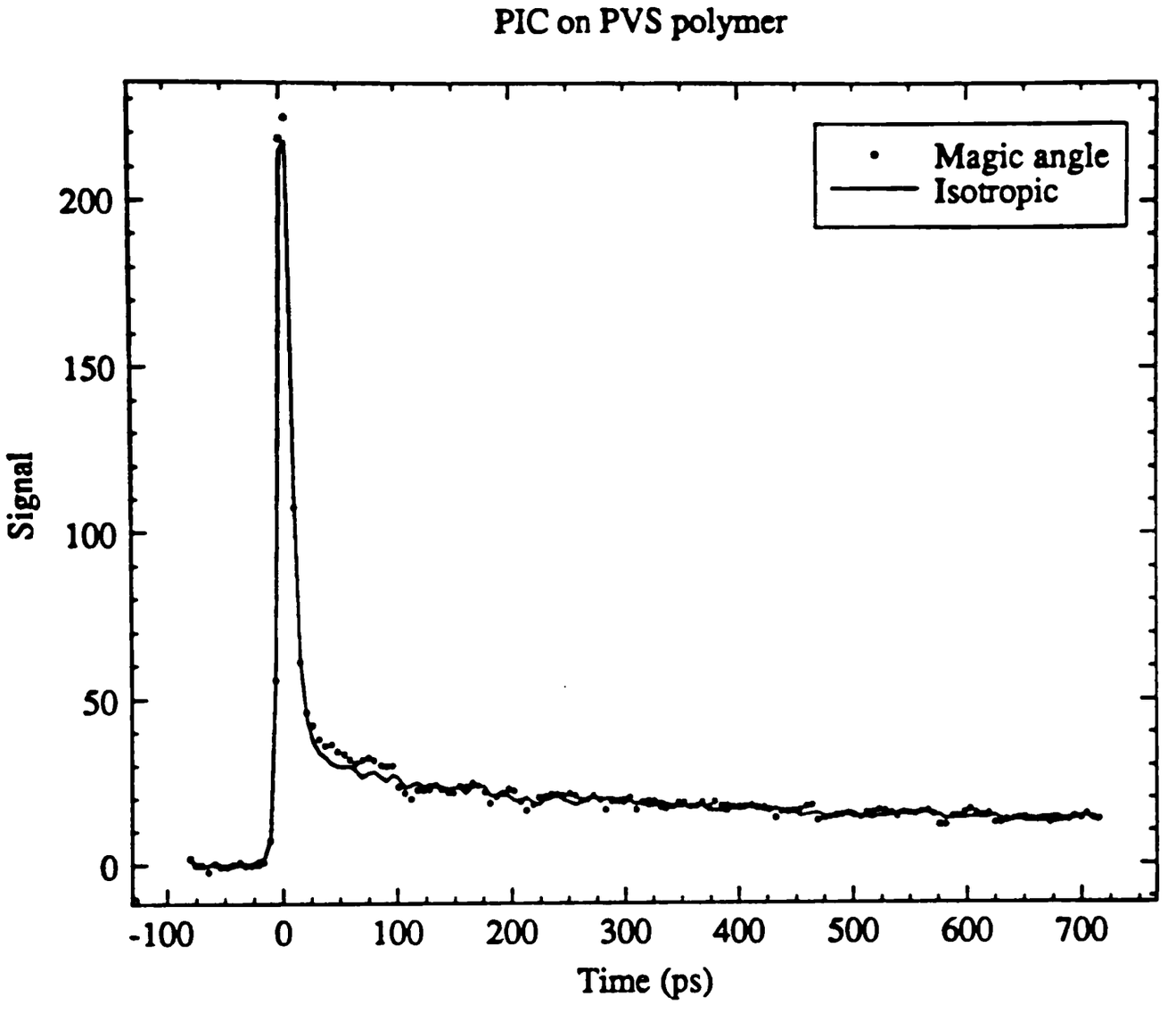

Figure 2.45. The curves isotropic and magic angle for J-aggregates in 0.5 mg/dl purified PVS solution at 565 nm with excitation intensity of 3.0×10^{12} photons cm^{-2} $pulse^{-1}$.

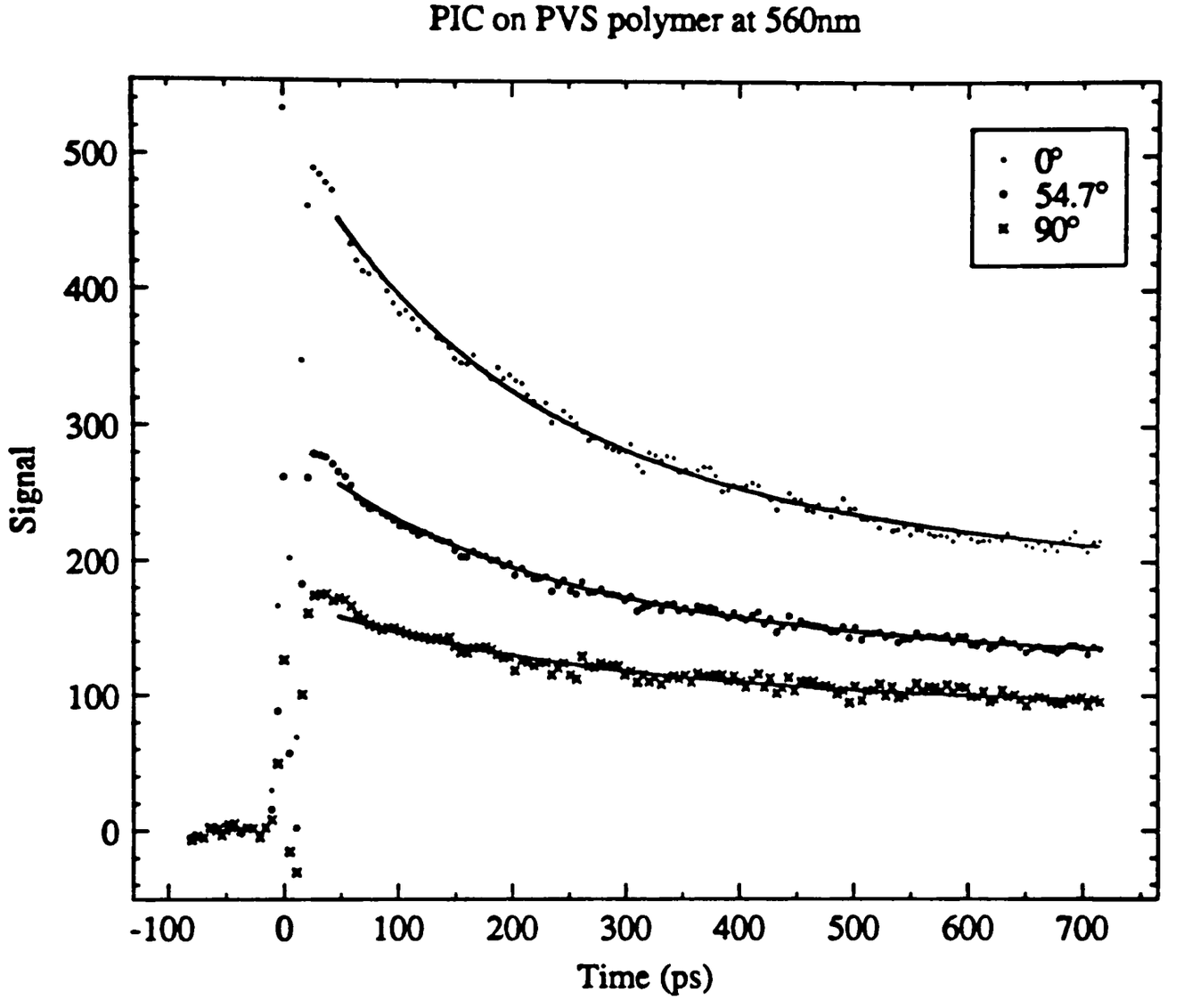

Figure 2.46. Fits of transient bleaching signals for J-aggregates in 0.5 mg/dl purified PVS solution with the polarization of the probe beam parallel, 54.7°, and perpendicular to the polarization of the pump beam at 560 nm. See Table 2.7 for fitting parameters.

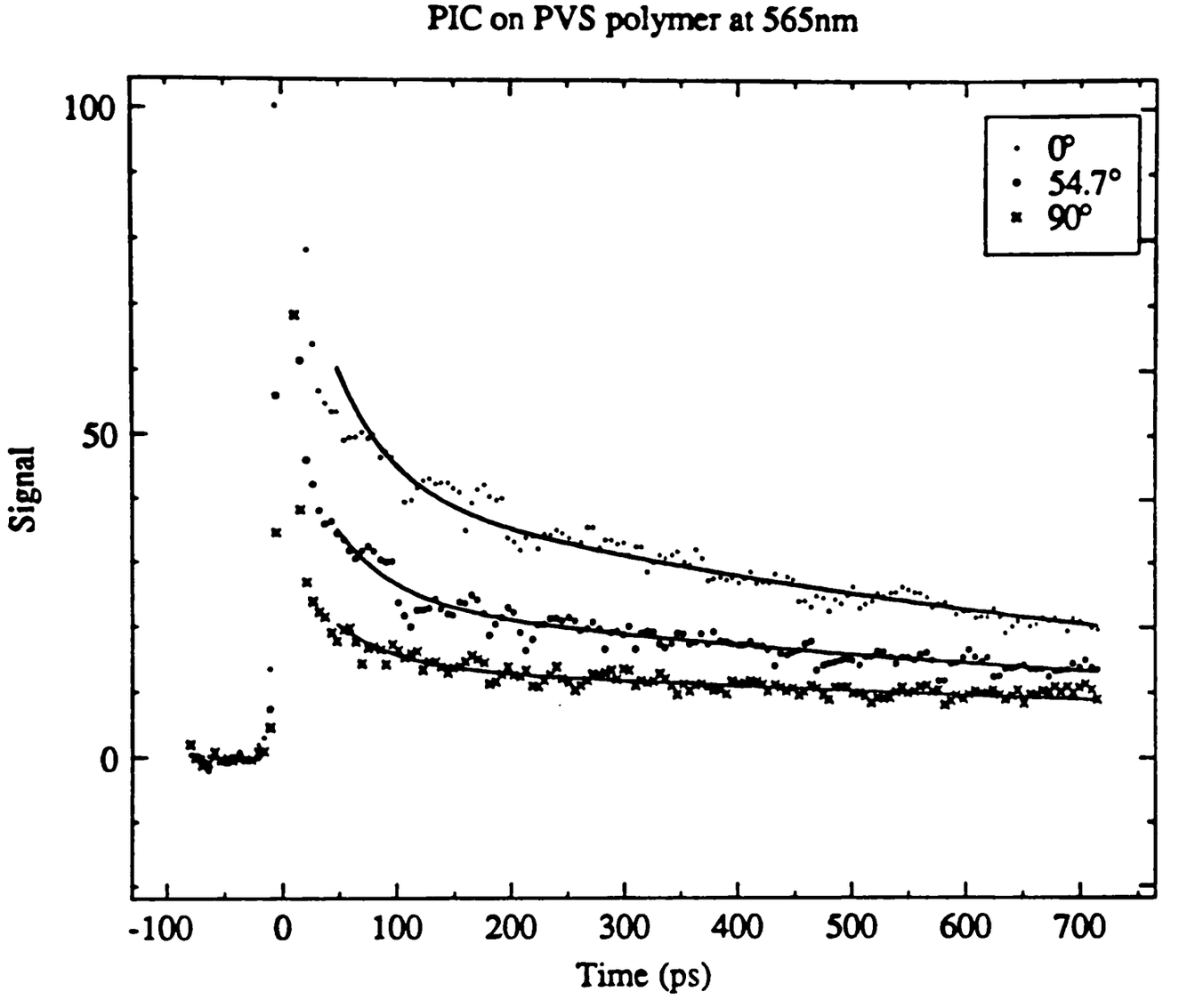

Figure 2.47. Fits of transient bleaching signals for J-aggregates in 0.5 mg/dl purified PVS solution with the polarization of the probe beam parallel, 54.7°, and perpendicular to the polarization of the pump beam at 565 nm. See Table 2.8 for fitting parameters.

Table 2.7. Fitting parameters of transient bleaching signals for J-aggregates in 0.5 mg/dl purified PVS solution at 560 nm.

Excitation intensity photons cm^{-2} $pulse^{-1}$	A_1	τ_1, ps	A_2	τ_2, ps	χ^2
3.0×10^{12}	0.46	198	0.54	4395	10.2
1.5×10^{12}	0.4	202	0.6	4335	5.9

Excitation intensity photons cm^{-2} $pulse^{-1}$	A	τ_{depol}, ps	a	χ^2
3.0×10^{12}	114.8	251	0.69	24.8

Table 2.8. Fitting parameters of transient bleaching signals for J-aggregates in 0.5 mg/dl purified PVS solution at 565 nm.

Excitation intensity photons cm^{-2} $pulse^{-1}$	A_1	τ_1, ps	A_2	τ_2, ps	χ^2
3.0×10^{12}	0.54	50	0.46	1157	2.3

Excitation intensity photons cm^{-2} $pulse^{-1}$	A	τ_{depol}, ps	a	χ^2
3.0×10^{12}	20.5	1545	0.32	2.8

solution is due to excitation-intensity-dependent decay kinetics.[116,117] Their study of the excitation-intensity dependence of pump-probe signals lends support to the earlier work of Brumbaugh et al.,[101] who showed that the excitation-intensity dependence of the nonexponential fluorescence decay can be explained by singlet-singlet exciton annihilation.

The transient photobleaching signals for J-aggregates in concentrated aqueous solutions of sodium chloride decay faster as the excitation intensities is increased. The excitation-intensity dependence of the decay kinetics of J-aggregates in solution indicates that exciton annihilation is occurring. They decay nonexponentially at high excitation intensities but exponentially at very low excitation intensities. Using an analysis based on an exciton annihilation model, Sundström[117] and co-workers deduced from their kinetic measurements that J-aggregates in solution contain 20,000-50,000 monomer units. They find that exciton annihilation occurs for laser intensities as low as $\approx 10^{11}$ photons cm^{-2} $pulse^{-1}$ and attribute this efficiency of annihilation to the very large size of the aggregates. However, an analysis of the absorption linewidth of the J-band gives an aggregate size of 60 monomer units. These results imply that the number of coherently coupled molecules in the aggregate is less than the actual number of molecules in the aggregate. The excitation is localized in a small domain of molecules in the aggregate. The decay of the anisotropy for J-aggregates in solution is caused by the migration of excitation from one domain of molecules to another domain in the aggregate.

Although the laser intensities used in our experiments are comparable to those used by Sundström et al.,[117] the transient photobleaching signals at 570 nm from J-aggregates of PIC on colloidal silica are independent of the excitation intensity and can be well-fitted by a biexponential decay function consisting of short and long

components. The absence of an intensity dependence indicates that exciton annihilation is not occurring. This is due to the fact that the J-aggregates of PIC are considerably smaller on colloidal silica than in solution. We attribute this difference to the fact that the J-aggregates on colloidal silica are smaller in size than the excitation wavelength. Their maximum size is limited by the finite number of binding sites on a colloid particle, which at pH 10.4 is 60–65.[118] The ratio of the concentration of dye to the concentration of colloid particles is 0.027 in a sample of 50 μM PIC in 7.5% colloidal silica. Hence, the number of coherently coupled molecules corresponds very closely to the actual number of molecules in the aggregate. Aggregation at such low coverages on colloidal silica occurs because of the favorable dispersion interactions between dye molecules in competion with the clustered tendency of dye cations to the negatively charged surface of colloidal silica. Transient photobleaching of the J-band in concentrated aqueous solutions (10^{-3} - 10^{-2} M) of PIC was previously studied by picosecond laser techniques.[109,110] The signals exhibited a rapid initial decay with a time constant of 15±3 ps and a very small residual decay with a much longer time constant (< 1 ns). It was suggested in these earlier studies of J-aggregates in solution that a distribution of aggregates was present.[109,110] Thus, the observed signals were the result of a distribution of aggregates each relaxing with different lifetimes. If one assumes that the J-band is homogeneously broadened, a mean exciton radiative lifetime of ≈ 1 x 10^{-4} second can be estimated from the 15-nm line width of the J-band. However, the lifetime calculated from the line width is less than the measured decay time, implying that the J-band is inhomogeneously rather than homogeneously broadened. A inhomogeneously broadened line is consistent with a distribution of relaxation times corresponding to different aggregates. The fact that relaxation times obtained from

the biexponential function was considerably longer than the lifetime calculated from the width of the J-band of colloidal silica system lends credence to the speculation that the nonexponential behavior arises from a distribution of J-aggregates with different relaxation times.

Another property that distinguishes the J-aggregates of PIC on colloidal silica from those in solution is the absorption anisotropy. The decay of absorption anisotropy is a measure of the rotation of the probed transition moment. Two sources of depolarization that can contribute to the decay of absorption anisotropy are molecular reorientation and exciton transport.[41,119] Because the J-aggregates in solution are large, molecular reorientation does not contribute to the decay of the anisotropy. In the case of J-aggregates on colloidal silica, binding of the dye molecules to the surface of the colloid inhibits molecular reorientation. Although the rotation of the colloid particles can contribute to the decay of the anisotropy, this motion is too slow to cause any change in the anisotropy in less than 300 ps. Using the Debye-Stokes-Einstein formula,[120]

$$\tau_{rot} = \frac{\eta V_{hyd}}{K_B T}, \qquad (61)$$

where V_{hyd} is the volume of a sphere rotating in a liquid with viscosity η, K_B is the Boltzmann constant, and T is the absolute temperature, we estimate that the rotational time τ_{rot} of a 40-Å-diameter colloid in water at room temperature is $\approx$ 7 ns. Exciton transport must therefore be the reason that the anisotropy decays for J-aggregates in solution but is constant for J-aggregates on colloidal silica. If the exciton interactions are greater than the exciton-phonon coupling, the exciton is delocalized.[121,122] If the exciton-phonon coupling is greater than exciton interactions, the exciton becomes localized on a single molecule of the aggregate. The J-band in the spectrum of PIC in

solution and on colloidal silica is a manifestation of excitons that are delocalized at the moment the light is absorbed. In our experiments and in the experiments of Sundström et al.,[117] the transition moment that is initially excited is probably that of a delocalized exciton in a small aggregate. For J-aggregates in solution, exciton hopping can occur between the loosely linked smaller aggregates. We expect this aggregate chain to have bends, as perhaps in a coiled polymer. As the exciton migrates down the chain, the probed transition moment will inevitably change its direction, causing the anisotropy to decay. In our experiments of aggregates on colloidal silica, exciton hopping between aggregates cannot occur, because most of the aggregates are bound to isolated colloids. Hence, the direction of the probed transition moment cannot change and the anisotropy remains constant.

The anisotropies of the two different colloidal silica systems are both constant. However, a lower value of 0.3 was observed for sample L. This value is less than the maximum theoretical value of 0.4. Cross and co-workers[123] showed that, in the presence of overlapping, coupled electronic states with different transition moments, the anisotropy initially decays rapidly. Thus, in J-aggregates of sample L, transitions between exciton states with different transition moments could cause the rapid decay of r(t). If the final result of a transition were a delocalized exciton, the anisotropy would not decay to zero but would remain at a high value. Unfortunately, the time resolution of our current apparatus is insufficient to observe a rapid component of the anisotropy decay. Careful time and frequency resolved experiments must be performed to resolve the uncertainty in the early time behavior of the anisotropy in J-aggregates of PIC on colloidal silica.

It is clear from our results that the ground state recovery of J-aggregates on colloidal silica after excitation to the first excited singlet S_1 cannot be described by a

single pathway of radiationless decay. Ground state recovery time is considerably longer than the lifetime of the fluorescent state, though we are unable to resolve fluorescence which decays with a lifetime much less than 185 ps, the FWHM of the instrumental response function. However, the presence of adsorbed transition-metal ions do not shorten the decay time. Thus, we rule out triplet state decay as a possible mechanism for causing the long decay component in our signals. Recently, the time-resolved fluorescence from the J-aggregates of 5,5'-dichloro-3,3'-disulfopropyl-9-ethylthiacarbocyanine adsorbed on silica gel was measured with a time-correlated single photon counting apparatus with higher time resolution than ours.[124] The decay time was 25 ps and independent of the excitation intensity. The size of these aggregates was estimated to be less than 50 monomer units. Thus, it is not surprising that the singlet-state dynamics of J-aggregates of this dye adsorbed on silica gel and of PIC adsorbed on colloidal silica are similar.

By adding polyanions to dilute aqueous solution of cationic dyes the dye molecules were held sufficiently close together on the surface of the polyanion to allow them to interact to form aggregates similar to those formed in a concentrated solution of the dye. A polymer such as PVS contains many single bonds, around which rotation is possible. If the configurations around sucessive carbon atoms are independent and unrelated, it will be seen that two parts of the polymer chain more than a few carbon atoms apart are essentially uncorrelated in regard to direction in space. The molecule is then statistically coiled and resembles a loose tangle of yarn. The absorption spectra of J-aggregates on purified and unpurified PVS seem inconsistent with the measured average molecular weight of purified and unpurified PVS polymers. It looks like purified PVS polymers have higher molecular weight, but J-aggregates on these polymers are smaller in size. To understand the difference

between the absorption spectra of dyes on purified and unpurified polymers we have to consider the following facts. The PVS polymer was purified by the method of precipitation and hence difficult to prevent fractionation. Thus, the molecular weight of purified polymer has a narrower distribution but unnecessarily the highest molecular weight of polymers. The dye molecule prefers to attach to sites adjacent to those already occupied by dye ions rather than randomly attach to available sites. The highest molecular weight polymers have more binding sites and hence a better chance to be attached by dye molecules. In unpurified PVS solution, the J-aggregates are most likely created on the highest molecular weight polymers. The molecular weight of polymers determined in section 2.1.1. was only the average molecular weight. Hence, the size of J-aggregates in unpurified PVS solution is actually bigger than those in purified PVS solution but the average molecular weight of purified PVS polymers are higher than those of unpurified PVS polymers.

The experimental results of J-aggregates on unpurified PVS polymers at low excitation intensity are very straightforward. The results of our experiments show that our dynamic measurements are consistent with the spectral results, and transient bleaching signals of the system are both wavelength and power dependent. The excited state of the system is densely spaced. Exciton-exciton annihilation occurs in the system. The dynamics of energy migration involves localized excitons in the system.

To analyze the decays for J-aggregates on unpurified PVS at high intensity turned out to be difficult. However, the wavelength dependent properties of a positive (absorption) and a negative (bleaching) signal levels can be qualitatively explained by the following model. We will first divide the kinetic curve of Figure 2.48 into three regions and then discuss each region in detail and relate to the

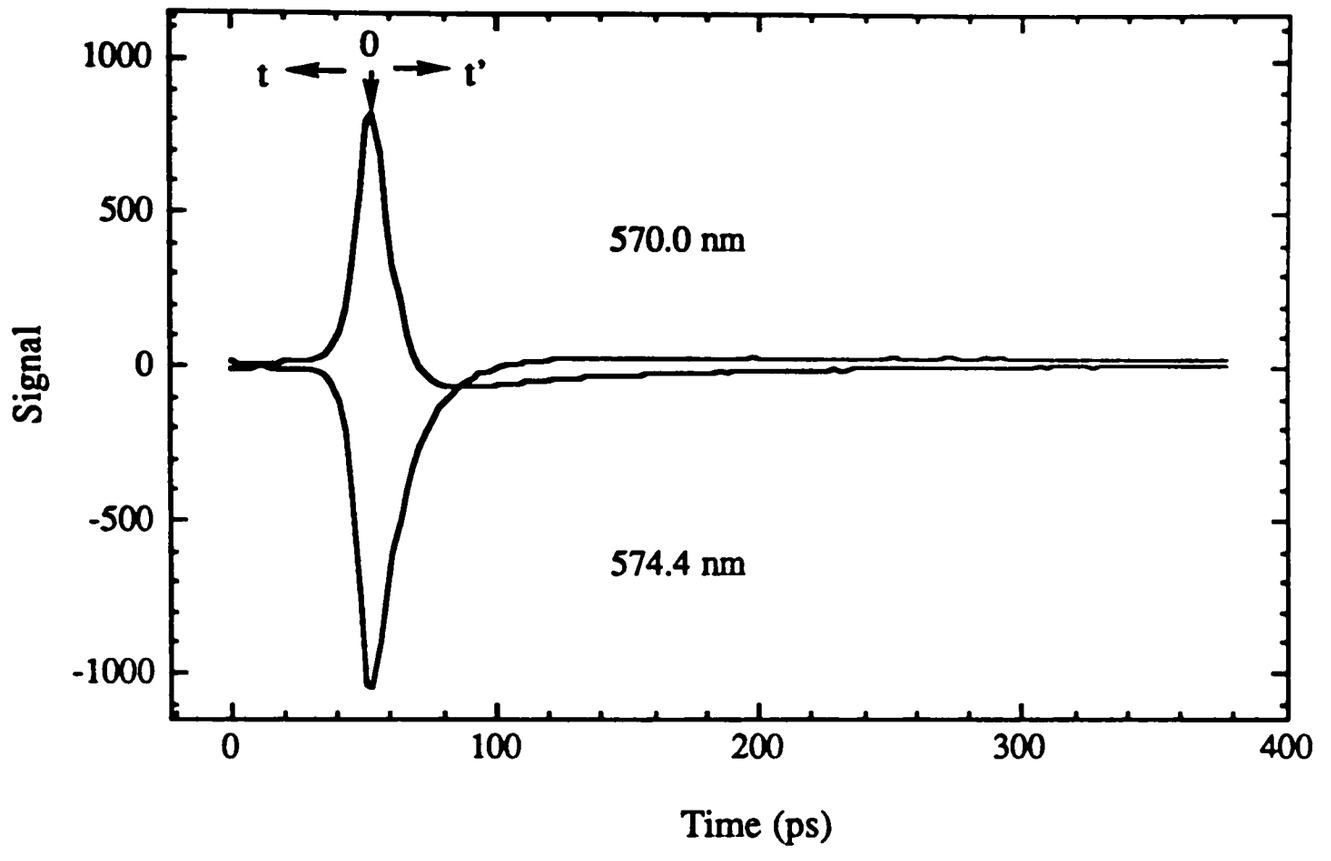

Figure 2.48. Kinetic curves for 100 μM PIC in 0.05 g/dl unpurified PVS at highest excitation intensity.

experimental observations. If the ground state extinction coefficient of the sample at the wavelength λ is denoted as ε_0, then the optical density OD(-t) of the sample at time t prior to the arrival of the pump pulse can be written in the form

$$OD(-t) = \varepsilon_0[S_0](-t) \tag{62}$$

where $[S_0](-t)$ is the ground state population at time t prior to the arrival of the pump pulse, and the effective optical pathlength has been omitted for simplification. Therefore, the optical density OD(0) at the arrival of pump pulse becomes

$$OD(0) = \varepsilon_0[S_0](0) + \varepsilon_1[S_1](0) \tag{63}$$

where ε_1 is the excited state extinction coefficient of the sample at the wavelength λ, and $[S_0](0)$ and $[S_1](0)$ are, respectively, the ground state and the excited state population at the arrival of pump pulse, and the conservation of matter gives the relation

$$[S_0](-t) = [S_0](0) + [S_1](0). \tag{64}$$

Hence, the optical density changes $\Delta OD(0)$ of the sample due to excitation can be expressed as

$$\Delta OD(0) = OD(0) - OD(-t) \tag{65}$$

$$= \varepsilon_0[S_0](0) + \varepsilon_1[S_1](0) - \varepsilon_0[S_0](-t) \tag{66}$$

$$= \varepsilon_1[S_1](0) + \varepsilon_0\{[S_0](0) - [S_0](-t)\}. \tag{67}$$

If we assume $\varepsilon_1[S_1](0) > |\varepsilon_0\{[S_0](0) - [S_0](-t)\}|$ at 570 nm, then $\Delta OD(0) > 0$, and the initial signal at 570 nm becomes an absorption as the experimental result. For the initial bleaching signal at 574.4 nm, $\Delta OD(0) < 0$, and $\varepsilon_1[S_1](0) < |\varepsilon_0\{[S_0](0) - [S_0](-t)\}|$. Therefore, $\varepsilon_0 > \varepsilon_1$ at 574.4 nm and $\varepsilon_0 < \varepsilon_1$ at 570 nm.

In the kinetic curve measured at 570 nm with the highest excitation intensity used, there is an initial fast recovery to a negative signal level, followed by a slower decay of the negative signal. As discussed previously, the fast recovery is attributed

to the singlet-singlet exciton annihilation. It is possible that a small fraction of the singlet-singlet exciton annihilation may lead to the following reaction

$$S_1 + S_1 \rightarrow S_0 + S_0 + \text{bottleneck.} \qquad (68)$$

This bottleneck can be formed by the phtoionization of aggregate and the temporarily trapped electron. Oxidation of the excited dye adsorbed on silver halide microcrystals by coadsorbed or diffusing oxygen has recently been observed by electron paramagnetic resonance (EPR) measurements.[125] The dye cation formed by this mechanism might act as an exciton trap and reduce the fluorescence lifetime. Thus, we propose that a bottleneck state is formed following the excited state annihilation in the system. If we assume that the bottleneck state has a population $[S_B](t')$ at time t' after the arrival of the pump pulse and extinction coefficient ε_B at wavelength λ, then OD(t') can be expressed as

$$OD(t') = \varepsilon_0[S_0](t') + \varepsilon_1[S_1](t') + \varepsilon_B[S_B](t'). \qquad (69)$$

The optical density changes $\Delta OD(t)$ of the sample after the excitation becomes

$$\Delta OD(t') = OD(t') - OD(-t) \qquad (70)$$

$$= \varepsilon_0[S_0](t') + \varepsilon_1[S_1](t') + \varepsilon_B[S_B](t') - \varepsilon_0[S_0](-t) \qquad (71)$$

$$= \varepsilon_0\{[S_0](t') - [S_0](-t)\} + \varepsilon_1[S_1](t') + \varepsilon_B[S_B](t'). \qquad (72)$$

The fast decay of the absorption at 570 nm is then caused by the rapidly decay of the highly absorbing of singlet excited sate due to exciton annihilation and the formation of the low absorbing bottleneck state. Finally, the slower decay rate is governed by the slow return of population from the bottleneck to the ground state and excited state decay. From the slower decay of the bleaching signal at 570 nm we deduce that $\varepsilon_B < \varepsilon_0 < \varepsilon_1$ at 570 nm. The same for the kinetic curve at 574.4 nm except that the rapid decay of the bleaching is caused by depopulation of the low absorbing excited state

and formation of the strongly absorbing bottleneck state. From the long-lived absorption tail at 574.4, we obtain that $\varepsilon_B > \varepsilon_0 > \varepsilon_1$ at 574.4 nm.

In a system as complex as this, there are of course other possible mechanisms which may also explain our observed ground state recovery. Hence, transient absorption measurements at these wavelengths are needed for further proof of this explanation. The formation of ionized aggregate can, in principle, be examined by using the accumulated photon echo technique.[10]

Pump-probe signals of J-aggregates on purified PVS polymer turn out all measured at high power region [Figure 2.49] that all signals exhibit singlet-singlet exciton annihilation. It is difficult to analyze the complicated decay kinetics of J-aggregates on purified PVS. However, the wavelength dependent properties can be qualitatively understood by the following energy level schemes [Figures 2.50 and 2.51]. The energy level diagram, shown in Figure 2.50, results in the following kinetic equations, neglecting the fast absorption rate:

$$\frac{d[N_1]}{dt} = -[N_1]k_r - [N_1]k_1 - [N_1]k_2 \tag{73}$$

$$\frac{d[N_B]}{dt} = [N_1]k_2 - [N_B]k_3 \tag{74}$$

$$\frac{d[N_0]}{dt} = [N_1]k_r + [N_1]k_1 + [N_B]k_3. \tag{75}$$

The symbols are explained in Figure 2.50. Immediately after the excitation pulse, at t = 0, $[N_1](0) = N_1 \neq 0$ and $[N_0](0) = N_0 - N_1$ where N_0 is the initial ground state population. These equations give the population in each level at any time, $t \geq 0$.

$$[N_1](t) = N_1 \exp(-k_S t) \tag{76}$$

$$[N_B](t) = \frac{k_2 N_1}{k_3 - k_S} \{\exp(-k_S t) - \exp(-k_3 t)\} \tag{77}$$

$$[N_0](t) = N_1 K_S(t) + N_0 \tag{78}$$

where $k_S = k_1 + k_2 + k_r$

and

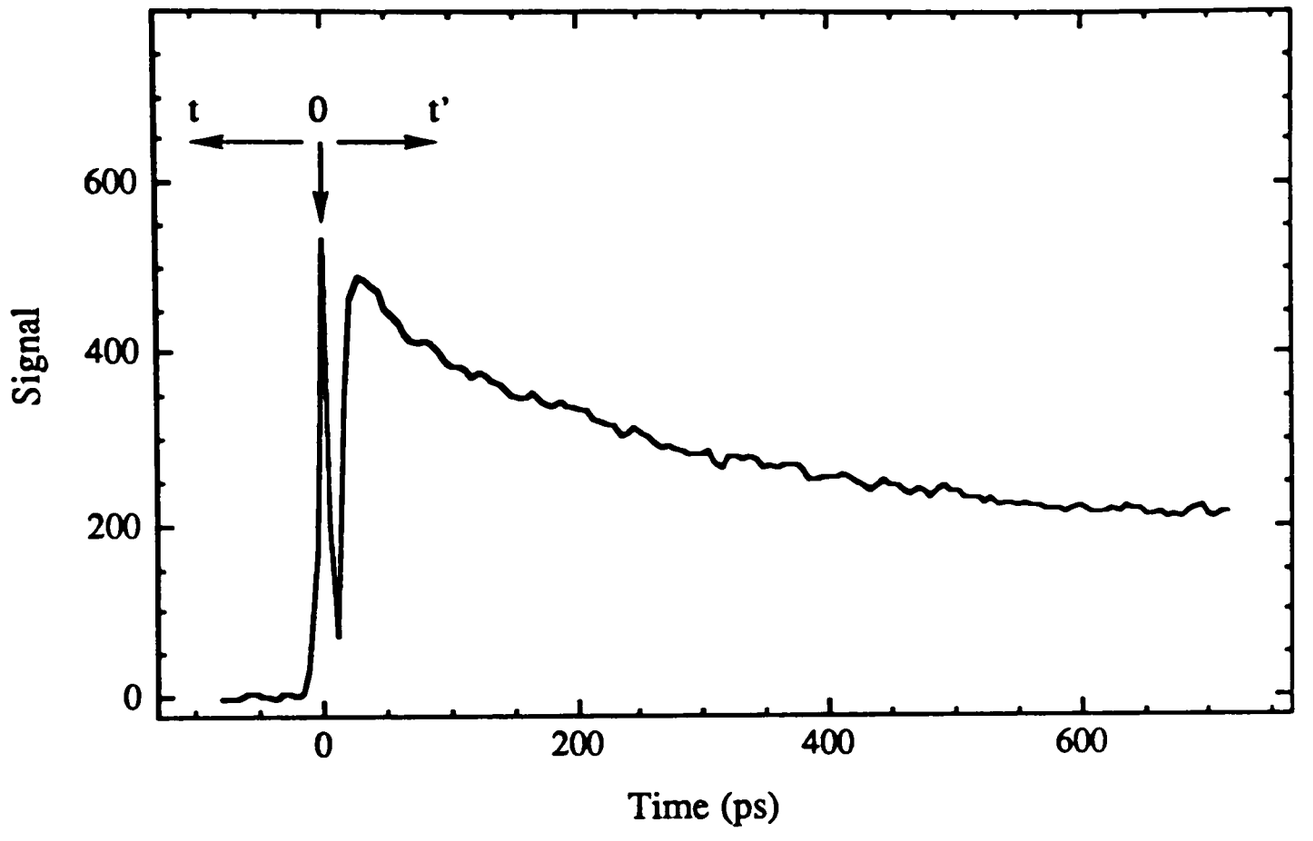

Figure 2.49. Transient photobleaching signals of J-aggregates on purified PVS solution turn out all measured at excitation intensities at which exciton annihilation occured.

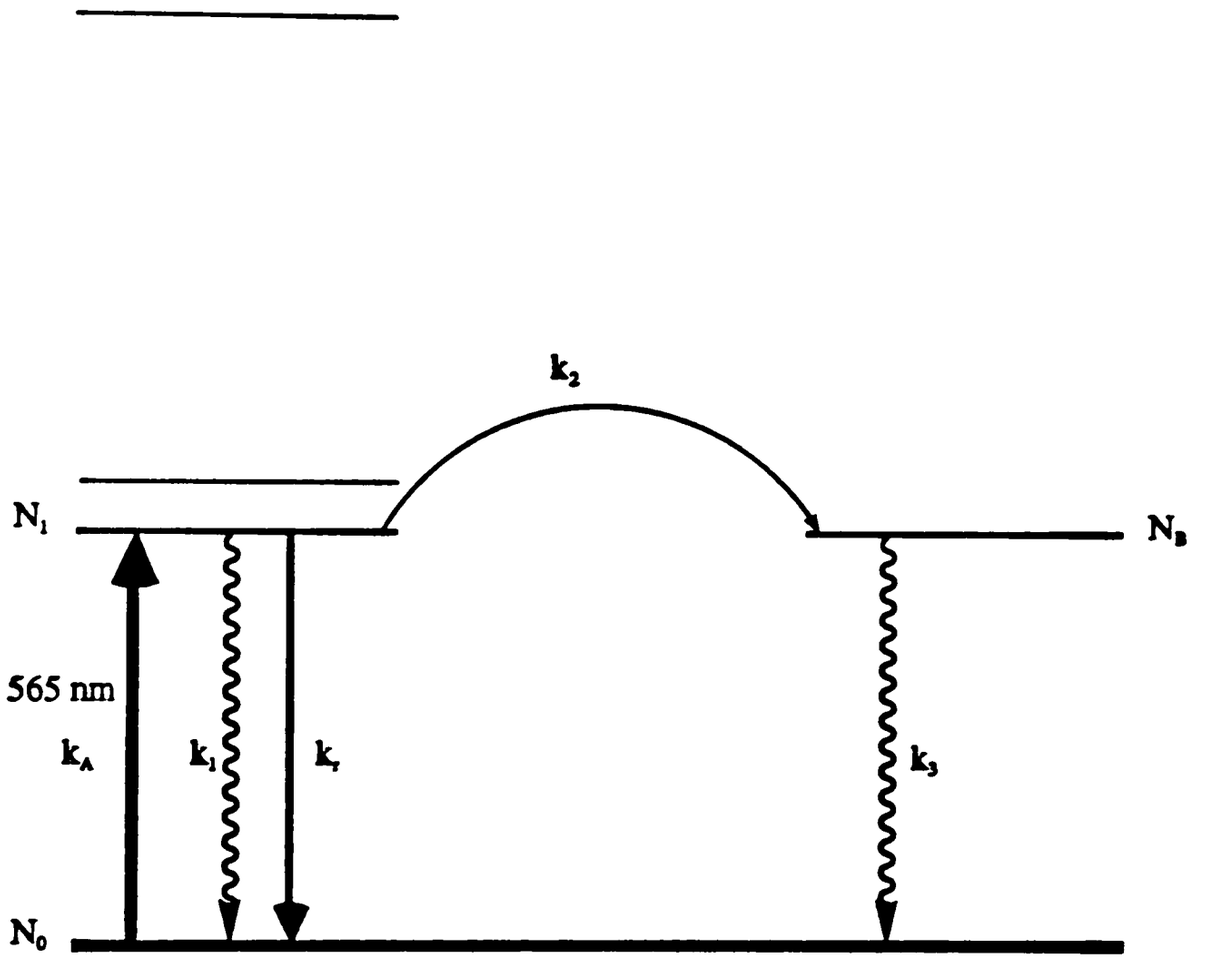

Figure 2.50. The energy level scheme for 565 nm.

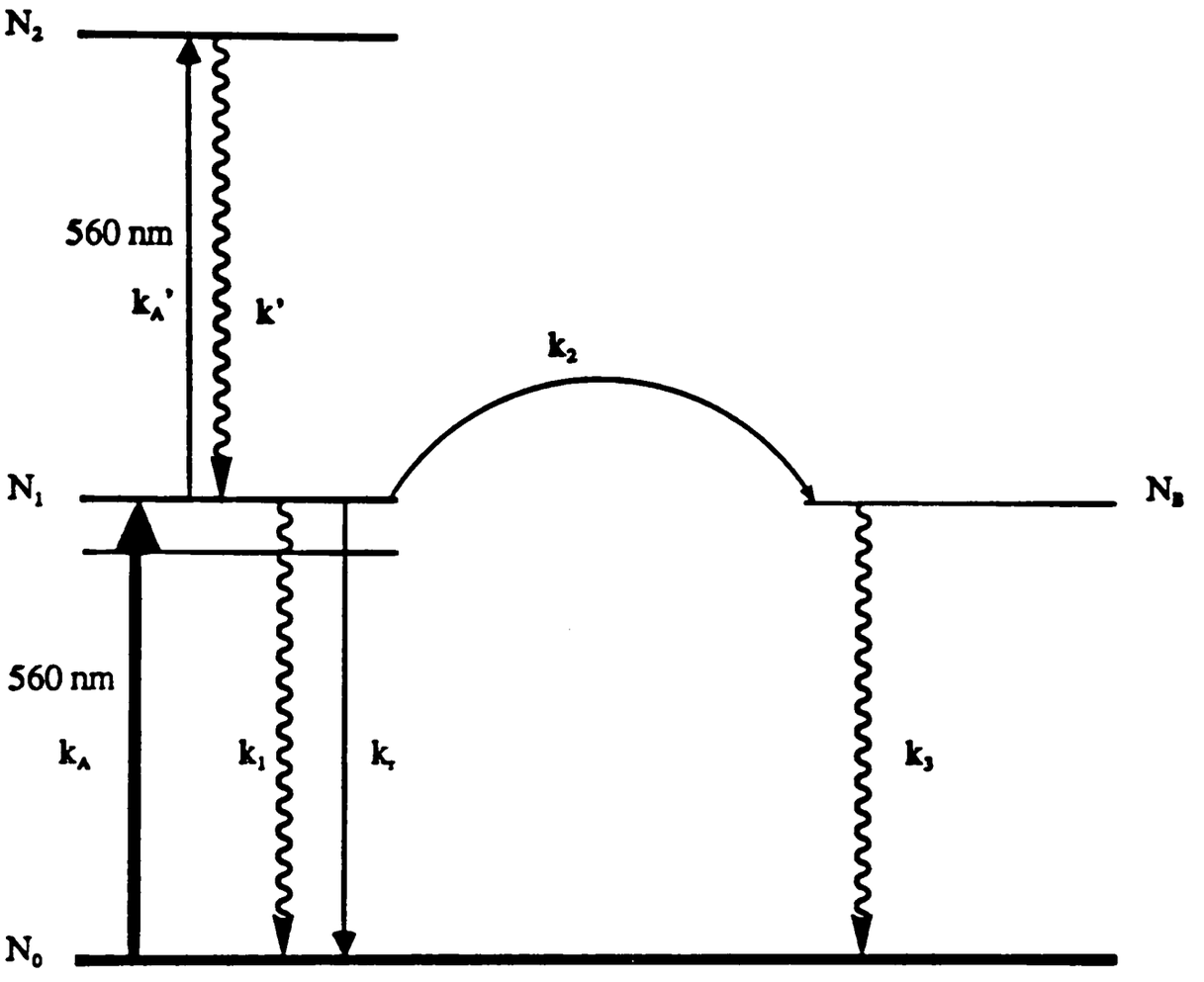

Figure 2.51. The energy level scheme for 560 nm.

$$K_S(t) = \frac{(k_3 - k_1 - k_r)\exp(-k_S t) - k_2\exp(-k_3 t)}{k_S - k_3}. \qquad (79)$$

Hence the decay curves at 565 nm should give better fits to the function shown below

$$R_i(t) = A_1\exp(-t/\tau_1) + A_2\exp(-t/\tau_2) + C \qquad (80)$$

where $C = N_0$, $A_1 = N_1(k_3 - k_1 - k_r)/(k_S - k_3)$ and $A_2 = N_1 k_2/(k_3 - k_S)$.

To explain the rapidly change of signal phases which occurs immediately after the excitation pulse at 560nm, we propose a two photon excitation mechanism. The initial sharp decay was caused by the excited state absorption of the probe light to a higher excited state. The rapidly lose of this absorption resulted from the quick depopulation of this excited state due to exciton annihilation and excited state decay.

CHAPTER III

DIMERIC STATE OF DCC

3.1. Experimental

DCC was obtained from Kodak Laboratory Chemical. No further purification was attempted. Dyes molecules were dissolved in deionized water. The dyes were adsorbed to the glass walls of volumetric apparatus and of the measuring cuvette. Thus all the volumetric apparatus and cuvettes were silanated with 1% dichlorodimethylsilane in toluene following by treating with methanol. All solutions were stored in tightly capped polyethylene bottles. Cuvette lengths of 0.02, 0.1 and 1.0 cm were used according to the molar extinction coefficients of the dyes. Absorption spectra were obtained using a Shimadzu UV-265 spectrophotometer at 21±0.5 °C. The experimental spectra were digitized and stored in a microcomputer for data processing. The programming language Turbo Pascal was used to write programs for analysis of dimer data.

3.2. Results

A dimer is the simplest kind of molecular aggregate. The study of the intermolecular interactions in a dimer should help understanding the complicated exciton states of polymeric systems such as molecular crystals.

The spectra of DCC are studied as a function of concentration over a range of 2.6×10^{-7} to 9.2×10^{-6} M. In this concentration range DCC seems to exist only in the form of monomers and dimers. The aggregation of the DCC in water with increasing concentration is shown in Figure 3.1. Upon increasing the dye concentration, the intensity of the monomer maximum at 604 nm is reduced and a

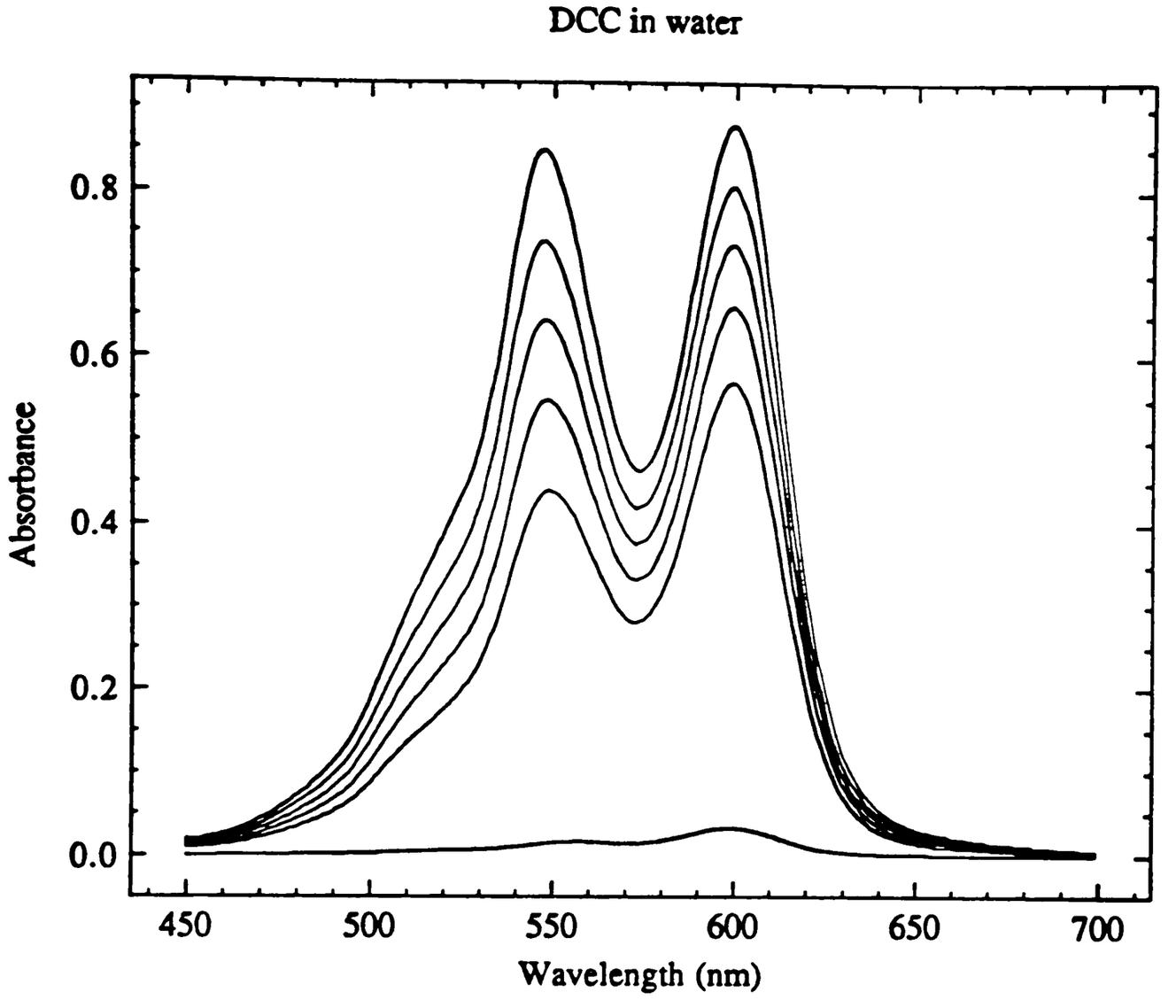

Figure 3.1. Measured spectra as function of concentration 0.26 μM, 5.1μM, 6.1 μM, 7.2 μM, 8.2 μM and 9.3 μM at room temperature. The observed spectrum is a superposition of monomer and dimer spectra.

new maximum at about 545 nm somewhat shorter than the vibrational shoulder of the monomer band appears. Over these concentrations, two isosbestic points appear in the family of absorption curves [Figure 3.2], one at a shorter wavelength (≈ 560 nm) and the other at a longer wavelength (≈ 630 nm) than the monomer maximum. Over this range of concentrations, therefore, according to the well-known properties of the isosbestic point,[73, 126-128] two colored species are in equilibrium. The persistence of the monomeric band shows that one of these species is the dye monomer, and it will be shown that the other is a dimeric form of the dye. Figure 3.3 shows the spectra of the pure monomer and dimer. The spectrum of the monomer is assumed to be the same as the spectrum of a very diluted solution of 2.6×10^{-7} M at the same temperature. The shape of monomer spectrum does not change by further dilution of the concentration. The experimental spectra were digitized and stored for processing in a microcomputer.

Assuming the law of mass action holds for the system, the composition of monomers and dimers is then governed by the same value of equilibrium constant K for each solution. For a given K value, the mole fraction of monomer in each concentration can be calculated. The observed spectrum needs to be treated so as to extract the spectrum of the dimerized molecules from that of the unassociated ones at a given concentration. We assume here that the first step of aggregation is the formation of dimers only. In the concentrated solution, where dimerization occurs, the equilibrium between monomer and dimer must exist.

$$2M \underset{K_d}{\overset{K}{\rightleftarrows}} M_2. \qquad (81)$$

The equilibrium constant K for dimerization is defined as

$$K = \frac{1}{Kd} = \frac{C_D}{C_M{}^2} \qquad (82)$$

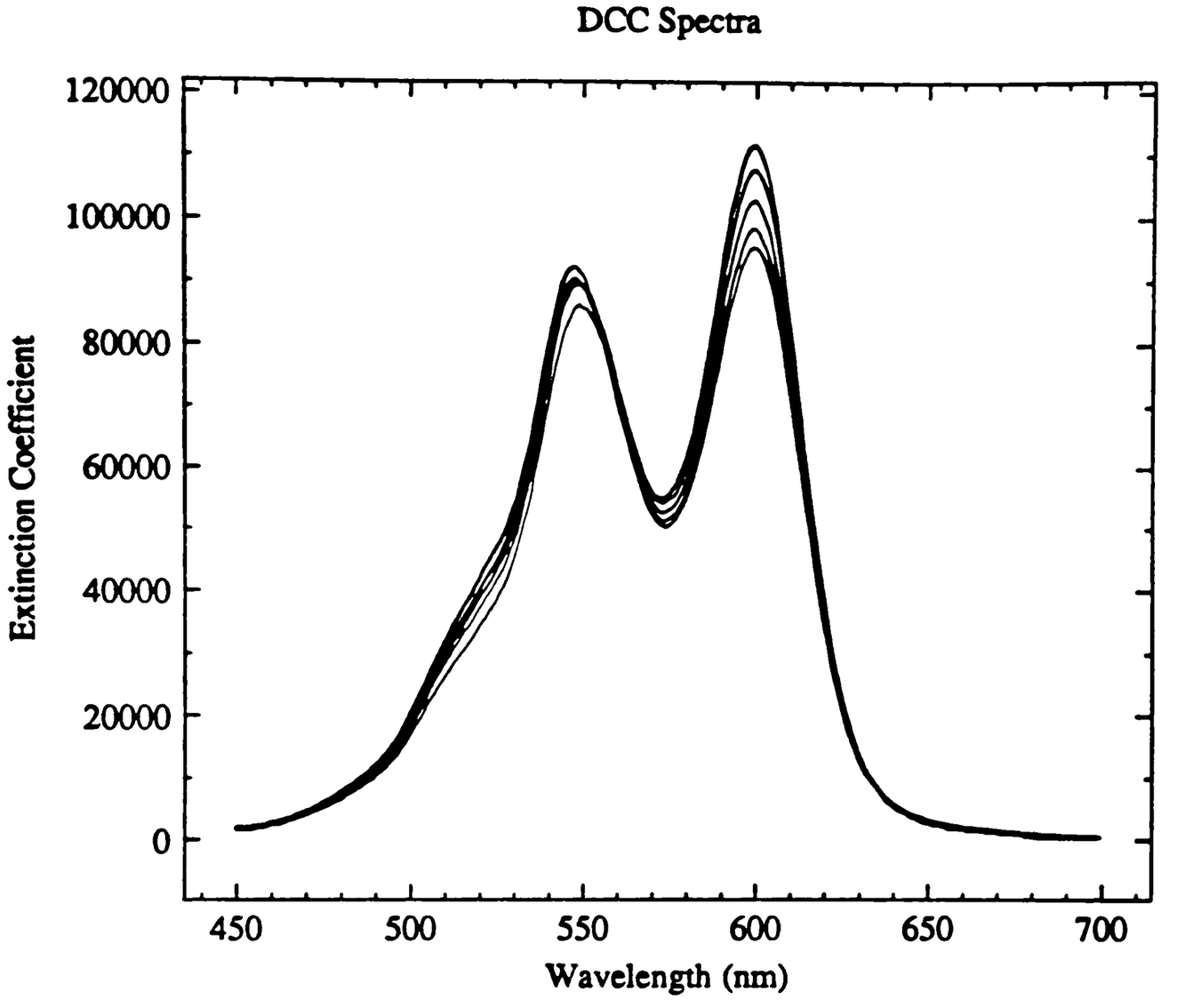

Figure 3.2. Two isosbestic points appear in the family of absorption curves for DCC in water.

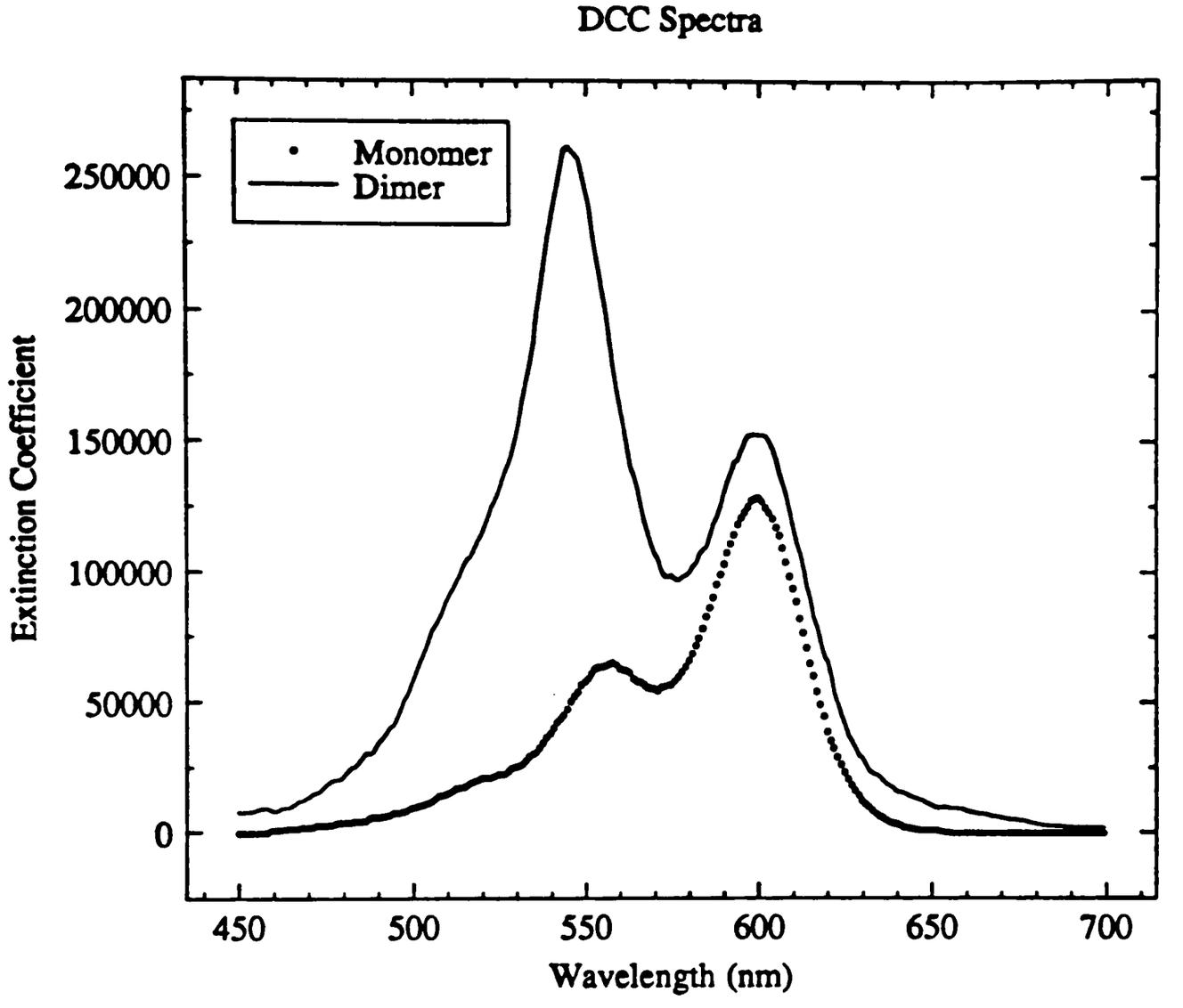

Figure 3.3. Molar extinction coefficients of pure monomer and dimer of aqueous DCC solutions.

where K_d is the dimer dissociation constant, C_M and C_D are the concentrations of monomers and dimers, respectively. Neglecting the formation of higher aggregates, K_d can be expressed in terms of ξ the mole fraction of molecules present as monomer

$$K_d = \frac{2C\xi^2}{1 - \xi} \tag{83}$$

where ξ is defined as

$$\xi = \frac{C_M}{C} \tag{84}$$

and C is the total concentration of the dye in moles/liter (M) given as

$$C = C_M + 2C_D. \tag{85}$$

Thus given the value of K_d, ξ can be obtain from

$$\xi = \frac{-K_d + \sqrt{K_d^2 + 8CK_d}}{4C}. \tag{86}$$

The molar extinction coefficient of the solution at the frequency υ is given by

$$\epsilon_\upsilon = \frac{A_\upsilon}{\ell\, C} \tag{87}$$

where A_υ is the optical density of the dye solution at a frequency υ, and ℓ is the pathlength. Assuming Beer's law to hold for each component, the apparent molar extinction coefficient ϵ_υ at frequency υ for a particular concentration is given by

$$\epsilon_\upsilon = \epsilon_\upsilon^M \alpha + \epsilon_\upsilon^D \left(\frac{1 - \xi}{2}\right) \tag{88}$$

where ϵ_υ^M and ϵ_υ^D are, respectively, the molar extinction coefficient of the monomer and dimer, and the concentration of dimer in the solution is given by $(1 - \xi)/2$. The ϵ_υ^M of monomer spectrum were readily determined from solutions with very low DCC concentrations. Equation (88) can be written as

$$\epsilon_\upsilon^D = \frac{2(\epsilon_\upsilon - \epsilon_\upsilon^M \xi)}{1 - \xi}. \tag{89}$$

One has determined the true dimer spectrum when the same value of ϵ_υ^D is obtained from equation (89) independent of concentration.

A check of the validity of the dimer spectrum was obtained by comparison between the experimental spectrum and the calculated spectrum at different concentration [Figure 3.4]. An analysis of the DCC monomer spectrum shows that the monomer spectrum consists of five Gaussian bands [Figure 3.5]. The dimer spectrum shows two absorption maxima. The frequency difference between these two maxima corresponds to the exciton band width. Deconvolution of the dimer spectrum into two component bands [Figures 3.6 and 3.7] allows determination of the geometry of the dimer, as will be described. Deconvolution was carried out with a spectral deconvolution program that uses a Gaussian function. The Gaussian function is described by the equation

$$\epsilon_\upsilon = \epsilon_{max}\exp\{-(\nu - \nu_{max})^2/2\sigma^2\} \qquad (90)$$

where ϵ_υ is the molar extinction coefficient at frequency ν, ϵ_{max} is the maximum molar extinction coefficient of the band, ν_{max} is the frequency at ϵ_{max}, and σ is the width of the Gaussian distribution. The full width at half maximum (FWHM) of the band is equal to 2.35σ.[129]

The oscillator strengths f of the monomer and dimer are determined from areas under the absorption curve, using the following equation.[130]

$$f = 4.31712 \times 10\text{-}9\int\epsilon\, d\bar{\nu} \qquad (91)$$

where $\bar{\nu}$ is the frequency in wavenumber (cm^{-1}) and ϵ is the molar extinction coefficient. Using the definition of oscillator strength for monomer[129]

$$f = 4.7027 \times 10^{29}\nu_{max}M^2 \qquad (92)$$

where M is the transition moment for the monomer in cm·statC, the expression for the excited state interaction energy U becomes[40]

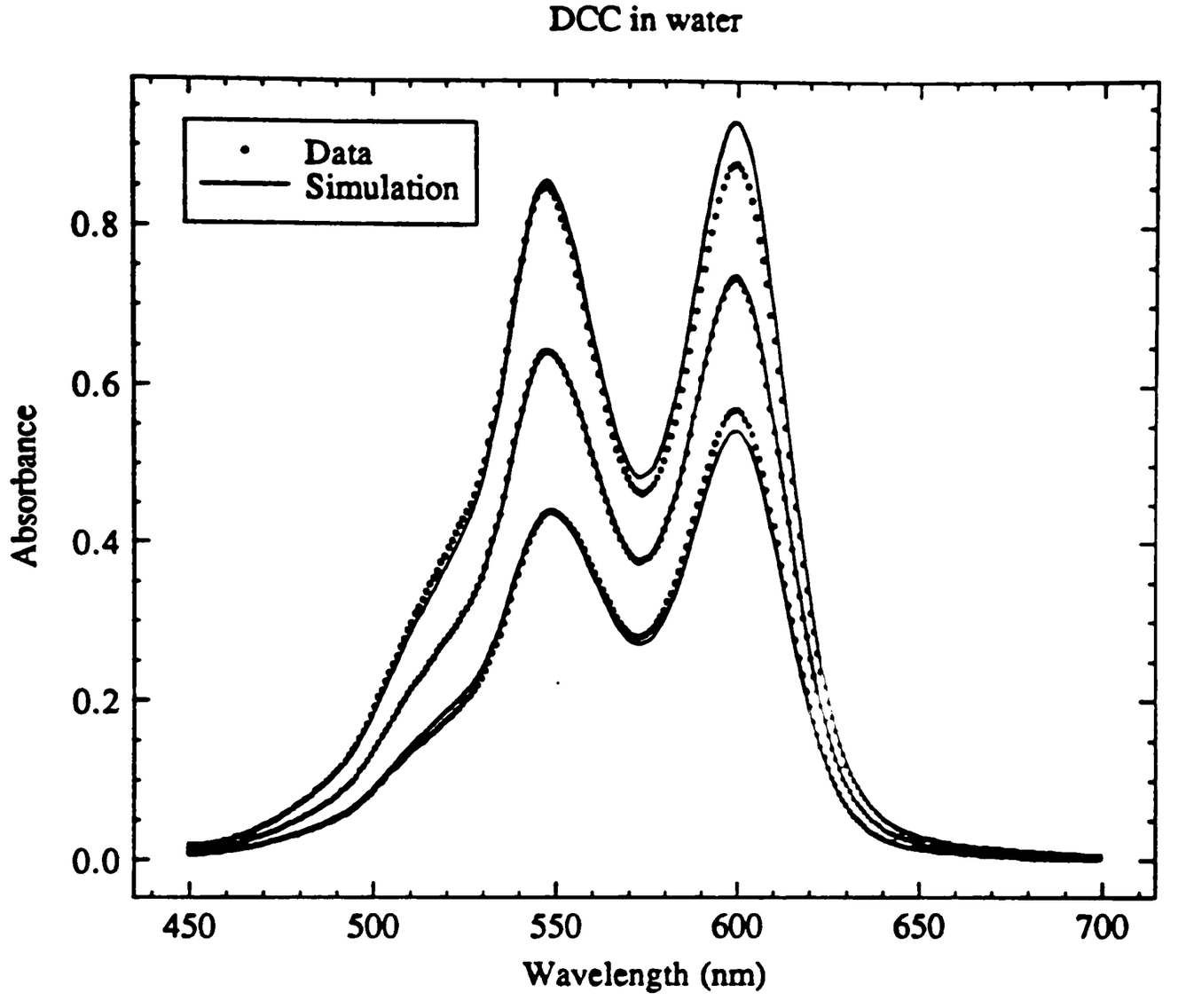

Figure 3.4. Comparisons between the experimental spectra and the calculated spectra at different concentration.

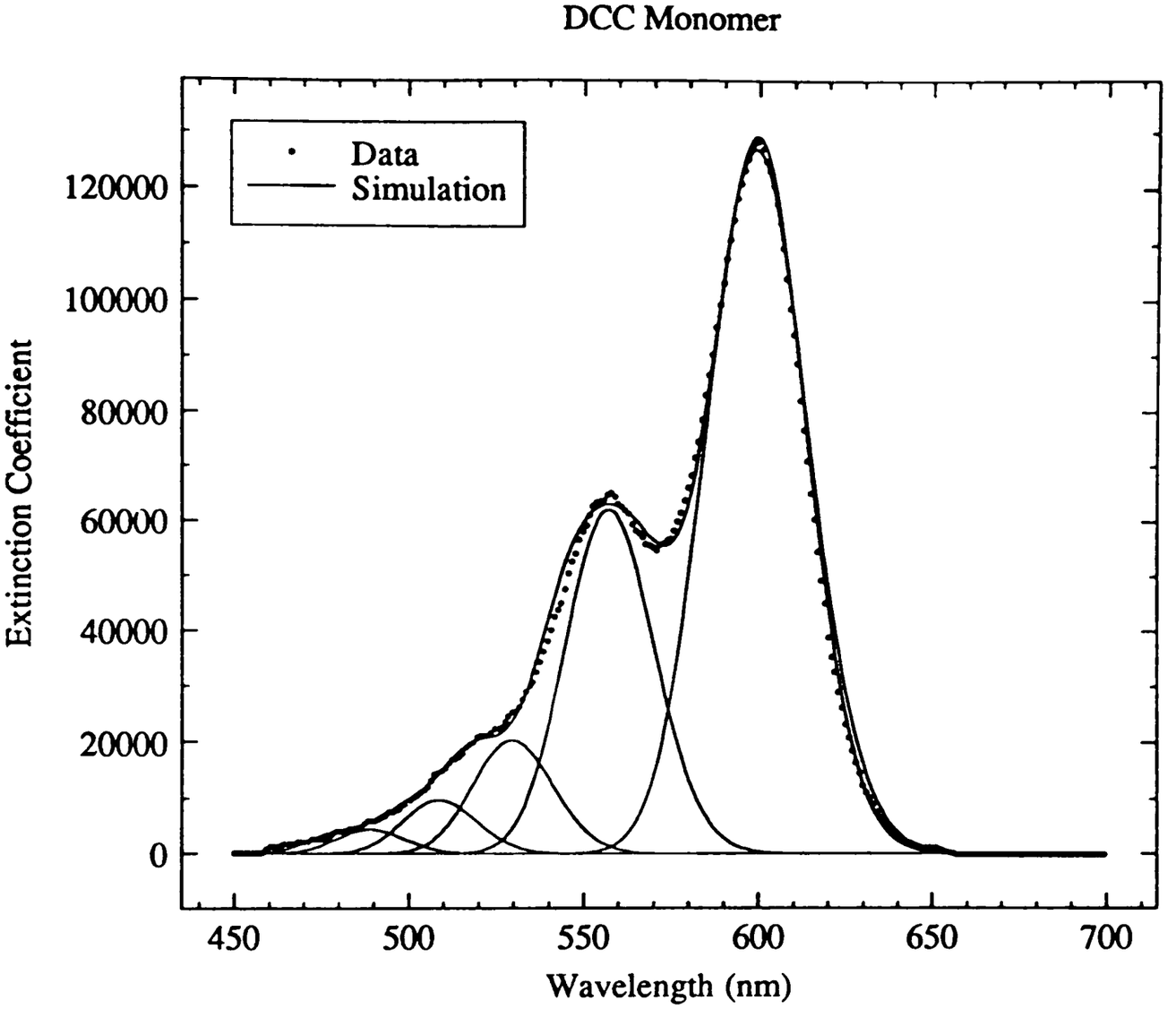

Figure 3.5. Observed and simulated monomer spectrum.

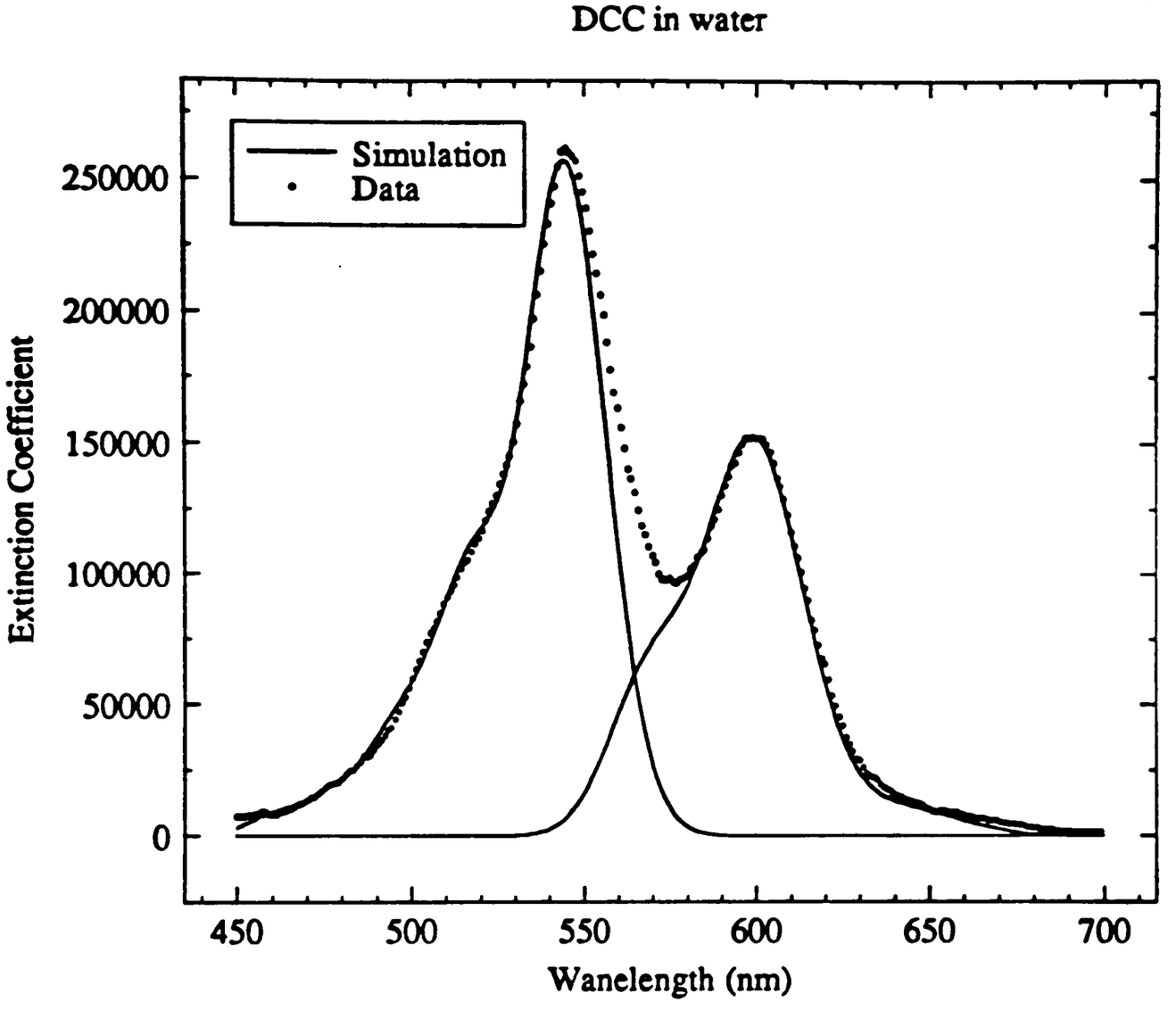

Figure 3.6. Dimer spectrum and component bands obtained by spectral deconvolution. Ratio of oscillator strengths is 1.862, giving a value of 72.5° for the angle between the DCC units.

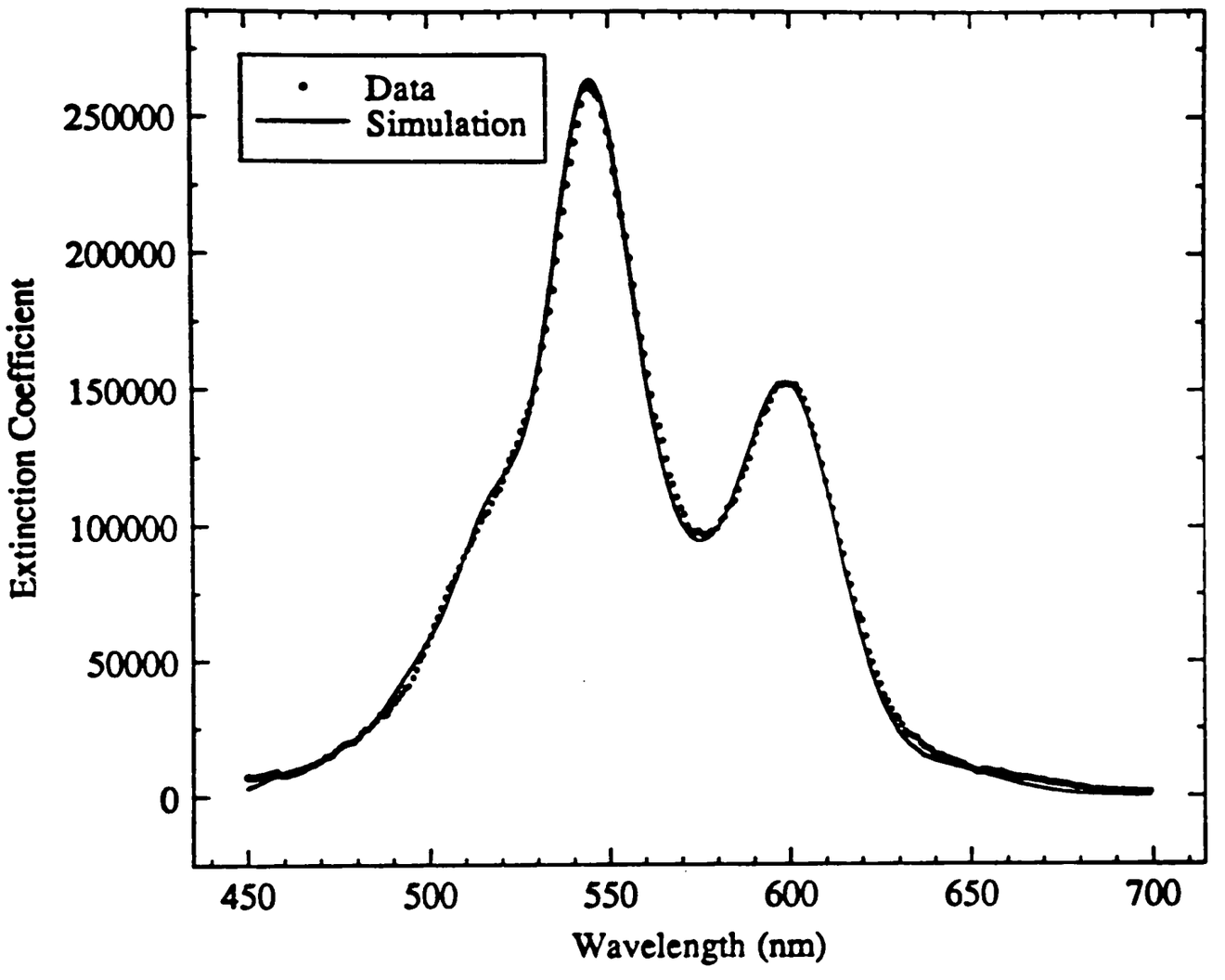

Figure 3.7. Observed and simulated dimer spectrum.

$$U = -\frac{M^2}{r^3}(1 - \cos^2\alpha) \qquad (93)$$

where r is the distance between centers of gravity of the two molecules and α is the angle between the long molecular axis and the dimer axis [Figure 1.15]. The angle α can be calculated from the equation[75]

$$\frac{f_s}{f_l} = \tan^2\alpha \qquad (94)$$

where f_s and f_l are the oscillator strengths for the shorter- and longer-wavelength band of the dimer spectrum, respectively. Electrostatic interactions between molecules with permanent dipole moments would lead to shifting of both bands as a whole rather than causing any extra splitting. Thus, the energy of interaction U would rather be a better approximation by half of the value of the exciton band width than the frequency difference between monomer and dimer maxima. Knowing α and r, the structure of the dimer can then be obtained. The information obtained about the dimer excited state from these spectral observations is summarized in Table 3.1.

3.3. Discussion

Investigations of the first step of aggregation of aqueous solutions of DCC suggest that almost all monomer units form dimers before higher aggregation occurs. The dimer spectrum was derived from a large number of measured spectra. Both monomer and dimer spectra could be well synthesized by several Gaussian functions. The analysis provides a distance of 10 Å between the two molecules and an angle of 72° between the transition moments of the monomer units in the dimer. A steric dimer model is consistent with the numerous data.

Table 3.1. Parameters obtained from spectra analysis.

Dimer

2U	K	α	β	r	ΔG^0
1686 cm^{-1}	124264 ℓ/mole	53.8°	72.5°	10Å	-6876.5 cal/mole

CHAPTER IV

CONCLUSIONS

Aggregates are of interest as they bridge the gap between a single molecule and a crystalline lattice. Interesting size effects on the spectroscopy and optical dynamics of aggregates are observed. The excitation-intensity dependence and the absorption anisotropy of the transient bleaching signals support the conclusion that the dynamics of energy migration involves localized excitons in large J-aggregates and delocalized excitons in isolated small J-aggregates.

In future experiments, the time-resolved fluorescence and fluorescence quantum yield of J-aggregates on colloidal silica should be measured, respectively, with better time resolution and higher precision. Further ground-state recovery measurements over a broader time range would be a good approach to understand the origin of the long decay component. These measurements should provide us with values for the radiative and nonradiative decay constants. A comparison of the radiative rate constants of the J-aggregate and the monomer will yield an estimate of the number of molecules in these aggregates. Studies of the effect of energy transfer on the anisotropy in systems consisting of fluorescent J-aggregates of PIC and nonfluorescent H-aggregates of DDC coadsorbed on colloidal silica will be useful in further understanding exciton transport in cyanine dye aggregates.

In the way of future work on the PVS system, it would seem important to directly measure the S_1 lifetimes using time-resolved fluorescence to provide a comparison with the estimates from ground state recovery. Transient absorption spectra would be a useful tool to clear the wavelength dependent properties of

J-aggregates on PVS polymer. Further ground-state recovery measurements over a broader time range are needed for a better understanding of the long decay component. The bottleneck state is formed by the ionized aggregate and the temporarily trapped electron. The dynamics of the returning electrons is a point for further study. The accumulated photon-echo technique can be successfully used to study the ultrafast optical dynamics of the J-band in the condensed phase. Improvement of our detection ability would help understanding of J-aggregates on purified PVS polymer at annihilation-free conditions. The transient bleaching measurements for J-aggregates on purified PVS polymers at 565 nm should be analyzed by using the biexponential plus constsnt function.

The dimer is a simpler system than the J-aggregate. Knowing the concentration ratio between monomer and dimer in a solution, it is possible to study the dynamic of excitation energy transfer between the units of the dimer by using the picosecond pump-probe technique.

REFERENCES

1. Worthy, W.; *Chem. Eng. News*, **1991**, 69, 41.

2. Borisov, A. Yu.; in *Photosynthesis in relation to model systems*, Barber, Ed., Elsevier, New York, **1979**, pp. 2-26.

3. Barsky, E. L.; Borisov, A. Yu.; *J. Bioenerg.*, **1971**, 2, 275.

4. Barsky, E. L.; Borisov, A. Yu.; Fetisova, Z. G.; Il'ina, M. D.; Samuilov, V. D.; *Mol. Biol.*, **1975**, 9, 221 (Engl. transl.).

5. Zuber, H.; *Photochem. Photobiol.*, **1985**, 42, 821.

6. Zuber, H.; in *Antennas and Reaction Centers of Photosynthetic Bacteria*, Michel-Beyerle, Ed., Springer-Verlag, **1985**, pp. 2-14.

7. Porter, G.; Archer, M.; *Interdiscip. Sci. Rev.*, **1976**, 1, 119.

8. Emerson, E. S.; Conlin, M. A.; Rosenoff, A. E.; Norland, K. S.; Rodriguez, H.; Chin, D.; Bird, G. R.; *J. Phys. Chem.*, **1967**, 71, 2396.

9. Graves, R. E.; Rose, P. I.; *J. Phys. Chem.*, **1975**, 79, 746.

10. De Boer, S.; Vink, K. J.; Wiersma, D. A.; *Chem. Phys. Lett.*, **1987**, 137, 99.

11. Nakahira, T.; Shinomiya, E.; Fukumoto, T.; Iwabuchi, S.; Kojima, K.; *Eur. Polym. J.*, **1978**, 14, 317.

12. Nakahira, T.; Minami, C.; Iwabuchi, S.; Kojima, K.; *Markromol. Chem.*, **1979**, 180, 2245.

13. Holden, D. A.; Ren, X. X.; Guillet, J. E.; *Macromol.*, **1984**, 17, 1500.

14. Zollinger, H.; *Color Chemistry*, VCH, New York, **1987**, 270-276.

15. Möbius, D.; *Acc. Chem. Res.*, **1981**, 14, 63.

16. Albery, W. J.; Foulds, A. W.; *J. Photochem.*, **1979**, 10, 41.

17. Dan, P.; Willner, I.; Dixit, N. S.; Mackay, R. A.; *J. Chem. Soc. Perkin. Trans. II*, **1984**, 455.

18. Wang, Y.; *Chem. Phys. Lett.*, **1986**, 126, 209.

19. De Boer, S.; Wiersma, D. A.; *Chem. Phys.*, **1989**, 131, 135.

20. West, W.; Gilman, P. B., Jr.; in *The Theory of The Photographic Process*; 4th ed.; James, Ed.; Macmillan; New York, **1977**, 251-290.

21. Takagi, K.; Kawabe, M.; Matsuoka, M.; Kitao, T.; *Dyes Pigm.*, **1985**, 6, 177.

22. Kim, S. H.; Matsuoka, M.; Kubo, Y.; Yodoshi, T.; Kitao, T.; *Dyes Pigm.*, **1986**, 7, 93.

23. Maeda, M.; in *Kinosei Shikiso no Kagaku (Chemistry of Functional Colouring Materials)*, Okawara et al., Eds., CMC Corp, Tokyo, **1981**, pp. 399.

24. Maeda, M.; *Laser Dyes*, Academic Press, Tokyo, **1984**.

25. Williams, C. H. G.; *Trans. Roy. Soc. Edinburgh*, **1856**, 21, 377.

26. Hamer, F. M.; in *The Chemistry of Heterocyclic Compounds, vol. 18, The Cyanine Dyes and Related Compounds*, Weissberger, Ed., Interscience, New York, **1964**.

27. Mills, W. H.; Hamer, F. M.; *J. Chem. Soc.*, **1920**, 117, 1550.

28. Mills, W. H.; *J. Chem. Soc.*, **1922**, 121, 455.

29. Sturmer, D. M.; Heseltine, D. W.; in *The Theory of The Photographic Process*, 4th ed.; James, Ed.; Macmillan; New York, **1977**, 194-234.

30. Griffiths, J.; *Colour and Constitution of Organic Molecules*, Academic Press, New York, **1976**.

31. Platt, J. R.; *J. Chem. Phys.*, **1956**, 25,80.

32. Jelley, E. E.; *Nature*, **1937**, 10, 631.

33. Scheibe, G.; *Angew. Chem.*, **1937**, 50, 212.

34. Mason, S. F.; *Proc. Chem. Soc.*, **1964**, 119.

35. Peticolas, W. L.; *J. Chem. Phys.*, **1964**, 40, 1463.

36. Bradley, D. F.; Wolf, M. K.; *Proc. Nat. Acad. Sci. USA*, **1959**, 45, 944.

37. Daltrozzo, E.; Scheibe, G.; Gschwind, K.; Haimerl, F., *Photogr. Sci. Eng.*, **1974**, 18, 441.

38. Brooker, L. G. S.; White, F. L.; Heseltine, D. W.; Keyes, G. H.; Dent, S. G., Jr.; Van Lare, E. J.; *J. Photogr. Sci.*, **1953**, 1, 173.

39. Herz, A. H.; *Photogr. Sci. Eng.*, **1974**, 18, 323.

40. McRae, E. G.; Kasha, M.; *Phys. Process. Radiation Biol.*, Proc. Intern. Symp., Mich. State Univ., **1963**, pp. 23-42.

41. Knox, R. S.; *Bioenergetics of Photosynthesis*, Govindjee, Ed., Academic Press, New York, **1975**, pp. 183-221.

42. Grad, J.; Hernandez, G.; Mukamel, S.; *Phys. Rev. A*, **1988**, 37, 3835.

43. Quitevis, E. L.; Horng, M. -L.; *SPIE*,**1990**, 1209, 198.

44. Craig, D. P.; *Phys. Process. Radiation Biol.*, Proc. Intern. Symp., Mich. State Univ., **1963**, pp. 1-9.

45. Frenkel, J. I.; *Phys. Rev.*, **1931**, 37, 17.

46. Davydov, A. S.; *Zh. Eksperim. i Teor. Fiz.*, **1948**, 18, 210.

47. Fano, U.; *Phys. Rev.*, **1960**, 118, 451.

48. Kasha, M.; *Radiat. Res.* , **1963**, 20, 55.

49. Wannier, G. H.; *Phys. Rev.*, **1937**, 52, 191.

50. Davydov, A. S.; *Theory of Molecular Excitons*, McGraw-Hill, New York, **1962**.

51. Knox, R. S.; *Radiat. Res.*, **1963**, 20, 77.

52. Simpson, W. T.; Peterson, D. M.; *J. Chem. Phys.*, **1957**, 26, 588.

53. Förster, T.; in *Comparative Effects of Radiation*, Burton et al. Eds., Wiley, New York, **1961**, pp. 300-319.

54. Förster, T.; in *Modern Quantum Chemistry*, vol 3, Sinanoğlu, Ed., **1965**, pp. 93-137.

55. McClure, D. S.; *Can. J. Chem.*, **1958**, 36, 59.

56. Craig, D. P.; Walmsley, S. H.; *Excitons in Molecular Crystals*, Benjamin, New York, **1968**.

57. McRae, E. G.; *Aust. J. Chem.*, **1961**, 14, 329.

58. Merrifield, R. E.; *Radiat. Res.*, **1963**, 20, 154.

59. Craig, D. P.; *J. Chem. Soc.*, **1955**, 2302.

60. Levinson, G. S.; Simpson, W. T.; Curtis, W.; *J. Am. Chem. Soc.*, **1957**, 79, 4314.

61. Kirkwood, J. G.; *J. Chem. Phys.*, **1937**, 5, 479.

62. Moffitt, W.; Fitts, D. D.; Kirkwood, J. G.; *Proc. Natl. Acad. Sci. USA*, **1957**, 43, 723.

63. Tinoco, I., Jr.; *J. Am. Chem. Soc.*, **1960**, 82, 4785.

64. Daltrozzo, E.; Scheibe, G.; Gschwind, K.; Haimerl, F.; *Photo. Sci. Eng.*, **1974**, 18, 441.

65. Margenau, H.; *Rev. Mod. Phys.*, **1939**, 11, 1.

66. Monger, T. G.; Parson, W. W.; *Biochim. Biophys. Acta*, **1977**, 360, 393.

67. Paillotin, G.; Swenberg, C. E.; Breton, J.; Geacintov, N. E.; *Biophys. J.*, **1979**, 25, 513.

68. Paillotin, G.; Swenberg, C. E.; *Ciba Found. Symp.*, **1979**, 61, 201.

69. Breton, J.; Geacintov, N. E.; *Biochim. Biophys. Acta*, **1980**, 594, 1.

70. Suna, A.; *Phys. Rev. B*, **1970**, 1, 1716.

71. Campillo, A. J.; Hyer, R. C.; Monger, T. G.; Parson, W. W.; Shapiro, S. L.; *Proc. Natl. Acad. Sci. USA*, **1977**, 74, 1997.

72. Bergmann, K.; O'Konski, C. T.; *J. Phys. Chem.*, **1963**, 67, 2169.

73. West, W.; Pearce, S.; *J. Phys. Chem.*; **1965**, 69, 1894.

74. Rohatgi, K. K.; Mukhopadhyay, A. K.; *Photochem. Photobiol.*, **1971**, 14, 551.

75. Valdes-Aguilera, O; Neckers, D. C.; *J. Phys. Chem.*, **1988**, 92, 4286.

76. Breslow, D. S.; Kutner, A.; *J. Polymer Sci.*, **1958**, 27, 295.

77. Andrews, D. A.; *Lasers in Chemistry*, 2nd ed., Springer-Verlag, New York, **1990**.

78. Exter, M. V.; Lagendijk, A.; *Rev. Sci. Instrum.*, **1986**, 57, 390.

79. Engh, R. A.; Petrich, J. W.; Fleming, G. R.; *J. Phys. Chem.*, **1985**, 89, 618.

80. Balk, M. W.; Fleming, G. R.; *J. Chem. Phys.*,**1985**, 83, 4300.

81. Levenberg, K.; *Quant. Appl. Math.*, **1944**, 2, 164.

82. Marquardt, D. W.; *J. Soc. Ind. Appl. Math.*, **1963**, 11, 431.

83. Lee, J.; Griffin, R. D.; Robinson, G. W.; *J. Chem. Phys.*, **1985**, 82, 4920.

84. Lee, J.; *J. Phys. Chem.*, **1990**, 94, 258.

85. Thomas, J. K.; *J. Phys. Chem.*, **1987**, 91, 267.

86. Weitz, D. A.; Garoff, S.; Gersten, J. I.; Nitzan, A.; *J. Chem. Phys.*, **1983**, 78, 5324.

87. Bard, A. J.; *J. Phys. Chem.*, **1982**, 86, 172.

88. Fox, M. A.; *Acc. Chem. Res.*, **1983**, 16, 314.

89. Iler, R. K.; *The Chemistry of Silica*, 2nd ed., Wiley, New York, **1979**.

90. Wheeler, J.; Thomas, J. K.; *J. Phys. Chem.*, **1984**, 88, 750.

91. Willner, I.; Yang, J. -M.; Laane, C.; Otvos, J. W.; Calvin, M.; *J. Phys. Chem.*, **1981**, 85, 3277.

92. Wheeler, J.; Thomas, J. K., In *Inorganic Reactions in Organized Media*, Holt, Ed., American Chemical Society, Washington, DC, **1982**, ACS Symp. Ser. No. 177, pp 98-111.

93. Knapp, E. W.; *Chem. Phys.*, **1984**, 85, 73.

94. Quitevis, E. L.; Horng, M. -L.; Chen, S. -Y.; *J. Phys. Chem.*, **1988**, 92, 256.

95. Horng, M. -L.; Quitevis, E. L.; *J. Phys. Chem.*, **1989**, 93, 6198.

96. Kemnitz, K.; Yoshihara, K.; Tani, T.; *J. Phys. Chem.*, **1990**, 94, 3099.

97. Linschitz, H.; Sarkanen, K.; *J. Am. Chem. Soc.*, **1958**, 80, 4826.

98. Porter, G.; Wright, M. R.; *Discuss. Faraday Soc.*, **1959**, 27, 18.

99. Linschitz, H.; Pekkarinen, L.; *J. Am. Chem. Soc.*, **1960**, 82, 2411.

100. Steel, C.; Linschitz, H.; *J. Phys. Chem.*, **1962**, 66, 2577.

101. Brumbaugh, D. V.; Muenter, A. A.; Knox, W.; Mourou, G.; Wittmershaus, B., *J. Lumin.*, **1984**, 31, 783.

102. Kihoshita, K.; Kawato, S.; Ikegami, A.; *Biophys. J.*, **1977**, 20, 289.

103. Jähnig, F.; *Proc. Natl. Acad. Sci. USA*; **1979**, 76, 6361.

104. Johansson, L. B. -Å.; Lindblom, G.; *Q. Rev. Biophys.*, **1980**, 13, 63.

105. Sundström, V.; Gillbro, T.; *Chem. Phys. Lett.* , **1983**, 94, 580.

106. Hofer, L. J. E.; Grabenstetter, R. J.; Wiig, E. O.; *J. Am. Chem. Soc.*, **1950**, 72, 203.

107. Buettner, A. V.; *J. Chem. Phys.*, **1967**, 46, 1398.

108. Teuchner, K.; Dähne, S.; Dresner, J.; Prochorow, J.; *J. Lumin.* , **1981**, 23, 413.

109. Kopainsky, B.; Kaiser, W.; *Chem. Phys. Lett.* , **1982**, 88(4), 357.

110. Rentsch, S. K.; Danielius, R. V.; Gadonas, R. A.; Piskarskas, A.; *Chem. Phys. Lett.* , **1981**, 84(3), 446.

111. Dorn, H. -P.; Müller, A.; *Chem. Phys. Lett.* , **1986**, 130, 426.

112. Ippen, E. P.; Shank, C. V.; Bergman, A.; *Chem. Phys. Lett.* , **1976**, 38(3), 611.

113. Humphry-Baker, R.; Grätzel, M.; Steiger, R.; *J. Amer. Chem. Soc.*, **1980**, 102, 847.

114. Fink, F.; Klose, E.; Teuchner, K.; Dähne, S., *Chem. Phys. Lett.* , **1977**, 45, 548.

115. Dorn, H. -P.; Müller, A.; *Appl. Phys. B*, **1987**, 43, 167.

116. Stiel, H.; Daehne, S; Teuchner, K.; *J. Lumin.* , **1988**, 39, 351.

117. Sundström, V.; Gillbro, T.; Gadonas, R. A.; Piskarskas, A.; *J. Chem. Phys.*, **1988**, 89, 2754.

118. Laane, C.; Willner, I.; Otvos, J. W.; Calvin, M.; *Proc. Natl. Acad. Sci. U.S.A.*, **1981**, 78, 5928.

119. Pearlstein, R. M.; in *Photosynthesis: Energy conversion by Plants and Bacteria*, Govindjee, Ed., Academic press, New York, **1982**, Vol. 1, pp 293-330.

120. Debye, P.; *Polar Molecules*, Dover, New York, **1929**, pp 84-85.

121. Grover, M.; Silbey, R.; *J. Chem. Phys.*, **1970**, 54, 4843.

122. Haken, H.; Strobl, G.; *Z. Phys.*, **1973**, 262, 135.

123. Cross, A. J.; Waldeck, D. H.; Fleming, G. R.; *J. Chem. Phys.*, **1983**, 78, 6455.

124. Kemnitz, K.; Yoshihara, K.; Tani, T.; *J. Phys. Chem.*, **1990**, 94, 3099.

125. Tani, T.; *J. Appl. Phys.*, **1987**, 62, 2456.

126. Zanker, V.; *Z. Phys. Chem.*, **1952**, 200, 250.

127. Mataga, N.; *Bull. Chem. Soc. Japan*, **1957**, 30, 375.

128. Zanker, V.; *Z. Phys. Chem.*, **1952**, 199, 225.

129. Taylor, J. R.; *An Introduction to Error Analysis*, University Science Books, Mill Valley, Califonia, **1982**.

130. Steinfeld, J. I.; Molecules and Radiation, 2nd ed.;The MIT Press, Cambridge, Massachusetts, 1985.

APPENDIX A

PUMP-PROBE SOFTWARE

The following computer program, written in Applesoft BASIC for Apple IIe system, has four functions: (1) control the translation stage to do multiple scans during pump-probe measurement, (2) convert an analog signal to a digital data point, (3) display signals on the computer screen while taking the data, and (4) store the data on a floppy diskette. Since this is a revised version of Dr. Kelly G. Casey's pump-probe software (dissertation of Kelly G. Casey, Texas Tech University, Lubbock, Tx, USA, 1988), only the modifications will be described below.

A subprogram consists of statements 10 and 20 that allows automatically log on to the main program, TAKING DATA, when the computer is turn on. Statement 10 start program and variable storage above high-resolution graphics page 1, beginning at address 16384 that allows the program a bit more breathing room.

Statements 150-202 check the number of Adalab A/D converter cards installed in the computer.

Statements 240-860 form the input routine for the control parameters, where R, F, and S are the stepping motor parameters indicated.

The heart of this program are statements 980-2720. Subroutine 5000 takes QQ number of analog signals and average them to give a digital data point output. Statements 1040-1300 move the translation stage backward and Statements 2040-2280 move the translation stage forward. Statements 1440-1680 and 2420-2700 display the data points on the computer screen.

Subroutine 4000 display the complete set of data taken. Finally, Statements 4580-4780 save data on a floppy diskette.

```
10  POKE 103, 1: POKE  104, 64: POKE 16384, 0
20  PRINT  CHR$ (4); "RUN TAKING DATA"
100 PRINT  CHR$ (4);"PR#3"
120 REM  Protecting High-Resolution Graphics & Program From Each Other.
140 HiMEM: 36095: D% = 0: DIM C%(5), Q%(5), D%(100), SA(500), FW(500),
    BW(500), TM(500)
150 CC$ = CHR$ (13) + CHR$ (4)
180 PRINT CC$;"BLOADQUICKI/O, A$8D00, S6, D1": IF PEEK (64448) = 224
    THEN POKE - 16374, 0
200 POKE 1010, 160: POKE 1011, 149: POKE 1012, 48: POKE 216, 0
202 CALL 36096: NCH = PEEK (36221)
203 C$ = "5": REM  Using  PRG QUICKI/O's  Analog Input
204 IN = ASC (C$) - 48
205 IF IN > 2 THEN GOSUB 3000
206 C$ = "2": REM  Using PRG QUICKI/O's Graph Output
207 OT = ASC (C$) - 48
208 IF OT > 2 THEN GOSUB  3000
209 IF OT = 2 THEN HG = 0: IX = 0: MAX = 2500: MIN = -2500: SC =
    155/(MAX - MIN): DT$ = "N": REM  "Y" For Draws High-Resolution lines
220 PRINT  CHR$ (4);"PR#3"
230 ZZ = 1
240 R = 250: REM    RATE   (1-255)
260 F = 250: REM  FACTOR (1-255)
280 S = 2: REM  SLOPE (1-255)
300 PRINT  TAB( 20);"Please position stage at starting point,"
320 PRINT : PRINT
340 PRINT  TAB ( 25);" and hit ";: FLASH : PRINT "RETURN;" NORMAL :
     PRINT " when finished."
360 GET ANS$: IF ANS$ = "" THEN 360: IF ANS$ < > CHR$ (13) THEN 360
380 HOME
400 INPUT " Please input distance of travel for stage (0.01-200.0 mm) : "; DST
420 IF DST < 0.01 OR DST > 200.0 THEN GOTO 400
440 PRINT : PRINT
460 INPUT "Input the number of data points you wish to take ( < 500 ):"; CHAN
480 IF CHAN < 0 OR CHAN > 500 THEN GOTO 460
500 PRINT : PRINT
520 JUMPSIZE = INT (100. * DST / CHAN): REM  Jumpsize Is in 10 Micron
Units
540 DETA = 2 * 3.33564E - 2: REM  DETA = (2*(10 MICRONS))/C
560 TIME = JUMPSIZE * DETA: FSC + TIME * (CHAN - 1)
580 PRINT : PRINT
600 PRINT "Time between data points is : ";time; "PS."
620 PRINT : PRINT
640 PRINT "The full scan is : ";FSC;" ps."
660 PRINT : PRINT
```

```
680 PRINT "Hit ";: INVERSE : PRINT "E";: NORMAL : PRINT " to edit these
    parameters";
700 PRINT " or hit ";: FLASH : PRINT "RETURN";: NORMAL : PRINT "  to
    continue.";
720 GET AS$: IF AS$ = "" THEN 720
740 IF AS$ < > "E" AND AS$ < >  CHR$ (13) THEN 720
760 IF AS$ = "E" THEN 380
770 CN = CHAN
775 ZZ = 1
780 PRINT : PRINT
800 PRINT "Input number of Adc conversions to make at each step. ( < 100)"
820 INPUT "Note : 20 conversions takes about 1 sec. ":QQ
840 PRINT : PRINT
860 INPUT "Input number of scans to be made : ";NSC
880 HOME
980 FOR I = 1 TO CHAN:SA(I) = 0:TM(I) = TIME * (I - 1): NEXT
1000 HGR
1020 IX = 0:II = 0:YY = 77:Y = 0:Z = 0
1030 IX = 0
1040  PRINT  CHR$ (4);"PR#3"
1060  & AIO: POKE 36295,1
1080  PRINT  CHR$ (4);"PR#3"
1090 CHAN = CN:AW = 0
1100 Z = Z + 1
1120 VTAB 24
1130 FOR I = 1 TO CHAN
1135 GOSUB 5000
1140 PRINT  CHR$ (4);"PR#2"
1160 PRINT  CHR$ (2);"LF DISABLE"
1180 PRINT  CHR$ (2);"TERM MODE"
1200 PRINT "R " +  STR$ (R)
1220 PRINT "S " +  STR$ (S)
1240 PRINT "F " +  STR$ (F)
1260 PRINT "N" +  STR$ (JUMPSIZE)
1280 PRINT "-"
1300 PRINT "G"
1440 BW(I) = KZ / QQ
1445 AW = 0
1450 PRINT  CHR$ (4);"PR#3"
1480 IX = IX + 1.8: IF IX > 279 THEN IX = 0
1500 DL = TIME * (I - 1)
1520 VTAB 24: PRINT  TAB(25);I; TAB( 30);"Time ";DL; TAB(50);"Value
";BW(I);
     TAB( 65);SA(I); TAB( 70);IX
1540 Y = 155 - (BW(I) - MIN) * SC
1560 IF Y > 155 THEN Y = 155
1580 IF Y < 0 THEN Y = 0
1600 IF IX = 0 THEN II = IX:YY = Y
1620 HCOLOR= 3
1640 HPLOT IX,Y:II = IX:YY = Y: NEXT
```

```
1650 IX = IX + 1.8:II = IX
1660  FOR I = 1 TO CHAN:SA(I) = SA(I) + BW(I): NEXT
1680  IF Z = NSC THEN GOTO 4000
2000  PRINT  CHR$ (R);"PR#3"
2020  & AIO: POKE 36259,1
2040  PRINT  CHR$ (4);"PR#3"
2050 CHAN = CN:AW = 0
2060 Z = Z + 1
2080  VTAB 24
2100  FOR I = 1 TO CHAN
2120  PRINT  CHR$ (4);"PR#2"
2140  PRINT  CHR$ (2);"LF DISABLE"
2160  PRINT  CHR$ (2);"TERM MODE"
2180  PRINT "R " +  STR$ (R)
2200  PRINT "F " +  STR$ (S)
2220  PRINT "F " +  STR$ (F)
2240  PRINT "N " +  STR$ (JUMPSIZE)
2260  PRINT "+"
2280  PRINT "G"
2300  GOSUB 5000
2420 FW(I) = KZ / QQ
2425 AW = 0
2430  PRINT  CHR$ (4);"PR#3"
2460 IX = IX - 1.8: IF IX < 0 THEN IX = 279
2480 DL = TIME * (CHAN - I)
2490 J = CHAN + 1 - I
2500  VTAB 24: PRINT  TAB( 25);I; TAB(30);"Time ";DL; TAB(
50);"Value";FW(I);
       TAB (65);SA(J); TAB ( 70);IX
2520 Y = 155 - (FW(I) - MIN) * SC
2540  IF Y > 155 THEN Y = 155
2560  IF Y < 0 THEN Y = 0
2580  IF IX = 279 THEN II = IX:YY = Y
2590  HCOLOR = 0
2600  HPLOT II,YY TO IX,Y:II = IX:YY = Y: NEXT
2650  FOR I = 1 TO CHAN:J = CHAN + 1 - I:SA(I) = SA(I) + FW(J): NEXT
2700  IF Z = NSC THEN GOTO 4000
2720  GOTO 1030
3000 IF NXH = 1 THEN CH = 0: RETURN
3010  PRINT " CARD#(0 - "NCH - 1")";: INPUT CH: IF CH < 0 OR CH > NC - 1
      GOTO 3010
3020  RETURN
4000  FOR I = 1 TO CHAN:SA(I) = SA(I) / NSC: NEXT
4020 IX = 0:II = 0:YY = 77:Y = 0
4040  HGR :HG = 1: HCOLOR= 3
4060  FOR I = 1 TO CHAN
4080 IX = IX + 1.8: IF IX > 279 THEN IX = 0
4100 DL = TIME * (I - 1)
4120  VTAB 24: PRINT  TAB ( 25);I; TAB( 30);"Time "; DL; TAB( 50);"Value ";
      SA(I)
```

```
4140 Y = 155 - (SA(I) - MIN) * SC
4160  IF Y > 155 THEN Y = 155
4180  IF Y < 0 THEN Y = 0
4200  IF IX = 279 THEN II = IX:YY = Y
4220  HPLOT II,YY TO IX,Y:II = IX:YY = Y: NEXT
4240  VTAB 24: PRINT "Hit any key to continue"
4260  GET HIT$: IF HIT$ = "" THEN 4260
4280 TEXT : HOME
4300  FOR I = 1 TO CHAN: PRINT I; TAB ( 5);TM(I); TAB( 20); SA(I): NEXT
4340  PRINT : PRINT
4360  PRINT "Do you want to save this data ? (Y or N)"
4380  GET ANS$: IF ANS$ < > "Y" AND ANS$ < > "N" THEN 4380
4400  IF ANS$ = "Y" THEN 4580
4420  HOME
4440  PRINT "Take More Data With These Parameters ? (Y or N)"
4460  GET AS$: IF AS$ < > "Y" AND AS$ < > "N" THEN 4380
4480  IF AS$ = "N" THEN GOTO 4562
4500  PRINT : PRINT
4520  PRINT "Please return stage to origin, then hit any key.";
4540  GET A$: IF A$ = "" THEN 4540
4560  GOTO 980
4562  PRINT : PRINT
4564  PRINT "Do you want to change any parameters ?"
4566  GET RP$ = IF RP$ < > "Y" AND RP$ < > "N" THEN 4484
4568  IF RP$ = "N" THEN END
4570  GOTO 400
4580  PRINT  CHR$ (4);"PR#3"
4600  INPUT "Name for raw data file : ";NAME$
4620  INPUT "Is data disk in drive 1 or 2 : ";DSK$
4640  IF DSK$ < > "1" AND DSK$ < > "2" THEN 4640
4660  PRINT  CHR$ (4);"OPEN ";NAME$;",S6,D";DSK$
4680  PRINT  CHR$ (4);"WRITE ";NAME$
4700  PRINT CHAN
4720  FOR I = 1 TO CHAN: PRINT TM(I): NEXT
4740  FOR I = 1 TO CHAN: PRINT SA(I): NEXT
4760  PRINT  CHR$(4);"CLOSE "
4780  PRINT  CHR$ (4);"LOCK ";NAME$
4800  GOTO 4420
5000 AW = 0
5020  FOR K = 1 TO QQ
5040  & AIO,K: REM  Input Devices Are Analog
5060 KZ = D%(K) + AW
5080 AW = KZ
5100  NEXT K
5120  RETURN
```

APPENDIX B

DIMER SOFTWARE

To analyze the structure of DCC dimer, the following procedure should be followed. The programs that are involved are OVERLAPDIGITIZER, DimericState, SpectrumDecomposition, OsStrength, and SpectraGeneration. The OVERLAPDIGITIZER program is written in Applesoft BASIC for Apple IIe system and used to digitize the absorption spectra of DCC. The original edition of digitization program was written by Dr. Kelly G. Casey (dissertation of Kelly G. Casey, Texas Tech University, Lubbock, Tx, USA, 1988) and revised by the author to fit our purpose. The revised version allows us to digitize spectra at exactly the same x-coordinates. The programs, DimericState, SpectrumDecomposition, OsStrength, and SpectraGeneration, are written in Turbo Pascal for all types of Macintosh systems. These programs are designed to read text data files only. The following format for data file should be followed. All data file should begin with an integer number which specified the number of data points in the data file. The x-coordinates of corresponding data points are listed right after the integer number and then the y-coordinates of these data points followed. The DimericState program uses the digitized data to determined the dimer spectrum of DCC. The dimer spectrum is then deconvoluted into several Gaussian bands by using the program SpectrumDecomposition. The OsStrength program is used to calculate the oscilator strength of the two component bands of the dimer spectrum. The dimer structure can be obtained from these spectra analysis. Finally, the composite spectra of monomers and dimers are synthesized by using the SpectraGeneration program and compare

with the measured spectra. The programs are described in more detail below, individually.

The following program, OVERLAPDIGITIZER, is a modification of an Applesoft BASIC digitization program (DIGITIZER) developed by Dr. Kelly G. Casey. In order to digitize the spectra at exactly the same wavelength coordinates, the measured spectra are all plotted in one spectra window before digitization. The front panel buttons of the plotter are used to move the digitizing sight to the digitizing points. The first step is to determine the digitzing window. Two coordinates (XN, YN and XX, YX) corresponding to the bottom-left and the upper-right corners of the spectra window are entered by moving the sight to the point and then pressing "Return" on the front panel of the computer. The digitizing step size (NDX) is entered through keyboard. Each digitized point is enter by moving the sight to the point and then pressing "Return". At the end, the digitized spectrum is rescaled and stored on a floppy diskette.

Subroutine 360 declares the frame within which spectra to be digitized. Statements 440-460, PR#3 sends output to computer slot number 3, and IN#1 accepts input from computer slot number 1. CHR$ (4) means end of transmission.

For statements 470-630, the initialize instruction IN returns the plotter's graphics conditions to the initial power-on state by program control. DC provides a means to terminate digitize mode. OC is the output commanded, position and pen status instruction. It is used to output the x- and y-coordinates and pen status (up or down) associated with the last valid pen position command. The pen position and status are output to the computer as integers in ASCII in the form of statements 490 and 610, where P1(1) and P2(1) are the X-coordinates of the digitized points in

plotter units, P1(2) and P2(2) are the Y-coordinates of the digitized points in plotter units, and P is the pen status when the point was entered.

Statements 122-127 return the sight to the starting point and get ready for digitization where SP is the pen select instruction that selects pen number PEN(1). IP sets scaling points (in plotter units) of statements 490 and 610. SC scales the digitizing area into user units (XN, XX, YN, YX). VS sets the pen velocity to its default velocity of 38.1 cm/s and acceleration to 980 cm/s^2. PU raises the pen at the coordinates indicated, programmatically. PD lowers the pen.

Statements 128-300 are the digitization routine where PR moves the sight to the points indicated by the increments (NDX, 0) relative to the previous pen position. Statements 336-347 smooths the digitized spectrum curve. Statements 640-970 save data on a floppy diskette. Statement 1200-1320 rescales the digitized spectrum.

```
10 REM PRG OVERLAPDIGITIZER
20 PRINT CHR$ (4);"PR#3"
30 Z = 1000
40 DIM X(Z), Y(Z)
45 TA = 0.0
60 GOSUB 360
70 PRINT : PRINT "Now input  min/max numbers that  correspond to the"
80 PRINT : PRINT "bottom-letf and upper-right hand corners."
90 PRINT
100 INPUT "Input  X & Y min. values: ";XN, YN
110 INPUT "Input X & Y max. values: ";XX, YX
115 PRINT  CHR$ (4);"PR#3"
120 PRINT : INPUT "Input incremental distance.  ";NDX
121 PRINT  CHR$ (4);"PR#3"
122 PRINT  CHR$ (4);"PR#1"
123 PRINT "IN;SP";PEN(1);"IP";P(1);",";P1(2);", "P2(1);",";P2(2)
124 PRINT "SC";XN;",";XX;",";YN;",";YX;";"
125 PRINT "VS "; "";";"
126 PRINT "PU";XN;",";YN
127 PRINT "PD"
128 PRINT  CHR$  (4);"PR#3"
129 KK = 1
130 PRINT : PRINT "Now move the plotter pen to a point you want to digitize."
140 PRINT : PRINT :Hit RETURN to accept the point."
150 PRINT
```

```
160 PRINT "Type N to stop, any key to continue."
170 GET A$: IF A$ = "" THEN 170
180 IF A$ = "N" THEN 310
190 PRINT  CHR$ (4);"PR#3"
200 PRINT  CHR$ (4);"PR#1"
210 PRINT  CHR$ (4);"IN#1"
220 PRINT "IN;DC;"
230 PRINT "IP";P1(1);","P1(2);","P2(1);",";P2(2)
240 PRINT "SC";XN;",";XX;",";YN;",";YX;","
250 PRINT "OC"
255 INPUT X(KK), Y(KK), P
260  PRINT "PR";NDX;",";0;"PD;"
270 PRINT  CHR$  (4);"PR#3"
276 PP = KK - 1
280 PRINT : PRINT : PRINT : PRINT "Point #, X, Y = ";KK, X(KK), Y(KK)
281 X(0) = X(KK)
282 Y(0) = Y(KK)
284 HL = ABS (X(KK) - X(PP))
286 VL = Y(KK) - Y(KK)
289 HT = Y(PP)
290 IF VL < 0 THEN HT = Y(KK)
291 SA = HL * HT + 0.5 * HL * ABS (VL)
292 TA = TA + SA
295 KK = KK + 1
300 GOTO 130
310 GOTO 320
320 PRINT  CHR$ (4);"PR#3"
330 FOR I = 1 TO KK - 1: PRINT I, X(I), Y(I): NEXT
332 PRINT "The total area is ";TA
333 PRINT " Hit any key to continue. "
334 GET AS$: IF AS$ = "" THEN 334
335 GOSUB 1200
336 PRINT : PRINT "Would you like to smooth the curve ? (Y pr N)"
337 GET AN$: IF AN$ <  > "Y" AND AN$ < > "N" THEN 337
338 IF AN$ = "N" THEN 349
339 J = 1
340 FOR I = 3 TO KK - 3
341 L = J + 1
342 M = L + 1
343 N = M + 1
344 U = N + 1
345 Y(M) = (Y(J) + Y(L) + Y(M) + Y(N) + Y(U)) / 5.0
346 J = J + 1
347 NEXT I
349 GOSUB 640
350 GOSUB 2000
351 GOTO 121
360 REM ************************************************
370 REM        DETERMINE  WINDOW  OF  PLOT
380 REM ************************************************
```

```
390 P1 = 0
400 PRINT : PRINT "using control panel, set the pen to the lower left-hand corner
of
    the graph."
410 PRINT : PRINT
420 PRINT "Hit any key when ready."
430 GET  A$: IF A$ = "" THEN 430
440 PRINT  CHR$ (4);"PR#3"
450 PRINT  CHR$ (4);"PR#1"
460 PRINT  CHR$ (4);"IN#1"
470 PRINT "IN;DC;"
480 PRINT "OC"
490 INPUT P1(1), P1(2), P
500 PRINT  CHR$ (4);"PR#3"
510 PRINT : PRINT
520 PRINT : PRINT "Using control panel, set the pen to the upper right-hand corner
of
    the graph."
530 PRINT : PRINT
540 PRINT "Hit any key when ready."
550 GET A$: IF A$ = "" THEN 550
560 PRINT  CHR$ (4);"PR#3"
570 PRINT  CHR$ (4);"PR#1"
580 PRINT  CHR$ (4);"IN#1"
590 PRINT "IN;DC;"
600 PRINT "OC"
610 INPUT P2(1), P2(2), P
620 PRINT  CHR$ (4);"PR#3"
630 RETRUN
640 REM ************************************************
650 REM                SAVE DATA
660 REM ************************************************
670 PRINT : PRINT "Do you want to save data? ( Y or N) ";
680 GET A$: IF A$ < > "Y" AND A$ < > "N" THEN 680
690 PRINT A$
700 IF A$ = "N" THEN RETURN
760 PRINT : PRINT "Please input data file name: ";
770 INPUT NME$
780 PRINT : PRINT : INPUT "Input drive number : ";D
810 IF D < > 1 AND D < > 2 THEN PRINT "Invalid drive number.  Try again.  ":
    GOTO 780
900 PRINT  CHR$ (4);"PR#3"
910 PRINT  CHR$ (4);"OPEN ";NME;",D"; D
920 PRINT  CHR$ (4);"WRITE ";NME$
930 PRINT KK - 1
940 FOR I = 1 TO KK - 1: PRINT X(I): NEXT
950 FOR I = 1 TO KK - 1: PRINT Y(I): NEXT
960 PRINT  CHR$ (4);"CLOSE"
970 RETURN
1200  REM ********** SCALE DATA  **********
```

```
1205 PRINT : PRINT "Would you like to rescale the Y axis ? (Y or N)"
1206 GET ANS$: IF ANS$ < > "Y" AND ANS$ < > "N" THEN 1206
1207 IF ANS$ = "N" THEN 1330
1225 N = KK - 1
1240 BIG = Y(1)
1250 FOR I = 1 TO N
1260 IF BIG - Y(I) > 0 THEN 1295
1280 BIG = Y(I)
1295 NEXT
1296 PRINT "The Ymax is : ";BIG
1297 PRINT
1298 PRINT : INPUT "Please input Ymax you want your data to be: ";YWANT
1300 FOR I = 1 TO N:
1302 Y9I) = Y(I) * (YWANT / BIG)
1310 PRINT I, X(I), Y(I)
1320 NEXT
1330 RETURN
2000 HOME
2010 PRINT "Continue for the next digitization ?"
2020 GET RPL$: IF RPL$ = "" THEN 2020
2030 IF RPL$ = "N" THEN END
2035 PRINT : INPUT "Enter the new Ymax value: ";YX
2040 HOME
2050 RETURN
```

Every Pascal program contains a header and a block. The header begins with the word PROGRAM. The block has two main parts, the declaration part and the statement part. The declaration part defines the various data items that are used within the program. These include labels, constants, type definitions, variables, functions, and procedures. The statement part contains the actural statements that cause actions to be taken.

This program, DimericState, extracts the dimer spectrum from composite spectra. The following orders are followed. First, number of digitized spectra files available (Fire) is entered at the beginning of the main program. The input routine includes PROCEDURE EnterName, EnterValue, and ReadFile. PROCEDURE EnterName reads the name of each spectrum file (FileName[Frame]) through keyboard starting from the file of the lowest concentration. The concentration (Conc) and pathlength (Path) of each file are entered from keyboard by PROCEDURE EnterValue.

PROCEDURE ReadFile reads in data from disk drive and converts wavelength from nm to cm^{-1} (line 17 of ReadFile). PROCEDURE ScaleXaxis, ScaleYaxis, and DrawingGraph display the data curves on the screen.

```
PROGRAM DimericState(DataFile,ResultFile);
USES MemTypes,QuickDraw,OsIntf,ToolIntf,PackIntf;
TYPE
   Xaxis = ARRAY [1..300] OF INTEGER;
   Yaxis = ARRAY [1..6,1..300] OF INTEGER;
   Map = ARRAY [0..7,1..300] OF REAL;
   Words = ARRAY [1..10] OF STRING;
   Strap = ARRAY [1..300] OF REAL;
   Short = ARRAY [1..6] OF REAL;

VAR
   Fire,Frame,Index,Row,Number,Mm:INTEGER;
   BufferFile,DataFile,ResultFile:TEXT;
   FileName,Phrase:Words;
   K,FinalK,DMax,DMin,Drange,Xrange,BestK,Walk,XSQ,Kd:REAL;
   Dband:LongInt;
   Conc,Path,Xi:Short;
   Spectra,Dimer:Map;
   Monomer,D:Strap;
   Name,Answer:STRING;
   X:Xaxis;
   Y:Yaxis;
   Box:rect;
   flag:boolean;

PROCEDURE EnterName;
BEGIN
 WRITELN;
 WRITE('Enter the file name of ',Phrase[Frame],' spectrum here : ');
 READLN(FileName[Frame]);
 WRITELN
END;

PROCEDURE EnterValue(VAR Value:Short);
BEGIN
 READLN(Value[Frame]);
 WRITELN
END;

PROCEDURE ReadFile(State:INTEGER;VAR Z:Map);
VAR
   flag : boolean;
```

```
  Axis:Strap;
  n:INTEGER;
BEGIN
 IF State = 1
  THEN
  Begin
   RESET(BufferFile,FileName[State]);
   READLN(BufferFile,Number);
   For Row:=0 To 1 Do
   For Index :=1 To Number Do
   READLN(BufferFile,Z[Row,Index]);
   CLOSE(BufferFile);
   For Index:=1 To Number Do
    Z[7,Index]:=1.0E7/Z[0,Index];
  End
  ELSE
  Begin
   RESET(BufferFile,FileName[State]);
   READLN(BufferFile,n);
   IF n <> Number
    THEN
    Begin
     CLOSE(BufferFile);
     WRITELN('Number of data mismatch !!')
    End
    ELSE
    Begin
     flag := true;
     Index:=1;
     REPEAT
      READLN(BufferFile,Axis[Index]);
      Index := Index + 1;
      IF (Axis[Index-1] <> Z[0,Index-1]) OR (Index > Number)
       THEN flag := false;
     UNTIL flag = false;
    IF Index > Number
     THEN
     Begin
      For Index :=1 To Number Do
      READLN(BUFFERFILE,Z[State,Index]);
      CLOSE(BufferFile)
     End
     ELSE
     Begin
      CLOSE(BufferFile);
      WRITELN('X axis of the file mismatch !!');
     End;
   End;
  End;
END;
```

```
PROCEDURE ScaleXaxis(Z:Map);
BEGIN
 Xrange:=390.0/(Z[7,1]-Z[7,Number]);
 For Index:=1 To Number Do
 X[Index]:=round((Z[7,Index]-Z[7,Number])*Xrange)+85;
END;

PROCEDURE ScaleYaxis(State:INTEGER;Z:Map);
VAR
   YMax,YMin,Yrange:real;
BEGIN
 For Index:=1 To Number Do
  Z[State,Index]:=Z[State,Index]/(Conc[State]*Path[State]);
 Ymax:=Z[State,1];
 Ymin:=Z[State,1];
 For Index:=2 To Number Do
 Begin
  IF Z[State,Index] > Ymax
   THEN
   Ymax:=Z[State,Index]
   Else
   IF Z[State,Index] < YMin
    THEN
    YMin:=Z[State,Index];
 End;
 Yrange:=240.0/(YMax-YMin);
 For Index:=1 To Number Do
 Y[State,Index]:=250-round((Z[State,Index]-YMin)*Yrange+5);
END;

PROCEDURE DrawingGraph(State:INTEGER);
BEGIN
 SetRect(Box,80,0,480,250);
 FrameRect(Box);
 MoveTo(X[1],Y[State,1]);
 for Index:=2 to Number do
 LineTo(X[Index],Y[State,Index]);
 Writeln('Hit "RETURN" to continue!');
 READLN;
END;

PROCEDURE Position(Wavelength:LongInt);
VAR
  Diff:REAL;
Begin
 ClearScreen;
 WRITELN('Processing!');
 Diff := abs(Spectra[0,1] - Wavelength);
 For Index := 1 To Number Do
```

```
    IF abs(Spectra[0,Index] - Wavelength) < Diff
     THEN
      Begin
       Diff := abs(Spectra[0,Index] - Wavelength);
       Mm := Index;
      End;
 ClearScreen;
End;

PROCEDURE ScaleDimerSpectra(Z:Map);
BEGIN
 Dmax:=Z[3,1];
 Dmin:=Z[3,1];
 For Index:=2 To Number Do
 Begin
  IF Z[3,Index] > Dmax
   THEN
   Dmax:=Z[3,Index]
   Else
   IF Z[3,Index] < DMin
    THEN
    DMin:=Z[3,Index];
 End;
 Drange:=240.0/(DMax-DMin);
 For Frame := 2 To Fire Do
 For Index:=1 To Number Do
 Y[Frame,Index]:=275-round((Z[Frame,Index]-DMin)*Drange+24);
END;

PROCEDURE PlotDimerSpectra;
BEGIN
 ClearScreen;
 SetRect(Box,80,0,480,275);
 FrameRect(Box);
 For Frame := 2 To Fire Do
 Begin
  MoveTo(X[1],Y[Frame,1]);
  for Index:=2 to Number do
  LineTo(X[Index],Y[Frame,Index]);
 End;
 IF walk > 0.0
 THEN
 Begin
  MoveTo(X[Mm],Y[3,Mm]);
  LineTo(X[Mm],263);
 End;
END;

PROCEDURE SelectWavelength;
VAR
```

```
  Plate:RECT;
  Frnt:LongInt;
  Digital:String;
  Spot:Point;
Begin
 WRITELN('Click at the dimer peak now!');
 GetMouse(Spot);
 With Spot Do
  Begin
   Case 0 of
   0:SetRect(Plate,0,260,78,280);
   End;
   Dband := round(1.0E7/((h -85)/Xrange + Spectra[7,Number]));
   Frnt := Dband;
   NumToString(Dband,Digital);
   MoveTo(3,273);
   DrawString(Digital);
  End;
 While Button = false Do
  Begin
     GetMouse(Spot);
     With Spot Do
     Begin
      Case 0 of
      0:SetRect(Plate,0,260,78,280);
      End;
      Dband := round(1.0E7/((h -85)/Xrange + Spectra[7,Number]));
      IF Dband <> Frnt
      THEN
       Begin
        Frnt := Dband;
        EraseRect(Plate);
        NumToString(Dband,Digital);
        MoveTo(3,273);
        DrawString(Digital);
       End;
     End;
  End;
 GetMouse(Spot);
 With Spot Do
 Begin
  Case 0 of
  0:MoveTo(h,270);
  End;
  LineTo(h,v);
 End;
 EraseRect(Plate);
 ClearScreen;
End;
```

```
PROCEDURE Result;
Begin
 ClearScreen;
 WRITE('Save the result dimer spectrum ? ');
 READLN(Answer);
 If (Answer = 'Y') OR (Answer = 'y')
 THEN
  Begin
   ClearScreen;
   WRITE('Enter file name of dimer here : ');
   READLN(Name);
   ClearScreen;
   WRITELN('Processing!');
   For Index := 1 To Number Do
    Begin
     D[Index] := 0.0;
     For Row := 2 To Fire Do
      D[Index] := D[Index] + Dimer[Row,Index]/(Fire-1);
    End;
   REWRITE(BufferFile,Name);
   WRITELN(BufferFile,Number);
   For Index := 1 To Number Do
    WRITELN(BufferFile,Spectra[0,Index]:7:3);
   For Index := 1 To Number Do
    WRITELN(BufferFile,D[Index]:13:6);
   WRITELN(BufferFile,'FileName    Concentration M   Pathlength cm');
   For Row := 1 To Fire Do
     WRITELN(BufferFile,FileName[Row],'   ',Conc[Row]:15,'
',Path[Row]:4:2);
    WRITELN(BufferFile,'K = ',BestK:8:2,' at ',Dband,' nm');
   CLOSE(BufferFile);
   ClearScreen;
   WRITE('Enter file name of monomer here : ');
   READLN(Name);
   ClearScreen;
   WRITELN('Processing!');
   REWRITE(BufferFile,Name);
   WRITELN(BufferFile,Number);
   For Index := 1 To Number Do
    WRITELN(BufferFile,Spectra[0,Index]:7:3);
   For Index := 1 To Number Do
    WRITELN(BufferFile,Monomer[Index]:13:6);
   WRITELN(BufferFile,'FileName    Concentration M   Pathlength cm');
   For Row := 1 To Fire Do
     WRITELN(BufferFile,FileName[Row],'   ',Conc[Row]:15,'
',Path[Row]:4:2);
    WRITELN(BufferFile,'K = ',BestK:8:2,' at ',Dband,' nm');
   CLOSE(BufferFile);
  End
 ELSE
```

```
   Begin
     ClearScreen;
     WRITELN('Processing!');
   End;
End;

PROCEDURE Calculation(Z:Map);
VAR
   I,J:INTEGER;
   Rock:boolean;
   EMM,Chi,Ck:REAL;
   EDM,T:Short;
   Front:LongInt;
   Rectangle:RECT;
   Idiom:STRING;
   S:Str255;
Begin
  S := '+';
 Rock := false;
 J := 0;
 EMM := Z[1,Mm]/(Conc[1]*Path[1]);
 REPEAT
  Front := round(K);
  NumToString(Front,Idiom);
  SetRect(Rectangle,0,260,75,280);
  MoveTo(3,273);
  DrawString(Idiom);
  Kd := 1.0/K;
  J := J + 1;
  Chi := 0.0;
  For Row := 2 To Fire Do
  Begin
    Xi[Row] := (sqrt(sqr(Kd)+8*Kd*Conc[Row])-Kd)/(4*Conc[Row]);
    EDM[Row] := 2*(Z[Row,Mm]/(Conc[Row]*path[Row])-EMM*Xi[Row])/(1.0-
Xi[Row]);
  End;
  For Row := 2 To Fire-1 Do
  For I := Row+1 To Fire Do
    Chi := Chi + sqr(EDM[Row]-EDM[I]);
  IF J = 1
  THEN
    Begin
      Ck := Chi/10.0;
      XSQ := Chi;
    End
  ELSE
    IF Chi < XSQ
    THEN
      Begin
      XSQ := Chi;
```

```
    BestK := K;
    IF (XSQ < 100.0) OR (XSQ < Ck)
    THEN
     Begin
    IF XSQ < Ck
    THEN Ck := XSQ/10.0;
     WRITELN('Processing!');
    For Index := 1 To Number Do
    For Row := 2 To Fire Do
     Begin
       Xi[Row] := (sqrt(sqr(Kd)+8*Kd*Conc[Row])-Kd)/(4*Conc[Row]);
       Dimer[Row,Index] := 2*(Z[Row,Index]/(Conc[Row]*path[Row])-
Monomer[Index]*Xi[Row])/(1.0-Xi[Row]);
     End;
    ScaleDimerSpectra(Dimer);
    PlotDimerSpectra;
     WRITELN('        K = ',K:6:2);
     WRITELN('Difference = ',Chi:12);
      End;
    End;
  K := K + Walk;
  EraseRect(Rectangle);
 Until K > FinalK;
 If (BestK <> FinalK) AND (Walk <10.0)
 THEN
  Begin
    WRITELN('Processing!');
   For Index := 1 To Number Do
   For Row := 2 To Fire Do
     Begin
       Xi[Row] := (sqrt(sqr(1.0/BestK)+8*(1.0/BestK)*Conc[Row])-
(1.0/BestK))/(4*Conc[Row]);
       Dimer[Row,Index] := 2*(Z[Row,Index]/(Conc[Row]*path[Row])-
Monomer[Index]*Xi[Row])/(1.0-Xi[Row]);
     End;
   ScaleDimerSpectra(Dimer);
   PlotDimerSpectra;
    WRITELN('        K = ',BestK:6:2);
    WRITELN('Difference = ',XSQ:12);
   READLN;
   WRITELN('Enter the name of the true dimer spectrum. ');
   WRITE('If you do not have one, enter N : ');
   READLN(Name);
    IF (Name = 'N') OR (Name = 'n')
   THEN
     Begin
       Result;
     End
   ELSE
     Begin
```

```
        RESET(BufferFile,Name);
        READLN(BufferFile,Number);
        For Index :=1 To Number Do
        READLN(BufferFile);
        For Index :=1 To Number Do
        READLN(BufferFile,D[Index]);
        CLOSE(BufferFile);
        For Index:=1 To Number Do
         Y[1,Index]:=275-round((D[Index]-DMin)*Drange+24);
        SetRect(Box,80,0,480,275);
        FrameRect(Box);
        For Index:=1 to Number do
         Begin
          MoveTo(X[Index],Y[1,Index]);
          DrawString(S);
         End;
        WRITELN('Hit "RETURN" to continue!');
        READLN;
        Result;
      End;
  End;
End;

PROCEDURE Approach;
BEGIN
 ClearScreen;
 WRITELN('Enter the starting equlibrium constant K below. ');
 READLN(K);
 IF K <= 0.0
 THEN
  Begin
   ClearScreen;
   WRITELN('This value is not acceptable!');
   WRITELN;
   WRITELN('Hit RETURN to start over.');
   READLN;
   EXIT;
  End;
 ClearScreen;
 WRITELN('Processing!');
 Walk := 0.0;
 Kd := 1.0/K;
 For Index := 1 To Number Do
  Monomer[Index] := Spectra[1,Index]/(Conc[1]*Path[1]);
 For Index := 1 To Number Do
 For Row := 2 To Fire Do
  Begin
   Xi[Row] := (sqrt(sqr(Kd)+8*Kd*Conc[Row])-Kd)/(4*Conc[Row]);
   Dimer[Row,Index] := 2*(Spectra[Row,Index]/(Conc[Row]*path[Row])-
Monomer[Index]*Xi[Row])/(1.0-Xi[Row]);
```

```
  End;
 ScaleDimerSpectra(Dimer);
 PlotDimerSpectra;
 SelectWavelength;
 Position(Dband);
 FinalK := 2.0*K;
 Walk := 0.1*K;
 REPEAT
 Calculation(Spectra);
 IF BestK = FinalK
 THEN
  Begin
   WRITELN;
   WRITELN('Processing!');
   For Index := 1 To Number Do
   For Row := 2 To Fire Do
    Begin
      Xi[Row] := (sqrt(sqr(1.0/BestK)+8*(1.0/BestK)*Conc[Row])-
(1.0/BestK))/(4*Conc[Row]);
      Dimer[Row,Index] := 2*(Spectra[Row,Index]/(Conc[Row]*path[Row])-
Monomer[Index]*Xi[Row])/(1.0-Xi[Row]);
    End;
   ScaleDimerSpectra(Dimer);
   PlotDimerSpectra;
 WRITELN('        K = ',BestK:6:2);
 WRITELN('Difference = ',XSQ:12);
    K := BestK;
    FinalK := 2.0*BestK;
    Walk := 0.1*K;
  End
 ELSE
  Begin
    FinalK := (FinalK - BestK)/5.0 + BestK;
    K := 1.2*BestK - 0.2*FinalK;
    Walk := 0.1*Walk;
  End;
 UNTIL (Walk < 1.0) OR (K > 1.0E7);
END;

BEGIN
 ClearScreen;
 WRITE('How many spectra do you have ? (maximum of 6) ');
 READLN(Fire);
 ClearScreen;
 IF Fire > 6
 THEN
  Begin
    WRITELN('Please enter a smaller number!');
    WRITELN;
    WRITELN('Hit RETURN to continue.');
```

```
    READLN;
    EXIT;
   End;
  Phrase[1] := 'the first';
  Phrase[2] := 'the second';
  Phrase[3] := 'the third';
  Phrase[4] := 'the fourth';
  Phrase[5] := 'the fifth';
  Phrase[6] := 'the sixth';
  For Frame := 1 To Fire Do
  Begin
   EnterName;
   WRITE('Enter the concentration of this spectrum here : ');
   EnterValue(Conc);
   WRITE('And the pathlength of this Spectrum is : ');
   EnterValue(Path);
   WRITELN('Thank You!');
   ReadFile(Frame,Spectra);
   ScaleXaxis(Spectra);
   ScaleYaxis(Frame,Spectra);
   ClearScreen;
   DrawingGraph(Frame);
   ClearScreen;
  End;
  Approach;
  ClearScreen;
  WRITELN('        K = ',BestK:6:2);
  WRITELN('Difference = ',XSQ:12);
  WRITELN('Walk = ',Walk:9:4);
  WRITELN('Hit RETURN to continue! ');
  READLN;
  flag := false;
  REPEAT
  ClearScreen;
  WRITE('Start over! Y/N ');
  READLN(Answer);
  IF (Answer = 'Y') OR (Answer = 'y')
  THEN
   Approach
  ELSE
   Begin
    WRITELN('Hit RETURN to exit! ');
    flag := true;
    READLN;
   End;
  UNTIL flag = true;
END.
```

```
PROGRAM SpectrumDecomposition2(Input,Output);
{$U+}
{$R-}
USES   MemTypes,QuickDraw,OsIntf,ToolIntf,PackIntf,SpeechIntf;
    TYPE
      bytes = packed array[1..5120] of char;
      byteptr = ^bytes;
      GrassI = ARRAY [1..10] OF INTEGER;
      TreeI = ARRAY [1..300] OF INTEGER;
      ForestI = ARRAY [0..10,1..300] OF INTEGER;
      GrassR = ARRAY [1..10] OF REAL;
      TreeR = ARRAY [1..300] OF REAL;
      ForestR = ARRAY [0..10,1..300] OF REAL;

    VAR
      Spot:Point;
      flag,gun,judge:boolean;
      FileName,Answer,DotLine,Reply,Speak:STRING;
      VX,VY,HX,HY:GrassI;
      Height,Sigma,Top,Width,Center:GrassR;
      X:TreeI;
      Y:ForestI;
      Block:rect;
      Spectra:ForestR;
      Index,J,K,Number,Row,Total,Share:INTEGER;
      Max,Min,Range,Test0,Test1,Test2,Xrange,Conc,Path:REAL;
      BufferFile:TEXT;

    PROCEDURE SpeakFile(Talk:STRING);
    VAR
      i:INTEGER;
      linein:bytes;
      lineptr:byteptr;
      f:text;
      output:Handle;
      theSpeech:SpeechHandle;
      j:integer;
      aChar:char;

    BEGIN
      i := SpeechOn('', theSpeech);
      IF (i <> 0) THEN exit;
      reset(f,Talk);
      for j:= 1 to 5120 do
      Begin
        read(f,achar);
        linein[j]:=achar;
      End;
```

```
  lineptr := @linein;
  output := NewHandle(0);
  i := Reader(theSpeech, POINTER(lineptr), 6000, output);
  i := MacinTalk(theSpeech, output);
  SpeechOff(theSpeech);
  DisposHandle(output);
  close(f)
END;

PROCEDURE EnterNameOfFile;
BEGIN
  WRITELN;
  WRITE('Enter the file name of the spectrum here : ');
  READLN(FileName);
  WRITELN;
  WRITE('The concentration (M) of this sample is : ');
  READLN(Conc);
  WRITELN;
  WRITE('and the pathlength (cm) is : ');
  READLN(Path);
  WRITELN
END;

PROCEDURE ReadFile(VAR Z:ForestR);
BEGIN
  RESET(BufferFile,FileName);
  READLN(BufferFile,Number);
  For Row:=0 To 1 Do
    For Index :=1 To Number Do
      READLN(BufferFile,Z[Row,Index]);
  CLOSE(BufferFile);
  For Index:=1 To Number Do
    Begin
      Z[0,Index]:=1.0E7/Z[0,Index];
      Z[1,Index]:=Z[1,Index]/(Conc*Path);
    End;
END;

PROCEDURE Delay;
VAR
    XYZ:ForestR;
    Lane,Alley,Nmb:INTEGER;
BEGIN
  RESET(BufferFile,FileName);
  READLN(BufferFile,Nmb);
  Nmb := Round(Nmb/5);
  For Lane:= 0 To 1 Do
    For Alley := 1 To Nmb Do
      READLN(BufferFile,XYZ[Lane,Alley]);
  CLOSE(BufferFile);
```

```
 For Alley:= 1 To Nmb Do
   Begin
     XYZ[0,Alley]:= 1.0E7/XYZ[0,Alley];
     XYZ[1,Alley]:= XYZ[1,Alley]/(Conc*Path);
   End;
END;

PROCEDURE ScaleXaxis(Z:ForestR);
BEGIN
  Xrange:=390.0/(Z[0,1]-Z[0,Number]);
  For Index:=1 To Number Do
    X[Index]:=round((Z[0,Index]-Z[0,Number])*Xrange)+85;
END;

PROCEDURE ScaleYaxis(Z:ForestR);
BEGIN
  Max:=Z[1,1];
  Min:=Z[1,1];
  For Index:=2 To Number Do
    Begin
      IF Z[1,Index] > Max
        THEN
        Max:=Z[1,Index]
        Else
        IF Z[1,Index] < Min
          THEN
          Min:=Z[1,Index];
    End;
  Range:=240.0/(Max-Min);
  For Index:=1 To Number Do
    Y[1,Index]:=275-round((Z[1,Index]-Min)*Range+24);
END;

PROCEDURE PlotData(A:STRING);
VAR
    Box:rect;
    Star:STR255;
BEGIN
  Star := '+';
  SetRect(Box,80,0,480,275);
  FrameRect(Box);
  IF (A = 'Y') OR (A = 'y')
  THEN
    Begin
      MoveTo(X[1],Y[Row,1]);
      For Index:=2 To Number Do
         LineTo(X[Index],Y[Row,Index]);
    End
  ELSE
    Begin
```

```
    For Index:= 1 To Number Do
     Begin
      MoveTo(X[Index],Y[Row,Index]);
      DrawString(Star);
     End;
   End;
END;

PROCEDURE PlotSpectra;
VAR
   Box:rect;
BEGIN
  SetRect(Box,80,0,480,275);
 FrameRect(Box);
 MoveTo(X[1],Y[Row,1]);
 For Index:=2 To Number Do
   LineTo(X[Index],Y[Row,Index]);
END;

PROCEDURE VerticalMouse;
VAR
   Rectangle:RECT;
   I:Integer;
   Front,Back,Frnt,Bk:LongInt;
   Words,Phrase,Idiom:String;
   Wrds:Str255;
   n:Array [1..5] Of Char;
Begin
  n[1] := '1';
  n[2] := '2';
  n[3] := '3';
  n[4] := '4';
  n[5] := '5';
 GetMouse(Spot);
 With Spot Do
   Begin
     Case 0 of
     0:SetRect(Rectangle,0,260,78,280);
     End;
     Front := round((h -85)/Xrange + Spectra[0,Number]);
     Frnt := Front;
     Back := round((275 - v - 24)/Range+Min);
     Bk := Back;
     NumToString(Front,Words);
     NumToString(Back,Phrase);
      Idiom:=Words+','+Phrase;
     MoveTo(3,273);
     DrawString(Idiom);
   End;
 While Button = false Do
```

```
    Begin
      GetMouse(Spot);
      With Spot Do
      Begin
       Case 0 of
       0:SetRect(Rectangle,0,260,78,280);
       End;
       Front := round((h -85)/Xrange + Spectra[0,Number]);
       Back := round((275 - v - 24)/Range+Min);
       IF (Front <> Frnt) OR (Back <> Bk)
       THEN
        Begin
         Frnt := Front;
         Bk := Back;
         EraseRect(Rectangle);
         NumToString(Front,Words);
         NumToString(Back,Phrase);
          Idiom:=Words+','+Phrase;
         MoveTo(3,273);
         DrawString(Idiom);
        End;
      End;
    End;
  GetMouse(Spot);
  With Spot Do
  Begin
   Case 0 of
   0:MoveTo(h,270);
   End;
   LineTo(h,v);
   VX[Row] := h;
   VY[Row] := v;
  End;
  Wrds := '#' + n[Row];
  MoveTo(VX[Row]+15,VY[Row]-1);
  DrawString(Wrds);
  Share := VX[Row];
  EraseRect(Rectangle);
End;

PROCEDURE HorizontalMouse;
VAR
   Rectangle:RECT;
   Front,Frnt:LongInt;
   I:Integer;
   Words:String;
Begin
 GetMouse(Spot);
 With Spot Do
  Begin
```

```
    Case 0 of
    0:SetRect(Rectangle,0,260,78,280);
    End;
    Front := round(abs((h -85)/Xrange + Spectra[0,Number]-Center[Row]));
    Frnt := Front;
    NumToString(Front,Words);
    MoveTo(30,273);
    DrawString(Words);
  End;
 While Button = false Do
  Begin
     GetMouse(Spot);
     With Spot Do
     Begin
      Case 0 of
      0:SetRect(Rectangle,0,260,78,280);
      End;
      Front := round(abs((h -85)/Xrange + Spectra[0,Number]-Center[Row]));
      IF Front <> Frnt
      THEN
        Begin
          Frnt := Front;
          EraseRect(Rectangle);
          NumToString(Front,Words);
          MoveTo(30,273);
          DrawString(Words);
        End;
     End;
  End;
 GetMouse(Spot);
 With Spot Do
 Begin
  Case 0 of
  0:MoveTo(Share,v);
  End;
  LineTo(h,v);
  HX[Row] := h;
  HY[Row] := v;
 End;
 EraseRect(Rectangle);
End;

PROCEDURE SelectPeaks;
VAR
  I:Integer;
Begin
 IF Row = 1
 THEN
  Begin
   WRITELN('Move the mouse to the peak');
```

```
        WRITELN('and click the mouse button.');
       End
      ELSE
       IF Row = 2
        THEN
         Begin
          WRITELN;
          WRITELN('Repeat the procedure, please.');
         End;
      VerticalMouse;
      Delay;
      Center[Row] := (VX[Row] -85)/Xrange + Spectra[0,Number];
      Height[Row] := (275 - VY[Row] - 24)/Range + Min;
      IF Row = 1
       THEN
        Begin
         WRITELN;
         WRITELN('Go to the halfwidth and click!');
        End;
      HorizontalMouse;
      Delay;
      Sigma[Row] := abs((HX[Row] -85)/Xrange + Spectra[0,Number] -
Center[Row]);
    End;

    PROCEDURE ByKeys;
    Begin
     For Row := 1 To Total Do
     Begin
      ClearScreen;
      WRITELN('Enter parameters for peak #',Row);
      WRITELN;
      WRITELN;
      WRITE('Center at (cm-1)  ');
      READLN(Center[Row]);
      WRITELN;
      WRITE('Height of the peak is  ');
      READLN(Height[Row]);
      WRITELN;
      WRITE('Sigma in (cm-1)  ');
      READLN(Sigma[Row]);
     End;
    End;

    PROCEDURE GaussianFunction(C,H,S:GrassR;VAR Z:ForestR);
    VAR
      Factor:REAL;
    Begin
     FOR Index := 1 To Number Do
      Begin
```

```
    Z[2,Index] := 0.0;
    FOR Row := 1 To Total Do
     Begin
       Factor := -sqr(Z[0,index]-C[Row])/(2*sqr(S[Row]));
       Z[2,Index] := Z[2,Index] + H[Row]*exp(Factor);
     End;
    Y[2,Index]:=275-round((Z[2,Index]-Min)*Range+24);
  End;
END;

PROCEDURE ChiSquare(Z:ForestR;VAR X2:REAL);
VAR
  DegFree:INTEGER;
  ChiSq,Deviation,Variance:REAL;
BEGIN
 DegFree := Number-3*Total-1;
 ChiSq := 0.0;
 Deviation := 0.0;
 For Index := 1 To Number Do
  Deviation := Deviation + (Z[2,Index]-Z[1,Index]);
 Variance := sqr(Deviation/Number);
 For Index := 1 To Number Do
  ChiSq := ChiSq+sqr(Z[2,Index]-Z[1,Index])/Variance;
 X2 := ChiSq/DegFree;
END;

PROCEDURE SaveYourResults(VAR Z:ForestR);
Begin
 REWRITE(BufferFile,FileName);
 WRITELN(BufferFile,Number);
 FOR Index := 1 TO Number DO
 Begin
  Z[0,Index]:=1.0E7/Z[0,Index];
  WRITELN(BufferFile,Z[0,Index]:8:3);
 End;
 FOR Index := 1 TO Number DO
 Begin
  Z[2,Index]:=Z[2,Index]*Conc*Path;
  WRITELN(BufferFile,Z[2,Index]:10:7);
 End;
 WRITELN(BufferFile,'Concentration = ',Conc:13:10);
 WRITELN(BufferFile,'Pathlength = ',Path:4:1);
 For Row := 1 To Total Do
  Begin
   WRITELN(BufferFile,'Peak #',Row);
   WRITELN(BufferFile,'Height = ',Height[Row]:10:2);
   WRITELN(BufferFile,'Center at ',Center[Row]:8:2);
   WRITELN(BufferFile,'Sigma is ',Sigma[Row]:7:2);
  End;
 Close(BufferFile);
```

```
End;

BEGIN
 Speak := 'Welcome';
 WRITELN('Welcome!');
 SpeakFile(Speak);
 ClearScreen;
 judge := true;
 EnterNameOfFile;
 ClearScreen;
 WRITELN('Processing!');
 WRITELN;
 ReadFile(Spectra);
 ScaleXaxis(Spectra);
 ScaleYaxis(Spectra);
 REPEAT
  ClearScreen;
  Row := 1;
  WRITE('Choose a line plot ? Y/N  ');
  READLN(DotLine);
  ClearScreen;
  WRITE('Enter parameters from Keyboard or Mouse ? K/M  ');
  READLN(Reply);
  ClearScreen;
  PlotData(DotLine);
   SetRect(Block,0,0,200,25);
  WRITELN('How many peaks can you tell ?');
  READLN(Total);
  IF Total <= 0
  THEN
   EXIT;
  EraseRect(Block);
   IF (Reply = 'K') OR (Reply = 'k')
  THEN
   ByKeys
  ELSE
   FOR Row := 1 To Total Do
    SelectPeaks;
  WRITELN;
  WRITELN('Processing!');
  GaussianFunction(Center,Height,Sigma,Spectra);
  ChiSquare(Spectra,Test0);
  ClearScreen;
  Row := 1;
  PlotData(DotLine);
  Row := 2;
  PlotSpectra;
  WRITELN('X2 = ',Test0:5:2);
  WRITELN;
  WRITELN('Do you wish to change parameters ?');
```

```
      READLN(Answer);
      IF (Answer =  'N') OR (Answer =  'n')
       THEN judge := false;
     UNTIL judge = false;
     For Row := 1 To Total Do
      Begin
        WRITELN('Height = ',Height[Row]:10:2);
        WRITELN('Center at ',Center[Row]:8:2);
        WRITELN('Sigma is ',Sigma[Row]:7:2);
      End;
     WRITELN;
     WRITE('Would you like to save this simulated spectra? (Y or N) ');
     READLN(Answer);
     IF (Answer = 'Y') Or (Answer = 'y')
     THEN
      Begin
        ClearScreen;
        WRITE('Enter the file name of the simulated spectrum : ');
        READLN(FileName);
        SaveYourResults(Spectra);
      End;
END.


PROGRAM OsStrength;
USES   MemTypes,QuickDraw,OsIntf,ToolIntf,PackIntf;
  Type
    Tree = ARRAY [1..300] OF REAL;
    Grass = ARRAY [1..6] OF REAL;
  Var
    Data_Block,BufferFile:TEXT;
     Counter,Number,Index,Gl,Gu,Row,Total:integer;
    Ab,AbWave:Tree;
    X,Y:ARRAY [1..300] OF INTEGER;
    Conc,Path,Average,Area,Os:REAL;
    Center,Height,Sigma:Grass;
    Word:Str255;
    FileName,Answer:STRING;

PROCEDURE ScaleXaxis(Z:Tree);
VAR
  Xrange:REAL;
BEGIN
 Xrange:=390.0/(Z[1]-Z[Number]);
 For Index:=1 To Number Do
  X[Index]:=round((Z[Index]-Z[Number])*Xrange)+85;
END;

PROCEDURE ScaleYaxis(Z:Tree);
```

```
VAR
   Max,Min,Range:REAL;
BEGIN
  Max:=Z[1];
  Min:=Z[1];
  For Index:=2 To Number Do
    Begin
     IF Z[Index] > Max
      THEN
      Max:=Z[Index]
      Else
      IF Z[Index] < Min
       THEN
       Min:=Z[Index];
    End;
  Range:=240.0/(Max-Min);
  For Index:=1 To Number Do
    Y[Index]:=275-round((Z[Index]-Min)*Range+24);
END;

PROCEDURE PlotSpectra;
VAR
   Box:rect;
BEGIN
  CLEARSCREEN;
  SetRect(Box,80,0,480,275);
  FrameRect(Box);
  MoveTo(X[1],Y[1]);
  For Index:=2 To Number Do
    LineTo(X[Index],Y[Index]);
END;

PROCEDURE GaussianFunction(C,H,S:Grass);
VAR
   Factor:REAL;
Begin
  FOR Index := 1 To Number Do
    Begin
     Ab[Index] := 0.0;
     FOR Row := 1 To Total Do
       Begin
        Factor := -sqr(AbWave[Index]-C[Row])/(2*sqr(S[Row]));
        Ab[Index] := Ab[Index] + H[Row]*exp(Factor);
       End;
   End;
END;

PROCEDURE AbArea;
VAR
   heigh,H,W:REAL;
```

```
Begin
  Area := 0.0;
  For Index := 2 To Number Do
    Begin
      IF Ab[Index] > Ab[Index-1]
      THEN
        heigh := Ab[Index-1]
      ELSE
        heigh := Ab[Index];
      H := abs(Ab[Index]-Ab[Index-1]);
      W := abs(AbWave[Index]-AbWave[Index-1]);
      Area := Area + (heigh + 0.5*H)*W;
    End;
  Os := 4.31712E-9*Area;
End;

BEGIN
    Word := 'Processing!';
   WRITE('Enter the file name of absorption spectrum here : ');
   READLN(FileName);
   WRITELN;
   WRITE('and the concentration in M is : ');
   READLN(Conc);
   WRITELN;
   WRITE('the pathlength in cm : ');
   READLN(Path);
   ClearScreen;
   MoveTo(200,100);
   DrawString(Word);
   RESET(Data_Block,FileName);
   READLN(Data_Block,Number);
   For Counter := 1 to Number do
   READLN(Data_Block,AbWave[Counter]);
   For Counter := 1 to Number do
   READLN(Data_Block,Ab[Counter]);
   CLOSE(Data_Block);
   For Counter := 1 to Number do
    Begin
      AbWave[Counter] := 1.0E7/AbWave[Counter];
      Ab[Counter] := Ab[Counter]/(Conc*Path);
    End;
   ScaleXaxis(AbWave);
   ScaleYaxis(Ab);
   PlotSpectra;
   WRITELN('Hit "RETURN" to continue!');
   READLN;
   ClearScreen;
   WRITELN('Calculate the area under gaussian functions ? Y/N');
   READLN(Answer);
   If (Answer = 'Y') OR (Answer = 'y')
```

```
        THEN
         Begin
          ClearScreen;
          WRITELN;
          WRITE('How many gaussian functions ? ');
          READLN(Total);
          For Row := 1 To Total do
           Begin
            ClearScreen;
             WRITELN('Enter #',Row,' Gaussian function parameters,');
            WRITELN;
            WRITE('Center at (cm-1) : ');
            READLN(Center[Row]);
            WRITELN;
            WRITE('the height is : ');
            READLN(Height[Row]);
            WRITELN;
            WRITE('Sigma in (cm-1) : ');
            READLN(Sigma[Row]);
           End;
          ClearScreen;
          MoveTo(200,100);
          DrawString(Word);
          GaussianFunction(Center,Height,Sigma);
         End;
        ClearScreen;
        MoveTo(200,100);
        DrawString(Word);
        AbArea;
        ClearScreen;
        WRITELN('The oscillator strength = ',Os:12);
        readln;
END.
```

```
PROGRAM SpectraGeneration;

USES
  MemTypes,QuickDraw;

TYPE
  TreeI = ARRAY [1..300] OF INTEGER;
  TreeR = ARRAY [1..300] OF REAL;

Var
  X,Y:TreeI;
  Alpha,Conc,Path,K:REAL;
  Data_Block:Text;
  FileName,Name,MName,DName:String;
```

```
  Counter,Index,Number,Row:integer;
  Wavelength,Monomer,Dimer,Spectrum:TreeR;

PROCEDURE ScaleXaxis(WN:TreeR);
VAR
  Xrange:REAL;
BEGIN
 Xrange:=390.0/(WN[1]-WN[Number]);
 For Counter:=1 To Number Do
  X[Counter]:=round((WN[Counter]-WN[Number])*Xrange)+85;
END;

PROCEDURE ScaleYaxis(EC:TreeR);
VAR
  Max,Min,Range:REAL;
BEGIN
 Max:=EC[1];
 Min:=EC[1];
 For Counter:=2 To Number Do
  Begin
   IF EC[Counter] > Max
    THEN
    Max:=EC[Counter]
    Else
    IF EC[Counter] < Min
     THEN
     Min:=EC[Counter];
  End;
 Range:=240.0/(Max-Min);
 For Counter:=1 To Number Do
  Y[Counter]:=275-round((EC[Counter]-Min)*Range+24);
END;

PROCEDURE Plotter;
VAR
  Box:rect;
BEGIN
 SetRect(Box,80,0,480,275);
 FrameRect(Box);
 MoveTo(X[1],Y[1]);
 For Counter:=2 To Number Do
  LineTo(X[Counter],Y[Counter]);
END;

PROCEDURE Results;
BEGIN
 REWRITE(Data_Block,FileName);
 WRITELN(Data_Block,Number);
 FOR Counter := 1 To Number Do
  WRITELN(Data_Block,Wavelength[Counter]:7:3);
```

```
 FOR Counter := 1 To Number Do
  WRITELN(Data_Block,Spectrum[Counter]:12:10);
 WRITELN(Data_Block,MName);
 WRITELN(Data_Block,DName);
 WRITELN(Data_Block,'Concentration = ',Conc:15);
 WRITELN(Data_Block,'Pathlength = ',Path:4:2);
 WRITELN(Data_Block,'Equilibrium constant K = ',1.0/K:10:2);
 Close(Data_Block);
 ScaleYaxis(Spectrum);
 ClearScreen;
 Plotter;
 Writeln('Hit "Return" when ready.');
 READLN;
 ClearScreen;
END;

PROCEDURE SpectraGeneration;
VAR
   Word:Str255;
   MConc,DConc:REAL;
   Filenumber:INTEGER;
BEGIN
 Word := 'Processing';
 WRITE('How many spectra do you need ? ');
 READLN(Filenumber);
 ClearScreen;
 WRITE('Enter the equilibrium constant of dimerization here: ');
 READLN(K);
 K := 1.0/K;
 ClearScreen;
 WRITE('Type the monomer file name here : ');
 READLN(MName);
 ClearScreen;
 MoveTo(200,150);
 DrawString(Word);
 RESET(Data_Block,MName);
 READLN(Data_Block,Number);
 For Index :=1 To Number Do
  READLN(Data_Block,Wavelength[Index]);
 For Index :=1 To Number Do
  READLN(Data_Block,Monomer[Index]);
 CLOSE(Data_Block);
 ScaleXaxis(Wavelength);
 ClearScreen;
 WRITE('Type the dimer file name here : ');
 READLN(DName);
 ClearScreen;
 MoveTo(200,150);
 DrawString(Word);
 RESET(Data_Block,DName);
```

```
        READLN(Data_Block);
        For Index :=1 To Number Do
         READLN(Data_Block);
        For Index :=1 To Number Do
         READLN(Data_Block,Dimer[Index]);
        CLOSE(Data_Block);
        FOR Row := 1 To Filenumber Do
         Begin
          ClearScreen;
          WRITE('Enter concentration of #',Row,' spectrum here : ');
          READLN(Conc);
          WRITELN;
          WRITE('and the pathlength is : ');
          READLN(Path);
          WRITELN;
          WRITE('Enter file name of this spectrum : ');
          READLN(FileName);
          ClearScreen;
          MoveTo(200,150);
          DrawString(Word);
          Alpha := (sqrt(sqr(K)+8*Conc*K)-K)/(4*Conc);
          MConc := Alpha*Conc;
          DConc:=(Conc-MConc)/2.0;
          FOR Counter := 1 To Number Do
           Spectrum[Counter] := (Monomer[Counter]*MConc +
Dimer[Counter]*DConc)*Path;
          Results;
         End;
      END;
      BEGIN
       SpectraGeneration;
END.
```